THE UNIVERSITY
of EDINBURGH

Quasi 2-Layer Morphodynamic Model and Lagrangian Study of Bedload

Sergio Maldonado-Villanueva

Doctor of Philosphy

THE UNIVERSITY OF EDINBURGH

2015

A mi papá, mamá y hermanos

All models are wrong. Some models are useful.

–G.E.P. Box

Eu o engenheiro, eu o civilizado, eu o educado no estrangeiro,

gostaria de ter outra vez ao pé da minha vista só veleiros e barcos de madeira.

(*I, the engineer, the civilised, educated abroad,*

would like to see once more only sailing boats and wooden ships.)

Álvaro de Campos (F. Pessoa). *Ode Marítima.*

Abstract

Conventional morphodynamic models are typically based on a coupled system of hydrodynamic equations, a bed-update equation, and a sediment-transport equation. However, the sediment-transport equation is almost invariably empirical, with numerous options available in the literature. Bed morphological evolution predicted by a conventional model can be very sensitive to the choice of sediment-transport formula. This thesis presents a physics-based model, where the shallow water-sediment-mixture flow is idealised as being divided into two layers of variable (in time and space) densities: the lower layer concerned with bedload transport, and the upper layer representing sediment in suspension. The model is referred to as a Quasi-2-Layer (Q2L) model in order to distinguish it from typical 2-Layer models representing stratified flow by two layers of different but constant and uniform densities. The present model, which does not require the selection of a particular empirical formula for sediment transport rates, is satisfactorily validated against widely used empirical expressions for bedload and total transport rates. Analytical solutions to the model are derived for steady uniform flow over an erodible bed. Case studies show that the Q2L model, in contrast to conventional morphodynamic approaches, yields more realistic results by inherently including the influence of the bed slope on the sediment transport. This conclusion is validated against experimental data from a steep sloping duct. An analytical study using the Q2L model investigates the influence of bed-slope on bedload transport; the resulting expressions are in turn used to modify empirical sediment transport formulae (derived for horizontal beds) in order to render them applicable to arbitrary streamwise slopes. The Q2L model provides an alternative approach to studying sediment-transport phenomena, whose adequate analysis cannot be undertaken following con-

ventional approaches without further increasing their degree of empiricism. The Q2L model can also lead to the enhancement of conventional morphodynamic models.

For coarse sediments and/or relatively low flow velocities, bedload transport is usually responsible for most sediment transport. Bedload transport consists of a combination of particles rolling, sliding and saltating (hopping) along the bed. Hence, saltation models provide considerable insight into near-bed sediment transport. This thesis also presents an analysis of the statistics and mechanics of a saltating particle model. For this purpose, a mathematically simple, computationally efficient, stochastic Lagrangian model has been derived. This model is validated satisfactorily against previously published experimental data on saltation. The model is then employed to derive two criteria aimed at ensuring that statistically convergent results are achieved when similar saltation models are employed. According to the first criterion, 10^3 hops should be simulated, whilst 10^4 hops ought to be considered according to the second criterion. This finding is relevant given that previous studies report results after only a few hundred, or less, particle hops have been simulated. The model also investigates sensitivity to the lift force formula, the friction coefficient, and the collision line level. A method is proposed by which to estimate the bedload sediment concentration and transport rate from particle saltation characteristics. This method yields very satisfactory results when compared against widely used empirical expressions for bedload transport, especially when contrasted against previously published saltation-based expressions.

Lay Summary

Theoretical models of natural systems are important tools that provide insight into the effect of climate variation and change, and human impacts on Earth surface processes such as sea level rise, river flows, soil erosion, and carbon exchanges. This thesis focuses on a theoretical model for predicting the transport of sediment in rivers, estuaries, and coastal waters. Its aim is to provide a more accurate means of calculating sediment transport in shallow water and predicting the evolution of such environments by including more of the physics in the analysis. This is achieved by dividing the shallow flow into upper and lower layers, and resolving the mass and momentum balances of water and sediment in each layer. It is found that the new model requires less tuning parameters and performs better than previous models based on empirical formulae obtained from extensive laboratory studies, when applied to a range of standard tests including the migration of a bed hump (sandbar) along the bed of a steady water stream. A secondary model is also presented, which studies the motion of sand or gravel grains as they are transported near the sea or river bed. Suggestions are included on how best to utilise this type of models in practice.

Acknowledgements

I would like to express my deepest gratitude to my supervisor, Prof. Alistair Borthwick, for his constant, thorough and very motivational guidance throughout my research. It has been a true pleasure to work with and learn from someone whose outstanding excellence as academic can only be outshined by his human quality.

This thesis has been nourished from diverse sources, ranging from brief talks to formal discussions, with academics and colleagues. I am indebted to all of them. In particular, I would like to thank Prof. N. Dodd (University of Nottingham), Dr. D. Pritchard (Strathclyde University), and Prof. Albert Falqués (Universitat Politècnica de Catalunya) and his group, for their insightful feedback on my work. I would especially like to extend my appreciation to Prof. P. Taylor (University of Oxford) for his sharp comments, which led to meaningful improvement of the study presented in Chapter 7; and to Prof. V. Nikora (University of Aberdeen), for his very profound remarks that yielded a significantly enhanced final version of this thesis.

My academic visit to Tsinghua University, China, turned out to be both professionally productive and personally satisfactory. For this, I am extremely grateful to Prof. BinLiang Lin, Dr. Jian Sun and their research group at the State Key Laboratory of Hydroscience and Engineering. Their warm hospitality and academic feedback are greatly appreciated. Here, I would also like to thank Gill Borthwick and (again) Prof. A. Borthwick, for 'adopting' me and kindly looking after me for good part of my stay in Beijing.

This thesis would have not been possible without the economic support received through scholarships awarded by Mexico's National Council for Science and Technology (Conacyt) (2011-2015) and the Mexican Ministry of Education (SEP) (2014-2015).

A very large number of people has contributed to making my PhD a memorable experience. I thank them all. Thanks to the people in IES and the office (Monika, Reza, Mahdi, Paul, Jenhao, Nacho, Joe, Siraj, Kaswar, Sara, Nicola, Rentao, and others) for creating such an enjoyable environment for doing research. Especially, I would like to thank Maggie for her sincere friendship and for all those rather philosophical and mutually motivating (in one way or another) conversations over lunch and coffee. Impossible not to acknowledge the contribution of people from University College Cork to this extraordinary experience. Particularly, I would like to express my gratitude to Edward, Paul (*eile*) and (Dr.) Vikram P. for the numerous and very entertaining (and occasionally even coherent!) talks about anything; but especially, for their valuable friendship. Lastly, the thesis examination period was rendered a rather enjoyable wait thanks to the hospitality of my old friend Jaime A. and Joanna Z. in the wonderful city of Barcelona, for which I am very grateful.

Finalmente, y a pesar de que estas líneas naturalmente no son suficientes, no me queda más que agradecer a quienes todo debo: mis papás y hermanos. No cabe duda de que, frente a su constante e inconmensurable apoyo y amor, el océano Atlántico ha parecido efectivamente no más que un diminuto charco, y cuatro años, apenas un parpadeo. Sus llamadas, visitas y mensajes fueron oxígeno vital para este logro. Agradezco también al resto de la familia, cuyos buenos deseos siempre me han acompañado. Many thanks to friends, at home and abroad, for their genuine concern and support during these years, which has been yet another source of motivation.

Declaration

I declare that this thesis was composed by myself, that the work contained herein is my own except where explicitly stated otherwise in the text, and that this work has not been submitted for any other degree or professional qualification except as specified.

Sergio Maldonado-Villanueva

Contents

Figures and Tables

Figures

Tables

Nomenclature and Abbreviations

Nomenclature

Note that some physical variables are defied by multiple symbols (e.g. bed shear stress). This obeys contextual reasons.

Common to all Chapters

A	proportionality coefficient in bedload formula (4.40);
A_r	aspect ratio;
B	proportionality coefficient in sheet flow formula (4.44);
c	volumetric sediment concentration;
c_b	sediment concentration in the bed;
c_f	friction coefficient for computation of τ;
c_y	constant for Yang *et al.*'s velocity profile;
c_0	sediment concentration in bedload layer L_0;
c_1	sediment concentration in upper layer L_1;
$c_{0\,\mathrm{mx}}$	maximum sediment concentration in bedload layer;
$c^{(b)}$	friction coefficient for computation of $\tau_0^{(b)}$;
$c^{(i)}$	friction coefficient for computation of $\tau^{(i)}$;
D	sediment particle diameter;
$e^{(b)}$	bed erosion rate;
F	proportionality coefficient in bedload generic expression (4.42);
F_β	bed-slope-related factor (see eq. 6.13);
g	gravitational constant;

h_T	$= h_0 + h_1$, total flow depth;
h'_T	h_T minus a small quantity, dh (i.e. $h'_T = h_T - \mathrm{d}h$);
h_0	thickness of bedload layer L_0;
h_1	depth of upper layer L_1;
$h_{1\,\mathrm{eq}}$	initial h_1;
$i^{(b)}$	net mass exchange through interface (b);
$i^{(i)}$	net mass exchange through interface (i);
$i_s^{(b)}$	net sediment mass exchange through interface (b);
$i_s^{(i)}$	net sediment mass exchange through interface (i);
$j^{(b)}$	net momentum exchange through interface (b);
$j^{(i)}$	net momentum exchange through interface (i);
j_c	convective or geomorphic momentum transfer;
j_d	diffusive or frictional momentum transfer;
L_b	bed layer;
L_0	bedload layer;
L_1	upper layer;
l	channel length;
M	mobility parameter (see eq. 4.47);
$p_w^{(b)}$	pore water pressure at the bed;
Q	discharge per unit width;
q_b	volumetric bedload sediment transport per unit width;
q_s	volumetric suspended sediment transport per unit width;
q_T	$= q_b + q_s$, volumetric total sediment transport per unit width;
S_b	$= \partial z_b / \partial x$, local bed-slope;
s	sediment relative density;
T	transport stage defined as ratio of bed shear stress to τ_c;
t	time;

t_l	lag time;
$\tan\varphi_d$	coefficient of dynamic friction;
$U(z)$	horizontal component of fluid velocity;
$U_{\mathrm{S}}(z)$	horizontal component of fluid velocity predicted by Soulsby (1997);
$U_{\mathrm{Y}}(z)$	horizontal component of fluid velocity predicted by Yang *et al.* (2004);
$U_{0\mathrm{Y}}$	flow velocity averaged over $z = z_0$ to $z = h_0$ (Yang *et al.*'s profile used);
$U_{1\mathrm{Y}}$	flow velocity averaged over $z = h_0$ to $z = h_0 + h_1$ (Yang *et al.*'s profile used);
$U_{0\mathrm{S}}$	flow velocity averaged over $z = 0$ to $z = h_0$ (Soulsby's profile used);
$U_{1\mathrm{S}}$	flow velocity averaged over $z = h_0$ to $z = h_0 + h_1$ (Soulsby's profile used);
U_{1L}	depth-averaged velocity in a 1-layer model;
$\bar{U}$	fluid velocity averaged over h_T;
U_*	bed shear velocity;
u	$= u(z)$, horizontal component of fluid velocity for Q2L model;
u_b	$(= 0)$, velocity of L_b;
u_0	horizontal velocity of water-sediment mixture in L_0;
u_1	horizontal velocity of water-sediment mixture in L_1;
u_{s0}	horizontal velocity of sediment particles in L_0;
u_{s1}	horizontal velocity of sediment particles in L_1;
$\bar{u}$	whole-depth-averaged velocity in Q2L model;
$\bar{u}_{z_2-z_1}$	flow velocity averaged over depth defined by $z_2 - z_1$;
$\forall_s$	volume of eroded sediment that yields $c_{0\mathrm{eq}}$ in L_0;
$\forall_0$	total volume of L_0;
x, y, z	spatial Cartesian coordinates;
z_b	bed elevation with respect to a datum;
z_0	zero-velocity level;
α	dip-correction factor;
β	angle of bed inclination with respect to the horizontal (negative = down-slope);

δ_{sh}	sheet layer thickness;
ε_b	bed porosity;
ε	bed-slope-related diffusivity parameter;
$\varepsilon_{B\&I}$	diffusivity parameter derived from Bailard & Inman (1981);
ε_T	diffusivity parameter derived from Π_T;
ε_{τ_0}	diffusivity parameter derived from Π_{τ_0};
η	free surface level from datum;
θ	non-dimensional bed shear stress;
θ_{sh}	Shields parameter;
θ_c	non-dimensional critical shear stress for sediment motion;
κ	von Kármán's constant;
μ	coefficient of fluid dynamic viscosity;
ν	coefficient of fluid kinematic viscosity;
ξ	term related to bed porosity;
Π_T	bed-slope influence for a given transport stage;
Π_{τ_0}	bed-slope influence for a given bed shear stress;
Π_1	$\equiv \rho_{0h}/\rho_{0\beta}$, for a given T;
Π_2	$\equiv \tau_{c\beta}/\tau_{ch}$, for a given T;
Π_3	$\equiv \rho_{0h}/\rho_{0\beta}$, for a given $\tau_0^{(b)}$ ($\Pi_3 \neq \Pi_1$);
Π_4	$\equiv (\tau_0^{(b)} - \tau_{c\beta})/(\tau_0^{(b)} - \tau_{ch})$, for a given $\tau_0^{(b)}$;
ρ	density;
ρ_b	bed average density;
ρ_s	sediment density;
ρ_w	water density;
ρ_0	depth-averaged density of L_0;
ρ_1	depth-averaged density of L_1;
$\sigma^{(b)}$	normal stress at interface (b);

$\sigma'^{(b)}$	effective normal stress at interface (b);
τ	bed shear stress;
τ_c	critical shear stress for sediment motion;
τ_{ch}	critical shear stress on horizontal bed;
$\tau_{c\beta}$	critical shear stress on sloping bed;
$\tau^{(i)}$	shear stress at interface (i);
$\tau_b^{(b)}$	shear stress at bottom of interface (b) (bed resistance);
$\tau_0^{(b)}$	shear tress at top of interface (b);
Φ	non-dimensional bedload transport; and
φ	angle of repose.

Subscripts:

eq	denotes sediment-transport equilibrium state;
h	denotes horizontal bed; and
β	denotes sloping bed.

In Chapter 7

C_D	drag coefficient;
C_L	lift coefficient for F_{L_2};
c_{0*}	$\equiv c_0/c_b$, non-dimensional bedload layer sediment concentration;
D_*	non-dimensional particle diameter;
e	restitution coefficient;
F_D	drag force;
F_G	submerged weight;
F_L	lift force;
f	friction coefficient;
h_b	bedload layer thickness;

h_{b*} $\equiv h_b/D$, non-dimensional bedload layer thickness;

K_c non-dimensional calibration constant for bedload expression (7.22);

k_s equivalent roughness height of Nikuradse;

m mass of the sediment particle;

Re particle Reynolds number;

R^2 correlation coefficient;

T_* $(= T)$ non-dimensional transport stage;

t_{in} time required by the particle to reach z_{in} (see splash function description);

t_s time elapsed between the particle rebound and eventual collision with the bed;

t_{s*} $\equiv \lambda_{s*}/u_{s*}$, non-dimensional saltation time;

U_B fluid horizontal velocity evaluated at the bottom of the particle;

U_T fluid horizontal velocity evaluated at the top of the particle;

U_{*c} critical shear velocity for sediment motion;

u_s $(\equiv \lambda_s/t_s)$ hop-averaged streamwise particle saltation velocity;

u_{s*} $\equiv u_s/U_*$, non-dimensional saltation velocity;

$\vec{V}$ $= (\dot{x}, \dot{z})$, particle velocity vector;

$\vec{V}_{in}$ $= (\dot{x}, \dot{z})_{in}$, particle velocity vector at collision;

$\vec{V}_{out}$ $= (\dot{x}, \dot{z})_{out}$, particle take-off velocity vector;

V_r particle relative velocity evaluated at its centroid;

V_{rB} relative velocity evaluated at the bottom of the particle;

V_{rT} relative velocity evaluated at the top of the particle;

V_{rx} streamwise component of V_r;

X any particle saltation characteristic (i.e. δ_s, λ_s or u_s);

X_* any non-dimensional particle saltation characteristic;

x streamwise particle's centroid displacement;

z bed-normal particle's centroid displacement;

z_{in} collision line level;

α_L	lift coefficient for F_{L_1};
α_m	added mass coefficient;
Δt	numerical time step;
β^-	bed-slope angle, where negative value denotes up-slope (i.e. $\beta^- = -\beta$);
δ_s	particle saltation height;
θ_{out}	take-off angle;
λ_s	particle saltation length;
λ_{s*}	$\equiv \lambda_s/D$, non-dimensional saltation length;
μ_s	take-off angle mean value;
σ_s^2	take-off angle variance;
τ_*	non-dimensional bed shear stress ($\tau_* = \theta$); and
τ_{*c}	non-dimensional critical shear stress for sediment motion ($\tau_{*c} = \theta_c$).

Abbreviations

CMM	Conventional Morphodynamic Model;
MTS	Modification of the Threshold of motion for Sloping beds;
Q2L	Quasi-2-Layer;
SPH	Smoothed Particle Hydrodynamics;
SSP	Simple Saltating Particle (model);
SWE	Shallow Water Equations; and
TS	Transport Stage.

Chapter 1

Introduction

This chapter presents an introduction and literature review concerned with morphodynamical modelling. The review bridges state-of-the-art models with the motivation for the present research. The aim, objectives and structure of this thesis are then stated.

1.1 Background

1.1.1 Why study morphodynamics?

The study of coastal and fluvial morphodynamics has very important societal, economic, and environmental implications. Coastal erosion hazard, dam sedimentation, scour at the base of offshore structures, vulnerability to fluvial and coastal floods, preservation of biologically-rich marshes and estuaries, potential effects of climate change on the river-ocean system (and vice versa), are just some examples of problems requiring an accurate understanding of the interaction between water flows and sediment (i.e. morphodynamics). The river-ocean system is very sophisticated, and man-made modifications disregarding its ability to respond to external perturbations can lead to severe consequences.

A good illustration is provided by the Yellow River ('the cradle of Chinese civilisation'), which has shaped the history of China throughout the centuries. The ability (or

lack of it) to protect the Chinese population from disastrous floods dictated the fate of several emperors in ancient times and, in turn, the nation. Inundations as those of 1332-1333, 1887 and 1931, were responsible for the deaths of millions of people, and as many as 1500 flooding disasters in the last 4000 years can be counted in Northern China alone (Hu *et al.*, 1998). The main cause of such floods is sedimentation of fine grained particles carried by the river from the Loess Plateau. This process of sediment settling is augmented by human activities such as the construction of multiple dams along the river, which not only increases the risk of floods and their potential severity, but has also reduced dramatically the sediment load delivered to the ocean, yielding various important environmental impacts (Wang *et al.*, 2007).

For the coastal environment, two scenarios are worth examining; namely, the case of Cancún, Mexico, and the Dutch Sand Engine project. The Caribbean city of Cancún is one of Mexico's major tourist attractions. With an infrastructure of up to 27,000 hotel rooms, Cancún provides the country with estimated revenue of 2-3 billion USD (1.2-2.0 billion GBP) per year (Silva Casarín *et al.*, 2012). However, the urban development of Cancún, whose planning procedures largely ignored the morphodynamic behaviour of the overall area (the lagoon-beach system), has compromised the natural capacity of its beaches to respond to extreme events. In 2005, hurricane Wilma passed near Cancún, and removed more than 7 million m^3 of sand from the shoreline. The destruction caused by this tropical cyclone led to an estimated loss of 1 billion USD (0.7 billion GBP) in tourism-related activities and costed more than 50 million USD (33 million GBP) in a consequent beach-nourishment program undertaken by the Mexican Federal Government (see Fig. 1.1). Silva Casarín *et al.* (2012) showed that, if the anthropogenic activities in the area had been planned according to an adequate understanding of the morphodynamic behaviour of the lagoon-beach system, the impact of hurricane Wilma on Cancún would have been significantly smaller.

In contrast, with one third of their territory below the mean sea level and under constant and growing threats related to sea level rise, the Dutch have learned important lessons with respect to coastal protection. From the 1700s, coastal engineers in the Netherlands have attempted to solve the problem of shore recession via classical alternatives (e.g. breakwaters, groynes), without properly achieving it in a sustainable manner (Stive *et al.*, 2013). Based on their long experience, Dutch experts recently proposed a so-called paradigm shift, where the perception of shore recession problems transforms from a fight against the forces of nature towards a view of working alongside nature to face such challenges in an integral fashion. In this context, the innovative project of The Sand Engine (Zand Motor, www.zandmotor.nl) has been conceived (see Fig. 1.2). The Sand Engine consists of a mega-nourishment (a localised artificial sand beach of 21.5 Mm^3, spanning 2.4 km longshore and 1 km offshore), planned according to environmental, ecological and social considerations, whose task is to provide (thanks to the action of the sea) the adjacent shoreline with a continuous source of sand, sufficient to avoid shore recession for the next 20 years. Preliminary results suggest that 'soft engineering' (as opposed to classic, concrete-built, tools), based on an integral understanding of the system's morphodynamics, may offer sensible solutions to the coastal challenges posed by global climate change in the 21st Century (Stive *et al.*, 2013).

Figure 1.1: Beach erosion in Cancún six years after hurricane Wilma. Despite government efforts, the beach has not returned to its pre-2005 state. Photograph from www.puertoaventurastravel.com

Figure 1.2: Aerial picture of the Sand Engine. Photograph taken from Stive *et al.* (2013).

The above examples illustrate the importance of accurate understanding and prediction of the morphodyamic behaviour of coasts and rivers. However, although the topic of near-shore and fluvial morhodynamics has been investigated by researchers over decades, accurate predictive methods are far from being mature and perfectly reliable (Cao & Carling, 2002a; Amoudry & Souza, 2011). This is hardly surprising, given

the complexity of the phenomena governing the system, the extremely wide range of time and spatial scales involved (from the order of millimetres to kilometres, and seconds to years or even centuries), and our imperfect understanding of some of the most fundamental mechanisms behind sediment transport (more on this below).

1.1.2 Classification of morphodynamic models

Different theories, often mutually incompatible, populate the scientific literature on coastal and river morphodynamics. In fact, arguably, a unifying theory in this field (as in Earth Sciences in general) may not be even possible (Kleinhans *et al.*, 2005; Sivakumar, 2004). The abundance of variables and complexity of their interactions, has encouraged morphodynamic modellers to adopt stochastic (e.g. Yen, 2002[1]; Parker *et al.*, 2000; Kleinhans & van Rijn, 2002; Ancey *et al.*, 2006; Ancey, 2010; Furbish *et al.*, 2012a; Tregnaghi *et al.*, 2012) and chaos-fractal approaches (e.g. Sivakumar, 2004; Shang & Kamae, 2005; Shang *et al.*, 2009; Ziaei *et al.*, 2005). Such approximations have yielded promising results. Nonetheless, their excessive and/or careless application may lead to introduction of unnecessary randomness in systems that are otherwise deterministic (Sivakumar, 2004), hence impeding or contaminating our further understanding of the underlying physics.

With regard to deterministic approaches, there exist several types of morphodynamic models available in the literature. Papers by Cao & Carling (2002a,b) and Amoudry & Souza (2011) provide sound reviews of approaches to the deterministic modelling of river and coastal morphodynamics. De Vriend *et al.* (1993) classifies coastal morphodynamic models according to spatial scales, dividing them into the following four categories: (1) Coastline models which deal with the long-term evolution of the shore-

1. This paper is an introduction to an issue by the *ASCE Journal of Hydraulic Engineering* specifically devoted to stochastic hydraulics.

line. (2) Coastal profile models which focus solely on the cross-shore evolution of the beach. (3) Coastal area models, also referred to as process-based models, which can include both horizontal dimensions (beach line and profile), and can either resolve the 3D nature of the flow, or be depth-averaged (2DH). (4) Local models which study small spatial scales; e.g. bottom boundary layer and ripple formation. Hybrids combining features from the different classes of models have also been developed. According to their primary purpose, models can also be labelled as 'academic' or 'applied' (Cao & Carling, 2002a). The former are devoted to the scientific explanation of certain phenomena (the *why* and *how*), whereas the latter are aimed at the quantitative and efficient modelling required by practitioners and policy makers.

The present thesis is principally concerned with the study of deterministic process-based models (although, in Chapter 7, a 'local', stochastic, particle-scale model is also considered). From now on, the term 'morphodynamic model' refers exclusively to this type of model.

1.1.3 Conventional morphodynamic models

Most Conventional Morphodynamic Models (CMMs) consist of a coupled system of hydrodynamic equations (e.g. the Shallow Water Equations), a bed-update equation, and a sediment-transport formula; as depicted in Figure 1.3.

Widely used models, such as Delft3d (http://oss.deltares.nl/web/delft3d), MIKE (www.mikepoweredbydhi.com) and Telemac (www.opentelemac.org), follow this general structure. Computationally speaking, CMMs are coupled by serial and recursive execution of three main modules (corresponding to the hydrodynamic, sediment-transport and morphological-evolution equations), where the output of one module serves as input data for the following module. The generic algorithm, applied to a given set of initial conditions, can be described as follows: a) in the first step,

the hydrodynamic model is solved, assuming a fixed bed; b) in the second step, the resulting hydrodynamic information is used to compute sediment transport rates; c) then, the bed elevation is updated according to the sediment transport rates previously estimated, while the flow velocities are assumed temporarily constant; and d) the new bathymetry is eventually used to recalculate the hydrodynamics (back to the first step). This methodology assumes an equilibrium state where the transport capacity of the flow is instantaneously achieved; in other words, the lag time required by a sediment particle to accelerate from its resting state on the bed to approximately the flow velocity is ignored. Such an assumption is justifiable when changes in the morphology occur at a much slower rate than variations in the hydrodynamics. Nevertheless, when fast morphological evolution takes place (e.g. during a dam-break over and erodible bed), the above methodology may not be valid anymore (Greco *et al.*, 2013). The frequency at which the computational hydrodynamic and morphological modules are updated may or not coincide (synchronous vs asynchronous solutions), which has also proven to impact the final results (Cao & Carling, 2002a; Cao *et al.*, 2002; Roelvink, 2006).

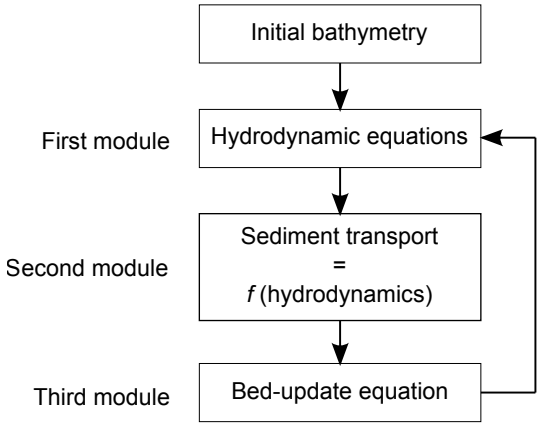

Figure 1.3: General structure of a Conventional Morphodynamic Model.

1.1.4 Dependency on empirical formulae

A feature common to virtually all CMMs (both 2DH and 3D) is the dependency on empirical or semi-empirical formulae for the estimation of sediment transport rates. However, the number of such formulae available in the literature is remarkably large. As an illustration, and for reference, Appendix A provides a compilation of various published works proposing either novel or enhanced versions of previously published formulae for bedload transport. The vast number of potentially-usable formulae yields uncertainty when model designers and final users need to select a particular expression. It is not uncommon for sediment transport formulae to be used outside their original range of validity, which clearly impacts on the final results from numerical simulations. Some research has focused on the inter-comparison of sediment transport formulae (e.g. Gomez & Church, 1989; Yang & Wan, 1991; Camenen & Larroudé, 2003; Barry *et al.*, 2004; Hinton, 2012; Van Emelen *et al.*, 2015). The findings from such investigations converge to a common conclusion: there is no best or universal expression. Different formulae perform better than others depending on the particular conditions to be simulated. This is to be expected, given that empirical formulae are derived for a given and limited range of parameters, and so universality should not be anticipated. Typical levels of accuracy in bedload empirical formulae fall within a factor of 5-10 (Amoudry & Souza, 2011).

Furthermore, many studies have shown that the final morphological results can be very sensitive to the selection of a particular sediment transport formula. For example, Garnier *et al.* (2006) showed that the time required for the formation of transverse sand bars depends strongly on the sediment transport formula used, with differences in the order of hundreds of days between the two choices explored. Similar conclusions were drawn by Dissanayake *et al.* (2009) in the context of complex patterns in tidal inlets,

for which different sediment transport expressions predicted formation times differing in the order of tens of years. These two examples illustrate the widely recognised observation that the high degree of empiricism involved in the estimation of sediment transport rates is a major source of uncertainty in Conventional Morphodynamic Models (Amoudry & Souza, 2011).

1.1.5 Ambiguity between bedload and suspended load

For coastal and river environments, sediment transport is typically divided into two modes of transport; namely, bedload and suspended load. The first mode of transport is commonly encountered when relatively low-flow rates and/or coarse sediments are present, and it involves rolling, sliding and saltation (hopping) of the sediment particles along and near the bed. Suspended load, on the other hand, takes place at flow velocities well beyond the threshold of motion, and is typically related to fine sediments. In this mode of transport, sediment is entrained into the stream (well above the bed), where it remains in suspension due to flow turbulent fluctuations, and is carried at the same speed as the current.

Nevertheless, although different mechanisms govern these two modes of transport, an objective criterion to distinguish one from the other has not yet been provided (Fredsøe & Deigaard, 1992). For example, bedload is often defined as the mode of transport taking place in the *vicinity* of the bed; however, a reliable method to determine the thickness of the bedload layer does not exist (except for the particular case of sheet flow, where a distinct transport layer can be identified). Soulsby (1997), for example, simply defines bedload as occurring *along the bed*. Bagnold (1973) states that bedload is confined to a zone *a few* particle diameters above the bed; Einstein (1950) considers this zone to be $2D$ thick (where D represents the particle diameter), whereas a maximum estimate of $\sim 20D$ can be deduced from van Rijn (1984a). Thus, the

ambiguity involved in the identification of the mode of transport present (i.e. bedload vs suspended load), is reflected in the selection of an appropriate sediment transport formula, hence, further increasing the uncertainty related to an adequate formulation of the sediment transport module.

1.1.6 Poor understanding of fundamental physics behind sediment motion

Further unreliability in CMMs arises from lack of understanding about the fundamental mechanics behind sediment transport. In particular, accurate knowledge and prediction of initiation of sediment motion remains a longstanding challenge to the scientific community. The most common approach to predicting initiation of sediment motion is by use of the Shields curve. However, the concept of a deterministic threshold of motion has long been questioned (see e.g. Lavelle & Mofjeld, 1987), based on the recurrent observation that the probability of initiation of motion well below the threshold predicted by the Shields curve may be small, but not zero[2] (Cheng, 2002). Hence, stochastic methods for prediction of initiation of sediment motion have also been explored (e.g. Kleinhans & van Rijn, 2002; Tregnaghi *et al.*, 2012). Diplas *et al.* (2008) put forward the idea that initiation of motion correlates better to a flow-exerted impulse instead of the magnitude of the time-averaged shear stress[3]. Radice *et al.* (2013), on the other hand, suggested that dislodgement of sediment may be associated with the presence of large-scale coherent structures; they also state that this theory may be compatible with that of Diplas *et al.* (2008).

---

2. In fact, as pointed out by Yen (2002), Shields (1936) presented the results in his original work as a band rather than a curve.
3. This hypothesis has previously been implied by researchers (e.g. Cheng, 2002), but Diplas *et al.* (2008) are accredited with having proved this for the first time through convincing experimental evidence.

Nonetheless, incorporation of the findings by Diplas *et al.* (2008) and Radice *et al.* (2013) into a morphodynamic model, requires reliable prediction of the time-varying near-bed turbulence, which is another major challenge in the field of fluid mechanics and key source of uncertainty in morphodynamic models (Cao & Carling, 2002b; Amoudry & Souza, 2011). Significant advances have been made in recent times with regard to near-bed turbulence in channels with fixed bottoms (e.g. Marusic *et al.*, 2010; Nikora *et al.*, 2007). However, less progress has been achieved for turbulent flows over movable beds. Nikora *et al.* (2013) have proposed a concept (i.e. double-averaged, in space and time, hydrodynamic equations for mobile rough beds) that may help reduce unpredictability in morphodynamic models associated with over-simplified treatment of near-bed hydrodynamics. More recently, Manes & Brocchini (2015) approached the problem of scour at the base of a cylinder, for the first time, by means of the phenomenological theory of turbulence, thus contributing to a better understanding of the physics behind erosion caused by turbulence.

Several other aspects contribute to the uncertainty found in morphodynamic models; for example: accurate estimation of bottom roughness, simplified numerical solutions, questionable assumptions behind mathematical formulations, lack of good-quality and extensive experimental or field data for model calibration, among others (Cao & Carling, 2002a; Amoudry & Souza, 2011).

1.1.7 Alternatives to conventional models

Alternatives to the CMMs described above include models based on Smoothed Particle Hydrodynamics (e.g. Zou, 2007; Razavitoosi *et al.*, 2014), two-phase (e.g. Bakhtyar *et al.*, 2009; Greco *et al.*, 2013), and two-layer models. In recent years, considerable progress has been achieved with regard to the robustness and applicability of Smoothed Particle Hydrodynamics (SPH), due to continuous advances in computing techniques.

However, the inclusion of an erodible bed in SPH is still in a very early stage of development. Two-phase and two-layer models are mutually similar, both in their conceptualisation of the phenomenon and computational performance and complexity. The two-phase model proposed by Greco *et al.* (2013), for example, proved to perform similarly well to previously published two-layer approaches, with the advantage over the latter that hyperbolicity of the governing equations (and thus, straightforward application of standard finite-volume numerical solvers) is guaranteed. Nevertheless, it must be noted that both the two-phase model presented by Greco *et al.* (2013) and the SPH-based approach by Zou (2007) suffer from a key shortcoming common to CMMs; namely, the dependence on highly empirical formulae for sediment motion.

1.1.8 Two-layer models

Two-layer models merit particular attention given their similarity with the morphodynamic model proposed in this thesis. Although two-layer shallow-flow approaches to simulate stratified fluids have been known for decades (e.g. Abbott, 1979), the inclusion of an erodible bed is relatively recent. The earliest works are accredited to Capart & Young (1998) and Fraccarollo & Capart (2002) in the context of sheet flow caused by dam-break-induced erosion of the bed. Fraccarollo & Capart (2002) introduced the idea of an erosion rate estimated from simple concepts borrowed from open channel hydraulics and soil mechanics, thus replacing some of the empiricism inherent to the typical estimation of sediment transport with physical mechanisms behind bed erosion. Fraccarollo & Capart's conceptualisation of the flow consisted of clear water flowing on top of a constant-density sediment-water-mixture, which in turn had the same average density as the non-movable bed underneath; both fluid layers moved at the same speed. Later, Spinewine (2005) extended Fraccarollo & Capart's model to account for different velocities and concentrations in both fluid layers (a study of the impact of such an enhancement is given by Zech *et al.*, 2008); the average

density of the transport layer, however, continued to be treated as constant. The latter restriction was recently removed by Li *et al.* (2013), who considered a variable-density lower layer; nonetheless, Li *et al.* still required an empirical formula for sediment transport rates in order to predict the variability in density. All of the aforementioned models (including most two-phase models) simulate clear water over a transport layer, and a distinct physical interface dividing both layers is assumed.

The above review has motivated the derivation of a quasi-2-layer shallow-flow morphodynamic model: an approach based on 2-layer models over an erodible bed, with particular characteristics detailed in later chapters. The main objectives of this thesis are stated in the next section.

1.2 Aim and Objectives

The aim of this thesis is to address the problem of uncertainty in morphodynamic modelling arising from the high degree of empiricism and ambiguity associated with the estimation of sediment transport rates. For this purpose, a physics-based, fully-coupled, quasi-2-layer model for shallow water-sediment flows is proposed. The model, free from empirical formulae for sediment transport rates, is applicable to a wide variety of problems, encompassing pure-water flows, bedload- and total-load-induced morphological changes, slow and fast geomorphic flows. The model may be considered to be of an academic nature given its primary goal to generate further insight into the physics of water-sediment flows over erodible beds. The insight gained can then be used to improve CMMs that are mostly founded on empirical ground. Three main objectives are identified; namely:

1. To present the derivation of the morphodynamic model and its validation against

established theory of sediment transport (including bedload, sheet flow and total load), and exploit its abilities to explore analytically diverse aspects of water-sediment science.

2. To use the model for the study of sediment transport phenomena that cannot be analysed adequately by CMMs without further increasing their level of empiricism. In particular, the objective is to undertake an investigation on the influence of bed-slope on bedload transport, with the goal of quantifying such influence in order to derive analytical expressions that can later be used to enhance Conventional Morphodynamic ('applied') Models.

3. To generate further insight into the mechanics and statistics of bedload transport, by means of a complementary mathematically-simple, computationally-efficient, robust model for stochastic saltation of a sediment particle along the bed.

1.3 Synopsis

The thesis is structured as described below. Note that Chapters 6 and 7 include their own literature review.

Chapter 2 introduces the phenomenological assumptions adopted and derives the governing equations of the quasi-2-layer morphodynamic model. **Chapter 3** presents an analytical treatment of the model for the case of a clear-water flow (no sediment transport), and a comparison against typical 1-layer (depth-averaged) hydrodynamic models. **Chapter 4** considers the case where exclusively bedload transport is present,

and compares the model's performance and predictions against established theory of bedload. In **Chapter 5**, the ability of the quasi-2-layer model to simulate total transport is explored. **Chapter 6** is devoted to the theoretical investigation and quantification, by means of the model proposed, of the influence of bed-slope on bedload. Model validation and comparison against previous predictors of the bed-slope-influence are included. In **Chapter 7**, a complementary model for stochastic particle saltation is proposed and then used to gain further insight into the mechanics and statistics of bedload, hence supplementing the investigation undertaken in previous chapters from an Eulerian, deterministic, larger-scale framework. **Chapter 8** provides some concluding remarks and recommendations for future research.

1.4 Published work

A significant part of the work presented in Chapter 7 has been published in the *ASCE Journal of Hydraulic Engineering* as Maldonado & Borthwick (2015). The remaining material in this thesis is currently in preparation for submission to peer-reviewed journals.

Chapter 2

Q2L Model description

This chapter presents the phenomenological assumptions on which the Quasi-2-Layer morphodynamic model is based. Then the governing equations are derived and estimation of closure terms is presented.

2.1 Phenomenological assumptions

The present model of sediment transport in shallow free surface flows idealises the water-sediment mixture as being divided into two layers: the lower one concerned with bedload transport, and the upper one representing sediment in suspension (presuming such modes of transport take place). The same hydrodynamic assumptions hold as for the conventional Saint-Venant or Shallow Water Equations (SWE). The water-sediment mixture is assumed to be an incompressible continuum, with each layer experiencing zero vertical acceleration such that the flow is hydrostatic and essentially two-dimensional – being predominantly in the horizontal plane. Uniform sediment size is considered. This thesis solely deals with the 1D version of the model. Uniform horizontal velocities (u) and sediment concentrations (c) are assumed within each of the two layers (see Figure 2.1); these velocities and concentrations can vary both in time and space.

The bedload layer is treated as a particular case of a lower layer in a classical 2-

Layer approach; i.e. as a layer with constant, arbitrary, vanishing thickness and variable density. This permits simulation of the (often ambiguously defined) bedload layer as a near-bed transport zone, whose sediment density can vary from zero for no sediment transport to a maximum or saturation value. The interface dividing the lower and upper layers is treated as an imaginary line rather than as a sharp physical interface or discontinuity in density (see §2.3.1).

The present model is referred to as Quasi-2-Layer (Q2L) model, in order to distinguish it from typical 2-Layer models representing a stratified flow consisting of two layers with different but constant, homogeneous densities (e.g. Fraccarollo & Capart, 2002; Spinewine, 2005; Zech *et al.*, 2008), where the interface between layers does correspond to a physical discontinuity in average densities.

The model is intended to simulate three different modes of transport:

- No sediment transport (Mode 0). For flow conditions below the threshold of sediment motion, both layers consist of pure water (Figure 2.1.b).
- Bedload only (Mode 1). In this case, flow conditions are such that only the lower layer carries sediment and the upper layer consists of pure water (Figure 2.1.c).
- Total load (Mode 2). For higher flow conditions, the bedload layer has reached a saturation point and sediment entrains into the upper layer, where it is treated as suspended load (Figure 2.1.d).

The assumed vertical structures of the fluid velocity and concentration profiles (Fig. 2.1) are closer to the observed vertical distributions in real channels, as compared to those of a 1-Layer model. The vertical profile of sediment concentration (e.g. Figure 2.1.d) reproduces accurately the occurrence of the maximum concentration in the near-bed zone (Pugh & Wilson, 1999). The vertical velocity distribution (Figure 2.1.a) also gives a closer representation of the near-bed (boundary layer) hydrodynamics.

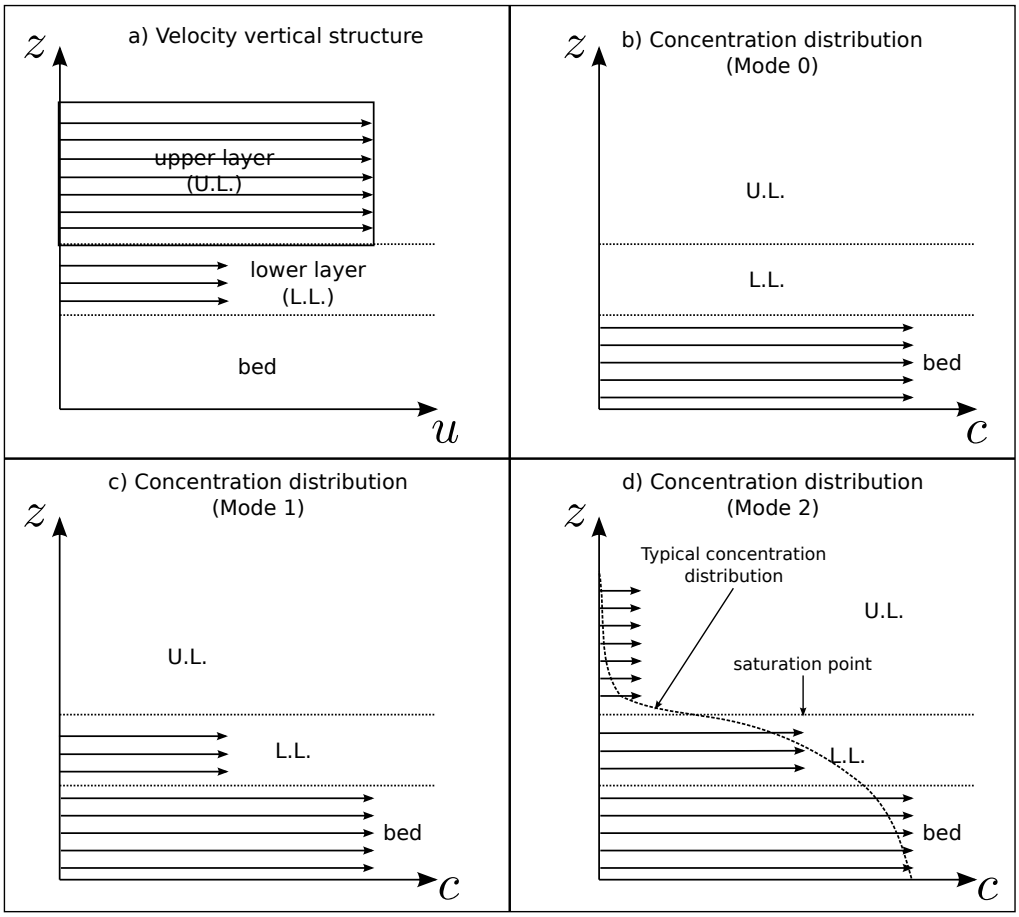

Figure 2.1: Assumed vertical structures for velocity and concentration: a) vertical structure of the fluid horizontal velocity; b), c) and d), vertical distribution of the sediment concentration in Modes of transport 0, 1 and 2, respectively.

Phenomena such as the event where different parts of the fluid column move in opposite directions (e.g. potentially during backwash and uprush in the beach) can be represented by the assumed velocity distribution.

The derivation of the model assumes a fluid in motion, encompassing low speed hydrodynamic conditions below the threshold of sediment motion (Mode 0), and higher speed flow where the velocity is sufficient to incorporate sediment into the lower layer (Mode 1) and eventually into the upper layer (Mode 2). Hence, particular cases such as still fluid or sediment being present in the upper layer when the lower one has not reached a saturation point (due perhaps to an external source of sediment) are

not considered as targets of the present study. Cases such as sudden entrainment into motion caused by strong turbulence (e.g. due to a breaking wave), or an adjacent source of sediment (e.g. in rivers) are not considered. Sheet-flow transport, where a distinct interface occurs between the lower transport layer and the upper pure-water layer, can be simulated by the present model (as Mode 1). It should nevertheless be borne in mind that the accurate physical representation of the phenomenon is not guaranteed. In other words, the well defined sheet-layer thickness may not coincide with the arbitrarily set bedload layer thickness; nonetheless, the overall sediment transport rate may still be accurately predicted by the model (see §4.4). Flows carrying highly concentrated suspended loads are also outside the scope of the present study, given that their appropriate treatment requires different approaches (e.g. Fang & Wang, 2000; Rosatti & Fraccarollo, 2006) in order to explain inherent phenomena, such as the minimum concentration occurring just above the bed instead of near the free surface (Ni *et al.*, 2000).

To simulate the entrainment of sediment into the stream and its deposition, the sediment erosion rate (a negative rate equals deposition) is estimated from the conservation of horizontal momentum at the bed interface, which is in turn related to the difference between the time-averaged shear stress exerted by the fluid on the bed surface and the effective bed resistance (more details in §2.3.1).

The remaining part of this chapter presents the derivation of the governing equations for the Q2L model, including the closure terms. Some remarks and comparisons against other models are also made.

2.2 Governing equations

The model essentially comprises mass and momentum conservation laws for a fluid vertically divided into 2 layers over an erodible bed (the bed can be thought of as a third, static layer), supplemented by empirical formulae for fluid-layers interface and bed shear stresses. The following derivation of the governing equations commences from the classical 2-Layer Shallow Water Equations (Abbott, 1979), after which certain assumptions are reviewed/imposed and source terms defined.

The 1D 2-Layer Shallow Water Equations can be written in their generic form (modified from Abbott, 1979) as:

$$\frac{\partial(\rho_1 h_1)}{\partial t} + \frac{\partial(\rho_1 h_1 u_1)}{\partial x} = i^{(i)} \tag{2.1a}$$

$$\frac{\partial(\rho_0 h_0)}{\partial t} + \frac{\partial(\rho_0 h_0 u_0)}{\partial x} = -i^{(i)} \tag{2.1b}$$

$$\frac{\partial(\rho_1 h_1 u_1)}{\partial t} + \frac{\partial}{\partial x}\left(\rho_1 h_1 u_1^2 + \frac{1}{2}\rho_1 g h_1^2\right) + \rho_1 g h_1 \frac{\partial(h_0 + z_b)}{\partial x} = j^{(i)} \tag{2.1c}$$

$$\frac{\partial(\rho_0 h_0 u_0)}{\partial t} + \frac{\partial}{\partial x}\left(\rho_0 h_0 u_0^2 + \frac{1}{2}\rho_0 g h_0^2\right) + g h_0 \left[\frac{\partial(\rho_1 h_1)}{\partial x} + \rho_0 \frac{\partial z_b}{\partial x}\right] = j^{(b)} - j^{(i)} \tag{2.1d}$$

where subscripts '1' and '0' refer to the upper and lower fluid layers, L_1 and L_0, respectively; ρ, h and u are the layers' density, depth and depth-averaged horizontal velocity, respectively; g denotes gravitational acceleration; z_b is the bed level with respect to the datum (subscript b refers to bed layer, L_b); and i and j represent mass and momentum net exchanges between layers (taken as positive in the upward direction) through the interfaces denoted by the superscripts (i) and (b). See Figure 2.2 for reference. Term $i^{(i)}$ represents the mass exchange between upper and lower layers when inter-layer fluxes take place; $j^{(i)}$ and $j^{(b)}$ then comprise the vertical flux of horizontal momentum through interfaces (i) and (b), respectively, resulting from mass exchange and interface shear stresses. For a fixed bed, $j^{(b)}$ can be translated into a bed shear stress.

Equations (2.1a) and (2.1b) represent conservation of mass of the water-sediment mixture in the upper and lower layers, respectively. Equations (2.1c) and (2.1d) are derived from conservation of horizontal momentum of the water-sediment mixture in the upper and lower layers. Note that the assumption of uniform velocity profiles implies a Boussinesq profile coefficient equal to one, which should otherwise be present in the momentum-conservation equations. A similar remark applies to the case of concentration profiles; i.e. a uniform (fully mixed) profile, in conjunction with a uniform velocity, implies a profile factor equal to one, which in another case should be included in the mass-conservation equations. Equations (2.1a) to (2.1d) are the governing equations of a system consisting of a shallow stratified flow over a fixed bed.

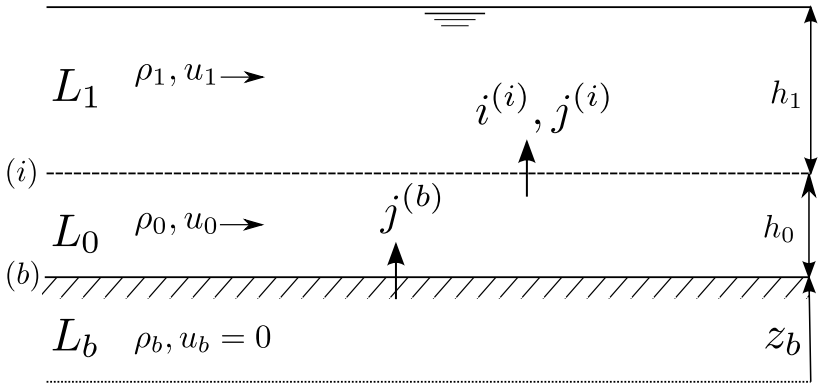

Figure 2.2: Definition sketch for the classical 2-Layer SWE.

The present morphodynamic model incorporates mass (and corresponding momentum) exchange between the bed (L_b) and the fluid layer above it (L_0) not considered in (2.1). Net mass exchange takes place through interface (b) and should be added as a source term in eq. (2.1b), leading to its right-hand side becoming: $i^{(b)} - i^{(i)}$. This mass exchange yields a change in the bed elevation, z_b, and so an equation governing the bed evolution must be also added. Conservation of overall mass in the bed layer, L_b,

gives:

$$\frac{\partial(\rho_b z_b)}{\partial t} = -i^{(b)}, \tag{2.2}$$

where ρ_b is the bed layer density. An assumption often implicitly underlying conventional morphodynamic models, and herein also adopted, is that the density of the bed remains constant (i.e. $\partial\rho_b/\partial t = \partial\rho_b/\partial x = 0$). Although the analysis of this assumption is not very important for conventional models, it is relevant for the present model (see §2.3.2). Consider the case of bedload only ($c_0 > 0, c_1 = 0$). When sediment transported in L_0 is deposited onto the bed, in order for the bed density to remain constant, a given quantity of water has to cross the interface (b) along with that sediment material. The water-sediment mixture crossing (b) has got to have an average density ρ_b, otherwise, the average porosity within the bed would decrease (alternatively, its concentration would increase). Hence, the water-sediment mass flux between layers L_b and L_0 corresponding to a volumetric exchange, or erosion/deposition rate, represented by $e^{(b)}$, is given by:

$$i^{(b)} = \rho_b e^{(b)}. \tag{2.3}$$

Using (2.3), and recalling that ρ_b is constant, eq. (2.2) can alternatively be written as:

$$\frac{\partial z_b}{\partial t} = -e^{(b)}. \tag{2.4}$$

A further assumption (key to the present model) is that the thickness of the lower layer is treated as a constant quantity in space and time; i.e.

$$\frac{\partial h_0}{\partial t} = \frac{\partial h_0}{\partial x} = 0. \tag{2.5}$$

This assumption yields a remark regarding eq. (2.4), which governs the morphology. Note that (2.4) differs from the bed-update equation typically used in conventional

morphodynamic models, known as the Exner equation, which includes the spatial gradient of the bedload transport; namely:

$$\frac{\partial z_b}{\partial t} + \xi \frac{\partial q_b}{\partial x} = 0, \tag{2.6}$$

where q_b represents the bedload sediment transport rate and ξ is related to bed porosity, ε_b. The Exner equation can be derived from the framework of the present model, proving (or confirming) that the Exner equation i) does not strictly represent conservation of mass in the bed –as commonly cited in the literature– but denotes conservation of sediment mass in the bed and bedload layer; and ii) considers sediment transport steady or quasi-steady conditions. For details on this proof, see Appendix B. Such observations on the Exner equation become relevant under certain morphodynamic conditions (see e.g. §6.5.4).

Furthermore, the assumption stated in (2.5) reduces the third term on the left-hand side of (2.1c) to $\rho_1 g h_1 \partial z_b/\partial x$. It also leads to a revised version of eq. (2.1b). Consider the case, depicted in Figure 2.3, of steady flow below the threshold of motion (no sediment transport, hence $\rho_0 = \rho_1 = \rho_w$), such that a horizontal gradient of the lower-layer water flow velocity exists in some part of the domain (i.e. $\partial u_0/\partial x \neq 0$). For this case, (2.1b) can be written as:

$$\rho_0 \frac{\partial h_0}{\partial t} + h_0 \frac{\partial \rho_0}{\partial t} + u_0 \frac{\partial (\rho_0 h_0)}{\partial x} + \rho_0 h_0 \frac{\partial u_0}{\partial x} = 0$$

$$\Rightarrow \rho_w \frac{\partial h_0}{\partial t} + h_0 \frac{\partial \rho_0}{\partial t} + u_0 \frac{\partial (\rho_w h_0)}{\partial x} + \rho_w h_0 \frac{\partial u_0}{\partial x} = 0. \tag{2.7}$$

Invoking (2.5), eq. (2.7) yields $\partial \rho_0/\partial t = -\rho_w \partial u_0/\partial x$, and so the model would predict a change in density within the lower layer (since $\partial \rho_0/\partial t \neq 0$) even for conditions

below the threshold of sediment motion. For this reason, eq. (2.1b) has to be replaced by an equation representing the conservation of *sediment* mass within the lower layer, namely:

$$\frac{\partial(\rho_s c_0 h_0)}{\partial t} + \frac{\partial(\rho_s c_0 h_0 u_0)}{\partial x} = i_s^{(b)} - i_s^{(i)}, \tag{2.8}$$

where i_s denotes net exchange of sediment mass (with density ρ_s) through interfaces. Due to the presence of the variable for sediment concentration in L_0, c_0, in (2.8), the potential incongruence described in the above paragraph is overcome.

Note that (2.8) implies that the particles transported in the bedload layer move at the same streamwise velocity as the whole water-sediment mixture. In other words, $u_{s0} = u_0$ is assumed, where u_{s0} represents the bedload particles streamwise velocity. Such an assumption may differ significantly from observations; however, use of the Lagrangian model presented in Chapter 7 to investigate the relationship between u_{s0} and u_0 shows that the final outputs of the model (i.e. sediment transport rates and morphological evolution) remain virtually unaffected (see Appendix C). Therefore, for the sake of simplicity and adopting a pragmatic position, this work assumes equivalence between sediment particle streamwise velocity and velocity of the corresponding water-sediment-mixture, unless otherwise explicitly stated.

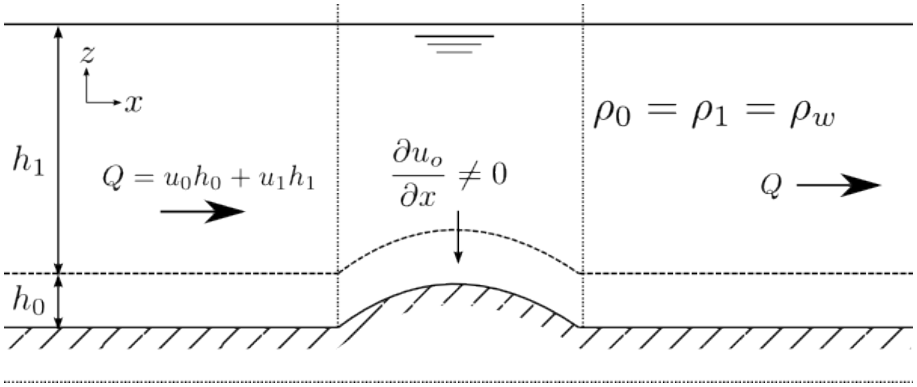

Figure 2.3: Illustration depicting a case where a gradient of u_0 exists in the central part of the domain.

In order to track the density variation within the upper layer, one further equation is required. This equation derives from conservation of sediment mass within the upper layer, namely:

$$\frac{\partial(\rho_s c_1 h_1)}{\partial t} + \frac{\partial(\rho_s c_1 h_1 u_1)}{\partial x} = i_s^{(i)}, \tag{2.9}$$

where c_1 is the sediment concentration in the upper layer. As before, (2.9) assumes $u_{s1} = u_1$, where u_{s1} is the streamwise velocity of sediment particles in L_1. Note, nonetheless, that such an assumption is more sensible than $u_{s0} = u_0$, given that for suspended load, sediment is expected to be transported by the current at roughly the same speed of the flow (Soulsby, 1997). This explains why a common approach to modelling suspended transport is the use of the advection-diffusion equation, where the advection velocity is that of the flow.

The Quasi-2-Layer morphodynamic model in 1D, depicted in Figure 2.4, is then defined by the following set of governing equations:

$$\frac{\partial(\rho_1 h_1)}{\partial t} + \frac{\partial(\rho_1 h_1 u_1)}{\partial x} = i^{(i)} \tag{2.10a}$$

$$\frac{\partial(\rho_s c_1 h_1)}{\partial t} + \frac{\partial(\rho_s c_1 h_1 u_1)}{\partial x} = i_s^{(i)} \tag{2.10b}$$

$$\frac{\partial(\rho_s c_0 h_0)}{\partial t} + \frac{\partial(\rho_s c_0 h_0 u_0)}{\partial x} = i_s^{(b)} - i_s^{(i)} \tag{2.10c}$$

$$\frac{\partial(\rho_1 h_1 u_1)}{\partial t} + \frac{\partial}{\partial x}\left(\rho_1 h_1 u_1^2 + \frac{1}{2}\rho_1 g h_1^2\right) + \rho_1 g h_1 \frac{\partial z_b}{\partial x} = j^{(i)} \tag{2.10d}$$

$$\frac{\partial(\rho_0 h_0 u_0)}{\partial t} + \frac{\partial}{\partial x}\left(\rho_0 h_0 u_0^2 + \frac{1}{2}\rho_0 g h_0^2\right) + g h_0 \left[\frac{\partial(\rho_1 h_1)}{\partial x} + \rho_0 \frac{\partial z_b}{\partial x}\right] = j^{(b)} - j^{(i)} \tag{2.10e}$$

$$\frac{\partial z_b}{\partial t} = -e^{(b)} \tag{2.10f}$$

In summary, the set of governing equations (2.10), corresponds to the horizontal conservation of: overall water-sediment mass in the upper layer (2.10a); sediment mass in the upper layer (2.10b); sediment mass in the lower layer (2.10c); overall water-sediment momentum in the upper layer (2.10d); overall water-sediment momentum in the lower layer (2.10e); and sediment mass in the bed (2.10f).

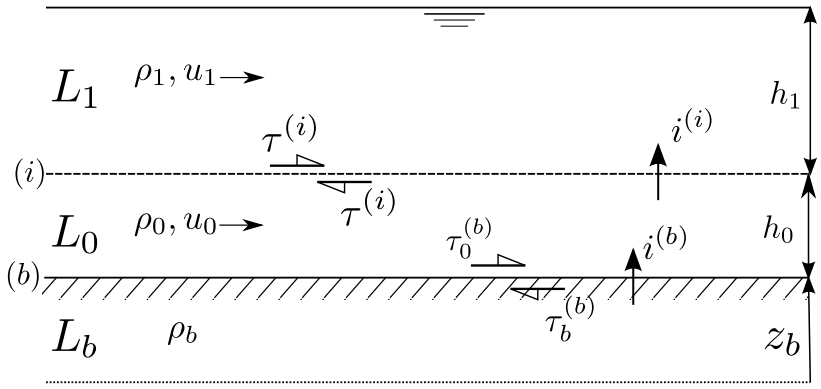

Figure 2.4: Definition sketch for the Quasi-2-Layer Model.

A key feature of the model is the definition of the source terms (right-hand side of eqs. 2.10), presented in the following section.

2.3 Source terms

First, the erosion rate and shear stresses acting on interfaces (i) and (b) are defined. Then, the inter-layer mass and momentum fluxes are described, hence closing the set of governing equations (2.10).

2.3.1 Erosion rate and shear stresses

The present model attempts to simulate the physical mechanism behind sediment transport phenomenon caused by bed erosion, which according to the conventional view can be described as follows. The flow exerts a shear stress on the surface of the channel bed,

which in turn resists erosion (Figure 2.4). When the shear stress exerted by the fluid exceeds a given threshold, sediment is eroded from the bed and carried by the fluid (see §1.1.6), thus promoting sediment transport and lowering the bed elevation with respect to a datum. Alternatively, when flow carrying sediment reaches a point in the channel where local hydrodynamic forces are not sufficient to maintain the sediment in motion, sediment is then deposited back onto the bed, raising the bed elevation.

Hence, the erosion rate (with deposition corresponding to a negative rate) is estimated as a function of the difference between the shear stress exerted by the fluid on the bed and the bed resistance, and the velocity jump between bed interface (see Fraccarollo & Capart, 2002; Spinewine, 2005); namely:

$$e^{(b)} = \frac{1}{\rho_b \left| u_0 \right|} (\tau_0^{(b)} - \tau_b^{(b)}), \tag{2.11}$$

where $\tau_0^{(b)}$ and $\tau_b^{(b)}$ represent the shear stress exerted by the fluid on the bed surface and the bed resistance, respectively. As stated in §2.1, the present idealisation assumes a fluid always in motion; however, should $u_0 = 0$ occur at some point in the domain at a certain time, the condition $e^{(b)} = 0$ for $u_0 = 0$ is imposed in order to avoid a mathematical error. Expression (2.11) derives from conservation of longitudinal momentum across the bed discontinuity (Spinewine, 2005). The linear relation that (2.11) proposes between erosion rate and bed shear stress yields, as proved later in this thesis, an expression for bedload far beyond the threshold of motion of the form $q_b \propto \tau_0^{(b)} U_* \therefore q_b \propto \left(\tau_0^{(b)} \right)^{3/2}$ (where U_* is the bed shear velocity), which is a widely accepted proportionality (Yalin, 1977; Bailard & Inman, 1981; Cheng, 2002).

The shear stress exerted by the water-sediment fluid on the bed surface (i.e. $\tau_0^{(b)}$) is commonly thought to be made up of three components: skin friction (viscous drag),

acting on the sediment grains; form drag, related to bed-surface features such as ripples; and a sediment-transport contribution, due to momentum being used to mobilise the sediment grains (Soulsby, 1997) and interchange of momentum due to particle collisions (Fredsøe & Deigaard, 1992; Bagnold, 1956). The dominant component will depend on the flow conditions; e.g. flat vs rippled bed, low vs intense sediment transport regime, etc. Common approaches to quantify the total shear stress consist in relating it to macroscopic characteristics through empirical expressions, which in turn require some tuning parameter. Herein, a mathematically simple approximation is adopted by estimating $\tau_0^{(b)}$ as a Chézy-type expression dependent on the squared velocity slip at the bed interface (b) and the bedload layer average density, ρ_0; namely:

$$\tau_0^{(b)} = c^{(b)} \rho_0 \left| u_0 \right| u_0, \tag{2.12}$$

where $c^{(b)}$ is a drag coefficient, considered as one of the main calibration parameters within the present model. By making $\tau_0^{(b)}$ dependent on the variable ρ_0 (as opposed to the density of water, ρ_w), the idea is to account for the effect of the skin-friction and sediment-transport contributions to the total bed shear stress. The influence of bed features could tentatively be represented by modifying accordingly the coefficient $c^{(b)}$, following the conventional approach. A discussion concerning the relation between $c^{(b)}$ and a friction coefficient in a 1-layer model is presented in §3.1.

The bed interface can be treated as a failure plane, and so the shear stress $\tau_b^{(b)}$ can be related to Terzaghi's effective normal stress, $\sigma'^{(b)}$, through Coulomb's law, which describes the stress state at failure for a rigid granular assembly as (Spinewine, 2005):

$$\tau_b^{(b)} = \tau_c + \sigma'^{(b)} \tan\varphi, \tag{2.13}$$

where τ_c is the critical yield stress, obtained from Shields' curve, and φ is the soil friction angle, assumed to be equal to the angle of repose. The effective normal stress, $\sigma'^{(b)}$, can be evaluated as the difference between the normal stress just beneath the bed interface assuming hydrostatic pressure, $\sigma^{(b)}$ $(= \rho_0 g h_0 + \rho_1 g h_1)$, and the pore water pressure at the bed, $p_w^{(b)}$ $(= \rho_w g(h_0 + h_1))$. Hence, $\sigma'^{(b)} = \sigma^{(b)} - p_w^{(b)}$, or:

$$\sigma'^{(b)} = [h_1(\rho_1 - \rho_w) + h_0(\rho_0 - \rho_w)]g \; ; \tag{2.14}$$

thus, allowing the bed resistance to be expressed in its generic form as:

$$\tau_b^{(b)} = \{\tau_c + [h_1(\rho_1 - \rho_w) + h_0(\rho_0 - \rho_w)]g \tan\varphi\} \, |u_0| / u_0, \tag{2.15}$$

where the term $|u_0| / u_0$ has to be included in order to ensure that $\tau_b^{(b)}$ acts as a resistive stress oriented in the direction opposite to the flow (as defined in Figure 2.4).

A comprehensive description of the methodology and assumptions underpinning the derivation of shear stresses and erosion rate functions stated above, can be found in Spinewine (2005) and Fraccarollo & Capart (2002).

A remark should be made at this point. Estimation of shear stresses at interface (b) (i.e. $\tau_0^{(b)}$ and $\tau_b^{(b)}$) represent the main source of empiricism in this model. Nevertheless, as will be proved later (see §4), the degree of empiricism involved in the present model is significantly lower than that of conventional moprhodynamic models, given that, unlike the latter models, the Q2L model does not require the selection of a particular empirical expression for computing sediment transport rates.

An additional note must be made concerning erosion as defined by (2.11). The shear

stress exerted by(on) a fluid on(by) a fixed and flat wall/bed is a relatively well understood phenomenon. However, this is not true for the case of sediment transport occurring due to a flow over an erodible irregular bed, given the technical complexities involving the accurate measurement of shear stress at that scale under those conditions, and the yet imperfect understanding of the mechanism behind initiation of motion (see §1.1.6). This has encouraged the adoption of a simple mathematical expression for $\tau_0^{(b)}$ in the present study. Moreover, the prevailing view is that, under bedload transport equilibrium conditions, the bedload layer acts as a 'shield' (Fernández Luque & van Beek, 1976) that prevents the upper water layer from eroding more sediment from the bed; or alternatively, a dynamic equilibrium state is achieved where the rate of entrainment of sediment from the bed equals the rate of deposition (Parker *et al.*, 2003). The present model does not intend to replicate the (yet to understand) micro-scale behaviour of the bed shear stress under sediment transport conditions. Nonetheless, the difference $\left(\tau_0^{(b)} - \tau_b^{(b)}\right)$ in eq. (2.11) could be taken as the *effective* shear stress acting on the bed surface, which decreases to zero when steady transport conditions are achieved[1] (see §4.2.4), hence allowing L_0 to act as a 'shield' that prevents L_1 from further eroding L_b, in agreement with the conventional view (see §4.2.4). Stresses $\tau_0^{(b)}$ and $\tau_b^{(b)}$, derive from theory borrowed from classical hydraulics and soil mechanics (Fraccarollo & Capart, 2002), and they should be taken as auxiliary concepts whose goal is to help quantify accurately the erosion rate, $e^{(b)}$, and associated sediment transport rate and bed evolution (primary aims of the present model), rather than as target terms themselves.

For L_1, the interface shear stress, $\tau^{(i)}$, can be treated as a bed resistance (Abbott, 1979), which in turn acts on L_0 as a driving stress (analogous to the free-surface interface in

1. In the Bagnoldian sense, it could alternatively be said that the *effective* shear stress $\left(\tau_0^{(b)} - \sigma'^{(b)}\right)$ decreases to the critical value τ_c, thus causing bed erosion to cease (see §4.2.4).

a wind-driven flow), with equal magnitude but opposite direction (see Figure 2.4). Although the shear stress at interface (i) is single-valued, there can be an exchange of mass between both layers as detailed in §2.3.2. A Chézy-type expression provides a simple way to estimate $\tau^{(i)}$, which is also consistent with the assumed vertical structure of the flow (uniform velocities). Hence, the inter-layer shear stress is calculated as:

$$\tau^{(i)} = c^{(i)} \rho_1 |u_1 - u_0| (u_1 - u_0), \tag{2.16}$$

where $c^{(i)}$ is a coefficient, considered as one of the two main tuning parameters within the model – the other being $c^{(b)}$ in eq. (2.12).

2.3.2 Inter-layer fluxes

Consider the case of initiation of sediment motion (Mode 1) as depicted in Figure 2.5. The assumption of constant h_0 (i.e. constant volume of L_0) implies that when the water-sediment mass mixture is eroded from the bed at a rate $i^{(b)}$, an equal volume of water has to be exchanged between L_0 and L_1 for the volume of L_0 to remain constant. For simplicity (though not necessarily correct from a phenomenological perspective), this can also be understood as follows: when eroded from the bed, the volume of water-sediment mixture 'pushes' an equal volume of water in L_0 up to L_1 (see Figure 2.5). Hence, for the case of bedload transport only (i.e. c_0 below its maximum allowed value, $c_{0\,\mathrm{mx}}$), for a mass flux through interface (b), $i^{(b)}$, there is a corresponding mass flux through interface (i) given by:

$$i^{(i)} = \rho_w e^{(b)}, \tag{2.17}$$

where ρ_w is the density of water. A similar exchange of water between fluid layers when bed erosion takes place is alternatively explained by Spinewine (2005) using

the concept of granular dilatancy, originally coined by Reynolds (1885). However, the analysis is not exactly the same given that in the 2-Layer model described by Spinewine (2005), the volume of L_0 does not necessarily remain constant (its density does).

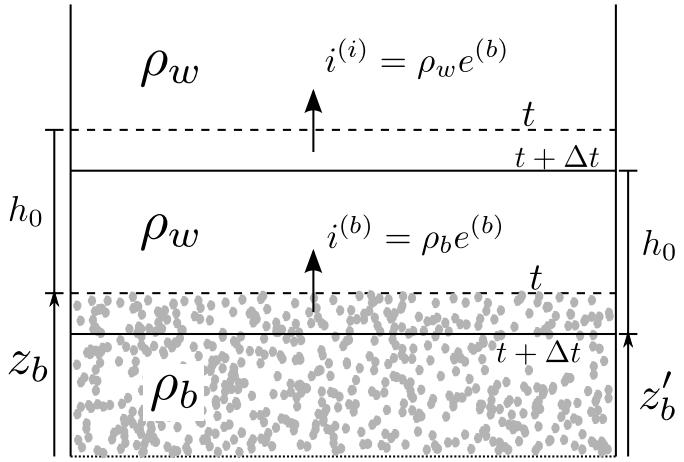

Figure 2.5: Sketch illustrating the initiation of erosion. Horizontal dashed(continuous) lines represent the instant immediately before(after) erosion takes place. z_b' denotes the new bed level (at $t + \Delta t$).

To illustrate the importance of including the water exchange $i^{(i)}$ when only bedload transport occurs (i.e. $c_0 \neq 0$ and $c_1 = 0$), consider the case of uniform flow such that $\partial(h_1 u_1)/\partial x = 0$; eq. (2.10a) would lead to:

$$\frac{\partial(\rho_1 h_1)}{\partial t} = \rho_w \frac{\partial h_1}{\partial t} = i^{(i)} = \rho_w e^{(b)},$$

which, invoking (2.4), gives:

$$\frac{\partial h_1}{\partial t} = e^{(b)} = -\frac{\partial z_b}{\partial t}. \tag{2.18}$$

Eq. (2.18) ensures that, when bed erosion occurs, the free surface level, given by $\eta = z_b + h_0 + h_1$, remains constant:

$$\frac{\partial \eta}{\partial t} = \frac{\partial z_b}{\partial t} + \frac{\partial h_0}{\partial t} + \frac{\partial h_1}{\partial t} = \frac{\partial z_b}{\partial t} + 0 - \frac{\partial z_b}{\partial t} = 0. \tag{2.19}$$

Note that not including the water exchange through interface (i) would yield $\partial h_1/\partial t = 0$, and hence, an unrealistic lowering of the free surface (given by $\partial \eta/\partial t = \partial z_b/\partial t$) when bed erosion is present.

This analysis also holds for the case of negative erosion (deposition); i.e. when water-sediment mass (with an average density equal to ρ_b) is deposited from L_0 onto the bed at a rate $e^{(b)}$, there is a compensating flux of water mass from L_1 to L_0 equal to $\rho_w e^{(b)}$.

For the case of total transport (Mode 2), L_0 has reached a saturation point and sediment enters L_1, where it is treated as suspended load. Given that the saturated L_0 cannot incorporate any more sediment, bed material (water-sediment mass) eroded from the bottom has to be compensated by the same (water-sediment) mass flux between fluid layers through interface (i). Hence, for the case of total transport (where $c_0 = c_{0\mathrm{mx}}$ and $c_1 \geq 0$):

$$i^{(i)} = i^{(b)} = \rho_b e^{(b)}. \tag{2.20}$$

At this point, it is convenient to make a note regarding the mechanics of suspended load. Suspended transport is related to fast flows (significantly above the threshold of motion) and fine sediments, which entrain suspension due to turbulent fluctuations. This is in agreement with the assumed mechanism within the present model, where Mode 2 occurs at fast flows relative to the threshold of motion. For sufficiently coarse sediments, suspension is not expected to take place even at high velocities; instead, sediment particles tend to be transported as bedload within a sheet layer (Fredsøe & Deigaard, 1992). This behaviour can also be replicated by the model, provided that an adequate value of h_0 has been selected; i.e. sufficiently large to ensure that $c_0 < c_{0\mathrm{mx}}$ is always met (for recommendations on the selection of h_0 refer to §4.4). Once said this, it should be remarked that, from a pragmatic viewpoint, the main objective of the

present model is the accurate quantification of the total sediment transport rate and its consequent effect on the bed morphology, rather than the precise representation of the bed-load and suspended-load components of the total transport (which is, in fact, a very challenging task, considering the inherent ambiguity in the definition of these modes of transport).

For the case of flow conditions below the threshold of motion (Mode 0), a logical condition has to be imposed in order to avoid unrealistic behaviour. Under these conditions, $\tau_0^{(b)} < \tau_b^{(b)}$ by definition, thus $e^{(b)} < 0$, which would predict deposition even when no sediment is available to be deposited by the flow (i.e. $c_0 = c_1 = 0$), so:

$$i^{(i)} = i^{(b)} = 0, \quad \text{if} \quad e^{(b)} < 0 \quad \text{and} \quad c_0 = c_1 = 0, \tag{2.21}$$

has to be stated.

Summarising the above discussed, net mass fluxes through interfaces can be expressed as:

$$i^{(b)} = \begin{cases} 0 & \text{if} \quad e^{(b)} < 0 \quad \text{and} \quad c_0 = c_1 = 0 \\ \rho_b e^{(b)} & \text{else} \end{cases} \tag{2.22}$$

and

$$i^{(i)} = \begin{cases} 0 & \text{if } \; i^{(b)} = 0 \\ \rho_w e^{(b)} & \text{if } \; c_0 \neq 0 \;\; \text{and} \;\; c_1 = 0 \\ \rho_b e^{(b)} & \text{if } \; c_0 = c_{0\text{mx}} \;\; \text{and} \;\; c_1 \geq 0 \end{cases} . \tag{2.23}$$

The corresponding sediment mass fluxes are the sediment components of the total water-sediment mass exchanges, which can be expressed as:

$$i_s^{(b)} = c_b \frac{\rho_s}{\rho_b} i^{(b)}, \tag{2.24}$$

and

$$i_s^{(i)} = \begin{cases} 0 & \text{if } \; c_0 < c_{0\text{mx}} \;\; \text{and} \;\; c_1 = 0 \\ c_b \rho_s e^{(b)} & \text{if } \; c_0 = c_{0\text{mx}} \;\; \text{and} \;\; c_1 \geq 0 \end{cases} . \tag{2.25}$$

The case of sediment being present in L_1 when L_0 has not reached its saturation point (i.e. $c_0 < c_{0\text{mx}}$ and $c_1 > 0$), may occur due to e.g. an external source of sediment. However, this special case is outside the scope of the present model, as already mentioned.

An exchange of horizontal momentum between layers can also take place when mass in motion (and thus, carrying momentum) from one layer crosses the interface into an adjacent layer. This occurs at both interfaces (i) and (b) when $i^{(b)} \neq 0$ (and hence $i^{(i)} \neq 0$). When $i^{(i)} > 0 (i^{(i)} < 0)$, L_1 experiences a gain(loss) in momentum equivalent to the magnitude of the mass crossing (i) multiplied by the velocity of its original horizontal velocity, i.e. $u_0(u_1)$. In other words:

$$j_c^{(i)} = \begin{cases} i^{(i)} u_0 & \text{if } \; i^{(i)} > 0 \\ \\ i^{(i)} u_1 & \text{if } \; i^{(i)} < 0 \end{cases}, \tag{2.26}$$

where the subscript c denotes the convective or geomorphic component of the overall momentum transfer, j. The other part being the resistive shear stress, which can be considered as a frictional or diffusive momentum exchange, j_d (Spinewine, 2005). Hence, $j = j_c + j_d$. For interface (i):

$$j_d^{(i)} = -\tau^{(i)}. \tag{2.27}$$

Note that the assumption of $\tau^{(i)}$ acting on both sides of interface (i) with equal magnitude (but opposite direction), implies that a gain(loss) of convective momentum experienced by L_1 yields a loss(gain) in L_0 of convective momentum of the same magnitude. This is not necessarily true for layers L_0 and L_b, as explained below.

Unlike interface (i), interface (b) experiences different shear stresses on its upper and lower sides, $\tau_0^{(b)}$ and $\tau_b^{(b)}$, respectively. However, at the interface, the total momentum exchange $j^{(b)}$ has to be single-valued. For this reason, $j^{(b)}$ can be computed based on variables from both sides; namely:

$$j^{(b)} = j_c^{(b)} + j_d^{(b)} = \begin{cases} i^{(b)} u_0 - \tau_0^{(b)} & \\ & \\ i^{(b)} u_b - \tau_b^{(b)} & = \; -\tau_b^{(b)} \end{cases}, \tag{2.28}$$

where u_b is the bed horizontal velocity, which is equal to zero by definition. Frictional momenta (shear stresses) necessarily act as diffusive terms on both sides of the interface. It should be noted that both expressions stated in (2.28) are mathematically

equivalent when either erosion or deposition take place (i.e. $e^{(b)} \neq 0$); however, the first formulation is adopted within the model for convenience (as explained in the next paragraph). Nevertheless, it is worth analysing both formulations in (2.28) from a phenomenological point of view. Focusing on L_0, when erosion occurs ($e^{(b)} > 0 \Rightarrow i^{(b)} > 0$), the aforementioned layer does not gain any additional convective momentum from L_b, because mass crossing the bed interface originally comes from rest ($u_b = 0$), and so the second expression (i.e. $j^{(b)} = -\tau_b^{(b)}$) makes more physical sense as L_0 is only experiencing dissipation of energy in the form of friction. On the other hand, when deposition takes place ($e^{(b)} < 0 \Rightarrow i^{(b)} < 0$), L_0 does lose some convective momentum due to the mass moving at a velocity u_0 being transferred onto L_b. In this case, the first formulation ($j^{(b)} = i^{(b)} u_0 - \tau_0^{(b)}$) appears more intuitively adequate as L_0 loses momentum in the form of mass transfer and friction. Note that in the case of deposition, the bed (L_b) may appear to gain some convective momentum (equal to that lost by L_0); however, this can be related to a gain in potential energy of the bed sediment due to a gain in the bed elevation.

The case of no sediment transport (Mode 0) requires special attention. Under this condition ($e^{(b)} = 0 \Rightarrow j_c^{(b)} = 0$), L_0 solely faces a resistive bed friction proportional to the square of its velocity ($j^{(b)} = j_d^{(b)} \propto u_0^2$). This behaviour would not be predicted by $j^{(b)} = -\tau_b^{(b)}$ given that, from eq. (2.15), $\tau_b^{(b)} = \tau_c$ (and hence, a constant value) for conditions below the threshold of motion. However, the first formulation for $j^{(b)}$ in (2.28) does replicate this behaviour; invoking eq. (2.12), for $e^{(b)} = 0 (\Rightarrow i^{(b)} = 0)$, $j^{(b)} = -\tau_0^{(b)} = c^{(b)} \rho_0 |u_0| u_0$ (thus, $j^{(b)} = j_d^{(b)} \propto u_0^2$). Hence, the overall momentum exchange through interface (b) is evaluated as:

$$j^{(b)} = i^{(b)} u_0 - \tau_0^{(b)}. \tag{2.29}$$

Combining (2.26) and (2.27), overall momentum transfer through (i) is given by:

$$j^{(i)} = \begin{cases} i^{(i)}u_0 - \tau^{(i)} & \text{if } \; i^{(i)} > 0 \\ i^{(i)}u_1 - \tau^{(i)} & \text{if } \; i^{(i)} < 0 \end{cases} . \tag{2.30}$$

Equations (2.29), (2.30), (2.22)-(2.25), (2.11) and shear stresses defined by (2.12), (2.15) and (2.16) close the set of governing equations given by (2.10).

2.4 Chapter summary

This chapter has introduced the phenomenological assumptions underlying the derivation of the Q2L model. The governing equations are derived from the classical 2-Layer SWE, reviewing some assumptions and imposing new conditions. A key feature of the model is the definition of the source terms associated with the erosion rate and interlayer fluxes. The erosion rate is in turn related to the shear stresses exerted at the bed interface. Estimation is provided of the closure terms (interface shear stresses), along with corresponding discussion.

The following three chapters deal with the three modes of transport that the Q2L model is capable of simulating.

Chapter 3

No sediment transport (Mode 0)

This chapter considers steady uniform flow over an inclined non-erodible bed. The analysis permits an insightful comparison between the present model and a classical 1-layer (SWE-based) hydrodynamical model. A methodology to calibrate the Q2L model based on purely hydrodynamic information of the flow (i.e. no sediment transport) is also presented.

3.1 Analytical solutions

A fixed bed (or flow below the threshold of sediment motion) implies the following: $e^{(b)} = 0 \Rightarrow i^{(b)} = i^{(i)} = 0$; $\partial z_b/\partial t = 0$; $\partial h_1/\partial t = 0$; $\rho_0 = \rho_1 = \rho_w$ (i.e. $c_0 = c_1 = 0$); $j^{(b)} = -\tau_0^{(b)}$; $j^{(i)} = -\tau^{(i)}$. In addition, the condition of uniform steady and unidirectional flow is imposed on the governing equations (2.10). Hence, (2.10d) can be expressed, invoking (2.16), as:

$$\tau^{(i)} = c^{(i)}\rho_w(u_1 - u_0)^2 = -\rho_w g h_1 \frac{\partial z_b}{\partial x}, \tag{3.1}$$

and (2.10e) becomes:

$$\tau^{(i)} - \tau_0^{(b)} = -\rho_w g h_0 \frac{\partial z_b}{\partial x}, \tag{3.2}$$

or, using eqs. (2.12) and (3.1):

$$\tau_0^{(b)} = c^{(b)} \rho_w u_0^2 = -\rho_w g h_T \frac{\partial z_b}{\partial x}, \tag{3.3}$$

where $h_T = h_0 + h_1$ is total channel depth.

From (3.1), it follows that:

$$c^{(i)} (u_1 - u_0)^2 = -g h_1 \frac{\partial z_b}{\partial x}, \tag{3.4}$$

and from eq. (3.3):

$$c^{(b)} u_0^2 = -g h_T \frac{\partial z_b}{\partial x}. \tag{3.5}$$

Expressions (3.4) and (3.5) can be used to compare the present model against a 1-layer hydrodynamic model. The 1D single-layer Shallow Water Equations can be expressed in conservative form for constant density as:

$$\frac{\partial h_T}{\partial t} + \frac{\partial (U_{1L} h_T)}{\partial x} = 0 \tag{3.6a}$$

$$\frac{\partial (U_{1L} h_T)}{\partial t} + \frac{\partial}{\partial x} \left(h_T U_{1L}^2 + \frac{1}{2} g h_T^2 \right) = -g h_T \frac{\partial z_b}{\partial x} - \frac{\tau}{\rho_w}, \tag{3.6b}$$

where U_{1L} denotes the depth-averaged horizontal velocity of the single layer, and τ represents the bed friction, often computed as:

$$\tau = c_f \rho_w U_{1L}^2, \tag{3.7}$$

with c_f representing the bed friction coefficient.

For a steady uniform flow over an inclined fixed bed, eq. (3.6b) can be simplified to:

$$c_f U_{1L}^2 = -g h_T \frac{\partial z_b}{\partial x}. \tag{3.8}$$

The depth-averaged flow velocity in a 1-layer model, U_{1L}, can be assumed to be equal to the horizontal velocity in the Q2L model averaged over the total depth, $\bar{u}$, (i.e. $\bar{u} = U_{1L}$) calculated as:

$$\bar{u} = \frac{1}{h_0+h_1}\int_0^{h_0+h_1} u \, \mathrm{d}z = \frac{1}{h_0+h_1}\left[\int_0^{h_0} u \, \mathrm{d}z + \int_{h_0}^{h_0+h_1} u \, \mathrm{d}z\right], \tag{3.9}$$

where u denotes the horizontal component of the flow velocity. Recalling the assumed vertical velocity distribution in the present model (Figure 2.1.a); namely:

$$u = \begin{cases} u_0 & \text{if } \ 0 \le z \le h_0 \\ \\ u_1 & \text{if } \ h_0 < z \le h_0+h_1 \end{cases}. \tag{3.10}$$

Equation (3.9) becomes:

$$\bar{u} = \frac{1}{h_0+h_1}\left[\int_0^{h_0} u_0 \, \mathrm{d}z + \int_{h_0}^{h_0+h_1} u_1 \, \mathrm{d}z\right]$$

$$\Rightarrow \quad \bar{u} = \frac{u_0 h_0 + u_1 h_1}{h_0+h_1}. \tag{3.11}$$

It is worth examining further the ratio of u_1 to u_0. For this purpose, eq. (3.4) is divided by (3.5), yielding:

$$\frac{c^{(i)}}{c^{(b)}}\left(\frac{u_1}{u_0}-1\right)^2=\frac{h_1}{h_T}$$

$$\Rightarrow\ \frac{u_1}{u_0}=\left(\frac{h_1 c^{(b)}}{h_T c^{(i)}}\right)^{1/2}+1. \tag{3.12}$$

The relation between coefficients c_f and $c^{(b)}$ can be studied by recalling the assumption that $\bar{u}=U_{1L}$ and dividing (3.5) by (3.8), giving:

$$\frac{c^{(b)}}{c_f}=\left(\frac{\bar{u}}{u_0}\right)^2, \tag{3.13}$$

which, invoking (3.11) and (3.12), can also be expressed as:

$$\frac{c^{(b)}}{c_f}=\left[\frac{h_0+(u_1/u_0)h_1}{h_0+h_1}\right]^2. \tag{3.14}$$

Eq. (3.13) illustrates de non-equivalence between coefficients $c^{(b)}$ and c_f, given that, from (3.12), it follows that $u_1>u_0$ and so $u_1/u_0>1\Rightarrow c^{(b)}>c_f$. Furthermore, eq. (3.14) demonstrates that $c^{(b)}$ cannot be directly related to a friction coefficient c_f (which is typically a function of a Chézy or Manning coefficient), because such a relation also depends on the selection of h_0 and $c^{(i)}$, which in turn determines the ratio u_1/u_0 (see eq. 3.12). It is then important to interpret $c^{(b)}$ as a particular friction indicator within the Q2L model, without confusing it with c_f, which is a measure (in the context of single-layer open channel hydraulics) of the bed resistance for a given bed composition and hydraulic conditions.

The analysis of eqs. (3.12) to (3.14) also illustrates the potential calibration of the model by using solely hydrodynamic information, as presented below. In §§4.3 and 5.2, it is shown that the model can also be calibrated using sediment (bedload and

total) transport data.

3.2 Methodology for hydrodynamic calibration

If, for a given open channel flow, there are available data on the vertical structure of the fluid horizontal velocity component, values of u_0 and u_1, corresponding to a given h_0 and h_1, can be calculated. This information can then be utilised to tune parameters $c^{(b)}$ and $c^{(i)}$. The goal of this section is to describe the methodology to calibrate the Q2L model by using solely hydrodynamic information, rather than proposing actual values for the tuning parameters. A proper calibration of the model is carried out in §§4.3 and 5.2.

First, $c^{(b)}$ can be related to the 1-Layer model's drag coefficient c_f through eq. (3.14), rewritten here as:

$$\frac{c^{(b)}}{c_f} = \left[\frac{1+(u_1/u_0)(h_1/h_0)}{1+h_1/h_0}\right]^2. \tag{3.15}$$

Then, $c^{(i)}$ can be estimated from $c^{(b)}$ by using (3.12), namely (in manipulated form):

$$\frac{c^{(b)}}{c^{(i)}} = \frac{h_T}{h_1}\left(\frac{u_1}{u_0}-1\right)^2. \tag{3.16}$$

In order to use eqs. (3.15) and (3.16), it is necessary to estimate u_1 and u_0, corresponding to a given h_1 and h_0. For this purpose, information on the vertical structure of the fluid velocity is required. Several expressions have been proposed to reconstruct the vertical distribution of the fluid velocity in an open channel flow (e.g. Yang *et al.*, 2004; Absi, 2011; Bonakdari *et al.*, 2008; Huai *et al.*, 2009; Pu, 2013). Herein, two equations are considered. The first one, proposed by Yang *et al.* (2004), is a log-law-based equation designed to reproduce the dip-effect (whereby the maximum velocity

occurs below the free surface) in smooth uniform open channel flows; namely:

$$\frac{U_{\mathrm{Y}}(z)}{U_*} = \frac{1}{\kappa}\ln\left(\frac{z}{z_0}\right) + \frac{\alpha}{\kappa}\ln\left(1-\frac{z}{h_T}\right), \tag{3.17}$$

where $U_{\mathrm{Y}}(z)$ represents the horizontal component of the fluid velocity as predicted by Yang *et al.* (2004); $\kappa = 0.4$ is the von Kármán constant; $z_0 = \nu/(c_y U_*)$ is the zero-velocity level; U_* denotes the shear velocity; ν represents the kinematic viscosity of water; c_y denotes a constant, that can be taken as equal to 9 for hydrodynamically smooth flows (Soulsby, 1997); $\alpha = 1.3\exp(-0.5A_r)$ is a dip-correction factor; and A_r is the aspect ratio. In this section, the datum ($z = 0$) is situated at the bed surface.

The second expression, proposed by Soulsby (1997), for use in tidal currents, is:

$$\frac{U_{\mathrm{S}}(z)}{\bar{U}} = \begin{cases} U'_{\mathrm{S}} = \left(\frac{z}{0.32h_T}\right)^{1/7} & \text{if } 0 < \frac{z}{h_T} < 0.5 \\ \\ U''_{\mathrm{S}} = 1.07 & \text{if } 0.5 < \frac{z}{h_T} < 1 \end{cases}, \tag{3.18}$$

where $U_{\mathrm{S}}(z)$ represents the horizontal velocity predicted by Soulsby (1997); and $\bar{U}$ is the depth-averaged fluid horizontal velocity.

Expressions (3.17) and (3.18) have been selected because of their different nature. Eq. (3.17) has been validated against flows in laboratory smooth flumes, where relatively small depths are considered (in the order of centimetres); and it has been chosen over the simple log-law due to its enhanced formulation designed to replicate real flows more accurately. On the other hand, (3.18) is derived for applications in tidal environments, where rough hydrodynamic flows and larger values of h_T are expected. The latter condition allows the present model to consider the effect of larger values of

the ratio h_1/h_0.

Note that because the aforementioned velocity profiles are not uniform, strictly speaking the momentum equations within the present model should account for such a property through Boussinesq profile coefficients or dispersion stresses. However, for uniform flow (herein considered) the non-linear terms in the equations affected by the profile-correction coefficients are zero, and so the present analysis remains valid.

Velocities u_0 and u_1 are computed according to the generic expression:

$$\bar{u}_{z_2-z_1} = \frac{1}{z_2 - z_1} \int_{z_1}^{z_2} u(z) \mathrm{d}z \,,$$

where $\bar{u}_{z_2-z_1}$ denotes a velocity averaged over the depth defined by $z_2 - z_1$.

From Yang *et al.* (2004), the layers' velocities are found as:

$$U_{0\mathrm{Y}} = \frac{1}{h_0 - z_0} \int_{z_0}^{h_0} U_{\mathrm{Y}}(z) \, \mathrm{d}z \,,$$

and

$$U_{1\mathrm{Y}} = \frac{1}{h_1} \int_{h_0}^{h_0+h_1} U_{\mathrm{Y}}(z) \, \mathrm{d}z \,,$$

which, using eq. (3.17), yield:

$$\begin{aligned} U_{0\mathrm{Y}} = \frac{1}{h_0 - z_0} \frac{u_*}{\kappa} \Bigg\{ & h_0 \ln \frac{h_0}{z_0} + z_0 - h_0 \\ & + \alpha \left[(h_0 - h'_T) \ln \left(1 - \frac{h_0}{h'_T} \right) - (z_0 - h'_T) \ln \left(1 - \frac{z_0}{h'_T} \right) + z_0 - h_0 \right] \Bigg\}, \end{aligned} \tag{3.19}$$

and

$$U_{1\mathrm{Y}} = \frac{u_*}{h_1\kappa}\left\{(h_0+h_1)\ln\left(\frac{h_0+h_1}{z_0}\right) - h_0\ln\frac{h_0}{z_0} - h_1 \right. \\ \left. + \alpha\left[(h_0+h_1-h'_T)\ln\left(1-\frac{h_0+h_1}{h'_T}\right) - (h_0-h'_T)\ln\left(1-\frac{h_0}{h'_T}\right)+h_1\right]\right\}. \quad (3.20)$$

$U_{0\mathrm{Y}}$ and $U_{1\mathrm{Y}}$ are the equivalent to u_0 and u_1, when Yang *et al.*'s velocity profile is used. In eqs. (3.19) and (3.20), h'_T has to be differentiated from $h_T(=h_0+h_1)$ by a small quantity (i.e. $h'_T = h_T - \mathrm{d}h$) in order to avoid a mathematical error in (3.20); i.e. $\ln 0$. Such error arises from the fact that Yang *et al.*'s velocity profile is not valid at the free surface, where $z = h_T$.

For the case of Soulsby (1997), assuming $h_0 < 0.5h_T$, the layers' velocities are given by:

$$U_{0\mathrm{S}} = \frac{\bar{U}}{h_0}\int_0^{h_0} U'_S \mathrm{d}z\,, \quad (3.21)$$

and

$$U_{1\mathrm{S}} = \frac{\bar{U}}{h_1}\int_{h_0}^{h_0+h_1} U_S(z)\mathrm{d}z$$

$$= \frac{\bar{U}}{h_1}\left(\int_{h_0}^{0.5h_T} U'_S\mathrm{d}z + \int_{0.5h_T}^{h_T} U''_S\mathrm{d}z\right). \quad (3.22)$$

Invoking eq. (3.18), the above pair of equations lead to:

$$U_{0\mathrm{S}} = \frac{7}{8}\left(\frac{h_0}{0.32h_T}\right)^{1/7}\bar{U}, \quad (3.23)$$

and

$$U_{1\mathrm{S}} = \frac{7}{8}\left(\frac{1}{0.32}\right)^{1/7}\left[\frac{h_T}{h_1}\left(\frac{1}{2}\right)^{8/7} - \frac{h_0}{h_1}\left(\frac{h_0}{h_T}\right)^{1/7}\right]\bar{U} + \frac{1.07}{2}\frac{h_T}{h_1}\bar{U}. \tag{3.24}$$

In order to express $c^{(b)}/c_f$ as function of h_1/h_0, it should also be feasible to formulate u_1/u_0 as $f(h_1/h_0)$. This is possible for Soulsby's profile by considering the simple transformations $h_T/h_1 = 1 + h_0/h_1$ and $h_0/h_T = (1 + h_1/h_0)^{-1}$. However, analysis of eqs. (3.19) and (3.20) demonstrates that the same is not true for Yang *et al.*'s profile, without assuming certain values. Hence, for this case, the experiments by Sarma *et al.* (1983) (against which Yang *et al.*'s formula is validated) are considered; which provide the following required parameters: $A_r = 6$; $h_T = 0.102$ m; and $U_* = 0.029$ m/s. For a total depth in the order of few centimetres, $h_0 = O(\mathrm{mm})$ is a reasonable assumption, yielding $h_1/h_0 \leq 100$. For tidal environments, depths in the order of meters are commonly found, hence allowing larger values of h_1/h_0 to be studied, given that $O(\mathrm{mm}) \leq h_0 \leq O(\mathrm{cm})$. Figures 3.1 and 3.2 depict ratios $c^{(b)}/c_f$ and $c^{(b)}/c^{(i)}$, respectively, as functions of h_1/h_0, for the two velocity profiles considered.

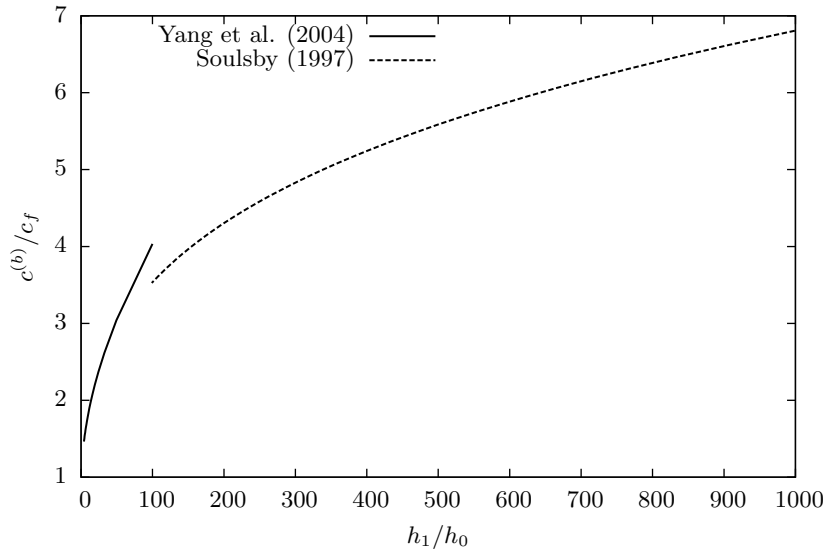

Figure 3.1: Relation between coefficients $c^{(b)}$ and c_f as function of the ratio h_1/h_0.

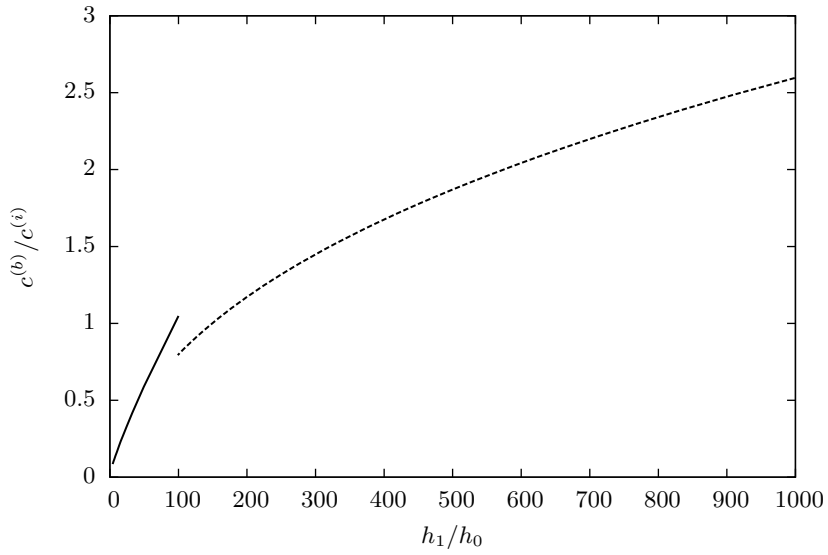

Figure 3.2: Relation between coefficients $c^{(b)}$ and $c^{(i)}$ as function of the ratio h_1/h_0. [Label as in Fig. 3.1]

Figures 3.1 and 3.2 demonstrate that both velocity-profile formulations exhibit congruent behaviour. Fig. 3.1 illustrates that $c^{(b)}$ and c_f have a similar order of magnitude; in fact, the range $c^{(b)}/c_f \in [4,6]$ can be expected to cover a wide range of practical applications. Estimation of the drag coefficient c_f, depends on the average flow velocity,

hydraulic radius and bed roughness; typical values of this parameter are in the range of 10^{-3} to 10^{-2} (Soulsby, 1997). Fig. 3.2 shows that $c^{(i)} \sim c^{(b)}$; in practice, $c^{(b)} > c^{(i)}$ is anticipated. Analysis of both figures also demonstrates an important feature of the present model; i.e. the weak dependence on the arbitrarily set h_0. Note that a small variation in h_0 (and hence in h_1/h_0) does not affect significantly the ratios $c^{(b)}/c_f$ and $c^{(b)}/c^{(i)}$. Section 4.4 presents a comprehensive discussion on the selection of h_0.

3.3 Chapter summary

The case of steady uniform flow over a non-erodible bed (or flow conditions below the threshold of sediment motion) has been considered. This permits analytical treatment of the Q2L model aimed at investigating the relation between the present model's tuning parameters $c^{(b)}$ and $c^{(i)}$, and a 1-Layer SWE-based model's friction coefficient c_f. A methodology to calibrate the model based on hydrodynamic data is presented, provided information on the vertical distribution of the fluid horizontal velocity is available (or that a theoretical velocity profile can be assumed reliably). For illustration purposes, two expressions to estimate the velocity profile in an open channel flow are considered. Design charts are produced with the intention of estimating, as a first approach, ratios $c^{(b)}/c_f$ and $c^{(b)}/c^{(i)}$ for a given h_1/h_0. Analysis of these charts shows that $c^{(b)} \sim c^{(i)}$ and $c^{(b)}/c_f \in [4,6]$ can be anticipated for a wide range of practical applications. These findings are later confirmed in §§4.3 and 5.2.

The following chapter examines bedload transport in isolation; i.e. when L_1 consists of pure water, whilst L_0 carries sediment.

Chapter 4

Bedload transport (Mode 1)

This chapter considers steady uniform flow over an erodible bed, such that only bedload transport occurs ($c_0 \leq c_{0\,\mathrm{mx}}$ and $c_1 = 0$). This case permits the derivation of exact and approximate analytical solutions to the Q2L model. Such expressions are used to compare the present model against bedload theory, including validation against empirical formulae. Analysis of the arbitrarily set h_0 is also presented. Then, the model is utilised to study the case of a migrating erodible hump due to a current. Comparison is made between the present model and a conventional morphodynamic model.

4.1 Analytical solutions

Bedload transport is defined by the quantity of sediment particles being transported by the flow at a given rate within the near-bed area. Hence, within the present model, where $u_0 = u_{s0}$ is assumed, bedload can be estimated as[1]:

$$q_b = h_0 c_0 u_0 \,, \tag{4.1}$$

where q_b represents the volumetric bedload transport rate. Under steady uniform flow initially above the threshold of sediment motion, equilibrium conditions for sediment

1. The *sediment* bedload rate should strictly be computed as $q_b = h_0 c_0 u_{s0}$. However, this would require and additional equation relating u_{s0} to the model's output variable u_0. Appendix C proves that the assumption $u_0 \approx u_{0s}$ appears sensible from a quantitative and pragmatic point of view.

transport are expected to be reached eventually. Given that h_0 is a constant within the present model, equilibrium-state values have to be found solely for c_0 and u_0 in order to compute q_b. These variables (and hence q_b) can, however, be estimated either as functions of channel physical characteristics or as dependent on the bed shear stress. The first option may be of interest to practitioner engineers wishing to compute bedload transport on rivers, for example. The second option is particularly useful when comparing the present model against bedload formulations (which are commonly derived as functions of the Shields parameter, θ). Exact and approximate solutions to the present model are presented below for the case of steady uniform flow.

4.1.1 Approximate solution as function of channel characteristics

For many practical cases, the condition $h_T \gg h_0$ will be met. Under this condition, it is reasonable to neglect the change in h_1 due to the water exchange through interface (i) caused by bed erosion; i.e. $\partial h_1/\partial t \approx 0$. Once bed erosion has initiated, steady sediment transport conditions can only occur once $e^{(b)}$ decreases to zero. This happens when both c_0 and u_0 have reached a given value such that the forces exerted by the water-sediment flow on the bed surface equal the latter's resistance to erosion. In order to find the equilibrium sediment concentration, $c_{0\,\mathrm{eq}}$, recall the equation governing bed erosion, namely:

$$e^{(b)} = \frac{1}{\rho_b |u_0|}(\tau_0^{(b)} - \tau_b^{(b)}) \,. \tag{4.2}$$

For $e^{(b)} = 0$ to occur, $\tau_0^{(b)} = \tau_b^{(b)}$ has to be verified. Note that $e^{(b)} = 0$ implies that $i^{(b)} = i^{(i)} = 0 \Rightarrow j^{(b)} = -\tau_0^{(b)}$ and $j^{(i)} = -\tau^{(i)}$. The bed shear stress $\tau_0^{(b)}$ can then be obtained from (2.10e) and (2.10d) by further invoking the condition of steady uniform

and unidirectional flow, giving:

$$\tau_0^{(b)} = -gS_b(\rho_w h_1 + \rho_0 h_0) \,, \tag{4.3}$$

where $S_b = \partial z_b/\partial x$ (notation changed solely for convenience). Recall that $\rho_1 = \rho_w$ for Mode 1 (only bedload present); which leads to eq. (2.15) becoming:

$$\tau_b^{(b)} = \tau_c + (\rho_0 - \rho_w) g h_0 \tan\varphi. \tag{4.4}$$

From the condition $\tau_0^{(b)} = \tau_b^{(b)}$, an expression can be found for the equilibrium bedload layer density, $\rho_{0\mathrm{eq}}$, by equating (4.3) to (4.4) and then solving for ρ_0; i.e.

$$\rho_{0\mathrm{eq}} = \frac{\rho_w g(h_0 \tan\varphi - h_1 S_b) - \tau_c}{g h_0(\tan\varphi + S_b)},$$

or using the definition of critical Shields parameter, θ_c ($\equiv \tau_c/[\rho_w g(s-1)D]$; where $s = \rho_s/\rho_w$ and D is the sediment diameter):

$$\rho_{0\mathrm{eq}} = \rho_w \frac{[h_0 \tan\varphi - h_1 S_b - (s-1)D\theta_c]}{h_0(\tan\varphi + S_b)}. \tag{4.5}$$

The bedload layer equilibrium concentration relates to $\rho_{0\mathrm{eq}}$ through:

$$c_{0\mathrm{eq}} = \frac{\rho_{0\mathrm{eq}} - \rho_w}{\rho_s - \rho_w}. \tag{4.6}$$

Hence,

$$c_{0\mathrm{eq}} = \frac{-S_b h_T - (s-1)D\theta_c}{(s-1)h_0(\tan\varphi + S_b)}. \tag{4.7}$$

To find the equilibrium bedload layer velocity, $u_{0\mathrm{eq}}$, recall the definition of $\tau_0^{(b)}$ stated in eq. (2.12) (i.e. $\tau_0^{(b)} = c^{(b)}\rho_{0\mathrm{eq}}u_0^2$, for the present case). Equating the latter to (4.3)

allows us to express $u_{0\mathrm{eq}}$ as:

$$u_{0\mathrm{eq}} = \left[\frac{-gS_b}{c^{(b)}}\left(h_0 + \frac{\rho_w}{\rho_{0\mathrm{eq}}}h_1\right)\right]^{1/2}. \tag{4.8}$$

Combining (4.1), (4.7) and (4.8), the bedload transport can be evaluated from:

$$q_b = \frac{-S_b h_T - (s-1)D\theta_c}{(s-1)(\tan\varphi + S_b)}\left[\frac{-gS_b}{c^{(b)}}\left(h_0 + \frac{\rho_w}{\rho_{0\mathrm{eq}}}h_1\right)\right]^{1/2}, \tag{4.9}$$

using (4.5) to compute $\rho_{0\mathrm{eq}}$.

In order to obtain further insight, $u_{0\mathrm{eq}}$ may be expressed in an alternative form by replacing $\rho_{0\mathrm{eq}}$ in (4.8) by (4.5) , yielding (after some algebraic manipulation):

$$u_{0\mathrm{eq}} = \left\{\frac{-gh_0S_b[h_T\tan\varphi - (s-1)D\theta_c]}{c^{(b)}[h_0\tan\varphi - h_1S_b - (s-1)D\theta_c]}\right\}^{1/2}.$$

If flow conditions well beyond the threshold of motion are considered, such that $\theta_c \approx 0$ can be assumed, the above equation becomes:

$$u_{0\mathrm{eq}} \approx \left[\frac{-gh_0S_bh_T\tan\varphi}{c^{(b)}(h_0\tan\varphi - h_1S_b)}\right]^{1/2} = \left[\frac{-gh_TS_b}{c^{(b)}(1-\frac{h_1S_b}{h_0\tan\varphi})}\right]^{1/2}. \tag{4.10}$$

By imposing the condition of $\theta_c \approx 0$ now to (4.7), the bedload transport, for conditions far beyond the threshold of motion, is estimated as:

$$q_b \approx \left[\frac{-h_TS_b}{(s-1)(\tan\varphi + S_b)}\right]\left[\frac{-gh_TS_b}{c^{(b)}(1-\frac{h_1S_b}{h_0\tan\varphi})}\right]^{1/2}. \tag{4.11}$$

Equations (4.9) and (4.11) can be used to estimate the bedload transport rate in a natural open channel (the latter for conditions well beyond the threshold of motion), given: the

channel slope (S_b), total depth (h_T) and bed sediment characteristics (D, ρ_s, φ); subject to the condition of $h_T \gg h_0 \Rightarrow h_1 \gg h_0$. Coefficient $c^{(b)}$ is the only tuning parameter required within the model for Mode 1 (i.e. the bedload transport rate is independent of coefficient $c^{(i)}$). Bedload expressions depend on h_0 (present in both eqs. 4.9 and 4.11); however, in §4.4 it is demonstrated that q_b is in fact weakly dependent on this arbitrary parameter for natural open channels. Although relatively complex in appearance, the sediment transport equations derived in this section represent alternative physics-based tools that can be used by, for example, fluvial engineers in order to estimate bedload transport in coarse-sediment-bed rivers, given their physical (i.e. morphological and hydrological) characteristics.

4.1.2 Exact solution as function of channel characteristics

For sufficiently shallow and fast flows where $h_T \sim h_1 \sim h_0$ and $e^{(b)}$ is very large, the change in h_1 due to the water flux from L_0 to L_1 may not be negligible. Hence, in order to derive an exact solution for bedload transport, the value of h_1 when equilibrium state has been reached, $h_{1\,\mathrm{eq}}$, has to be found. As stated in eq. (2.18), the magnitude of the total changes in h_1 and z_b have to be equal due to conservation of volume in the vertical; i.e. $|\Delta h_1| = |\Delta z_b|$. The total change in the bed elevation can be found by considering the total volume of bed sediment that yields the equilibrium concentration within the bedload layer, $c_{0\mathrm{eq}}$; namely: $\forall_s = |\Delta x \Delta y \Delta z_b| c_b$, where y is the coordinate orthogonal to x and z. The bedload layer equilibrium volumetric sediment concentration is given by the total volume of sediment eroded, $\forall_s$, divided by the volume of the layer L_0, $\forall_0$; i.e.

$$c_{0\mathrm{eq}} = \frac{\forall_s}{\forall_0} = \frac{|\Delta x \Delta y \Delta z_b| c_b}{|\Delta x \Delta y h_0|} = \frac{|\Delta z_b|}{h_0} c_b \,. \tag{4.12}$$

Recalling that $|\Delta h_1| = |\Delta z_b|$:

$$h_{1\,\mathrm{eq}} = h_{1\,\mathrm{in}} + |\Delta z_b| = h_{1\,\mathrm{in}} + \frac{c_{0\,\mathrm{eq}}}{c_b} h_0 \,, \tag{4.13}$$

where $h_{1\,\mathrm{in}}$ denotes the initial h_1. The above equation can also be expressed in terms of $\rho_{0\,\mathrm{eq}}$; namely:

$$h_{1\,\mathrm{eq}} = h_{1\,\mathrm{in}} + \frac{(\rho_{0\,\mathrm{eq}} - \rho_w)}{c_b(\rho_s - \rho_w)} h_0 \,. \tag{4.14}$$

The exact value of $\rho_{0\,\mathrm{eq}}$ can then be found again from the consideration of $e^{(b)} = 0 \Rightarrow \tau_0^{(b)} = \tau_b^{(b)} \Rightarrow -gS_b(\rho_{0\,\mathrm{eq}} h_0 + \rho_w h_{1\,\mathrm{eq}}) = \rho_w g(s-1)D\theta_c + (\rho_{0\,\mathrm{eq}} - \rho_w)h_0 g \tan\varphi \Rightarrow$

$$\rho_{0\,\mathrm{eq}} = \rho_w \frac{\left[h_0 \tan\varphi - h_1 S_b + h_0 S_b c_b^{-1}(s-1)^{-1} - (s-1)D\theta_c\right]}{h_0\left[\tan\varphi + S_b + S_b c_b^{-1}(s-1)^{-1}\right]}. \tag{4.15}$$

Invoking (4.6):

$$c_{0\,\mathrm{eq}} = \frac{-S_b h_T - (s-1)D\theta_c}{(s-1)h_0\left[\tan\varphi + S_b + S_b c_b^{-1}(s-1)^{-1}\right]}. \tag{4.16}$$

The bedload layer velocity comes from rewriting eq. (4.3) as $\tau_0^{(b)} = -gS_b(\rho_w h_{1\,\mathrm{eq}} + \rho_{0\,\mathrm{eq}} h_0)$, and equating it to $\tau_0^{(b)} = c^{(b)}\rho_{0\,\mathrm{eq}} u_0^2$, yielding (using eq. 4.14):

$$u_{0\,\mathrm{eq}} = \left\{ \frac{-gS_b}{c^{(b)}\rho_{0\,\mathrm{eq}}} \left[\rho_{0\,\mathrm{eq}} h_0 + \rho_w h_1 + \frac{h_0}{c_b(s-1)}(\rho_{0\,\mathrm{eq}} - \rho_w) \right] \right\}^{1/2}. \tag{4.17}$$

Comparison between (4.17) and the approximate solution (4.8) illustrates that both equations differ by the term $h_0(\rho_{0\,\mathrm{eq}} - \rho_w)c_b^{-1}(s-1)^{-1}$, which is present in the former equation. Note that for $h_1 \gg h_0$, then $\rho_{0\,\mathrm{eq}} h_0 + \rho_w h_1 \gg h_0(\rho_{0\,\mathrm{eq}} - \rho_w)c_b^{-1}(s-1)^{-1}$, and so under this condition both solutions tend to the same expression. A similar analysis can be applied to the exact and approximate solutions for $c_{0\,\mathrm{eq}}$ previously derived, leading to the same conclusion.

Equations (4.15), (4.16) and (4.17) can then be used to compute the bedload transport (as $q_b = h_0\, c_{0\mathrm{eq}}\, u_{0\mathrm{eq}}$) for all values of the ratio h_T/h_0 and flow conditions; thus representing the universal solution to the Q2L model for bedload transport in an inclined erodible open channel as a function of its physical characteristics.

4.1.3 Exact solution as function of bed shear stress

A solution as a function of bed shear stress may be of less utility for practitioners than the alternative solutions derived in the two previous sections, given that estimation of the bed shear stress in turn requires information on the physical characteristics of the channel. However, such a solution is important as it allows us to compare the present model against widely used empirical and semi-empirical bedload expressions, leading to relevant conclusions.

Following the same methodology as in previous sections, the equilibrium bedload layer density is found from the condition of $e^{(b)} = 0 \Rightarrow \tau_0^{(b)} = \tau_b^{(b)} \Rightarrow \tau_0^{(b)} = \tau_c + (\rho_0 - \rho_w) h_0 g \tan\varphi \Rightarrow$

$$\rho_{0\mathrm{eq}} = \frac{\tau_0^{(b)} + \rho_w g h_0 \tan\varphi - \tau_c}{g h_0 \tan\varphi}, \tag{4.18}$$

and, using (4.6),

$$c_{0\mathrm{eq}} = \frac{\tau_0^{(b)} - \tau_c}{(\rho_s - \rho_w) g h_0 \tan\varphi}. \tag{4.19}$$

From the definition of $\tau_0^{(b)} (= \rho_{0\mathrm{eq}}\, c^{(b)} u_{0\mathrm{eq}}^2)$, $u_{0\mathrm{eq}}$ is expressed as:

$$u_{0\mathrm{eq}} = \left(\frac{\tau_0^{(b)}}{\rho_{0\mathrm{eq}}\, c^{(b)}} \right)^{1/2}. \tag{4.20}$$

Hence, the bedload transport rate, equal to $h_0\, c_{0\mathrm{eq}}\, u_{0\mathrm{eq}}$, is computed as:

$$q_b = \frac{(\tau_0^{(b)} - \tau_c)}{(\rho_s - \rho_w) g \tan\varphi} \left(\frac{\tau_0^{(b)}}{\rho_{0\,\mathrm{eq}}\, c^{(b)}} \right)^{1/2} . \tag{4.21}$$

The above equation provides a straightforward way of estimating the bedload transport rate as function of bed shear stress, sediment characteristics (ρ_s, D and τ_c) and a main tuning parameter, $c^{(b)}$. Note that predicted bedload is also dependent on h_0, through ρ_0 (see eq. 4.18), but as will be shown later, such a dependence is rather weak. The following sections are devoted to comparison between the present model and well-established theory on bedload transport.

4.2 Analytical validation

The Q2L model can be treated analytically in order to compare it against bedload transport theory (including sheet flow). This section derives analytical solutions for bedload transport in non-dimensional form, analyses the case of flow well beyond the threshold of sediment motion, estimates the sheet layer thickness by manipulating previously derived solutions, and presents a discussion of the 'shield' effect attributed to the bedload transport layer.

4.2.1 Mathematical agreement with bedload formulae

Empirical expressions for bedload transport are (by definition) curve fits to experimental data. These formulations are often expressed in terms of non-dimensional variables for the sake of universality. Commonly, a non-dimensional bedload transport rate, Φ, is expressed as function of a non-dimensional bed shear stress, known as the Shields parameter, θ_{sh}. Φ relates the measured sediment transport rate to sediment

characteristics through the following conventional definition:

$$\Phi \equiv \frac{q_b}{[g(s-1)D^3]^{1/2}}. \tag{4.22}$$

The Shields parameter relates the bed shear stress to sediment characteristics through:

$$\theta_{\mathrm{sh}} \equiv \frac{\tau}{g(\rho_s-\rho_w)D} = \frac{\rho_w c_f U_{1L}^2}{\rho_w g(s-1)D} = \frac{U_*^2}{g(s-1)D}. \tag{4.23}$$

Hence, the Shields parameter can also be thought as relating the bed shear velocity to sediment characteristics. This observation becomes relevant in the context of the present model, as explained below.

Essentially, non-dimensional variables are arbitrarily defined numbers, which use should aid in achieving an effective interpretation of the experimental observations; e.g. by allowing recognisable tendencies (curves) to be found between combinations of measurable quantities, hence generating insight into the physics of observed phenomena. For example, the critical Shields parameter θ_c, relates the bed shear stress at which particles on the bed surface will move, τ_c, to their density relative to water $s = \rho_s/\rho_w$ and diameter D. It can be argued that the definition of θ_{sh} implies a low concentration of sediment within the transport layer (note that the Shields parameter was originally employed in the study of initiation of motion, where $c_0 = c_1 = 0$ by definition). This argument is also supported by experimental evidence showing that concentrations within the near-bed transport layer tend to be small (Fernández Luque & van Beek, 1976). Under these conditions, most of the bed shear stress is caused by the frictional interaction between the fluid (water) and the grains on the bed surface. However, for the sheet-flow regime, concentrations within the transport layer can be significant and the sediment-transport contribution to the total bed shear stress may not be negligible. This does

not necessarily contradict the definition of θ_{sh} stated in (4.23), given that the typical practice is to account for the sediment-transport contribution to total bed shear through modifying the drag coefficient c_f (and hence U_*) (Soulsby, 1997). Nevertheless, and unlike the aforementioned approach, the present model attempts to account for the sediment-transport contribution by defining $\tau_0^{(b)}$ as a function of ρ_0 (as discussed in §2.3.1), which can vary considerably from ρ_w for sufficiently fast flows. Therefore, the specification of the non-dimensional bed shear stress, θ, is not a trivial matter. Three different alternatives are explored, namely:

$$\theta_1 \equiv \frac{\tau_0^{(b)}}{g(\rho_s - \rho_0)D} = \frac{c^{(b)} u_0^2}{g[(\rho_s/\rho_0) - 1]D} \,, \tag{4.24}$$

$$\theta_2 \equiv \frac{\tau_0^{(b)}}{\rho_0\, g(s-1)D} = \frac{c^{(b)} u_0^2}{g(s-1)D} \,, \tag{4.25}$$

and

$$\theta_3 \equiv \frac{\tau_0^{(b)}}{g(\rho_s - \rho_w)D} \,. \tag{4.26}$$

θ_1 is consistent with θ_{sh} in that the former relates a form of bed shear velocity ($= c^{(b)} u_0^2$) to the particle's diameter and density relative to that of the water-sediment flow that causes the total shear (i.e. ρ_s/ρ_0). Following the same rationale, θ_2 is similar to θ_{sh} because it relates the same form of bed shear velocity to the sediment density relative to water (i.e. $s \equiv \rho_s/\rho_w$) and particle diameter. On the other hand, θ_3 associates the total bed shear stress (instead of shear velocity) to the particle diameter and density, just as θ_{sh} does. Arguably, all three formulations then have equally valid physical foundations, and so it is worth comparing them in detail. Note that for low concentrations, the three alternative definitions tend to the same expression, which is the same as θ_{sh}; i.e. for

$c_0 \to 0,\ \rho_0 \to \rho_w \therefore \theta_1 \to \theta_2 \to \theta_3 \to \theta_{\text{sh}}$.

It is also important to highlight that the definition of a non-dimensional bed shear stress is only important within the present model for the purpose of comparing it against empirical formulations. Morphodynamic results (sediment transport rates and bed evolution) are solely dependent on the dimensional bed shear stress $\tau_0^{(b)}$.

Following the same methodology presented in §4.1.3, analytical solutions for bedload transport can be found, in this case, as functions of a non-dimensional bed shear stress. The condition of $\tau_0^{(b)} = \tau_b^{(b)}$ (which yields $e^{(b)} = 0$) is considered in order to find equilibrium sediment transport conditions. However, different definitions of θ lead to different analytical solutions.

If θ_1 is used, then $\tau_0^{(b)} = \tau_b^{(b)} \Rightarrow g(\rho_s - \rho_0)D\theta_1 = \tau_c + (\rho_0 - \rho_w)gh_0 \tan\varphi \Rightarrow$

$$\rho_{0\text{eq}} = \frac{\rho_s g D\theta_1 + \rho_w g h_0 \tan\varphi - \tau_c}{gD\theta_1 + gh_0 \tan\varphi}. \tag{4.27}$$

Invoking (4.6),

$$c_{0\text{eq}} = \frac{(\rho_s - \rho_w)gD\theta_1 - \tau_c}{(\rho_s - \rho_w)(gD\theta_1 + gh_0 \tan\varphi)}. \tag{4.28}$$

And from $\tau_0^{(b)} = \rho_0 c^{(b)} u_0^2 = g(\rho_s - \rho_0)D\theta_1$, we obtain:

$$u_{0\text{eq}} = \left(\frac{g(\rho_s - \rho_{0\text{eq}})D\theta_1}{\rho_{0\text{eq}}\, c^{(b)}} \right)^{1/2}. \tag{4.29}$$

Similarly as with the non-dimensional bed shear stress, different non-dimensional bedload transport rates can be derived within the framework of the Q2L model. Hence,

the criterion to follow is the consistency with the corresponding definition of θ. θ_1 uses the sediment's density relative to that of the bedload layer (i.e. ρ_s/ρ_0); thus, for the sake of congruence, the corresponding non-dimensional bedload transport rate should be defined as:

$$\Phi_1 \equiv \frac{q_b}{[g(\rho_s/\rho_{0\mathrm{eq}} - 1)D^3]^{1/2}}. \tag{4.30}$$

Using eqs. (4.27) to (4.29) to compute $q_b = h_0 c_{0\mathrm{eq}} u_{0\mathrm{eq}}$, and invoking the definitions of $\theta_c \equiv \tau_c/[g(\rho_s - \rho_w)D]$ and Φ_1, the latter can be expressed as[2]:

$$\Phi_1 = \frac{h_0(\rho_s - \rho_w)gD(\theta_1 - \theta_c)}{[g\frac{(\rho_s - \rho_{0\mathrm{eq}})}{\rho_{0\mathrm{eq}}}D^3]^{1/2}(\rho_s - \rho_w)g(D\theta_1 + h_0\tan\varphi)} \left(\frac{g(\rho_s - \rho_{0\mathrm{eq}})D\theta_1}{\rho_{0\mathrm{eq}}\, c^{(b)}}\right)^{1/2}$$

$$\Rightarrow \Phi_1 = \frac{h_0}{\sqrt{c^{(b)}}(D\theta_1 + h_0\tan\varphi)}(\theta_1 - \theta_c)\,\theta_1^{1/2}. \tag{4.31}$$

If θ_2 is employed, then $\tau_0^{(b)} = \tau_b^{(b)} \Rightarrow \rho_0 g(s-1)D\theta_2 = \tau_c + (\rho_0 - \rho_w)gh_0\tan\varphi \Rightarrow$

$$\rho_{0\mathrm{eq}} = \frac{\rho_w g h_0\tan\varphi - \tau_c}{gh_0\tan\varphi - g(s-1)D\theta_2}. \tag{4.32}$$

---

2. Note that the case of θ_c is not similar to that of θ regarding potential alternative definitions, because for conditions of incipient motion $c_1 = c_0 = 0 \therefore \rho_1 = \rho_0 = \rho_w$.

Employing (4.6),

$$c_{0\mathrm{eq}} = \frac{\rho_w g(s-1)D\theta_2 - \tau_c}{(\rho_s - \rho_w)[gh_0 \tan\varphi - g(s-1)D\theta_2]}$$

$$= \frac{\rho_w g(s-1)D(\theta_2 - \theta_c)}{(\rho_s - \rho_w)[gh_0 \tan\varphi - g(s-1)D\theta_2]}$$

$$= \frac{D(\theta_2 - \theta_c)}{h_0 \tan\varphi - (s-1)D\theta_2}, \tag{4.33}$$

and, from $\tau_0^{(b)} = \rho_0 c^{(b)} u_0^2 = \rho_0 g(s-1)D\theta_2$,

$$u_{0\mathrm{eq}} = \left(\frac{g(s-1)D\theta_2}{c^{(b)}}\right)^{1/2}. \tag{4.34}$$

For the case of θ_2, Φ_2 can be defined according to the convention given by (4.22); hence:

$$\Phi_2 = \frac{h_0\, D(\theta_2 - \theta_c)}{[g(s-1)D^3]^{1/2}\,[h_0 \tan\varphi - (s-1)D\theta_2]} \left(\frac{g(s-1)D\theta_2}{c^{(b)}}\right)^{1/2}$$

$$= \frac{h_0}{\sqrt{c^{(b)}}\,[h_0 \tan\varphi - (s-1)D\,\theta_2]} (\theta_2 - \theta_c)\,\theta_2^{1/2}. \tag{4.35}$$

If θ_3 is utilised, then $\tau_0^{(b)} = \tau_b^{(b)} \Rightarrow g(\rho_s - \rho_w)D\theta_3 = \tau_c + (\rho_0 - \rho_w)gh_0 \tan\varphi \Rightarrow$

$$\rho_{0\mathrm{eq}} = \frac{g(\rho_s - \rho_w)D\theta_3 + \rho_w g h_0 \tan\varphi - \tau_c}{gh_0 \tan\varphi}$$

$$= \frac{(\rho_s - \rho_w)D(\theta_3 - \theta_c) + \rho_w h_0 \tan\varphi}{h_0 \tan\varphi}. \tag{4.36}$$

Therefore (through eq. 4.6),

$$c_{0\,\mathrm{eq}} = \frac{D\,(\theta_3 - \theta_c)}{h_0 \tan\varphi}. \tag{4.37}$$

From $\tau_0^{(b)} = \rho_0\, c^{(b)} u_0^2 = g(\rho_s - \rho_w) D\theta_3$:

$$u_{0\,\mathrm{eq}} = \left(\frac{g(\rho_s - \rho_w) D\theta_3}{\rho_{0\,\mathrm{eq}}\, c^{(b)}} \right)^{1/2}. \tag{4.38}$$

θ_3 is consistent with the original definition of Φ, and so eq. (4.22) can be used to compute Φ_3, yielding:

$$\Phi_3 = \frac{h_0\, D(\theta_3 - \theta_c)}{[g(s-1)D^3]^{1/2}\, h_0 \tan\varphi} \left(\frac{g(\rho_s - \rho_w) D\theta_3}{\rho_{0\,\mathrm{eq}}\, c^{(b)}} \right)^{1/2}$$

$$= \frac{1}{\tan\varphi} \sqrt{\frac{\rho_w}{\rho_{0\,\mathrm{eq}}\; c^{(b)}}}\; (\theta_3 - \theta_c)\, \theta_3^{1/2}. \tag{4.39}$$

Inspection of equations (4.31), (4.35) and (4.39), shows that all three bedload transport expressions can be written in the generic form of:

$$\Phi = A\,(\theta - \theta_c)\, \theta^{1/2}, \tag{4.40}$$

with

$$A = \begin{cases} \frac{h_0}{\sqrt{c^{(b)}}(D\theta + h_0 \tan\varphi)} & \text{if } \theta \equiv \theta_1 \\ \frac{h_0}{\sqrt{c^{(b)}}\,[h_0 \tan\varphi - (s-1)D\theta]} & \text{if } \theta \equiv \theta_2 \\ \left\{ \frac{h_0}{c^{(b)} \tan\varphi [(s-1)D(\theta - \theta_c) + h_0 \tan\varphi]} \right\}^{1/2} & \text{if } \theta \equiv \theta_3 \end{cases}. \tag{4.41}$$

A vast number of empirical and semi-empirical formulations for bedload transport are available in the literature (see Appendix A), many of which can be expressed in the form of $\Phi = f(\theta, \theta_c)$, through the general expression:

$$\Phi = F\left(\theta^{m1} - \theta_c^{m2}\right)^{n1}\left(\theta^{m3} - \theta_c^{m4}\right)^{n2}\theta^{n3}, \tag{4.42}$$

where $n1, n2, n3, m1, ..., m4$ are are power indices; and F is a variable whose computation depends on the particular formula selected. As an illustration, Table 4.1 gives the values of the exponents in (4.42) for the formulae by Meyer-Peter & Müller (1948), Bagnold (1963), van Rijn (1984a), Yalin (1963), Ashida & Michue (1972), Wilson (1966), Nielsen (1992), Fernández Luque & van Beek (1976), and Soulsby (1997). From analysis of Table 4.1, it can be seen that the formulae by Bagnold (1963), Yalin (1963), Nielsen (1992) and Soulsby (1997), share the same form as the solutions for Φ derived herein; i.e. $\Phi = F(\theta - \theta_c)\,\theta^{1/2}$. This proves the potential ability of the present model to simulate bedload in agreement with widely used empirical and semi-empirical expressions.

Table 4.1: Values for exponents in eq. (4.42), for different bedload formulations. Values not shown (since they are not relevant) when $n1 = 0$ or $n2 = 0$.

Formula	$m1$	$m2$	$m3$	$m4$	$n1$	$n2$	$n3$
Meyer-Peter and Müller (1948)	1	1	-	-	3/2	0	0
Bagnold (1963)	1	1	-	-	1	0	1/2
van Rijn (1984)	1/2	1/2	-	-	2.4	0	1/2
Yalin (1963)	1	1	-	-	1	0	1/2
Ashida and Michiue (1972)	1/2	1/2	1	1	1	1	0
Wilson (1966)	-	-	-	-	0	0	3/2
Nielsen (1992)	1	1	-	-	1	0	1/2
Fernández Luque and van Beek (1976)	1	1	-	-	3/2	0	0
Soulsby (1997)	1	1	-	-	1	0	1/2

The variable F also merits some discussion. F is taken as a constant by certain authors

(e.g. Meyer-Peter & Müller, 1948; Ashida & Michue, 1972; Wilson, 1966; Nielsen, 1992; Soulsby, 1997; Fernández Luque & van Beek, 1976), and as a function of various parameters by other researchers. For example, for Bagnold (1963), F depends on c_f, φ and S_b; whereas for van Rijn (1984a), $F = f(c_f, D, h_T)$. Yalin (1963) estimates F as $f(\theta, \theta_c, s)$; and for Madsen (1991), $F = f(\varphi)$. The diversity in computing both F and the exponents in (4.42) reflects the well-established uncertainty involved in accurate quantification of sediment transport rates. Fernández Luque & van Beek (1976) argue that variations reported in the value of F depend on the flow conditions and sediment characteristics considered in a given experiment. Note that A in eq. (4.40) (analogous to F in eq. 4.42) is dependent on parameters $c^{(b)}$, h_0, D, s, φ and θ (see eq. 4.41); in agreement with the aforementioned methods to compute F. This further confirms the agreement between the present theoretical development and previous experimental observations.

The attempt to match the present model with a particular empirical formula is not an aim of this study because, as has been mentioned previously, analytical solutions to the Q2L model in non-dimensional form depend on the somewhat arbitrary definition of the non-dimensional quantities involved. However, for a quantitative comparison between solutions derived here and empirical formulae, see §4.3.

4.2.2 Sheet flow as a function of velocity cubed

Sheet flow is considered as an special case of bedload transport that takes place at relatively fast flows, when $\theta \gg \theta_c$; approximately at $\theta > 0.8$ (Nnadi & Wilson, 1992; Soulsby & Damgaard, 2005). During this transport regime, bed forms are washed out (if initially present) and sediment is transported within a well-defined layer a few millimetres thick. The transport rate under sheet-flow conditions can be described satisfactorily as being dependent on the flow velocity cubed (Ribberink & Al-Salem,

1994; Capart & Young, 1998); i.e. $q_b = f(\bar{u}^3)$. A commonly used formula, popular because of its simplicity (Hudson & Sweby, 2003), is $q_b = B\bar{u}^3$, where B is a constant related to the flow and sediment characteristics. The cubic dependence on velocity can be deduced from most empirical expressions presented in Table 4.1, where if $\theta - \theta_c \approx \theta$ is assumed (given that $\theta \gg \theta_c$), $\Phi = F\theta^{3/2}$ is obtained. Then, if definition (4.23) is invoked, $\theta = c_f U_{1L}^2/[g(s-1)D]$ and so $\Phi = f(U_{1L}^3)$. In this section, it is demonstrated, through two different approaches, that the present model also predicts $q_b = f(U_{1L}^3)$ (or equivalently, $q_b = f(\bar{u}^3)$) for sheet-flow conditions.

For the first approach, consider the analytical solution derived for dimensional bedload given by (4.21). For sheet flow, $\tau_0^{(b)} \gg \tau_c \Rightarrow \tau_0^{(b)} - \tau_c \approx \tau_0^{(b)}$. Under these conditions, eq. (4.21) can be rewritten as:

$$q_b = \frac{1}{\left(\rho_{0\,\mathrm{eq}}\, c^{(b)}\right)^{1/2} (\rho_s - \rho_w) g \tan\varphi} \left(\tau_0^{(b)}\right)^{3/2}$$

$$= \frac{\rho_{0\,\mathrm{eq}}\, c^{(b)}}{(\rho_s - \rho_w) g \tan\varphi} u_0^3 \,. \tag{4.43}$$

Therefore $q_b \propto u_0^3$. From eq. (3.13), it is observed that u_0 and the whole-depth averaged velocity $\bar{u}$ exhibit a linear relationship; hence $q_b \propto \bar{u}^3$, confirming consistency between the present model and sheet-flow theory.

Furthermore, eq. (4.43) can be used to provide a bedload equation of the form $q_b = B\bar{u}^3$ by invoking expressions derived in §3.1, subject to the condition of $h_1 \gg h_0$ ($\because \rho_1 h_1 \gg \rho_0 h_0$). If eq. (3.13) relating u_0 to $\bar{u}$ is employed, bedload transport under sheet-flow

conditions can be calculated from:

$$q_b = B\bar{u}^3, \tag{4.44}$$

with

$$B \approx \frac{\rho_{0\,\mathrm{eq}}\, c^{(b)}}{(\rho_s - \rho_w) g \tan\varphi} \left(\frac{c_f}{c^{(b)}}\right)^{3/2}. \tag{4.45}$$

Note that B is dependent on sediment and flow characteristics, in agreement with established knowledge. The ratio $c_f/c^{(b)}$ can be estimated from Figure 3.1. The equilibrium density $\rho_{0\,\mathrm{eq}}$ is related to $c_{0\,\mathrm{eq}}$ (through $\rho_0 = c_0\rho_s + (1-c_0)\rho_w$), which, for sheet flow, has been observed to fall in the range of 0.21 to 0.25 (Spinewine, 2005).

The second approach follows an analysis undertaken by Fraccarollo & Capart (2002). For $\tau_c \approx 0$, the erosion rate can be expressed as:

$$\begin{aligned} e^{(b)} &= \frac{1}{\rho_b u_0}\left(\tau_0^{(b)} - \tau_b^{(b)}\right) \\ &= \frac{1}{\rho_b u_0}\left[\rho_0 c^{(b)} u_0^2 - (\rho_0 - \rho_w) g h_0 \tan\varphi\right] \\ &= \frac{g h_0 \tan\varphi}{\rho_b u_0}\left[\frac{\rho_0 c^{(b)}}{g h_0 \tan\varphi} u_0^2 - (\rho_0 - \rho_w)\right]. \end{aligned} \tag{4.46}$$

Analysis of (4.46) yields the following interpretation. The increment (in relation to no-sediment-transport conditions) in the bedload layer density given by $(\rho_0 - \rho_w)$ tends asymptotically to the equilibrium value $(\rho_{0\,\mathrm{eq}} - \rho_w) = [(\rho_{0\,\mathrm{eq}} c^{(b)})/(g h_0 \tan\varphi)]u_0^2$; which ensures a balance between shear stresses at both sides of the bed interface, and

hence cessation of erosion. It is then straightforward to see that:

$$q_b = h_0 c_{0\,\mathrm{eq}} u_0 = \frac{h_0(\rho_{0\,\mathrm{eq}} - \rho_w)u_0}{(\rho_s - \rho_w)} = \frac{\rho_{0\,\mathrm{eq}}\, c^{(b)}}{(\rho_s - \rho_w) g \tan\varphi} u_0^3 \,,$$

which is the same expression as eq. (4.43), thus confirming again that $q_b \propto \bar{u}^3$. However, the relevance of this second approach lies in the analysis that arises from rearranging (4.46) as:

$$e^{(b)} = \frac{1}{t_l}\left(M u_0^2 - \frac{\rho_0 - \rho_w}{\rho_0} h_0\right), \tag{4.47}$$

where $M = c^{(b)}/(g\tan\varphi)$ is a mobility parameter; and $t_l = \rho_b u_0/(\rho_0 g \tan\varphi)$ is a lag time related to the inertia of the sediment that has to be accelerated from rest to be incorporated into the sheet flow (when erosion takes place). This is in agreement with the view that sediment transport does not respond immediately to changes in bed shear stress, but instead it has a characteristic time of relaxation (Parker *et al.*, 2003). This relaxation time is often neglected (under the assumption of instantaneous response of a sediment particle to the imposed shear stress) without serious consequences for slow morphological changes; however, for the study of fast morphological changes, the lag time is significantly important. The term $(\rho_0 - \rho_w)h_0/\rho_0$ can be related to the transport capacity of the sheet layer. Similar quantities have been found within the framework of alluvial hydraulics and dam-breaks (e.g. Armanini & Di Silvio, 1988; Fraccarollo & Capart, 2002).

4.2.3 Sheet layer thickness

The thickness of the sheet layer, δ_{sh}, can be estimated by considering the balance of vertical forces for the particles in the sheet layer, and further assuming a vertical distribution of the sediment concentration within the layer, varying linearly from a maximum equal to c_b, to zero at the sheet-layer surface (see e.g. Fredsøe & Deigaard, 1992). This leads to express δ_{sh} as (Soulsby & Damgaard, 2005):

$$\delta_{\mathrm{sh}} = \frac{2(\tau - \tau_c)}{c_b(\rho_s - \rho_w)g\tan\varphi_d}, \tag{4.48}$$

where $\tan\varphi_d$ is the coefficient of dynamic friction, and $c_b/2$ is assumed to be the average concentration of the sheet layer (i.e. c_0). Note that the equation for $c_{0\mathrm{eq}}$ given by (4.19) is consistent with (4.48). The present model assumes a varying density within a fixed layer defined by h_0. However, δ_{sh} could be estimated from the Q2L model by fixing $c_{0\mathrm{eq}}$ for sheet-flow conditions ($0.21 \lesssim c_{0\mathrm{eq}} \lesssim 0.25$) and then solving (4.19) for h_0, yielding:

$$\delta_{\mathrm{sh}} \approx h_0 = \frac{(\tau_0^{(b)} - \tau_c)}{c_0(\rho_s - \rho_w)g\tan\varphi}. \tag{4.49}$$

Note that (4.49) equals (4.48) if $c_0 = c_b/2$ and $\tan\varphi = \tan\varphi_d$ are assumed. The first assumption is perfectly justified given that both c_0 and $c_b/2$ are defined as being the average concentration of the sheet layer. Regarding the second assumption, it is not unreasonable to consider $\tan\varphi \sim \tan\varphi_d$, given that $\tan\varphi_d$ has been found to have values in the range of 0.50 to 0.65 (Fredsøe & Deigaard, 1992), which are also commonly expected values for $\tan\varphi$. In fact, Kovacs & Parker (1994) argue that both variables do not differ greatly from each other and assume $\tan\varphi = \tan\varphi_d$. The linear relationship between the sheet layer thickness and bed shear stress has also been reported by e.g. Wilson (1987); Capart & Young (1998). This finding further confirms the agreement

between the present model and general theory of bedload transport.

4.2.4 The 'shield' effect

According to Fernández Luque & van Beek (1976), the bedload layer (L_0) acts as a 'shield' that prevents the upper water layer (L_1) from further eroding the bed. Bagnold (1956) proposed that this occurs due to the fluid component of the bed shear stress being reduced to the value of τ_c at the bed surface by the presence of particles in the bedload layer. However, this theory has been criticised (see e.g. Fernández Luque & van Beek, 1976; Niño & García, 1998b; Seminara *et al.*, 2002; Parker *et al.*, 2003), especially for low concentrations of particles within the bedload layer. Here, we show that the present model conforms with the aforementioned views without favouring or contradicting a particular one.

For equilibrium bedload conditions, the present model requires $\tau_0^{(b)} = \tau_b^{(b)}$. Here, $\tau_b^{(b)}$ can be interpreted as a 'critical' bed stress in the Bagnoldian sense, hence agreeing with his –somehow intuitive– idea of a fluid stress being reduced to a critical value in order for erosion to cease. Moreover, as evidenced by (4.21) (and because $\tau_b^{(b)} > \tau_c$), the presence of bedload necessarily verifies the condition $\tau_0^{(b)} > \tau_c$. Thus, for a natural steady regular flow (where $-S_b > 0$), the following expression can be deduced from (2.10e):

$$\tau^{(i)} - \tau_0^{(b)} = -\rho_0 g h_0 S_b > 0,$$

leading to:

$$\tau^{(i)} > \tau_0^{(b)} > \tau_c. \tag{4.50}$$

The above equation implies that the bedload layer indeed acts as a 'shield' throughout which the fluid shear stress at the top of the bedload layer $\tau^{(i)}$ is reduced to a value

$\tau_0^{(b)}$ at the bed surface, which in turn is larger than τ_c. Note that $\tau_0^{(b)}$ represents the shear stress exerted by the sediment-water mixture defining the bedload layer, and not exclusively the fluid shear stress (see §2.3.1). However, for low values of c_0 ($\because \rho_0 \approx \rho_w$), $\tau_0^{(b)}$ can be taken as the fluid component of the bed shear stress, in agreement with Fernández Luque & van Beek (1976). Furthermore, the erosion rate $e^{(b)}$ should be read as a *net* transfer of mass between the bed and the bedload layer, such that the condition $e^{(b)} = 0$ required for steady transport represents a dynamic, rather than static, state. This agrees with the view that simultaneous entrainment and deposition of sediment take place under stable conditions (Fernández Luque & van Beek, 1976; Parker *et al.*, 2003).

The above observations yield the conclusion that the current model reconciles (or least is not in contradiction with) the conceptualisation of bed shear stress in the presence of bedload described by Bagnold and those of his critics.

4.3 Validation against empirical formulae

Fig. 4.1 compares the solutions in non-dimensional form derived in §4.2.1 against bedload formulae by Meyer-Peter & Müller (1948) (MP & M), Yalin (1963) (Y), Ashida & Michue (1972) (A & M), Wilson (1966) (W), Nielsen (1992) (N) and Fernández Luque & van Beek (1976) (FL & vB). These formulae have been selected because they do not require any additional assumptions (e.g. value of drag coefficient), other than the sediment characteristics (used to compute θ_c). A particle diameter of 1.0 mm, $s = 2.65$ and $\varphi = 32.1^\circ$ are considered; these values of s and φ are used hereinafter unless otherwise stated. For the evaluation of analytical solutions given by (4.40) and (4.41), $c^{(b)} = 0.03$ is employed. A value of $h_0 = 10D$ is assumed.

Fig. 4.1 gives rise to the following observations. Predictions by the present model

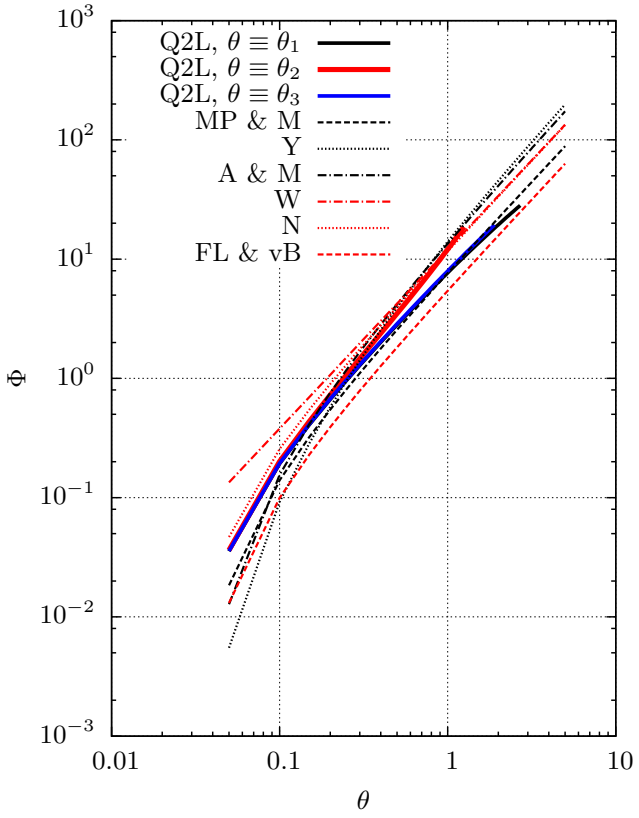

Figure 4.1: Comparison between the non-dimensional bedload predicted by the Q2L model against various empirical and semi-empirical formulae. [Acronyms defined in corresponding paragraph]

fall within the band of estimates delimited by the empirical formulae considered; this band illustrates the well-known uncertainty in the quantification of bedload. Solutions Φ_1 ($\Phi_1 = f(\theta_1)$) and Φ_3 ($\Phi_3 = f(\theta_3)$) exhibit more similar behaviour, as compared with Φ_2 ($\Phi_2 = f(\theta_2)$), to the empirical formulae for increasing values of θ. Bedload rates Φ_1 and Φ_3 also allow computation of bedload for larger values of θ than Φ_2; model predictions have been truncated where $c_0 = c_{0\mathrm{mx}}$ is reached (here $c_{0\mathrm{mx}} = 0.3$ is considered). However, unlike Φ_1 and Φ_3, Φ_2 predicts an increasing value of the proportionality coefficient A (see eqs. 4.40 and 4.41) with θ. This behaviour has been widely reported in the literature (see e.g. Fernández Luque & van Beek, 1976; Wilson, 1987; Camenen & Larson, 2005; Ribberink, 1998) and is a major reason for the discrepancies in proposed values of A. Experiments at low shear stresses yield a smaller

value of A (e.g. Fernández Luque & van Beek, 1976) than those involving higher flow velocities (e.g. Meyer-Peter & Müller, 1948; Wilson, 1966). On this basis, θ_2 appears to be the most adequate definition of the non-dimensional bed shear stress. Recall, nevertheless, that non-dimensionalisation of τ (or $\tau_0^{(b)}$) is only useful in the framework of the present model for comparison against bedload formulae. The quantification of sediment transport rates and morphological evolution is solely dependent on the estimation of dimensional bed shear stress, as discussed previously.

Near the incipient-motion regime (i.e. at low values of θ), the three analytical solutions converge, as expected (see §4.2.1). Values of the drag coefficient (for 1-layer models) typically fall in the range of $10^{-3} \lesssim c_f \lesssim 10^{-2}$ (Soulsby, 1997), and so $c^{(b)} = 0.03$ is in agreement with the values of the ratio $c^{(b)}/c_f$ derived in §3.2 (see Fig. 3.1). For example, a value of $c^{(b)}/c_f \approx 4$ would yield $c_f \approx 7.5 \times 10^{-3}$ for the present case, which implies a relatively rough hydrodynamic flow. Flows over beds composed by coarse sands (such as the one considered herein) can be treated as hydrodynamically rough (Soulsby, 1997), and so these findings validate both the potential of the present model to simulate bedload and the predictions of the ratio $c^{(b)}/c_f$ undertaken previously and based solely on hydrodynamic (i.e. no sediment transport) considerations.

In order to avoid ambiguity related to the definition of θ within the framework of the present model, the analytical solution derived in dimensional form (eq. 4.21) is now contrasted against the same empirical expressions depicted in Fig. 4.1. Figure 4.2 illustrates such a comparison. Empirical expressions are computed as $f(\tau)$, whereas the solution to the present model is evaluated as $f(\tau_0^{(b)})$; in other words, $\tau = \tau_0^{(b)}$ is assumed. Two particle diameters are considered; i.e. 0.5 and 2.0 mm. These particle sizes represent medium-coarse and very coarse sands, respectively, according to the Wentworth grain size scale. The reason to study coarse sand is that, for a bed composed

of such material, bedload is expected to be the main mode of transport (for $D > 0.3$ mm, according to Soulsby & Damgaard, 2005). Three values of $c^{(b)}$ are investigated; namely, 0.01, 0.03 and 0.06. The bedload layer thickness, h_0, is taken as equal to $10D$.

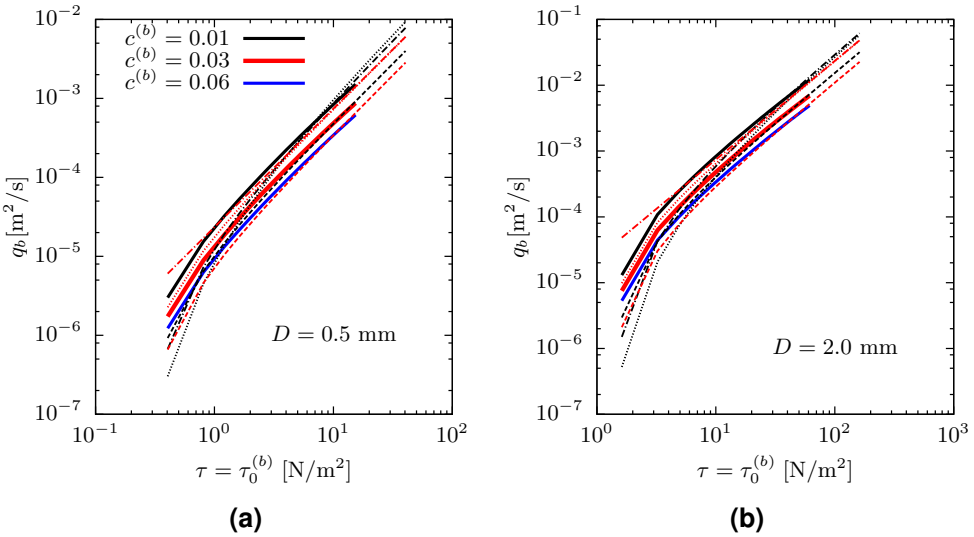

Figure 4.2: Comparison between dimensional bedload predicted by the Q2L model against some empirical and semi-empirical expressions, for two particle diameters. [The rest of the legend as in Fig. 4.1]

Fig. 4.2 confirms the agreement between the predictions by the present model and the formulae considered. For increasing values of the bed shear stress, the behaviour of the solution given by (4.21) adheres to the empirical curves, confirming the ability of the present model to simulate potential sheet flow, as concluded in §4.2.1 through mathematical analysis. Comparison between Figures 4.2a and 4.2b demonstrates that the overall behaviour of the Q2L in relation to the formulae is independent of the particle size within the range considered. The recommended value of $c^{(b)}$ depends on the reference formula. For flow conditions well above incipient motion, $c^{(b)} = 0.01$ yields a very good agreement between the present model and formulations by Yalin (1963), Ashida & Michue (1972), Wilson (1966) and Nielsen (1992); $c^{(b)} = 0.06$ leads to a better match with the expression by Fernández Luque & van Beek (1976); and for the middle value of $c^{(b)} = 0.03$, the model is closer to the formula by Meyer-Peter

& Müller (1948). Based on the empirical equations herein considered, the range of $0.01 \leq c^{(b)} \leq 0.06$ can be taken as a suggested operational range when calibrating the Q2L model.

Fig. 4.3 compares the approximate and exact solutions given in §§4.1.1 and 4.1.2, respectively, for different values of the ratio h_1/h_0. These solutions are derived as functions of channel features, and so the following parameters, representative of a practical situation, are assumed: $D = 1.0$ mm, $c^{(b)} = 0.03$, $h_T = 2.5$ m, and a varying channel slope in the range of $S_b \in [-1.5 \times 10^{-2}, -1.0 \times 10^{-3}]$. For these values of S_b, the influence of the bed-slope on the estimation of θ_c can be neglected (this point becomes relevant in Chapter 6). Here, the value of h_0 is changed for each value of S_b as to ensure a value of the bedload layer equilibrium concentration of $c_{0\,\mathrm{eq}} \approx 0.24$, which is a common value for sheet flow. Fig. 4.3 shows that the exact and approximate solutions converge for increasing h_1/h_0, as it would be expected; i.e. when $h_1 \gg h_0$, the change in h_1 caused by the flux of water to L_1 due to erosion (see §2.3.2) is negligible. Differences between both solutions can be perceived for relatively shallower flows; however, such differences also seem negligible from a pragmatic perspective. Note that the relative shallowness of a flow, here given by h_T/h_0, is equal to $h_1/h_0 + 1$, and so for the present case $h_T/h_0 \approx h_1/h_0$ can be assumed.

Figure 4.4 depicts a comparison between exact analytical solution, approximate analytical solution, and numerical predictions. To this end, governing equations (2.10) are solved through a second-order central finite difference scheme, and integrated in time using a fourth-order Runge-Kutta method. Three particle diameters (i.e. 0.5, 1.0 and 2.0 mm) are investigated and the following parameters are considered: $c^{(b)} = 0.03$, $h_T = 1.0$ m and $h_0 = 10D$. Curves are shown up to a point where $c_0 = c_{0\,\mathrm{mx}} = 0.3$. It can be observed that the numerical solution is in virtually perfect agreement with the exact solution. Differences between the exact and approximate solutions become

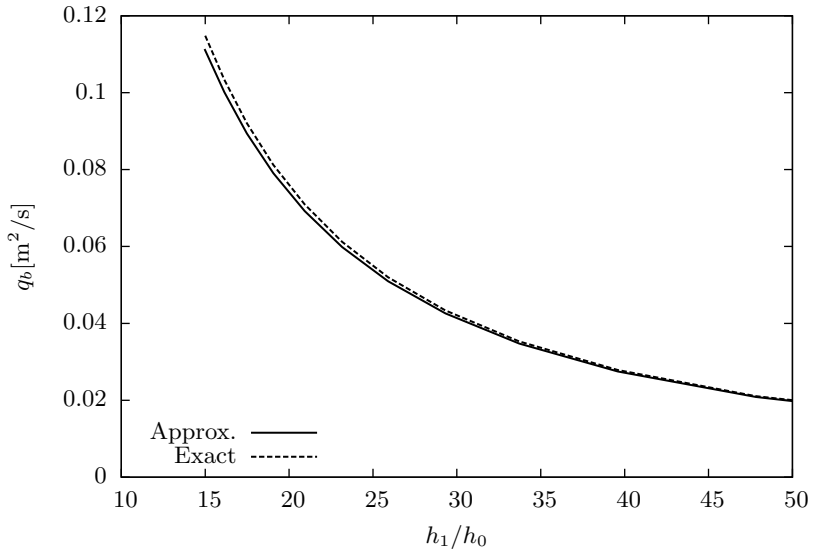

Figure 4.3: Comparison between approximate and exact analytical solutions to the Q2L model for varying h_1/h_0 and fixed $c_{0\,\mathrm{eq}}$ and h_T; $D = 1.0$ mm.

perceptible at steeper slopes (for a fixed h_T, this equates faster flows). This can be understood as follows: a faster flow yields a larger erosion rate, which in turn leads to a larger exchange of water mass from L_0 to L_1 (equal to $\rho_w e^{(b)}$). However, these differences again seem negligible from a practical viewpoint, and hence, the use of the simpler approximate solution (4.9) is recommended for most practical applications, excluding very shallow and fast flows.

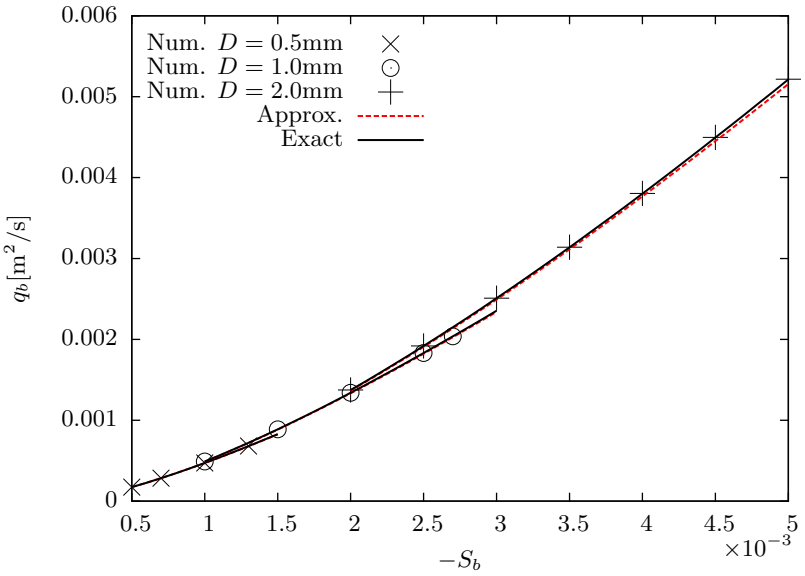

Figure 4.4: Comparison between analytical (approximate and exact) and numerical solutions to the Q2L model for varying bed-slopes and three particle diameters; h_T fixed.

4.4 Bedload layer thickness, h_0

The bedload is, in general terms, defined as the mode of transport taking place *near* the bed, as opposed to the suspended load, that occurs away from the channel bottom. However, as discussed in §1.1.5, a reliable method to determine the thickness of the bedload layer does not exist (except for the particular case of sheet flow, where a distinct transport layer can be identified).

In the present model, the layer L_0 (defined by h_0) seeks to represent the bedload zone. Hence, Fig. 4.5 investigates the sensitivity of the bedload transport predicted by the model to values of h_0 in the range of $[2D\,, 20D]$. This range is selected based on estimates of bedload layer thickness by Einstein (1950) and van Rijn (1984a). A diameter of 1.0 mm has been selected, which is representative of the behaviour

followed by other diameters in the range of 0.5 – 2.0 mm. It can be observed that the influence of the arbitrary h_0 in the predicted q_b, for a given $\tau_0^{(b)}/\tau_c$, is small. For $\tau_0^{(b)}/\tau_c = 20$ (where sheet flow is expected), the discrepancies between curves are negligible. The most significant effect of the selected value of h_0 is the variation in the range of validity of the model when operating as Mode 1. The curves are plotted up to a point where $c_0 = c_{0\,\mathrm{mx}} = 0.3$, beyond which, sediment transport would be considered as suspended load (Mode 2) within the framework of the Q2L model. A larger value of h_0 allows the model to operate as Mode 1 for a wider range of $\tau_0^{(b)}$.

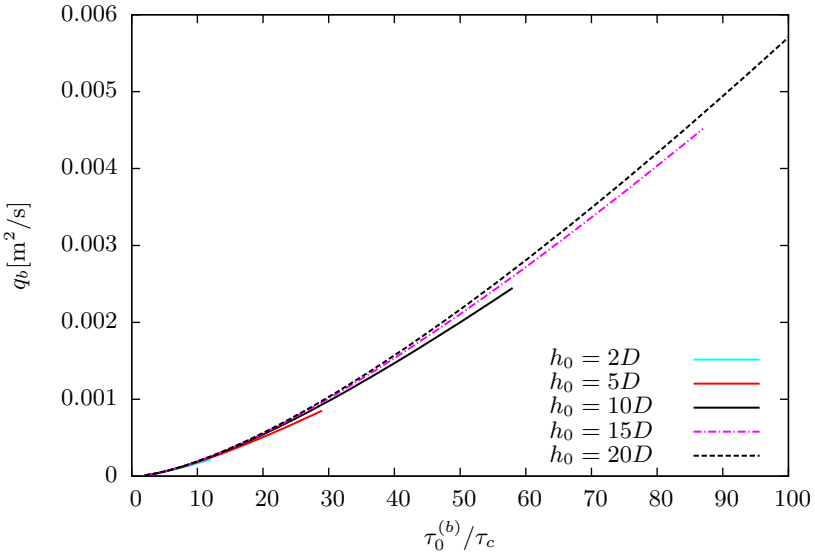

Figure 4.5: Predicted bedload vs non-dimensional bed shear stress for different values of h_0.

In Appendix C it is shown that when bedload is estimated as a function of u_{s0} instead of u_0, q_b is not dependent on h_0 at all. This apparent advantage, however, is counterbalanced by the fact that in such a case, additional calibration parameters are required (in this case, they are estimated by means of the Lagrangian model presented in Chapter 7). Thus, the weak dependence of q_b on h_0 here demonstrated is a very relevant conclusion that allows to reduce, from a practical perspective, the calibration of the model for bedload to a single variable (i.e. $c^{(b)}$).

Consider now the expression (4.48) given in §4.2.3 to determine the thickness of a sheet layer, rewritten here as:

$$\frac{\delta_{\mathrm{sh}}}{D} = \frac{2(\theta - \theta_c)}{c_b \tan\varphi_d}. \tag{4.51}$$

An alternative criterion to set the thickness of L_0 is to select a value of h_0 that ensures $h_0 \geq \delta_{\mathrm{sh}}$ when sheet flow is simulated. In other words, if it is known a priori that sheet flow will be modelled, as well as the expected values of θ, h_0 should be selected as to meet the condition $h_0 \geq \delta_{\mathrm{sh}}$, with δ_{sh} estimated from (4.51). This would ensure that the Q2L model treats the sheet flow as bedload (Mode 1), and not as bedload plus suspended load (Mode 2). For example, assuming standard values of $\tan\varphi_d \approx 0.65$, $\theta_c \approx 0.05$ and $c_b/2 \approx 0.3$, eq. (4.51) varies linearly from $\left(\delta_{\mathrm{sh}}/D\,|_{\theta/\theta_c=1}\right) = 0$ to $\left(\delta_s/D\,|_{\theta/\theta_c\approx 50}\right) \approx 10$. Therefore, $h_0 = 10D$ would ensure sheet flow is treated as bedload by the model for conditions up to $\tau_0^{(b)} \approx 50\tau_c$ (note, from Fig. 4.5, that for $h_0 = 10D$, Mode 1 is valid up to $\tau_0^{(b)} \approx 60\tau_c$). Hence $h_0 \sim 10D$ is recommended given the relatively wide range of validity (for Mode 1) that such an assumption yields. The value $h_0 = 10D$ is used hereinafter as default unless otherwise stated.

4.5 The case of a migrating hump

The case of a submerged erodible hump subject to a steady subcritical flow is now considered. This scenario represents a simple but very informative case study for morphological models. The behaviour followed by the initially symmetrical hump is known: the hump migrates in the downstream direction and its downstream face (lee) steepens with time. A comparison is made between the behaviour predicted by the Q2L model and that of a conventional morphological model consisting of a coupling between hydrodynamic equations, a bed-update equation and a sediment-transport empirical formula. The latter model represents the basic structure of conventional 2DH

morphological models widely used in coastal and river engineering (e.g. MIKE21, TELEMAC, Delft3D).

Hudson & Sweby (2003) developed an approximate analytical solution for this case based on the Method of Characteristics, assuming a rigid lid (i.e the water surface level, η, remains constant in time and space), constant discharge throughout the domain, and a horizontal frictionless bed. The first two assumptions are valid for a bed interacting slowly with the flow. The set of governing equations adopted by Hudson & Sweby (2003) consisted of a coupled version of the 1D Shallow Water Equations (fluid density = water density), a bed-update equation (commonly known as Exner equation) and a bedload equation applicable to sheet flow (sometimes referred to as Grass equation); namely:

$$\frac{\partial h_T}{\partial t} + \frac{\partial (\bar{u} h_T)}{\partial x} = 0 \tag{4.52a}$$

$$\frac{\partial (\bar{u} h_T)}{\partial t} + \frac{\partial}{\partial x}\left(h_T \bar{u}^2 + \frac{1}{2} g h_T^2 \right) = -g h_T \frac{\partial z_b}{\partial x} - \frac{\tau}{\rho_w} \tag{4.52b}$$

$$\frac{\partial z_b}{\partial t} + \xi \frac{\partial q_b}{\partial x} = 0 \tag{4.52c}$$

$$q_b = B \bar{u}^3 \tag{4.52d}$$

In equations (4.52), $\bar{u}$ is used instead of U_{1L} for convenience (alternatively, $\bar{u} = U_{1L}$ is assumed).

Figure 4.6 compares the evolution of the hump predicted by the approximation derived by Hudson & Sweby (2003) with the numerical solution to eqs. (4.52). The analytical

approximation is valid up to the point where the characteristics cross; for this reason, the approximate solution is not shown for the right-most curve. For the numerical solution, equations (4.52) are discretised using a second-order central finite difference scheme and integrated in time via a fourth-order Runge-Kutta method. The following parameters are considered: channel length, $l = 1000\text{m}$; $B = 0.001\,\text{s}^2/\text{m}$; $\xi = 1/0.6$ ($\varepsilon_b = 0.4$); $h_T = 10\text{m}$ (at the upstream boundary) and discharge per unit width, $Q = 10\,\text{m}^2/\text{s}$.

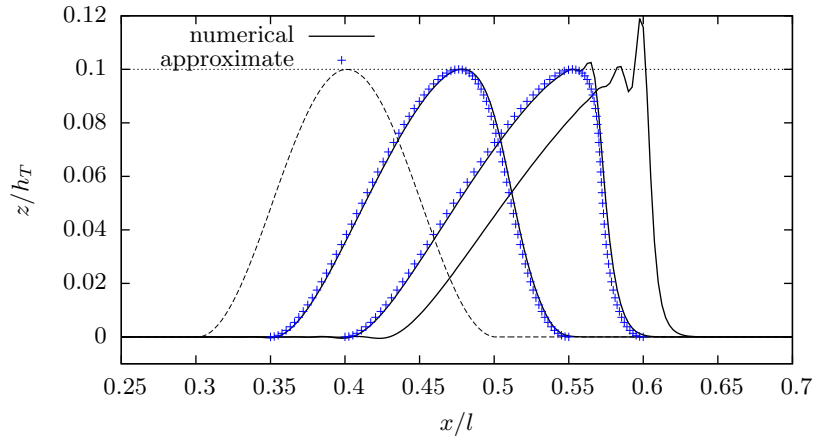

Figure 4.6: Evolution of a hump predicted by eqs. (4.52). Comparison between numerical and approximate analytical solutions. Results shown at $t = 0\text{s}$ (dashed line) and at (from left to right) $t = 100 \times 10^3$, 200×10^3 and $250 \times 10^3\text{s}$.

After $200 \times 10^3\text{s}$, the numerical solution starts to develop instabilities at the crest and base of the upstream face (stoss) of the hump. These instabilities continue to increase with time, as clearly perceived after $250 \times 10^3\text{s}$ of simulation, and eventually render the model unstable. The appearance of these unrealistic oscillations can be related to the neglected influence of the local bed-slope on the bedload transport. The role of such an influence is to introduce diffusion into the bed-update equation, which prevents such oscillations from developing (Johnson & Zyserman, 2002). Note that the analytical approximation implies that no diffusion is considered in the bed-update equation, given the nature of the method followed by Hudson & Sweby (2003), where

points in the original bathymetry move strictly parallel to the flow (advection without diffusion). Castro Díaz *et al.* (2008) carried out laboratory experiments similar to this numerical test, but considering a 'squared' hump. Their experimental results provide evidence the importance of slope-related diffusion – numerical simulations neglecting the influence of the slope diverge significantly from measurements.

The same case study is now approached by means of the Q2L model. A direct comparison with the previous approach is not possible for several reasons. Hudson & Sweby (2003) assume a horizontal frictionless bed, which, though physically unrealistic, does not represent an impediment for the model described by eqs. (4.52). However, in the framework of the Q2L model, erosion and sediment transport cannot occur in a frictionless bottom ($e^{(b)}$ is defined by the bed friction). A horizontal channel would require an extra source of momentum to produce a constant flow (e.g. a pump); Hudson & Sweby (2003) overcame this by assuming a frictionless bed and setting fluid in motion as initial condition. Despite these limitations, a qualitative comparison between the two morphological models can be undertaken. To study the evolution predicted by the Q2L model, the channel with a hump is slightly inclined with respect to the horizontal, and bed friction is considered. The angle of inclination has to be sufficiently small as to justifiably neglect any additional influence of the slope; in this case, an angle of -0.006° is adopted. In the case of Hudson & Sweby (2003), the average migration speed of the hump is solely dependent on the parameter B, whereas in the Q2L, such a speed depends on several parameters (see e.g. equations 4.45 and 4.15). Achieving an equal speed for hump migration between models is not an aim of the present qualitative comparison.

Figure 4.7 illustrates the evolution of the hump predicted by the Q2L model. The same technique used previously for the numerical solution of eqs. (4.52) is employed in

this case. The following parameters are considered: $h_T = 10$m; $D = 2.0$mm; $h_0 = 10D$; $c^{(b)} = 0.02$; $c_b = 0.6$ ($\varepsilon_b = 0.4$). It can be observed that the model captures correctly the qualitative behaviour of the hump; i.e. the hump migrates downstream and its lee steepens with time. However, in contrast with the previous approach, high-frequency oscillations are not present in the hump, presumably due to an inherent diffusive component within the model that prevents small perturbations from forming. This theory is supported by the fact that the hump losses height with time (diffusive behaviour). Based upon phenomenological arguments, Johnson & Zyserman (2002) state that diffusion (or smoothing effect) is related to the local bed-slope. In order to test whether this is the case within the present model, a longer-term simulation is carried out. Fig. 4.8 depicts the hump evolution after 1.2×10^6s ($\approx$ 14 days). The height of the hump seems to converge with time, which supports the idea that the diffusion component of the model vanishes for small local slopes, and hence, that such a diffusion is indeed related to the bed-slope. A thorough investigation on the influence of the bed-slope is carried out in Chapter 6.

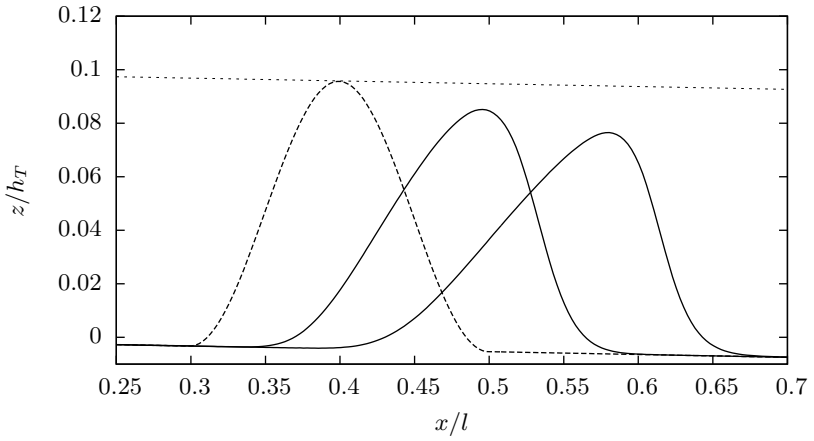

Figure 4.7: Evolution of a hump predicted by the Q2L model. Results shown at $t = 0$s (dashed line), $t = 200 \times 10^3$s (central curve) and $t = 400 \times 10^3$s (right curve). Dotted line is tangent to the initial crest of the hump.

A last comparison between the two approaches is worth being made. Equations governing the morphology in both models are different. Rewritten below for convenience,

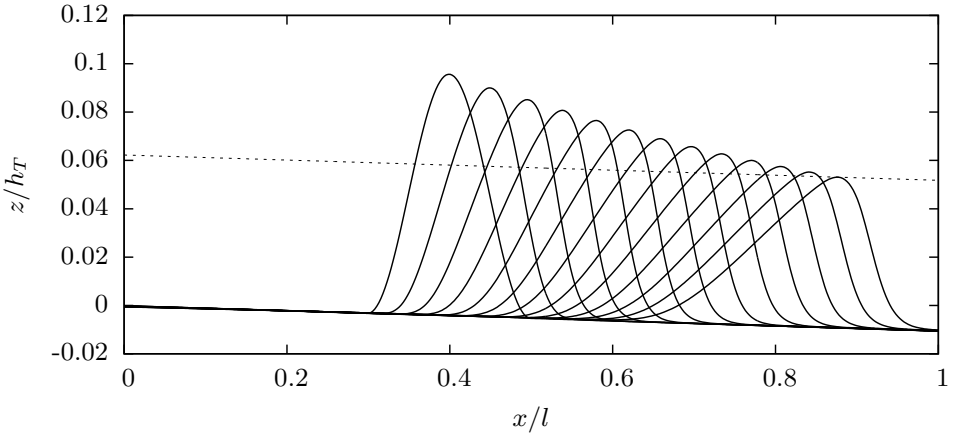

Figure 4.8: Evolution of a hump predicted by the Q2L model after 1.2×10^6s. Results shown every 100×10^3s. Dotted line is tangent to the final crest of the hump (parallel to the otherwise flat bed).

morphology is governed in the case of Hudson & Sweby (2003) by the following equation:

$$\frac{\partial z_b}{\partial t} = -\xi \frac{\partial q_b}{\partial x}, \tag{4.53}$$

whereas, in the Q2L model, bed evolution is described by:

$$\frac{\partial z_b}{\partial t} = e^{(b)}. \tag{4.54}$$

For the case study herein considered, a gradient of the whole-depth-averaged velocity, $\bar{u}$, is expected in the region above the hump (due to the constant discharge); i.e. $\partial \bar{u}/\partial x \neq 0$. Given that $q_b = B\bar{u}^3$, it follows that $\partial q_b/\partial x \neq 0$ in this region. Invoking (4.53), a migration of the hump is thus explicitly prescribed in the model used by Hudson & Sweby (2003); i.e. a positive(negative) gradient of $\bar{u}$ (and hence of q_b) yields bed erosion(accretion). The derivation of the approximate solution depicted in Fig. 4.6 demonstrates that the steepening of the hump's lee takes place due to different levels of the bed travelling in the direction of the stream at different celerities (Hudson &

Sweby, 2003; Huang *et al.*, 2008).

The Q2L model is different in this regard. Equation (4.54) states that the bed level changes according to the erosion rate, $e^{(b)}$. However, $e^{(b)} = f(\tau_0^{(b)}, \tau_b^{(b)})$; and recalling that $\tau_0^{(b)} = f(u_0, \rho_0)$ and $\tau_b^{(b)} = f(\rho_0)$, it follows that changes in z_b depend on the local values of u_0 and ρ_0, rather than on gradients of these variables. Note that initial conditions for this case study are perfectly symmetrical, and so the Q2L model's governing equations do not explicitly predict migration (nor necessarily evolution) of the hump. Nevertheless, as the simulation progresses, the model captures differences in the local values of u_0 and ρ_0 within the domain, so as to erode bed material from the stoss and deposit it on the lee of the hump, allowing not only its migration but also correct deformation (i.e. steepening of the lee). It is then hypothesised that the Q2L model captures correctly the physics behind the phenomenon of a migrating hump, especially concerning the influence of the bed-slope on bedload transport. This influence is commonly parametrised or ignored in widely used morphological models described by a set of equations similar or equal to eqs. (4.52). The hypothesis is further investigated in Chapter 6.

4.6 Chapter summary

The case of steady uniform flow over an erodible bed such that only bedload transport takes place has been considered. This allows the derivation of (approximate and exact) analytical solutions to the Q2L model for Mode 1. Such solutions are derived as functions of i) key channel features; and ii) bed shear stress. The former can be of interest to, for example, practitioner fluvial engineers wishing to estimate bedload transport rates in coarse-sediment-bed rivers; whereas the latter is useful when comparing the present model against popular empirical expressions for bedload. For the case of bedload only,

the Q2L model requires solely one calibration parameter; namely, $c^{(b)}$.

The model is then compared against bedload theory by means of analytical treatment of the governing equations. Solutions are derived for bedload in non-dimensional form. Three versions are obtained given the different possible definitions of the non-dimensional bed shear stress within the framework of the present model. All three solutions can be expressed in the form of $\Phi = A(\theta - \theta_c)\theta^{1/2}$, which is common to several empirical and semi-empirical available formulations. Furthermore, the predicted coefficient A is shown to depend on flow and sediment characteristics, confirming previous findings.

The sheet flow regime is also considered. In this case, the model predicts a transport rate proportional to the cubed average flow velocity, in agreement with well-established theory. An expression for B in $q_b = B\bar{u}^3$ is proposed. The lag time, related to the non-immediate response and adaptation of sediment particles to the flow velocity, is analytically extracted from the model. The ability of the model to predict the sheet layer thickness in agreement with previous (and different) theoretical approaches is also demonstrated. The 'shield' effect, due to which the bedload layer prevents the upper water layer from further eroding the bed, is replicated by the model. It is shown that in the context of the Q2L model, previous contradictory views about the behaviour of the shear stress under bedload conditions, may not necessarily be in conflict.

The model is then validated satisfactory against widely used empirical and semi-empirical bedload formulae. Values of the calibration parameter in the range of $0.01 \leq c^{(b)} \leq 0.06$ are suggested as first approximations. These values are congruent with the estimations of the ratio $c^{(b)}/c_f$ derived in Chapter 3. Exact and approximate analytical solutions to the model respectively diverge for very fast and shallow flows. The model

is weakly dependent on the arbitrarily defined h_0 for practical applications. A default value of $h_0 = 10D$ is recommended.

The case study of a migrating hump subject to a steady subcritical flow is lastly addressed. This case permits an insightful comparison against a conventional morphodynamic model composed of a coupling between the 1D SWE, the Exner equation, and the Grass sheet-flow formula. The same numerical technique is employed in order to solve both sets of governing equations. Unlike the conventional approach, the Q2L model does not predict the development of unrealistic oscillations at the crest and base of the hump. This is presumably due to the model inherently accounting for the diffusive influence of the local bed-slope on bedload transport. Such an hypothesis is thoroughly investigated in Chapter 6.

The following chapter explores the capability of the Q2L model to simulate simultaneous bedload and suspended sediment transport.

Chapter 5

Total transport (Mode 2)

For sufficiently fast flows, sediment will entrain upper parts of the transporting fluid well above the near-bed zone (suspended load), which, in conjunction with bedload, constitutes the total transport. According to the conceptualisation of the sediment transport phenomenon given in §2.1, the scenario is now considered where the bedload layer has reached a saturation point and sediment is thus entrained into the upper layer L_1. As with bedload, the assumption of steady uniform flow over a flat erodible bed permits the derivation of analytical solutions. This brief chapter presents the development of an analytical solution for total transport as a function of key channel parameters, and comparison against empirical formulae for total transport available in the literature.

5.1 Analytical solution

Formulae for total transport typically depend directly on channel physical parameters (e.g. h_T, D). Hence, for the sake of easy comparability, an analytical solution for the present model as function of channel features is derived. Total transport can be computed as the addition of bedload and suspended load; namely:

$$q_T = q_b + q_s, \tag{5.1}$$

where q_T and q_s represent the total and suspended loads, respectively. In the framework

of the present model, $q_b(q_s)$ represents the sediment transported in layer $L_0(L_1)$.

Equilibrium bedload is calculated considering that L_0 has reached its maximum transport capacity; in other words:

$$q_{b\,\mathrm{eq}} = q_b|_{c_0=c_{0\mathrm{mx}}} = h_0\, c_{0\mathrm{mx}}\, u_0|_{c_0=c_{0\mathrm{mx}}}\ . \tag{5.2}$$

Recall that $c_{0\mathrm{mx}}$ represents the maximum sediment concentration allowed within the bedload layer, or saturation point; approximately $0.21 \lesssim c_{0\mathrm{mx}} \lesssim 0.25$ (see §4.2.2).

Analogous to bedload, suspended load is computed as the product $h_1 c_{1\mathrm{eq}} u_{1\mathrm{eq}}$. Observe that, as mentioned before, the implicit assumption of $u_1 = u_{1s}$ is here justified given the fast flows associated to suspended load, where the sediment is transported at practically the same speed as the carrying fluid. In order to derive expressions for the equilibrium values of c_1 and u_1, uniform steady unidirectional flow is considered. Following the methodology employed previously, equilibrium sediment transport conditions are achieved when $\tau_0^{(b)} = \tau_b^{(b)}$. Suspended transport normally occurs at flow velocities well beyond the threshold of motion, and so $\tau_c = 0$ can be assumed. Aiming for a simpler mathematical expression, $h_1 \gg h_0$ is considered, so that the flux of water from L_0 to L_1 due to bed erosion can be neglected, yielding $h_1 =$ constant. Invoking (4.3) and (2.15), we have:

$$-gS_b(\rho_1 h_1 + \rho_{0\mathrm{mx}} h_0) = [h_1(\rho_1 - \rho_w) + h_0(\rho_{0\mathrm{mx}} - \rho_w)]\, g \tan\varphi, \tag{5.3}$$

where $\rho_{0\mathrm{mx}} = \rho_0|_{c_0=c_{0\mathrm{mx}}} = (1 - c_{0\mathrm{mx}})\rho_w + c_{0\mathrm{mx}}\rho_s$. From the above equation, the equilibrium density for the upper layer can be found, namely:

$$\rho_{1\mathrm{eq}} \approx \frac{\rho_w h_T \tan\varphi - h_0 \rho_{0\mathrm{mx}} (\tan\varphi + S_b)}{h_1 (\tan\varphi + S_b)}, \tag{5.4}$$

and, from $c_1 = (\rho_1 - \rho_w)/(\rho_s - \rho_w)$,

$$c_{1\mathrm{eq}} \approx \frac{h_0 \tan\varphi - h_1 S_b - h_0 (\rho_{0\mathrm{mx}}/\rho_w)(\tan\varphi + S_b)}{(s-1) h_1 (\tan\varphi + S_b)}. \tag{5.5}$$

For the aforementioned flow conditions, conservation of momentum for the upper layer (eq. 2.10d) reduces to $\tau^{(i)} = c^{(i)} \rho_{1\mathrm{eq}} (u_{1\mathrm{eq}} - u_0)^2 = -\rho_{1\mathrm{eq}} g h_1 S_b$, yielding:

$$u_{1\mathrm{eq}} = u_{0\mathrm{eq}} + \left(\frac{-g h_1 S_b}{c^{(i)}} \right)^{1/2}, \tag{5.6}$$

where $u_{0\mathrm{eq}} = u_0|_{c_0 = c_{0\mathrm{mx}}}$, can be estimated invoking (4.8), namely:

$$u_{0\mathrm{eq}} = u_0|_{c_0 = c_{0\mathrm{mx}}} = \left[\frac{-g S_b}{c^{(b)}} \left(h_0 + \frac{\rho_w}{\rho_{0\mathrm{mx}}} h_1 \right) \right]^{1/2}. \tag{5.7}$$

Employing equations (5.5)-(5.7), total transport can be computed as:

$$q_T = h_0 \, c_{0\mathrm{mx}} \, u_{0\mathrm{eq}} \; + \; h_1 \, c_{1\mathrm{eq}} \, u_{1\mathrm{eq}}. \tag{5.8}$$

The above analytical solution is next compared against empirical formulae for total transport.

5.2 Validation against empirical formulae

Two empirical expressions for total transport are considered; namely, those of Engelund & Hansen (1967) and van Rijn (1984b) (see Soulsby, 1997). These formulae are selected due to their wide use and because they were originally derived for applications in rivers (steady currents). The following parameters are assumed: $h_T = 10$ m; $D = 0.2$ mm (uniform sediment); $h_0 = 10D$ (hence, $h_1 \gg h_0$ is verified); $c_{0\text{mx}} = 0.25$.

Inspection of the analytical solution derived in the previous section reveals that, for total load, the present model requires two tuning parameters; namely, $c^{(b)}$ and $c^{(i)}$. This additional degree of freedom for calibration (with respect to the case of bedload only) can nonetheless be reduced by proposing a value for the ratio $c^{(b)}/c^{(i)}$ based on hydrodynamic considerations. In §3.2, a methodology has been derived aimed at estimating $c^{(b)}/c^{(i)}$ as function of h_1/h_0 given a velocity profile. For the parameters herein considered (where $h_1/h_0 \approx 5,000$), and assuming that the current follows the velocity profile described by Soulsby (1997), a value of $c^{(b)}/c^{(i)} = 5$ is prescribed. Model calibration for bedload has been carried out in §4.3 (see Fig. 4.2), where it is suggested that $0.01 \leq c^{(b)} \leq 0.06$. Fig. 5.1 compares the predictions obtained by the empirical formulae (considered here) and the present model for values of $c^{(b)}$ =0.05, 0.056, 0.06 and $c^{(b)}/c^{(i)} = 5$.

For values of $c^{(b)} \in [0.05, 0.06]$ and $c^{(b)}/c^{(i)} = 5$ (consistent with the hydrodynamic and bedload calibrations), the present model favours the formula by Engelund & Hansen (1967) over that of van Rijn (1984b). In fact, for $c^{(b)} = 0.056$, the agreement between the model prediction and Engelund & Hansen's formula is outstanding over the range of parameters studied. Note that disagreement between the two empirical expressions considered can reach a factor of up to 2 (this factor increases if other formulae, such

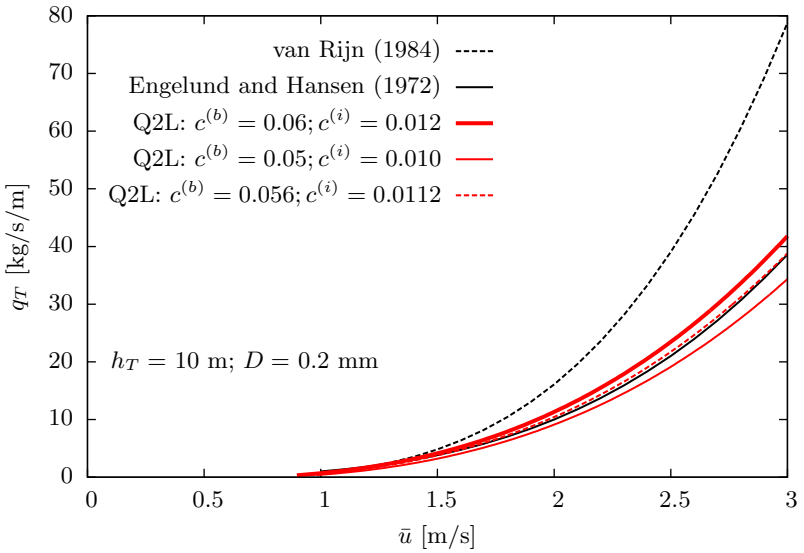

Figure 5.1: Comparison between the Q2L model predictions and empirical formulae for total sediment transport as function of flow average velocity. Three values of $c^{(b)}$ are considered; the ratio of $c^{(b)}/c^{(i)} = 5$ is fixed.

as that of Ackers & White, 1973, are included in the comparison). This level of uncertainty is unlikely to be improved upon significantly, given that inter-comparison of empirical data exhibits a similar degree of accuracy (Soulsby, 1997). At low velocities, the agreement between the model and both formulae is satisfactory. At fast flows, discrepancies become relevant.

If the values for the ratio $c^{(b)}/c^{(i)}$ suggested from hydrodynamic considerations are disregarded (for example, due to lack of information or reliable assumptions about the velocity profile), and both $c^{(b)}$ and $c^{(i)}$ are manipulated independently, the model predictions can be closer to those of van Rijn (1984b). This can be perceived in Fig. 5.2, where $c^{(b)} = 0.04$ and 0.06 (consistent with the bedload calibration) and $c^{(b)}/c^{(i)} = 1.5$ and 2.4 are considered. The agreement with van van Rijn's formula is less satisfactory than that with Engelund & Hansen's expression observed in Fig. 5.1. Nevertheless, the results prove that, if no reliable information(assumptions) about the flow hydrodynamics is accessible(can be made), no conclusions should be drawn regarding what

empirical expression yields the best agreement with the present model. Under such circumstances, the model should be calibrated directly against data for sediment transport rates. However, for practical applications, and in the absence of hydrodynamic and sediment transport information, the recommendation is to assume a standard velocity profile and then follow the methodology described in §3.2 in order to estimate the ratio $c^{(b)}/c^{(i)}$ (Fig. 3.2 can be used as a first approximation for rough hydrodynamic and relatively deep flows; e.g. tidal flows).

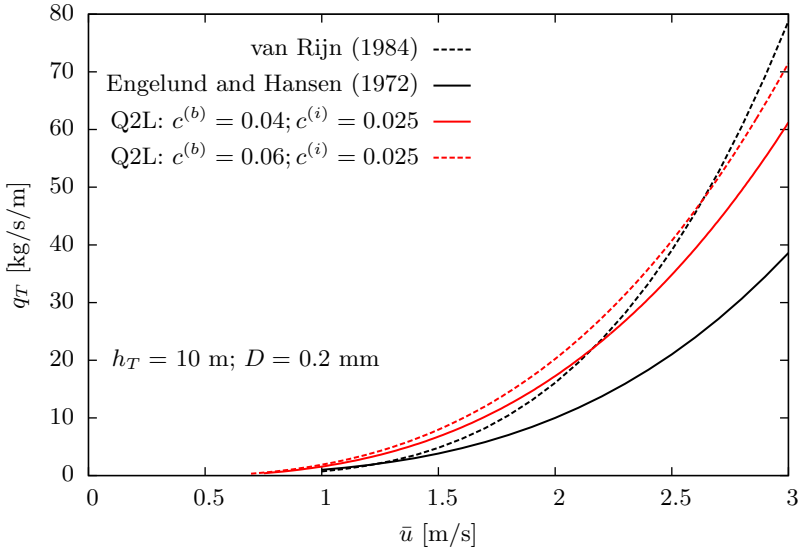

Figure 5.2: Comparison between the Q2L model predictions and empirical formulae for total sediment transport as function of flow average velocity. Values of $c^{(b)} = 0.04$, 0.06 and $c^{(b)}/c^{(i)} = 1.5$, 2.4 are considered.

5.3 Chapter summary

This chapter has illustrated the ability of the model to simulate with acceptable accuracy fast flows over fine-sediment beds, where suspended load is expected to be the predominant mode of transport. Analytical solutions have been derived for the case of steady uniform flow over an erodible bed. For total load, the model required two calibration parameters; namely, $c^{(b)}$ and $c^{(i)}$. The additional degree of freedom (with

respect to Mode 1) represented by $c^{(i)}$ was reduced by utilising prescribed values of the ratio $c^{(b)}/c^{(i)}$ derived in Chapter 3.

The Q2L model has been validated against empirical formulae for total transport obtained by Engelund & Hansen (1967) and van Rijn (1984b). The values for $c^{(b)}$ and $c^{(i)}$ necessary for satisfactory validation of the model are consistent with those found previously from hydrodynamic and bedload calibrations. For values of $c^{(b)}$ and $c^{(b)}/c^{(i)}$, consistent with predictions derived in Chapters 4 and 3, respectively, the model predictions are in very good agreement with the formula by Engelund & Hansen (1967). Agreement with van Rijn (1984b) can nonetheless be improved if values of the ratio $c^{(b)}/c^{(i)}$ derived in Chapter 3 are disregarded, while nevertheless retaining realistic values of both $c^{(b)}$ and $c^{(i)}$.

When dealing with suspended load, the present model should be utilised with care, avoiding, for example, its use for simulation of hyper-concentrated flows (see §2.1). The maximum concentrations simulated in this chapter are in the order of 0.001, well below the hyper-concentrated regime, and so the conclusions achieved herein are valid for dilute concentrations. Also, it should be recalled that analytical solutions for bedload and total load derived in this and the previous chapter, are strictly valid for steady uniform flows exclusively.

So far, mild bed-slopes have been considered. In the following chapter, the effect of steeper bed-slopes on bedload transport is investigated.

Chapter 6

Bed-slope influence on bedload

In the present chapter, the Q2L model is validated against empirical data for bedload in a steep sloping duct, and compared against other methods and semi-empirical expressions derived for sloping channels. The model is then used to undertake a thorough investigation of the bed-slope influence on bedload. Analytical expressions to account for such an influence are proposed. Morphological models using bedload formulae derived for horizontal beds can be enhanced by incorporating slope-related terms derived from the framework of the present model. The chapter concludes with presentation of several case studies and final remarks.

6.1 Introduction

Much of the study on sediment transport (and hydraulics in general) derives originally from considering the fluvial environment. Pioneering works in the field, such as those of Du Boys (1879), Shields (1936), Einstein (1950), and Bagnold (1963)[1], were all based on steady unidirectional flows over mild bed-slopes. The findings from these investigations were later adapted and applied to other environments, such as coastal areas (e.g. Fleming & Hunt, 1976), which are hydrodynamically different from rivers. To achieve this, it was assumed that the sediment motion is solely dependent on the

1. Some of the earliest scientific studies on hydraulics can be traced back to prominent characters such as E. Torricelli (1608–1647), Galileo Galilei (1564–1642) and Leonardo da Vinci (1452–1519) (Graf, 1984).

fluid velocity and that the sediment particle adapts immediately to the local flow velocity (Soulsby, 1997). Even so, this assumption overlooks other fundamental differences between these two environments; namely, that the coastal areas present steeper bed-slopes and the occurrence of adverse flow (i.e. in the up-slope direction, usually due to tide flows or during a swash event). Arguably, the assumption of immediate adaptation of the velocity of the sediment particle to that of the hydrodynamic flow could account for the difference between environments; in other words, the local slope is expected to have an impact on the local velocity. However, it has been shown through laboratory tests that the bed-slope does influence the sediment transport rate for a given flow velocity (e.g. Smart, 1984; Damgaard *et al.*, 1997; Dey & Debnath, 2001). This is unsurprising, considering that this mode of transport takes place very close to the bed, where local gradients in the bed elevation are expected to influence near-bed phenomena (Amoudry & Souza, 2011).

Neglect of the potential influence of bed-slope on bedload transport is justifiable in practice for most problems encountered in river hydraulics, given that the bed-slopes commonly encountered in such environments are very small, in the order of $< 0.05^{\circ}$ (Abbott, 1979). At the coast, however, beach slopes can be as large as $\sim 11^{\circ}$ (Komar, 1998), and so the influence of the bed-slope on sediment transport, and hence on morphological evolution, may not be negligible.

Mountain streams provide another example of environments where the influence of the bed-slope may be very important to predict. Such streams are usually composed of coarse sediments and have bed-slopes that are sufficiently large to affect the overall flow behaviour, including the sediment transport rate (Bayazit, 1983). This is relevant given that bedload is expected to be the predominant mode of transport over beds composed of coarse sediments.

Commonly, the bed-slope influence is accounted for through two methods: (i) Modification of the Threshold of motion for Sloping beds (MTS); and (ii) addition of a slope-related term to the bedload formulae derived for a horizontal channel. In the first approach, the threshold of sediment motion is modified by including a gravity-related component (see e.g. Fernández Luque & van Beek, 1976; Engelund, 1981; Fredsøe & Deigaard, 1992; Soulsby, 1997), which reduces(increases) the critical shear stress for down(up)-sloping beds. The second approach requires an additional empirically-determined (calibration) diffusivity parameter (e.g. Johnson & Zyserman, 2002; Watanabe, 1988), thus further increasing the level of empiricism involved. Alternatives to these approaches include semi-empirical models based on Bagnoldian ideas (e.g. Bagnold, 1963; Bailard & Inman, 1981; Kovacs & Parker, 1994), which are analysed later in this section; and formulae explicitly derived for sloping beds, which often imply a significant degree of empiricism or complexity (e.g. Smart, 1984; Chiari *et al.*, 2010; Parker *et al.*, 2003). Experimental study of bed-slope influence also faces obstacles of a technical nature. For example, uniform flow in open channels is very difficult to achieve on steep slopes and impossible on an adverse slope (Chiew & Parker, 1994; Dey & Debnath, 2001). This is why experiments in steep channels are often conducted in closed ducts. These complexities are reflected by the relative lack of empirical data concerning bedload transport on steep slopes.

In the following section, the Q2L model is validated against empirical data obtained by Damgaard *et al.* (1997) for bedload in steep sloping beds, and compared with the semi-empirical expression for sloping channels by Bagnold (1963) and the MTS-method.

6.2 Validation against empirical data

The model is compared against experimental data measured by Damgaard *et al.* (1997). The data set of Damgaard *et al.* (1997) is selected because it encompasses the widest range of slopes analysed (i.e. approximately ±angle of repose), compared to other studies. For example, Fernández Luque & van Beek (1976) and Smart (1984) considered sediment transport solely over down-sloping beds, whereas Dey & Debnath (2001) worked with a range of $-25^\circ \leq \beta \leq 15^\circ$. It should be noted that studies of sediment transport over transverse slopes (e.g. Sekine & Parker, 1992; Talmon *et al.*, 1995; Dey, 2003; Chen *et al.*, 2010) are not relevant for the 1D-case investigated herein.

The formula by Bagnold (1963) (as presented by Soulsby, 1997, and applicable to sloping beds without additional modifications) is also considered. The MTS-method is investigated, using the Meyer-Peter and Müller formula as a basis.

The experimental conditions reported by Damgaard *et al.* (1997) are replicated; namely: $-29^\circ \leq \beta \leq 30^\circ$; $D = 0.208$mm; $\rho_s = 2630$ kg/m^3; $\varphi = 32.1^\circ$; θ =0.11, 0.18 and 0.33. To avoid uncertainties within the present model related to the definition of the non-dimensional bed shear stress, θ (see §4.2.1), the validation is carried out in dimensional form. The conventional definition $\theta \equiv \tau/[\rho_w g(s-1)D]$ $(= \tau_0^{(b)}/[\rho_w g(s-1)D])$, is used for the conversion into dimensional quantities. For the calibration of both the Q2L model and Bagnold's formula, the criterion is to optimise the fit to the experimental data for the horizontal cases ($\beta = 0$). In both approaches, a single tuning parameter is required – the 'transport efficiency factor' for Bagnold's formula and $c^{(b)}$ for the Q2L model. For the present model, a value of $c^{(b)} = 0.07$ yields the best results, which is close to the values found during the validation undertaken in §4.3. The modification of the threshold of motion for sloping beds, which defines the MTS-method but is

required also by both the Q2L model (where the analytical solution given by eq. 4.21 is employed) and Bagnold's formula, arises from the contribution of gravity to the resting particle, leading to:

$$\frac{\tau_{c\beta}}{\tau_{ch}} = \frac{\sin(\varphi+\beta)}{\sin\varphi}, \tag{6.1}$$

where $\tau_{c\beta}$ represents the threshold of motion for an arbitrary sloping bed, and τ_{ch} is the threshold of motion for a horizontal channel. Recall that a negative(positive) value of β denotes down(up)-sloping bed. Relationship (6.1) is widely used as a means by which to account for the influence of the slope on bedload transport (see e.g. Fernández Luque & van Beek, 1976; Engelund, 1981; Fredsøe & Deigaard, 1992; Soulsby, 1997).

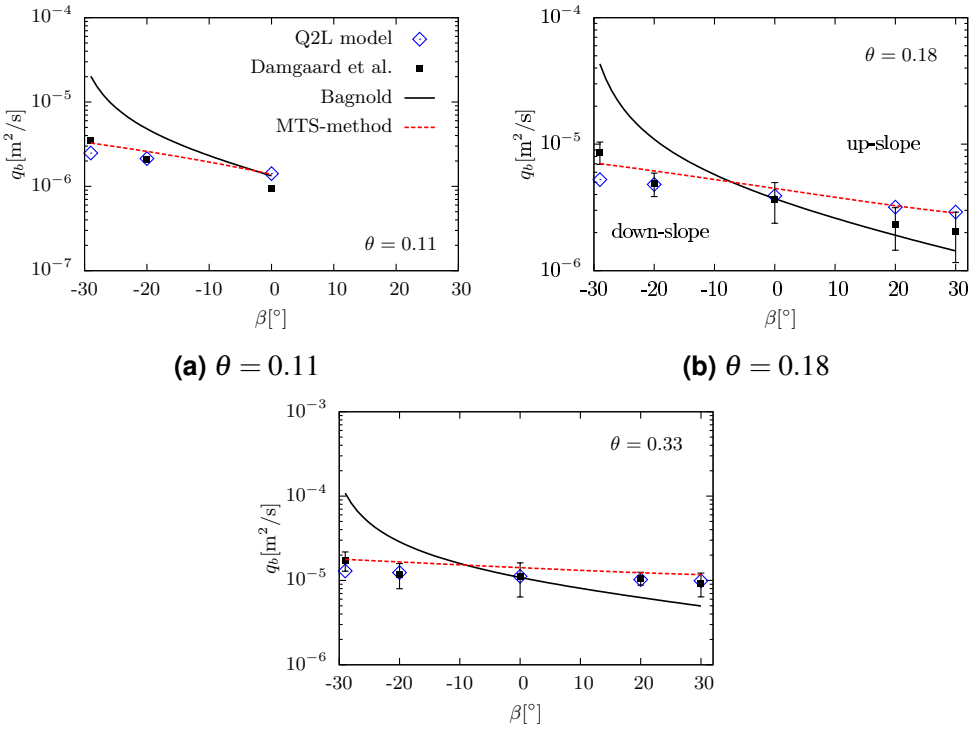

(a) $\theta = 0.11$ **(b)** $\theta = 0.18$

(c) $\theta = 0.33$

Figure 6.1: Comparison between dimensional bedload for sloping channels predicted by the Q2L model against experimental data from Damgaard *et al.* (1997) and the approaches by Bagnold (1963) and the MTS-method, for three values of the bed shear stress. Negative(positive) values of β denote down(up)-sloping beds.

Fig. 6.1 compares the model predictions of bedload transport rate versus bed-slope for different values of non-dimensional bed shear stress, against the empirical data by Damgaard *et al.* (1997), the semi-empirical formula by Bagnold (1963) and the MTS-method based on the Meyer-Peter and Müller formula. Bagnold's formula overestimates significantly the bedload for down-sloping conditions, as previously observed by Damgaard *et al.* (1997). The MTS-method yields good agreement with the experimental data, with a slight tendency to overestimate q_b as compared to the empirical mean values, except for the case of steep negative slopes.

The Q2L model predictions are in very good agreement with experimental data, with the estimates falling within the range of values reported by Damgaard *et al.* in most cases. Certain discrepancies can be observed near the angle of repose for down-sloping beds; however, such differences are smaller than a factor of 2, which is a very good level of accuracy for sediment transport predictions (Amoudry & Souza, 2011). A potential explanation for the discrepancies near $\beta = -\varphi$ may be found in the significant uncertainty involved in the estimation of the threshold of motion for steep-sloping channels (Chen *et al.*, 2010). Chiew & Parker (1994) analysed experimentally the incipient motion of sediment in channels with slopes of $-10^\circ \leq \beta \leq 31^\circ$, concluding that, in general, the relationship given by eq. (6.1) reproduces correctly the influence of bed-slope on the threshold of motion, except for steep adverse slopes. However, although not remarked upon by Chiew & Parker (1994), their data also suggest that eq. (6.1) may not represent accurately the influence of slope for cases involving steep down-sloping beds. This observation is further supported by empirical data reported by Whitehouse & Hardisty (1988), who carried out similar experiments[2]. Furthermore,

2. Note that the lack of accuracy in the estimation of the threshold of motion for steep adverse slopes is less relevant than for steep down-sloping beds. This is because larger values of the bed shear stress are required on steep adverse slopes in order for sediment to entrain motion. However, for these conditions, hydrodynamic forces become dominant in promoting sediment-transport and so the bed-slope influence tends to vanish. The opposite can be said about steep down-sloping slopes.

Bathurst *et al.* (1983) argues that in steep channels with a small ratio of h_T/D the Shields curve fails to predict accurately the initiation of sediment motion.

The Q2L model yields better agreement with the empirical data for larger values of bed shear stress than the MTS-method.

A cautionary remark has to be made regarding the use of the model for problems involving steep slopes. The present model follows the fundamental assumptions underlying the classical Shallow Water Equations (see e.g. Abbott, 1979; Falconer, 1993), including the assumption of a mild slope such that $\sin\beta \approx \tan\beta \approx \beta$. For sufficiently steep slopes ($|\beta| \gtrsim 20°$) this assumption does not hold any more, and the governing equations (eqs. 2.10) should be modified accordingly (see e.g. Denlinger & O'Connell, 2008; Hergarten & Robl, 2015; Ancey *et al.*, 2008; Pritchard, 2005). Note, however, that the analytical solution plotted in Fig. 6.1 (eq. 4.21) is derived as a direct function of the bed shear stress, and so the conclusions herein achieved remain valid, as long as (in practice) the bed shear stress is estimated accurately for a sloping channel.

The bed-slope influences predicted by the approaches considered herein are investigated in more detail next.

6.3 Quantification of the bed-slope influence

The model is now used to derive analytical expressions to quantify the influence of bed-slope on bedload transport. Two approaches are examined; namely, (i) as a function of the transport stage; and (ii) as a function of the bed shear stress.

6.3.1 Bed-slope influence as function of transport stage

The bed-slope influence, for a given transport stage, is defined as:

$$\Pi_T \equiv \frac{q_b\big|_{\tau_c=\tau_{c\beta},\tau_0^{(b)}=T\tau_{c\beta}}}{q_b\big|_{\beta=0.\because\tau_c=\tau_{ch},\tau_0^{(b)}=T\tau_{ch}}}, \tag{6.2}$$

where T represents the transport stage, defined as:

$$T \equiv \frac{\tau_o^{(b)}}{\tau_c}, \tag{6.3}$$

with $\tau_c = f(\beta,\varphi)$. Thus $\tau_c = \tau_c(\beta,\varphi) = \tau_{c\beta}$ and $\tau_c(\beta=0,\varphi) = \tau_{ch}$. Hereinafter, subscripts β and h refer to arbitrary and horizontal beds, respectively.

By invoking eq. (4.21), the bed-slope influence is given by:

$$\Pi_T \equiv \frac{q_b\big|_{\tau_c=\tau_{c\beta},\tau_0^{(b)}=T\tau_{c\beta}}}{q_b\big|_{\beta=0.\because\tau_c=\tau_{ch},\tau_0^{(b)}=T\tau_{ch}}} = \frac{(T\tau_{c\beta}-\tau_{c\beta})}{(T\tau_{ch}-\tau_{ch})}\left(\frac{T\tau_{c\beta}\,\rho_{0h}}{\rho_{0\beta}\,T\tau_{ch}}\right)^{1/2}$$

$$\Rightarrow \Pi_T = \left(\frac{\rho_{0h}}{\rho_{0\beta}}\right)^{1/2}\left(\frac{\tau_{c\beta}}{\tau_{ch}}\right)^{3/2},$$

or

$$\Pi_T = \Pi_1^{1/2}\Pi_2^{3/2}, \tag{6.4}$$

where $\Pi_1 = \rho_{0h}/\rho_{0\beta}$ and $\Pi_2 = \tau_{c\beta}/\tau_{ch}$. The ratio $\rho_{0h}/\rho_{0\beta}$ can be expressed (by means of eq. 4.18) as:

$$\Pi_1 = \frac{\rho_{0h}}{\rho_{0\beta}} = \frac{T\tau_{ch} + \rho_w g h_0 \tan\varphi - \tau_{ch}}{T\tau_{c\beta} + \rho_w g h_0 \tan\varphi - \tau_{c\beta}}$$

$$= \frac{(T-1)\tau_{ch} + \rho_w g h_0 \tan\varphi}{(T-1)\tau_{c\beta} + \rho_w g h_0 \tan\varphi}. \tag{6.5}$$

Note that the subscript 'eq' originally present in equations derived in §4.1.3, standing for the equilibrium state, has been dropped for convenience. Substituting (6.5) in (6.4), the latter can be written as:

$$\Pi_T = \left[\frac{(T-1)\tau_{ch} + \rho_w g h_0 \tan\varphi}{(T-1)\tau_{c\beta} + \rho_w g h_0 \tan\varphi}\right]^{1/2} \left(\frac{\tau_{c\beta}}{\tau_{ch}}\right)^{3/2}. \tag{6.6}$$

As observed in the above equation, the bed-slope influence depends on several parameters other than β; i.e. T, h_0, φ and τ_{ch}. To assess the sensitivity of eq. (6.6) to these parameters, the following values are considered: $D = 0.5$ and 2.0 mm; $s = 2.63$ (τ_{ch} depends on D and s); $h_0 = 5D$ and $15D$; $T = 2$, 6, 10 and 14 (for sufficiently large values of T the influence of the slope vanishes; see e.g. Damgaard *et al.*, 1997); and φ =31, 34 and 37° (i.e. typical values for sand; Chiew & Parker, 1994).

Fig. 6.2 depicts the 48 combinations generated. Three families of curves are produced corresponding to the three values of φ considered, illustrating that the dominant parameter in the bed-slope influence (as defined by eq. 6.2) is the angle of repose. To further investigate sensitivity to the other parameters, $\Pi_1^{1/2}$ is plotted in Fig. 6.3 for the representative value of $\varphi = 32°$, with the other parameters (i.e. T, h_0 and D) retaining their aforementioned values. Fig. 6.3 demonstrates that for all cases considered, the value of the term $\Pi_1^{1/2}$ falls in the range of $1 \pm 12\%$, hence contributing relatively little to the overall bed-slope influence, Π_T. Note that Π_2 is solely dependent on β

and φ (see eq. 6.1). The largest deviations from unity in $\Pi_1^{1/2}$ can be observed for increasing values of T. However, it should be remarked that for increasing bed-shear conditions (and hence, increasing T), the influence of bed-slope on bedload is eclipsed by the effect of the hydrodynamics (as shown later in this section). An increasing value of h_0/D (for a given D) tends to reduce the influence of $\Pi_1^{1/2}$. The term $\Pi_1^{1/2}$ is relatively insensitive to the selection of D (as compared to the choice of h_0/D). A curve corresponding to the suggested default value of h_0, $h_0 = 10D$ (see §4.4) has also been included for $T = 14$ and $D = 2.0$ mm, which maximises the value of $\Pi_1^{1/2}$ within the range of values considered. For $h_0 = 10D$, $\Pi_1^{1/2}$ falls within a range of $1 \pm 6\%$.

The influence of the slope on bedload is expected to reach a maximum at conditions near the threshold of motion (i.e. $T \to 1$). For relatively small slopes, a good approximation of the bed-slope influence can then be proposed by considering $\Pi_1^{1/2} \approx 1$, yielding:

$$\Pi_T \approx \left(\frac{\tau_{c\beta}}{\tau_{ch}} \right)^{3/2}. \tag{6.7}$$

This expresses the bed-slope influence as a simple function solely of β and φ.

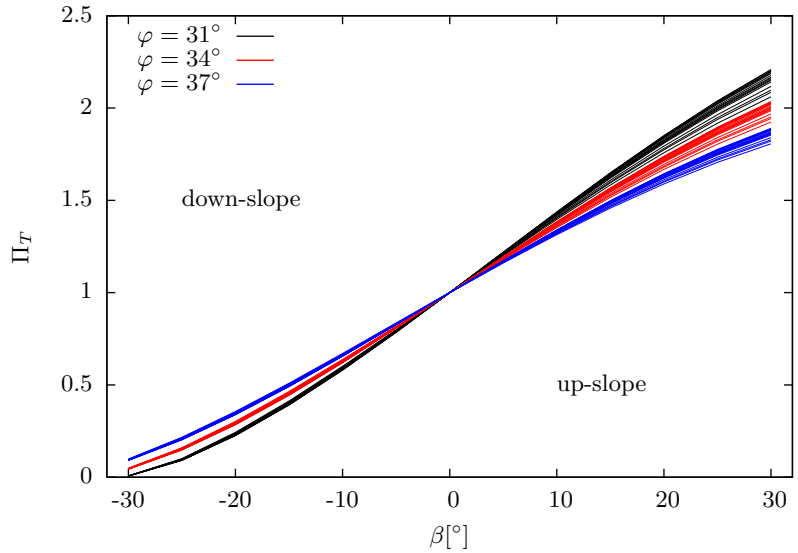

Figure 6.2: Bed-slope influence on bedload for a given transport stage vs bed-slope angle. Forty-eight curves (generated from combinations of different values of φ, T, h_0 and D) are plotted, grouped into three families corresponding to the three values of φ analysed.

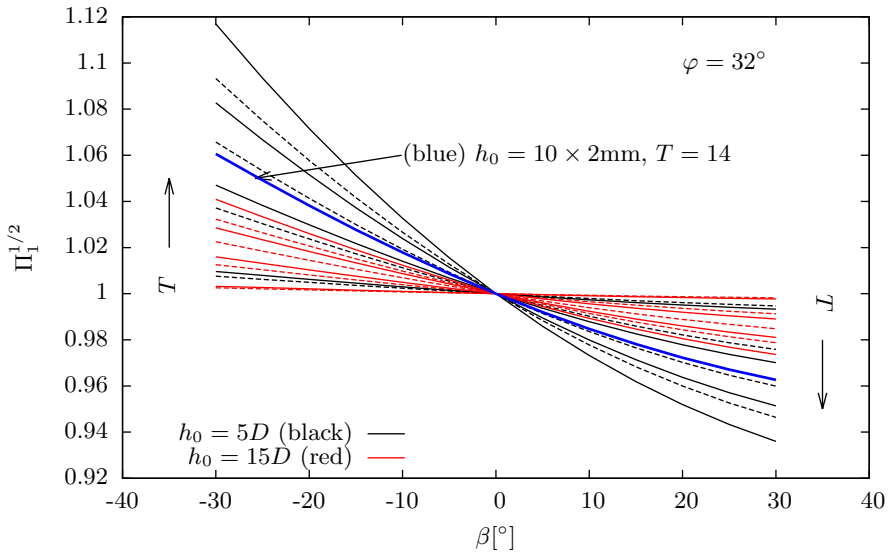

Figure 6.3: $\Pi_1^{1/2}$ vs bed-slope angle, for $\varphi = 32°$. Dashed(continuous) lines correspond to $D = 0.5(2.0)$ mm; black(red) colour represents $h_0 = 5D(15D)$. Increasing values of T are in the directions indicated by the vertical arrows.

Misinterpretation of Fig. 6.2 could lead to the erroneous conclusion that the bed-slope influence (derived in this section) does not vanish for up-sloping beds, as it should

according to previous studies (e.g. Damgaard *et al.*, 1997). However, attention ought to be paid to the present definition of bed-slope influence, Π_T; i.e. as the ratio of the bedload on an arbitrary slope to the bedload on a horizontal bed, for a given transport stage, T (see eq. 6.2). Fig. 6.4 depicts the model predictions of bedload against bed shear stress, for different bed-slopes, illustrating the vanishingly small effect of bed-slope for increasing bed shear stress, in agreement with experimental findings. This property is further confirmed in the next section.

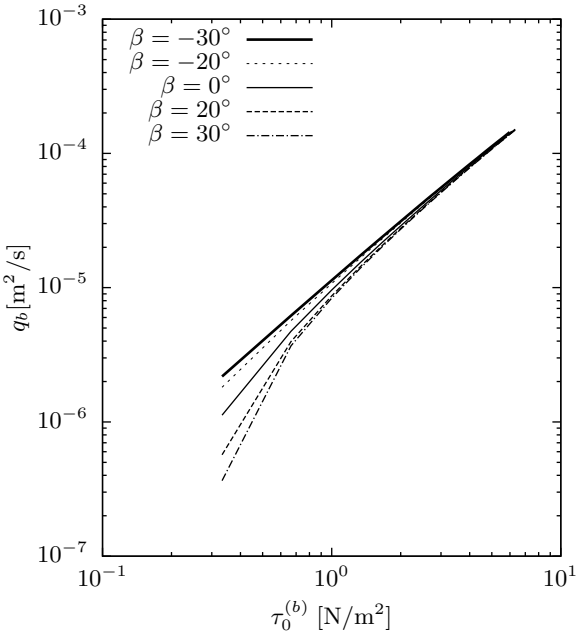

Figure 6.4: Model predictions for bedload vs bed shear stress for different bed-slopes.

6.3.2 Bed-slope influence as function of bed shear stress

Empirical formulae for bedload tend to be expressed as functions of the bed shear stress instead of the transport stage, and so it is worth analysing the influence of bed-slope for a fixed value of bed shear stress. This facilitates a comparison between the bed-slope influence predicted by the Q2L model and other methods (see §6.3.3). The bed-slope influence as a function of the bed shear stress is defined as:

$$\Pi_{\tau_0} \equiv \frac{q_b|_{\tau_c=\tau_{c\beta}}}{q_b|_{\beta=0 \therefore \tau_c=\tau_{ch}}}. \tag{6.8}$$

Through (4.21), which is derived as a function of $\tau_0^{(b)}$, the above equation becomes:

$$\Pi_{\tau_0} = \frac{(\tau_0^{(b)} - \tau_{c\beta})}{(\tau_0^{(b)} - \tau_{ch})} \left(\frac{\tau_0^{(b)}}{\rho_{0\beta} c^{(b)}} \frac{\rho_{0h} c^{(b)}}{\tau_0^{(b)}} \right)^{1/2}$$

$$\Rightarrow \Pi_{\tau_0} = \left(\frac{\rho_{0h}}{\rho_{0\beta}} \right)^{1/2} \left(\frac{\tau_0^{(b)} - \tau_{c\beta}}{\tau_0^{(b)} - \tau_{ch}} \right)$$

$$= \Pi_3^{1/2} \Pi_4, \tag{6.9}$$

where $\Pi_4 = (\tau_0^{(b)} - \tau_{c\beta})/(\tau_0^{(b)} - \tau_{ch})$ and $\Pi_3 = \rho_{0h}/\rho_{0\beta}$ is equal to (using eq. 4.18):

$$\Pi_3 = \frac{\rho_{0h}}{\rho_{0\beta}} = \frac{\tau_0^{(b)} + \rho_w g h_0 \tan\varphi - \tau_{ch}}{\tau_0^{(b)} + \rho_w g h_0 \tan\varphi - \tau_{c\beta}}. \tag{6.10}$$

Combination of (6.9) and (6.10) yields:

$$\Pi_{\tau_0} = \left(\frac{\tau_0^{(b)} + \rho_w g h_0 \tan\varphi - \tau_{ch}}{\tau_0^{(b)} + \rho_w g h_0 \tan\varphi - \tau_{c\beta}} \right)^{1/2} \left(\frac{\tau_0^{(b)} - \tau_{c\beta}}{\tau_0^{(b)} - \tau_{ch}} \right). \tag{6.11}$$

Note that $\Pi_1 \neq \Pi_3$ and $\Pi_T \neq \Pi_{\tau_0}$. Similar to its analogue derived in the previous section (see eq. 6.6), the above equation depends on other variables besides β; namely: τ_{ch}, $\tau_0^{(b)}$, φ and h_0. Hence, a sensitivity analysis is undertaken assuming the following values: $D = 0.5$ and 2.0 mm; $s = 2.63$; $h_0 = 5D$ and $15D$; $\tau_0^{(b)}/\tau_{ch}$ (not to be confused with $T \equiv \tau_0^{(b)}/\tau_{c\beta}$) = 2, 5 and 20; and φ =31 and 37°. Fig. 6.5 shows the results of the sensitivity analysis. The bed-slope influence seems to be governed by the bed shear

stress and the angle of repose, and appears to be insensitive to the selection of D and h_0/D within the ranges of values considered. The bed-slope influence also vanishes ($\Pi_{\tau_0} \to 1$) for large values of the bed shear stress, in agreement with experimental findings reported in the literature. This can be mathematically confirmed. Eq. (6.11) can be rewritten as:

$$\Pi_{\tau_0} = \left(\frac{\tau_0^{(b)} + \rho_w g h_0 \tan\varphi - \tau_{ch}}{\tau_0^{(b)} + \rho_w g h_0 \tan\varphi - \tau_{c\beta}} \right)^{1/2} \left(\frac{1/\tau_0^{(b)}}{1/\tau_0^{(b)}} \right)^{1/2} \left(\frac{\tau_0^{(b)} - \tau_{c\beta}}{\tau_0^{(b)} - \tau_{ch}} \right) \left(\frac{1/\tau_0^{(b)}}{1/\tau_0^{(b)}} \right)$$

$$= \left(\frac{1 + \rho_w g h_0 \tan\varphi/\tau_0^{(b)} - \tau_{ch}/\tau_0^{(b)}}{1 + \rho_w g h_0 \tan\varphi/\tau_0^{(b)} - \tau_{c\beta}/\tau_0^{(b)}} \right)^{1/2} \left(\frac{1 - \tau_{c\beta}/\tau_0^{(b)}}{1 - \tau_{ch}/\tau_0^{(b)}} \right),$$

and so it can be seen that,

$$\lim_{\tau_0^{(b)} \to \infty} \Pi_{\tau_0} = 1\,.$$

To study further the sensitivity of Π_{τ_0} to D and h_0, Fig. 6.6 plots the variation of $\Pi_3^{1/2}$ with bed-slope (Π_4 does not depend on D and h_0). Fig. 6.6 illustrates that for all combinations of the values herein considered, $\Pi_3^{1/2}$ falls in the range of $1\pm \sim 1\%$, which justifies the assumption of $\Pi_3^{1/2} \approx 1$, hence simplifying the bed-slope influence as a function of the bed shear stress as:

$$\Pi_{\tau_0} \approx \frac{\tau_0^{(b)} - \tau_{c\beta}}{\tau_0^{(b)} - \tau_{ch}}. \tag{6.12}$$

Note that the above equation is solely dependent on β, φ and the bed shear stress, $\tau_0^{(b)}$.

It also worth remarking that the expressions herein derived for quantifying the bed-slope influence on bedload are independent of the calibration parameter $c^{(b)}$.

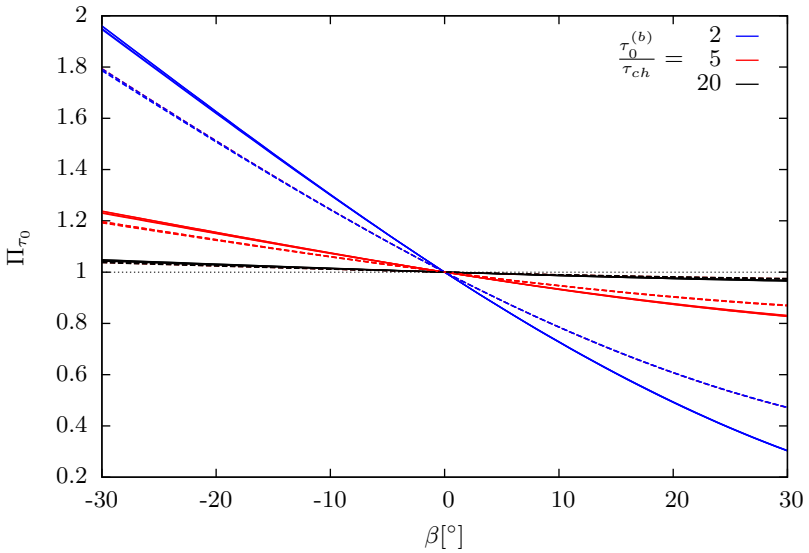

Figure 6.5: Bed-slope influence on bedload for a given bed shear stress vs bed-slope angle. Twenty-four curves (generated from the combinations of the different values of φ, $\tau_0^{(b)}/\tau_{ch}$, h_0 and D considered) are plotted, grouped in six families corresponding to the six combinations of φ and $\tau_0^{(b)}/\tau_{ch}$ analysed. Solid(dashed) lines correspond to $\varphi = 31(37)^\circ$; blue, red and back colours represent $\tau_0^{(b)}/\tau_{ch} = 2$, 5 and 20, respectively.

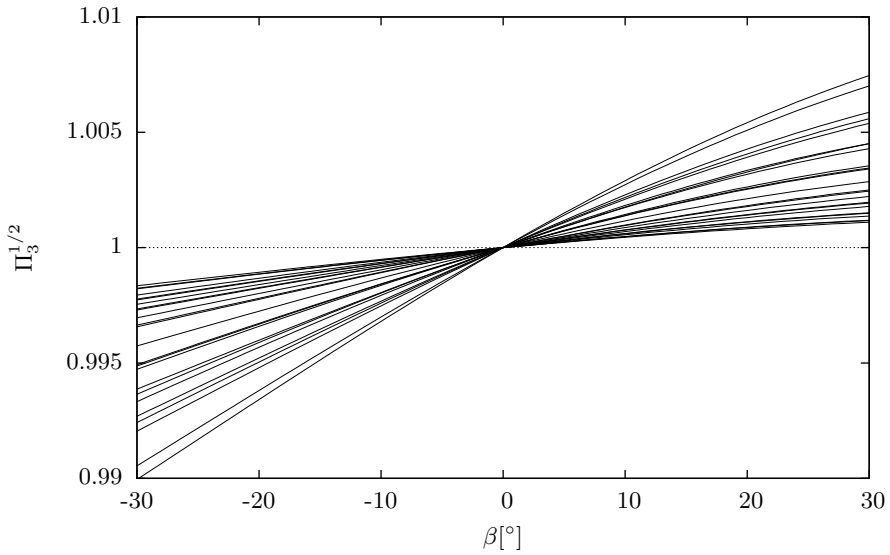

Figure 6.6: $\Pi_3^{1/2}$ vs bed-slope angle, for all combinations of φ, $\tau_0^{(b)}/\tau_{ch}$, h_0 and D considered.

6.3.3 Comparison against other predictors of the bed-slope influence

The bed-slope influence predicted by the present model is now compared against that obtained using the following approaches: (i) the expression proposed by Damgaard *et al.* (1997), derived on the basis of their own experimental observations; (ii) the MTS-method applied to the Meyer-Peter and Müller formula; and (iii) the formula for sloping channels by Bagnold (1963).

The comparison is first undertaken adopting the definition of bed-slope influence given by (6.8) (as a function of the bed shear stress), and applying it to each of the aforementioned approaches. Parameters reported in the experiments by Damgaard *et al.* (1997) are employed, including the values of the non-dimensional bed shear stress, θ (= 0.11, 0.18 and 0.33). The results of the comparison are shown in Fig. 6.7. An ability to predict the vanishing effect of the slope for adverse slopes is common to all approaches. The tendency of Bagnold's formula to overestimate the slope influence in down-sloping beds is further confirmed and clearly illustrated.

For the sake of clarity, Bagnold's model is excluded from Fig 6.8, where the influence of the particle diameter is also analysed. For the second particle diameter ($D = 2.0$ mm), values of $\tau/\tau_{ch} = \theta/\theta_{ch} = [0.11, 0.18, 0.33]/0.05$ ($\theta_{ch} \approx 0.05$ in Damgaard *et al.*'s experiments) are considered. Fig. 6.8 shows that the influence of D (which only affects the estimation of τ_c) is negligible. The behaviour followed by Damgaard *et al.*'s predictor diverges from that of the other two approaches for steep down-sloping beds. This is in agreement with the tendency of the present model and the MTS-method to underestimate the bedload reported by Damgaard *et al.* (1997) for steep negative slopes, as remarked upon in §6.2. This discrepancy between the MTS-method and the

Q2L model, and the experimentally-based expression derived by Damgaard *et al.* may be caused by uncertainty in the estimation of $\tau_{c\beta}$ via eq. (6.1), as discussed in §6.2.

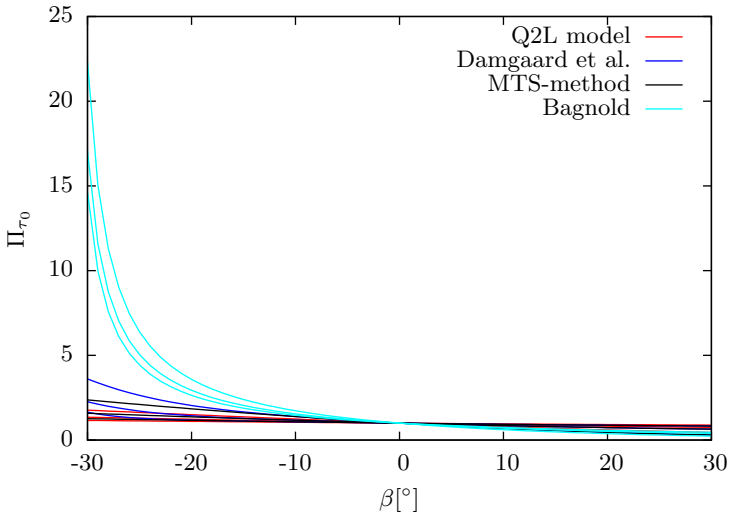

Figure 6.7: Comparison between different slope-influence predictors vs bed-slope angle for different bed shear stresses.

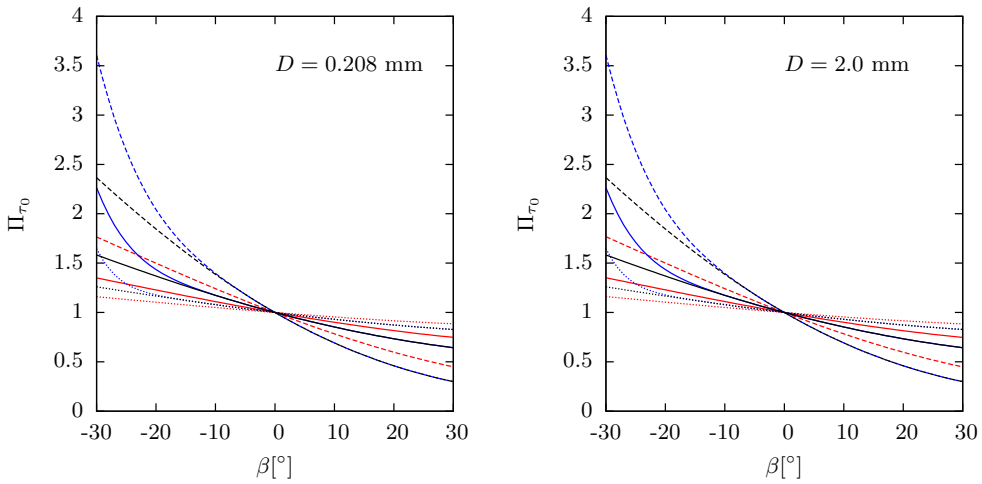

Figure 6.8: Comparison between different slope-influence predictors (Bagnold's approach excluded) vs bed-slope angle for three different bed shear stresses and two particle diameters. Dashed, solid and dotted lines correspond to $\tau/\tau_{ch} = 2.2$, 3.6 and 6.6, respectively. Colours as in Figure 6.7.

To analyse further the bed-slope influence predicted by the different approaches, the

slope influence as a function of the transport stage (eq. 6.2) is now considered. This allows us to express the bed-slope influence predicted by all approaches considered in the following form:

$$\Pi_T = F_\beta \left(\frac{\tau_{c\beta}}{\tau_{ch}} \right)^{3/2}, \tag{6.13}$$

where,

$$F_\beta = \begin{cases} \left[\frac{(T-1)\tau_{ch} + \rho_w g h_o \tan\varphi}{(T-1)\tau_{c\beta} + \rho_w g h_o \tan\varphi} \right]^{1/2} & \text{for Q2L model} \\ f_\beta & \text{for Damgaard } \textit{et al.} \\ 1 & \text{for MTS-method} \\ \left(\frac{\tan\varphi}{\tan\varphi + \tan\beta} \right) & \text{For Bagnold} \end{cases}, \tag{6.14}$$

and,

$$f_\beta = \begin{cases} 1 + 0.8 \left(\frac{\tau_{ch}}{T\tau_{c\beta}} \right)^{0.2} \left(1 - \frac{\tau_{c\beta}}{\tau_{ch}} \right)^{(1.5 + T\tau_{c\beta}/\tau_{ch})} & \text{for } -\varphi < \beta \leq 0 \\ 1 & \text{for } 0 < \beta < \varphi \end{cases}. \tag{6.15}$$

By comparing the different slope-influence predictors using Π_T instead of Π_{τ_0}, a potential bias (possibly present in Figures 6.7 and 6.8) is avoided. This potential bias arises from the fact that both Damgaard *et al.*'s predictor and the MTS-method as herein defined utilise the Meyer-Peter and Müller formula as a basis. However, when defining the slope-influence as a function of the transport stage instead of the bed shear stress, this fact becomes irrelevant given that any empirical bedload formula that complies

with the condition of $\Phi \propto \theta^{3/2}$ for $\theta \gg \theta_c$ ($\because \theta - \theta_c \approx \theta$) would lead to an expression for slope-influence of the form of (6.13). It should be noted that most bedload formulae indeed comply with this condition; e.g. Meyer-Peter & Müller (1948), Bagnold (1963), Yalin (1963), Ashida & Michue (1972), Wilson (1966), Nielsen (1992), Fernández Luque & van Beek (1976), Soulsby (1997).

The term F_β in (6.13) represents the differentiating factor between the different approaches considered. For this reason, the behaviour of F_β for all predictors and for different transport stages (note that only for the cases of Damgaard *et al.* and the Q2L model, F_β depends on T) and $\varphi = 32.1^\circ$ is analysed in Fig. 6.9. The term F_β has been divided by $(\tau_{c\beta}/\tau_{ch})^{3/2}$ in order to compare the magnitude of both multiplicands in (6.13). Fig. 6.9 further confirms the remarks made before in this section; namely: the slope influence predicted by Damgaard *et al.* (1997), the MTS-method and the Q2L model lead to similar results, and these predictions are significantly different from those derived from Bagnold's formula. The largest discrepancies between the present model and Damgaard *et al.*'s approach are found near $\beta = -\varphi$ (steep negative slopes); however, such discrepancies never exceed a factor of 2. For a increasing bed shear stress, the difference between these two approaches decreases. For steep negative slopes, F_β becomes significantly larger (up to two orders of magnitude) than $(\tau_{c\beta}/\tau_{ch})^{3/2}$, whereas for adverse slopes, $F_\beta \sim (\tau_{c\beta}/\tau_{ch})^{3/2}$, for all predictors herein studied.

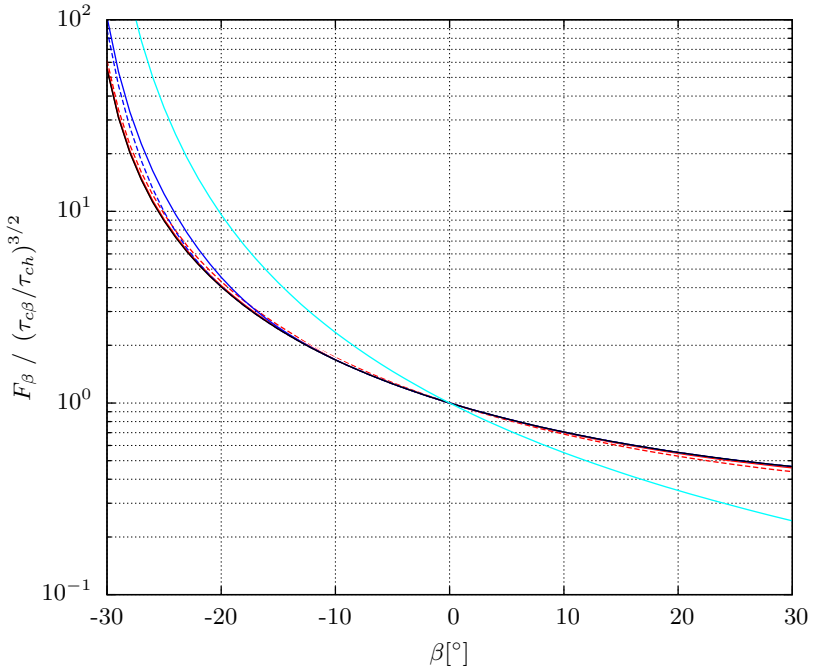

Figure 6.9: Differentiating term between various bed-slope-influence predictors, F_β, divided by $(\tau_{c\beta}/\tau_{ch})^{3/2}$, vs bed-slope angle for different transport stages. Dashed lines correspond to $T = 20$; solid lines correspond to $T = 2$ and 5 (discrepancies not perceivable). Colours as in Figure 6.7.

Overall, the present model appears to capture correctly the influence of the bed-slope on bedload transport, as illustrated by the comparison against the empirical data and experimentally-derived expression for bedload on steep channels from Damgaard *et al.* (1997). The predictor for the bed-slope influence derived from the Q2L model vanishes for large bed shear stresses (and steep adverse slopes, which often imply large values of $\tau_0^{(b)}$), and small bed-slopes, in agreement with laboratory findings. It has been shown that the choice of expressing the slope-influence as a function of the transport stage or the bed shear stress is relevant, and one option may be more convenient than the other depending on the application. This is further exemplified in the next section.

6.4 Slope-related diffusivity parameters

A common practice to account for the influence of the slope is to modify the bedload formulae originally derived for horizontal channels, by adding a term that promotes(inhibits) sediment transport in down(up)-sloping beds (see e.g. Johnson & Zyserman, 2002; Watanabe, 1988; Bailard & Inman, 1981). Such a term is proportional to the bed-slope, and can be added as follows:

$$q_{b\beta} = q_{bh} + \varepsilon |q_{bh}| S_b, \tag{6.16}$$

where $S_b = \partial z_b / \partial x = \tan\beta$ is the local bed-slope, and ε is a proportionality parameter related to diffusion, often taken as an additional tuning parameter in morphological models (Johnson & Zyserman, 2002; Watanabe, 1988), thus further increasing their level of empiricism. The modifying term $\varepsilon |q_{bh}| S_b$ vanishes for small slopes and acts (thanks to $|q_{bh}|$) in the direction of the bed-slope, promoting(inhibiting) bedload for down-sloping(adverse) beds. Eq. (6.16) can be rewritten (assuming for convenience a positive unidirectional flow; i.e. $\bar{u} > 0 \therefore q_{bh} > 0$) as:

$$\frac{q_{b\beta}}{q_{bh}} = 1 + \varepsilon S_b. \tag{6.17}$$

The above equation represents the equation of a line, where the ratio $q_{b\beta}/q_{bh}$ is the dependent variable, S_b represents the independent variable, ε is the slope of the line, and the y-intercept is equal to 1. From Figures 6.2 and 6.5, it can be observed that the expressions herein derived for $q_{b\beta}/q_{bh}$ (i.e. Π_T and Π_{τ_0}), exhibit linear behaviour for a relatively wide range of β consistent with (6.17). Thus, expressions for ε can be proposed based on the bed-slope influence predicted by the present model, as detailed next.

6.4.1 Diffusivity parameter from Π_T

For a given set of parameters, the bed-slope influence as a function of T varies linearly with β (for small angles, $\beta \approx \tan\beta$) for values of the bed-slope near $\beta = 0$ (see Fig. 6.2). Hence, the diffusivity parameter can be found from the slope of the bed-slope-influence curve at the origin; namely:

$$\varepsilon_T = \frac{\partial \Pi_T}{\partial S_b}\Big|_{\beta=0}. \tag{6.18}$$

As discussed previously in this chapter, the bed-slope influence vanishes for large values of the bed shear stress (and hence T). For small values of T and β, eq. (6.7) can be used to approximate the bed-slope influence, Π_T, yielding:

$$\frac{\partial \Pi_T}{\partial S_b} = \frac{3}{2}\left(\frac{\tau_{c\beta}}{\tau_{ch}}\right)^{1/2} \frac{\partial(\tau_{c\beta}/\tau_{ch})}{\partial S_b}. \tag{6.19}$$

Invoking (6.1),

$$\frac{\partial(\tau_{c\beta}/\tau_{ch})}{\partial S_b} = \frac{\partial}{\partial \tan\beta}\left[\frac{\sin(\varphi+\beta)}{\sin\varphi}\right] = \frac{\cos(\varphi+\beta)}{\sin\varphi}\frac{\partial(\varphi+\beta)}{\partial\tan\beta}$$

$$= \frac{\cos(\varphi+\beta)}{\sin\varphi}\cdot\frac{\partial\beta}{\partial\tan\beta} = \frac{\cos(\varphi+\beta)}{\sin\varphi}\cdot\frac{1}{\partial\tan\beta/\partial\beta}$$

$$= \frac{\cos(\varphi+\beta)}{\sin\varphi}\cdot\frac{1}{\sec^2\beta} = \frac{\cos(\varphi+\beta)}{\sin\varphi}\cos^2\beta. \tag{6.20}$$

Hence, combining eqs. (6.18) – (6.20) the slope-related diffusivity parameter is given by:

$$\varepsilon_T = \frac{3}{2}\left\{\left[\frac{\sin(\varphi+\beta)}{\sin\varphi}\right]^{1/2}\left[\frac{\cos(\varphi+\beta)}{\sin\varphi}\cos^2\beta\right]\right\}\Bigg|_{\beta=0}$$

$$\Rightarrow\ \varepsilon_T = \frac{3}{2}\cdot\frac{1}{\tan\varphi}. \tag{6.21}$$

Eq. (6.21) represents a constant value dependent solely on the angle of repose. Fig. 6.10 compares the bed-slope influence expressed by the exact solution (6.6) against the approximation given by the line with slope ε_T (eq. 6.21). Values of $T = 2$ and 20 are considered. Near the threshold of motion ($T \to 1$), the linear approximation describes accurately the bed-slope influence predicted by (6.6) for a range of $-0.2 \lesssim \tan\beta \lesssim 0.3$ ($-11° \lesssim \beta \lesssim 17°$). This is fortunate because in practice, steep slopes, such as those found in coastal environments, are of the order of $|\beta| \lesssim 11°$ (Komar, 1998). For increasing T, the range of $\tan\beta$ for which the agreement between (6.6) and the linear approximation is very good, is reduced. Nonetheless, it should be recalled that at sufficiently large values of T (and hence $\tau_0^{(b)}$), accurate prediction of the slope-influence becomes less relevant (see §6.3).

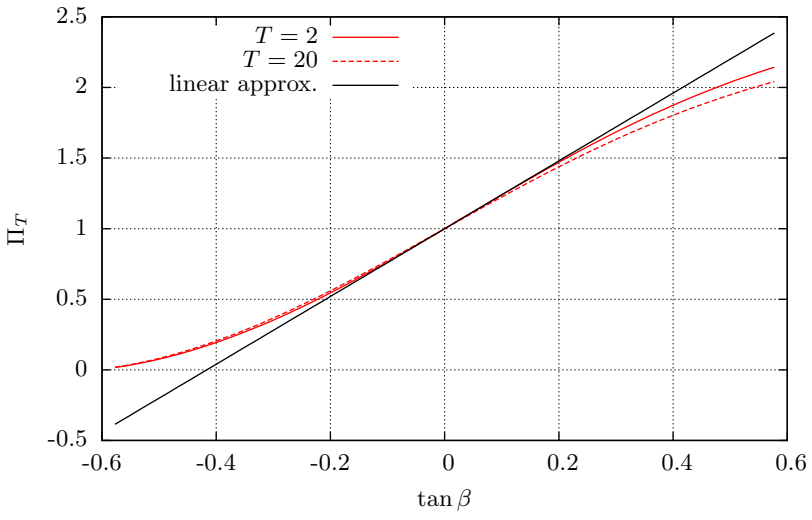

Figure 6.10: Bed-slope influence as function of transport stage vs bed-slope for two values of T ($\varphi = 32°$). Comparison between eq. 6.6 (red curves) and linear approximation.

An alternative expression for ε_T can be derived using eq. (6.6) (i.e. the exact solution for Π_T) instead of the approximation given by (6.7). This yields the following expression:

$$\varepsilon_T = \left\{ \frac{-(T-1)\tau_{ch}}{2[(T-1)\tau_{ch} + \rho_w g h_0 \tan\varphi]} + \frac{3}{2} \right\} \frac{1}{\tan\varphi}. \tag{6.22}$$

Unlike (6.21), eq. (6.22) includes the effect of T. Fig. 6.11 compares Π_T predicted by (6.6) against the line with slope, ε_T, given by (6.22), for two values of T. The lines prescribed by the slope, ε_T, given by (6.22), describe correctly the linear behaviour of (6.6) over a wider range of $\tan\beta$. However, from a pragmatic viewpoint, the improvement presented by (6.22) as compared to (6.21) does not seem to justify the increased complexity involved in the quantification of ε_T. Note that (6.21) depends solely on the constant parameter φ, whereas (6.22) is a function of φ, T, τ_{ch} and h_0. Furthermore, the enhancement proposed by (6.22) becomes relevant at large values of T, precisely where the influence of the bed-slope vanishes. Thus, the potential advantages of estimating the linear approximation to Π_T as a function solely of φ outweigh the relatively small disadvantage of losing some accuracy for large transport stages. Hence, the use of (6.21) over (6.22) is recommended. Note, however, that the linear approximation should not be used for steep negative slopes ($\tan\beta \lesssim -0.3 \therefore \beta \lesssim -17°$). For steep adverse slopes, the linear approximation also loses accuracy; however, this is not so important because steep adverse slopes imply relatively high bed shear stresses (as has been discussed before), and so the slope-influence is expected to vanish (see Fig. 6.4).

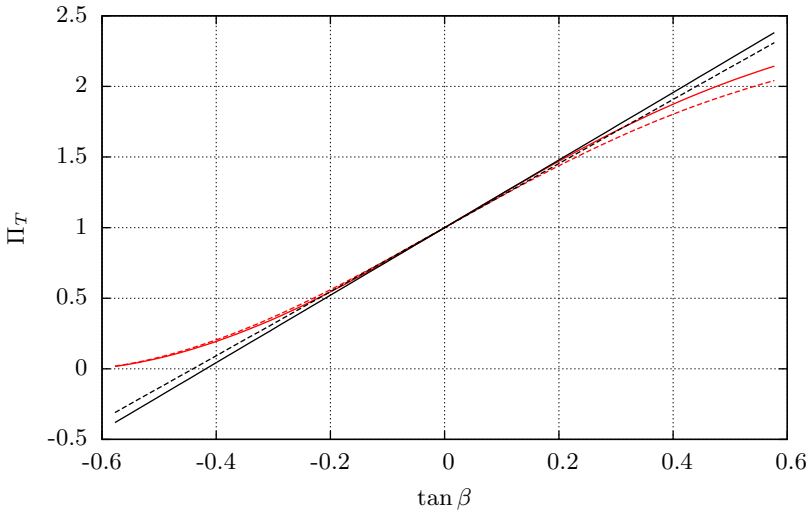

Figure 6.11: Bed-slope influence as function of transport stage vs bed-slope for two values of T ($\varphi = 32°$). Comparison between eq. (6.6) (red curves) and linear approximations with slope, ε_T, given by (6.22) (black lines). Solid(dashed) lines represent $T = 2(20)$.

6.4.2 Diffusivity parameter from Π_{τ_0}

The bed-slope influence defined as a function of $\tau_0^{(b)}$, also exhibits a linear behaviour for a wide range of values of the main governing parameters (i.e. β and $\tau_0^{(b)}$), as depicted in Fig. 6.5. Hence, (6.18) can be used to extract a slope-related diffusivity parameter from the curve Π_{τ_0}, using:

$$\varepsilon_{\tau_0} = \frac{\partial \Pi_{\tau_0}}{\partial S_b}\bigg|_{\beta=0}. \tag{6.23}$$

As demonstrated in §6.3.2, a satisfactory approximation for the slope-influence is given by (6.12), which can be rewritten as follows:

$$\Pi_{\tau_0} \approx \frac{\tau_0^{(b)} - \tau_{c\beta}}{\tau_0^{(b)} - \tau_{ch}} = \frac{\tau_0^{(b)} - \tau_{ch}(\tau_{c\beta}/\tau_{ch})}{\tau_0^{(b)} - \tau_{ch}}. \tag{6.24}$$

The partial derivative of the above expression with respect to $\tan\beta$ can be found by

invoking (6.20), as follows:

$$\frac{\partial \Pi_{\tau_0}}{\partial S_b} = \frac{-\tau_{ch}}{\tau_0^{(b)} - \tau_{ch}} \cdot \frac{\partial (\tau_{c\beta}/\tau_{ch})}{\partial S_b}$$

$$= \frac{-\tau_{ch}}{\tau_0^{(b)} - \tau_{ch}} \cdot \frac{\cos(\varphi + \beta)}{\sin \varphi} \cos^2 \beta. \tag{6.25}$$

A diffusivity parameter extracted from (6.12) can be obtained by evaluating the above expression at $\beta = 0$, yielding:

$$\varepsilon_{\tau_0} = \left(\frac{-\tau_{ch}}{\tau_0^{(b)} - \tau_{ch}} \right) \left(\frac{1}{\tan \varphi} \right). \tag{6.26}$$

Eq. (6.26) is in agreement with (6.21) in that both predict a diffusivity inversely proportional to the angle of repose. However, in the case of (6.26), such a proportionality depends on τ_{ch} and $\tau_0^{(b)}$ (for eq. 6.21, it is a constant equal to 3/2). Eq. (6.26) illustrates the vanishing effect of the bed-slope for high bed shear stresses; i.e. $\varepsilon_{\tau_0} \to 0$ for $\tau_0^{(b)} \to \infty$. Fig. 6.12 compares the bed-slope influence predicted by the exact solution (6.11) against the approximation given by the line with slope ε_{τ_0} (eq. 6.26). The agreement between predictions is very good for all negative slopes, mild adverse slopes and high bed shear stresses. Discrepancies grow for low $\tau_0^{(b)}$ and steep adverse slopes. The bed-slope influence is well described by the linear approximation for $\tan \beta \lesssim 0.2 \therefore \beta \lesssim 11°$, for all bed shear stresses herein considered, with the range of validity (for β) widening for increasing $\tau_0^{(b)}$ and negative β. In fact, the linear approximation adheres well to the exact solution for $0 \leq \beta \lesssim -\varphi$ in all cases.

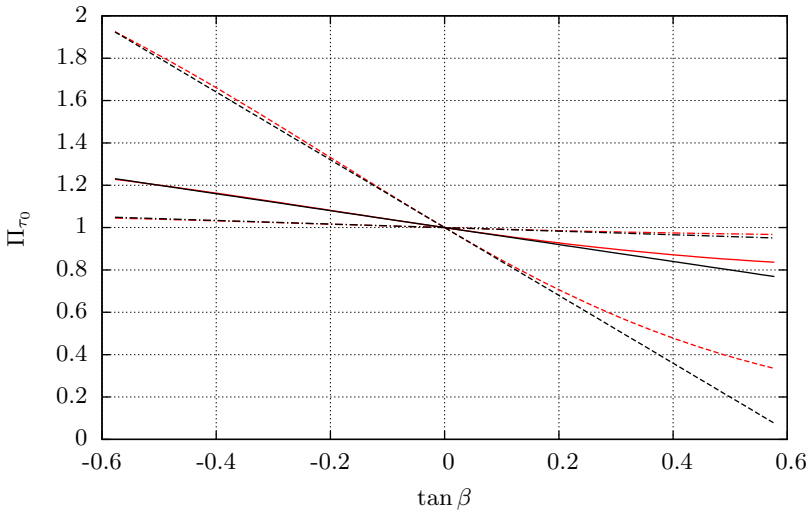

Figure 6.12: Bed-slope influence as function of bed shear stress vs bed-slope for three values of $\tau_0^{(b)}/\tau_{ch}$ ($\varphi = 32°$). Comparison between eq. 6.11 (red curves) and linear approximation (black lines). Dashed, solid and dashed-dotted lines correspond to $\tau_0^{(b)}/\tau_{ch} = 2$, 5 and 20, respectively.

The diffusivity parameter ε_{τ_0} can also be extracted from the exact solution to Π_{τ_0} given by (6.11), yielding:

$$\varepsilon_{\tau_0} = \left[\frac{\tau_{ch}}{2\left(\tau_0^{(b)} + \rho_w g h_0 \tan\varphi\right)} - \frac{\tau_{ch}}{\tau_0^{(b)} - \tau_{ch}}\right]\left(\frac{1}{\tan\varphi}\right). \tag{6.27}$$

However, the above expression is not only more complicated and dependent on more variables than (6.26), but its quantitative difference from (6.26) is negligible, as observable in Fig. 6.13. This confirms that (6.12) provides a very good approximation for Π_{τ_0} in general, as discussed in §6.3.2. The use of (6.26) over (6.27) is thus strongly recommended.

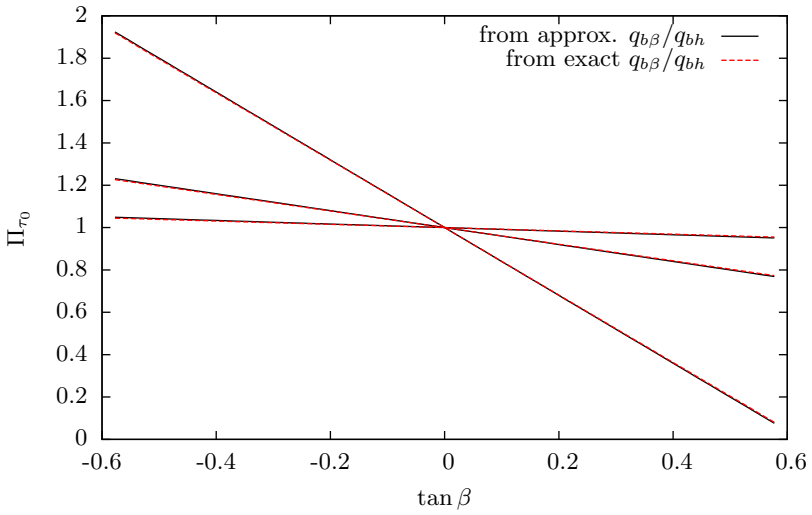

Figure 6.13: Linear approximation to the bed-slope influence as function of bed shear stress vs bed-slope for $\tau_0^{(b)}/\tau_{ch} = 2$, 5 and 20 (increasing $\tau_0^{(b)}/\tau_{ch}$ in the counter-clockwise direction). Comparison between the gradients predicted by (6.26) (derived from approximate solution, eq. 6.12) and (6.27) (derived from exact solution, eq. 6.11).

6.4.3 Application to the case of a migrating hump

To illustrate the effect of the diffusivity parameter ε, let us consider the case of the migrating hump described in §4.5. For the assumptions adopted by Hudson & Sweby (2003), the bed-update equation (4.52c) can be written as an advection equation, as follows:

$$\frac{\partial z_b}{\partial t} + \xi \frac{\partial q_b}{\partial x} = \frac{\partial z_b}{\partial t} + \left(\xi \frac{\partial q_b}{\partial z_b} \right) \frac{\partial z_b}{\partial x} = 0, \tag{6.28}$$

where the term $\xi \partial q_b / \partial z_b$ is related to the celerity at which the hump migrates in the stream-wise direction. By modifying the bedload via (6.16) in order to account for the influence of the bed-slope, the above expression can be expressed as an advection-diffusion equation as follows:

$$\frac{\partial z_b}{\partial t} + \xi \frac{\partial q_{b\beta}}{\partial x} = \frac{\partial z_b}{\partial t} + \xi \frac{\partial}{\partial x} \left(q_{bh} + \varepsilon q_{bh} \frac{\partial z_b}{\partial x} \right)$$

$$\Rightarrow \frac{\partial z_b}{\partial t} + \left(\xi \frac{\partial q_{bh}}{\partial z_b}\right) \frac{\partial z_b}{\partial x} = -\frac{\partial}{\partial x}\left(\xi q_{bh} \varepsilon \frac{\partial z_b}{\partial x}\right). \tag{6.29}$$

The right-hand side of (6.29), dependent on ε, represents the diffusive term in the advection-diffusion equation.

The choice of using either ε_T or ε_{τ_0} should be based on the final application. For example, at low bed shear stresses, ε_T may yield a better approximation of the bed-slope influence for steep adverse slopes. However, ε_{τ_0} is a better option for high bed shear stresses and steep negative slopes. An important difference between ε_T and ε_{τ_0} (see eqs. 6.21 and 6.26) is that the former is solely dependent on φ, whereas the latter depends on φ, $\tau_0^{(b)}$ and τ_{ch}. This may be particularly relevant when using analytical means to solve the bed-update equation; i.e. a constant value of ε may be very convenient when using mathematical tools to solve the diffusive component of (6.29). Nevertheless, the major criterion to choose between ε_T or ε_{τ_0} is perhaps whether the bedload formula employed (i.e. q_{bh}) is expressed as a function of transport stage or bed shear stress (or a quantity related to the bed shear stress).

In the case study considered in §4.5, the empirical formula for bedload adopted (eq. 4.52d) is a function of the flow velocity, which can be directly related to the bed shear stress through $\tau = c_f \rho_w \bar{u}^2$, and so ε_{τ_0} is herein utilised (with $\tau = \tau_0^{(b)}$). This decision is further supported by the fact that $\tau \gg \tau_c$ is assumed in the original case study. The initial local bed-slopes are in the range of $|\tan\beta| < 0.02$, which justifies use of the linear approximation to the bed-slope influence; the condition of small bed-slopes for all t is checked *a posteriori* during the simulation.

A few drawbacks have to be overcome before the slope-related diffusivity parameter

can be applied. First, the use of a bedload formula independent of τ_{ch} is justified by Hudson & Sweby (2003) by considering sheet flow (where $\tau - \tau_c \approx \tau$). Nonetheless, estimation of τ_{ch} is fundamental for the evaluation of ε_{τ_0}, and so assumptions have to be made regarding the bed composition. Bedload is expected to be the predominant mode of transport for coarse sediments with $D > 2.0$ mm (Soulsby & Damgaard, 2005); thus, $D = 2.0$ mm is adopted, with a common value for quartz sand of $s = 2.65$. This allows the estimation of τ_{ch} from the Shields curve. A second problem arises from the physically-unrealistic assumption by Hudson & Sweby (2003) of a frictionless bed ($c_f = 0$), which would lead to $\tau = 0$. This is overcome by considering no bed friction in the momentum-conservation equation (4.52b), but estimating a value of c_f for the evaluation of $\tau_0^{(b)}$ in (6.26), from the following approach.

The bedload formula by Soulsby & Damgaard (2005) for sheet-flow conditions reads $\Phi = 12\theta^{3/2}$ (see also Wilson, 1966; Nielsen, 1992); or in dimensional form:

$$q_{bh} = \frac{12\tau^{3/2}}{g(s-1)\rho_w^{3/2}},$$

which, recalling that $\tau = c_f \rho_w \bar{u}^2$, can be written as:

$$q_{bh} = \frac{12 c_f^{3/2}}{g(s-1)} \bar{u}^3. \tag{6.30}$$

Comparison between the above equation and eq. 4.52d (i.e. $q_{bh} = B\bar{u}^3$), shows that the former can be used to estimate c_f as a function of B (through eq. 6.31), which has been set to $B = 0.001\,\mathrm{s}^2/\mathrm{m}$ in the case studied in §4.5. Note, however, that this approach has been developed purely to overcome the problem posed by an unrealistic frictionless bed. Under normal circumstances, the same approach to calculate the bed resistance in (4.52b) is used to compute ε_{τ_0}. It is also worth comparing the expression herein

proposed for B (i.e. $B = 12\,c_f^{3/2}/[g(s-1)]$) against that derived from the Q2L model (eq. 4.45). For standard values of $s = 2.65$, $c^{(b)} = 0.03$, $\varphi = 32^\circ$ and $\rho_{0\mathrm{eq}}|_{c_0=0.25} = 1,412.5$ kg/m^3, eq. (4.45) yields $B \approx 13\,c_f^{3/2}/[g(s-1)]$. This is in good agreement with the approach derived from the work by Soulsby & Damgaard (2005).

$$c_f = \left[\frac{Bg(s-1)}{12}\right]^{2/3}. \tag{6.31}$$

Fig. 6.14 illustrates the effect of accounting for the influence of bed-slope on bedload transport through inclusion of ε_{τ_0} in the estimation of q_b (via eq. 6.16). The modification of the bedload formula (4.52d) avoids the formation of unrealistic oscillations otherwise present in the bed elevation, while reproducing the correct qualitative behaviour of the migrating hump (i.e. the steepening of its lee). Note that the inclusion of slope-related diffusion is not only a tactic to avoid high-frequency oscillations, but it is a fundamental component of the sediment-transport phenomenon (see §6.5.1). This also allows us to carry out simulation of bed evolution for a longer term (the spurious oscillations otherwise present render the model unstable). The steepest bed-slopes for this case are of the order of $\tan\beta \approx -0.06$, which justifies the use of ε_{τ_0}.

Given that the bed-slope influence predicted by the Q2L model has been satisfactorily validated against experimental data from steep sloping channels (see §6.2), the expressions obtained herein for quantifying the effect of bed-slope on bedload (i.e. Π_T, Π_{τ_0}, ε_T and ε_{τ_0}) can be used to enhance conventional morphodynamic models based on a set of equations similar to (4.52).

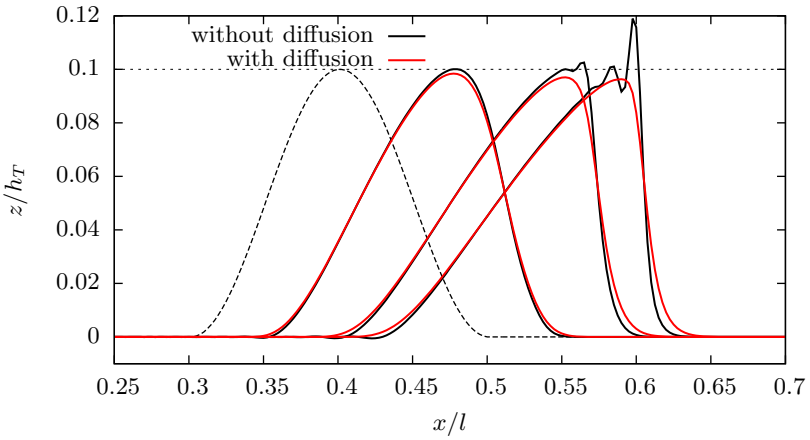

Figure 6.14: Evolution of a hump predicted by eqs. (4.52), illustrating the effect of local bed-slope on bedload through inclusion of the slope-related diffusivity parameter ε_{τ_0}. Results shown at $t = 0$s (dashed line) and at (from left to right) $t = 100 \times 10^3$, 200×10^3 and 250×10^3s.

The case of the bedload formula for sloping channels by Bailard & Inman (1981) is worth noting. Based on the work by Bagnold (1963), Bailard & Inman (1981) proposed a formula for the bedload transport of the form of (6.16), provided that $\tan\beta \ll \tan\varphi$. Hence, a slope-related diffusivity parameter can be deduced from their work, yielding:

$$\varepsilon_{B\&I} = \frac{1}{\tan\varphi}. \tag{6.32}$$

The above expression is derived from the definition of bed-slope influence given by (6.8) being applied to Bailard & Inman's formula, and so $\varepsilon_{B\&I}$ is directly comparable to ε_{τ_0} (instead of ε_T). Note that following different methodologies, both $\varepsilon_{B\&I}$ and ε_{τ_0} predict an inverse proportionality with $\tan\varphi$ (this is also true for ε_T). However, unlike ε_{τ_0}, $\varepsilon_{B\&I}$ depends solely on the angle of repose and, thus, is independent of bed shear stress (does not vanish at large τ). A similar expression to $\varepsilon_{B\&I}$ has been used by other authors (e.g. Dodd *et al.*, 2008).

Fig. 6.15 compares the roles of ε_{τ_0} and $\varepsilon_{B\&I}$ in the evolution of the hump previously

considered. Note that, although the two approaches prevent high-frequency oscillations from developing, only the Q2L-model-based diffusivity predicts a realistic evolution of the hump (i.e. steepening of its lee) – the use of $\varepsilon_{B\&I}$ yields over-attenuation of the hump's profile. The apparently-over-diffusive behaviour of $\varepsilon_{B\&I}$ may be explained by the fact that such an expression is derived from Bagnoldian ideas, which have been proven to over(under)estimate significantly bedload on negative(positive) bed-slopes (see §§6.2 and 6.3.3). This comparison further favours the hypothesis that the Q2L model captures correctly the physics behind bedload on sloping beds.

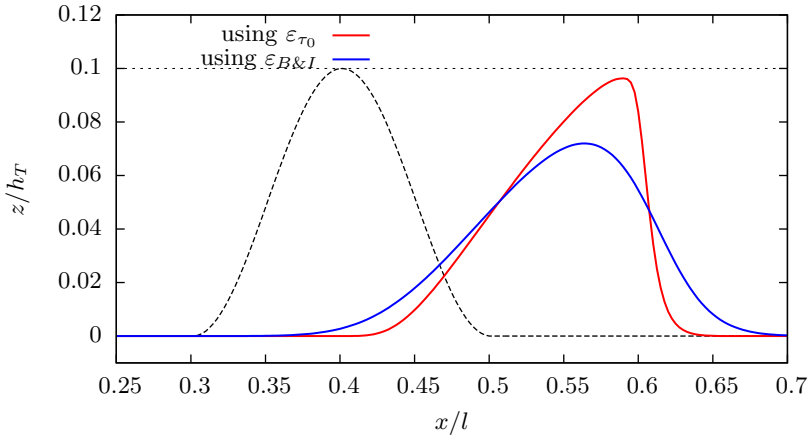

Figure 6.15: Evolution of a hump predicted by eqs. (4.52). Comparison of the effect of the bed-slope-related diffusivity parameters ε_{τ_0} and $\varepsilon_{B\&I}$. Results shown at $t = 0$s (dashed line) and at $t = 250 \times 10^3$s (continuous lines).

6.4.4 A curious fact

A curious fact arises from analysis of the diffusivity constant given by (6.21). Note that for common values (for sand and gravel) of φ, $\varepsilon_T = (3/2)/\tan\varphi \approx 1/\kappa$ (a realistic value of $\varphi \approx 31.6^\circ$ would correspond to the commonly accepted value of $\kappa = 0.41$). Consider now the following treatment of the linear approximation to Π_T:

$$\Pi_T = \frac{q_{b\beta}}{q_{bh}} = 1 + \varepsilon_T \tan\beta$$

$$\Rightarrow \frac{q_{b\beta} - q_{bh}}{q_{bh}} = \frac{\Delta q_{b\beta}}{q_{bh}} = \varepsilon_T \tan\beta$$

$$\Rightarrow \frac{\Delta q_{b\beta}/q_{bh}}{\tan\beta} = \varepsilon_T = \frac{1}{2/3\tan\varphi}. \tag{6.33}$$

Then, compare (6.33) with the definition of von Kármán constant from the log-law:

$$\frac{\Delta q_{b\beta}/q_{bh}}{\tan\beta} = \varepsilon_T = \frac{1}{2/3\tan\varphi} \approx \frac{1}{\kappa} = \frac{u(z)/u_*}{\ln(z/z_0)}. \tag{6.34}$$

The above expression can be explained physically as follows. The ratios between the non-dimensional variables $\Delta q_{b\beta}/q_{bh}$ and $u(z)/u_*$ (which depend, respectively, on β and z) to the non-dimensionalisations of the independent variables given by $\tan\beta$ and $\ln(z/z_0)$, have quasi-constant values expressed as $1/[(2/3)\tan\varphi]$ and $1/\kappa$, respectively, which are approximately equal to $1/0.41$. Moreover, the angle of repose, φ, is not a universal constant, but rather a parameter with a variable value commonly close to 30° for natural sands and gravels. Similarly, κ has also been reported not to be a universal constant (contrary to still-common belief), but to have a quasi-constant value near 0.41. Interestingly, major deviations of κ from 0.41 have been measured when sediment transport is present (see e.g. Gaudio *et al.*, 2010; Yeganeh *et al.*, 2000). The proportionality given by $1/\kappa$ holds for a limited range of z (near the wall/bed), just as the proportionality described by ε_T is valid for a given range of β only. Both, the log-law and the bed-slope influence on bedload describe near-bed phenomena. At the time of writing, the author cannot state whether there is a physical connection between

the aforementioned parallels or whether these are mere coincidences. Further research in this regard is encouraged.

6.5 Case studies

In the preceding part of this chapter, the effect of bed-slope on bedload transport rate has been analysed. Now, the impact of such an influence on the changing morphology is examined via several case studies.

6.5.1 An erodible hole under subcritical flow

The behaviour of an erodible hole subject to a subcritical flow is simulated as a 'negative-height' case of the migrating hump described in §4.5 (the remaining parameters are kept constant). Figure 6.16 depicts the evolution of the hole predicted by the Q2L model. The hole significantly shrinks with time. This is in agreement with field measurements of excavated holes in the surfzone by Moulton *et al.* (2014). Moulton *et al.* (2014) also estimated the slope-related morphological diffusivity. Although their treatment of such a diffusivity differs from the present one, their conclusions support the hypothesis, proposed also herein, that the slope-related diffusivity is proportional to the three-halves power of the bed shear stress and inversely proportional to the angle of repose. Furthermore, the investigation by Moulton *et al.* (2014) proves that inclusion of slope-related diffusion in the bed-update equation is underpinned by phenomenological observations and should not be interpreted as an auxiliary tool which sole target is to avoid oscillations arising from the numerical technique employed (for numerical strategies aimed at preventing such oscillations see e.g. Johnson & Zyserman, 2002; Hudson & Sweby, 2003; Callaghan *et al.*, 2006). This remark is also supported by the findings by Castro Díaz *et al.* (2008).

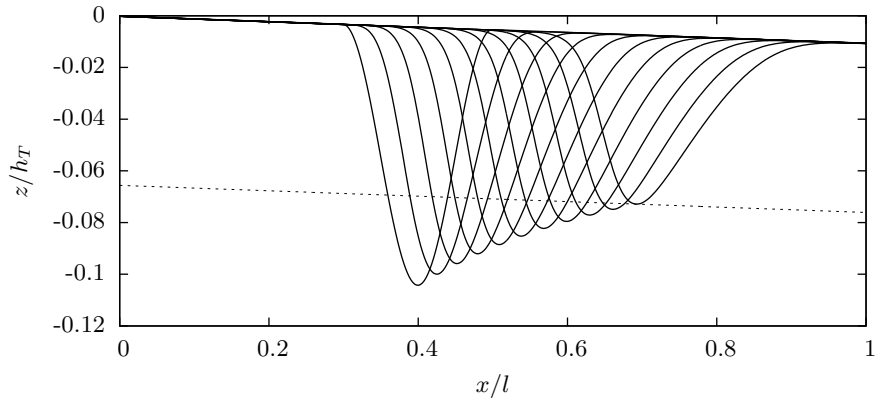

Figure 6.16: Evolution of a hole subject to a subcritical flow predicted by the Q2L model. Results shown (left to right) from $t = 0$ to $t = 1 \times 10^6$ s, every 100×10^3 s.

6.5.2 A partially-sinusoidal bed

The combined effect of a hump and a hole is now studied by considering a partially-sinusoidal bed. The bed is originally flat, except for a sinusoidal elevation profile of amplitude equal to 0.5 m, located from $x = 300$ m to 600 m . The remaining parameters (including $h_T = 10m$ at the upstream boundary) are as previously stated. Fig. 6.17 illustrates the evolution of the sinusoidal hump-hole predicted by the Q2L model. As expected, the sinusoidal protuberance migrates down the stream, with the hump and hole losing height and depth, respectively. The plane joining the crest and trough also steepens with time.

Fig. 6.18 compares the evolution of the hump-hole predicted by the conventional approach described by eqs. (4.52), with and without accounting for the slope-influence. The methodology employed in §6.4.3 to include the influence of bed-slope (via ε_{τ_0}) is herein utilised. The remaining parameters are as in the case of the hump (§4.5).

As for the migrating hump, inclusion of the slope-influence prevents formation of unrealistic oscillations at the crest and base of the hump. Regarding the hole, instabilities are not present in any of the two cases. However, the conventional approach without

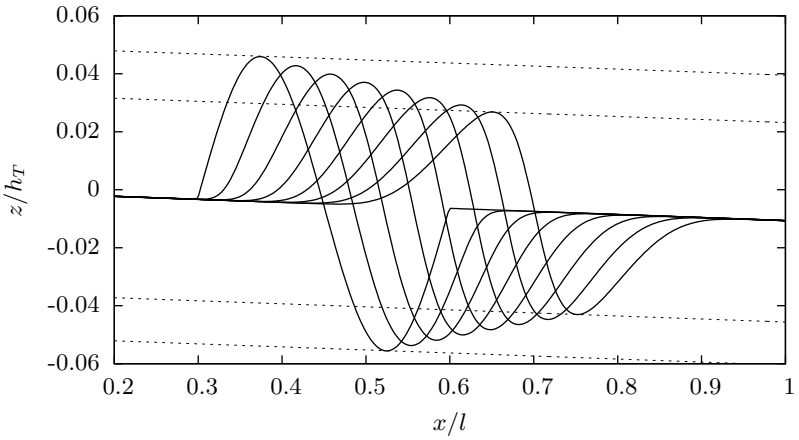

Figure 6.17: Evolution of a sinusoidal protuberance under subcritical flow predicted by the Q2L model. Results shown (left to right) from $t = 0$ to $t = 700 \times 10^3$ s, every 100×10^3 s.

slope-related diffusivity does not predict the expected (from a phenomenological perspective) decrease in hole depth, as discussed previously.

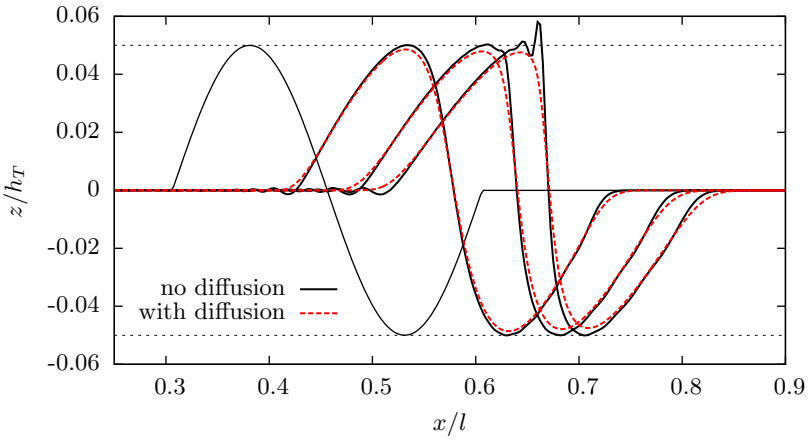

Figure 6.18: Evolution of a sinusoidal protuberance predicted by the conventional approach prescribed by (4.52), with and without considering the slope-related diffusion. Results shown at (left to right) $t = 0$, 200×10^3, 300×10^3 and 350×10^3 s.

6.5.3 A ramp

The case is now studied of a ramp located in the central area of a channel under subcritical flow. The aim is to investigate the evolution of an initially constant adverse slope.

Fig. 6.19 depicts the behaviour predicted by the Q2L model. All parameters are as in the previous cases (h_T denotes the total fluid depth at the upstream boundary). The ramp migrates downstream, with its average slope decreasing with time (similar to the upstream-face of a migrating hump). The edges at the base and top of the ramp are eventually smoothed out by the flow.

Fig. 6.20 shows the evolution of the ramped bed computed by the conventional approach (eqs. 4.52), with and without considering the bed-slope influence on bedload. This time, the channel is also slightly inclined in the conventional model. This permits the direct computation of the slope-related diffusivity parameter ε_{τ_0} via (6.26). Again, neglect of slope-influence causes oscillations to develop at the base of the ramp, which are not present when the slope-influence is considered. Note that oscillations do not occur at the top of the ramp, where flow velocities are higher. This demonstrates that the effect of bed-slope on bedload is most significant at low velocities.

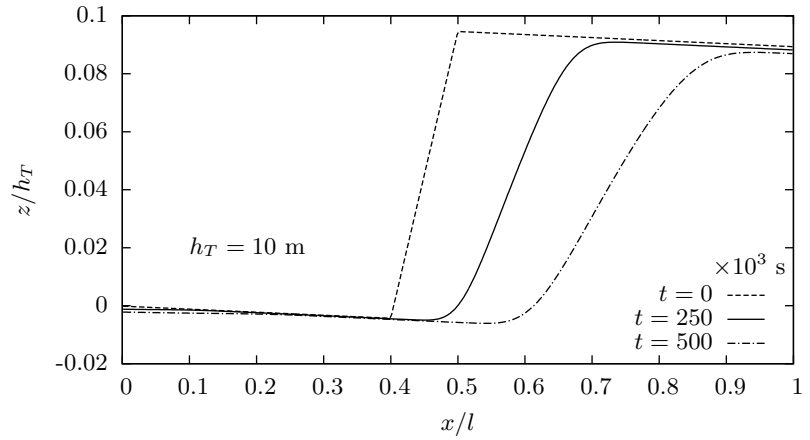

Figure 6.19: Evolution of a ramp in a channel under subcritical flow predicted by the Q2L model.

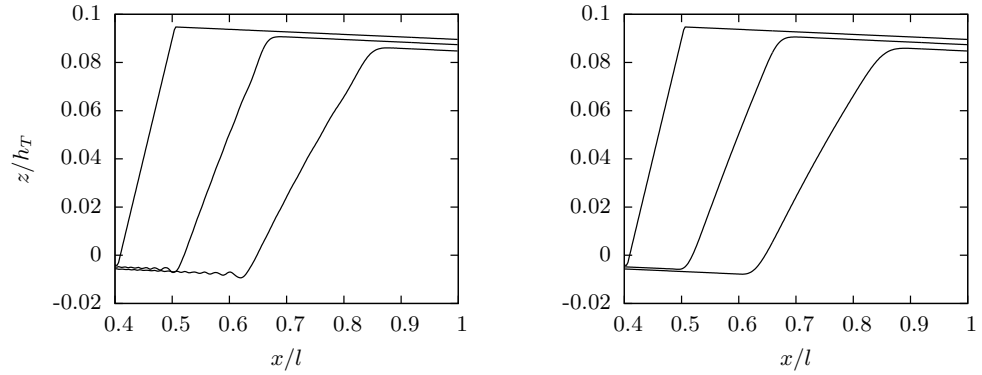

(a) without slope-influence **(b)** with slope-influence

Figure 6.20: Evolution of a ramp subject to subcritical flow predicted by the conventional approach (eqs. 4.52), with and without including the slope-influence on bedload. Results shown at (left to right) $t = 0$, 200×10^3 and 400×10^3 s.

Further insight into this case study can be gained by plotting the bed gradients of the final states predicted by all three approaches (estimated through second-order central finite differences), as in Fig. 6.21. The smoothing effect related to the inclusion of the slope-influence is clearly illustrated. Oscillations in the bed gradient exist throughout the entire domain when no slope-influence is considered. The Q2L model exhibits more (bed-slope-related) diffusive behaviour than the enhanced conventional approach. However, this case does not provide conclusive observations, because the

parameters employed in the simulations do not guarantee equal flow velocities and migration celerities of the ramp for the different models utilised. This is confirmed by the fact that, in the case of the Q2L model, it takes 100×10^3 s more for the ramp to migrate roughly the same distance downstream than in the case of the conventional approach. Nevertheless, it is interesting to observe that for approximately same distances of migration (≈ 200 m), all three approaches predict a similar mean slope of the ramp, roughly equal to 0.004.

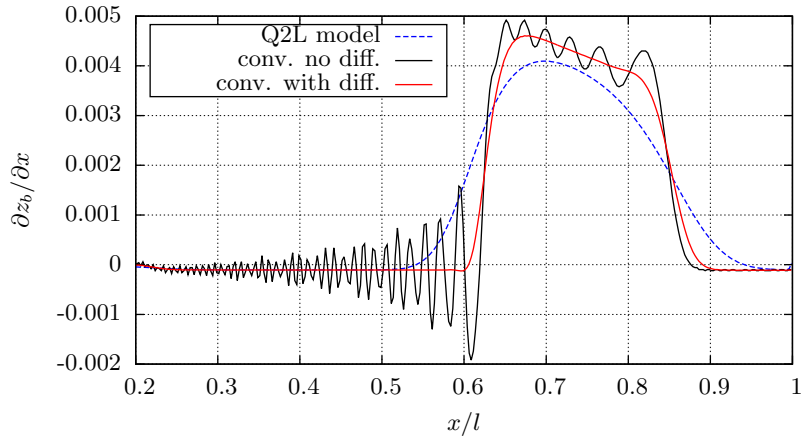

Figure 6.21: Bed gradients for the final states of the ramp predicted by all three approaches considered.

6.5.4 A dam-break over a flat erodible bed

In its current state of development, the Q2L model cannot be applied to cases including sharp changes in the free surface elevation and the flow velocity, such as in the case of dam-breaks. However, in order to assess the potential effect of bed-slope on bathymetry when fast morphological changes take place, the enhanced conventional approach (i.e. eqs. 4.52 with a slope-related modification in the bedload formula) is employed. For the solution of the hydrodynamic equations (eqs. 4.52a and 4.52b), a shock-capturing scheme is used; namely a HLLC Riemann solver with MUSCL-Hancock second-order time integration (see Toro, 2001). The bed-update equation (4.52c) is discretised using

a second-order central finite difference scheme and integrated in time using the second-order Adams-Bashforth method.

Fig. 6.22 illustrates the initial and final states of the simulated dam-break event. The water is tranquil at $t = 0$. The initial water depth at the upstream boundary, h_T, is set to 1.0 m, and the channel length is $l = 50$ m. The same values are adopted for the parameters governing bedload employed previously. Bed-slope influence is calculated following the method described in §6.4.3. The bed is assumed frictionless, noting that bed friction affects the free surface profile but its presence does not nevertheless modify the conclusions reached regarding the morphology. Fig. 6.23 shows the time evolution of the free surface, whereas Fig. 6.24 depicts the time evolution of the erodible bed, with and without considering slope-related diffusivity. As observed in Fig. 6.24, inclusion of the bed-slope influence has negligible effect in this case. This is unsurprising given the small bed gradients (the bed is originally flat) and high velocities ($T \approx 30$) involved. For these conditions, the bed-slope influence vanishes, as discussed previously.

Analysis of Figs. 6.23 and 6.24 yields the following observations. A sediment bore is propagated along the bed, driven by the hydraulic bore. Both bores propagate at roughly the same speed, namely ≈ 3.12 m/s. The rarefaction wave upstream of the dam is associated with smooth widening of the initial bed scour in the upstream direction. The scour originated by the dam-break causes a nearly-stationary hydraulic jump.

One more remark is worth making regarding the sediment bore. Such a bore manifests itself as a raised elevation of the bed level. This result appears to be in contradiction with experiments on dam-breaks over erodible channels (see e.g. Cao *et al.*, 2004; Fraccarollo & Capart, 2002), which report scour under the propagating hydraulic shock,

caused by the consequent high velocities. Two explanations for this seeming contradiction are proposed.

From a mathematical perspective, the present bed-update equation (the Exner equation, eq. 4.52c), widely employed for problems concerning bedload, is dependent on the flow velocity gradient, and not on the magnitude of the local velocity. Hence, a morphological model based on the Exner equation will predict deposition as long as the flow velocity gradient is negative, regardless of the magnitude of the local velocities, as is the case here (see also Haddadian *et al.*, 2014). This does not occur when the bed is updated according to expressions dependent on the magnitude of the local flow velocity, as is typical for problems dealing with suspended transport (e.g. Cao *et al.*, 2004).

A second explanation can be found in the interpretation of the Exner equation. The bed-update equation (4.52c) is often quoted in the literature as representing conservation of mass (or volume) 'in the bed'. However, as discussed in §2.2, such an equation in fact represents the conservation of sediment mass in the bed and the transport layer immediately above it (i.e. the bedload layer). Interpreting the Exner equation like this, reconciles the aforementioned apparently-contradictory results. For example, it is worth considering the experimental results reported by Fraccarollo & Capart (2002) or Zech *et al.* (2008). When tracking the 'immovable' bed (here, L_b) in their results, scour under the shock is observed. However, when examining the sediment mass in the bed and the transport layer above it ($L_b + L_0$), the behaviour shown in Fig. 6.24 can be identified.

In cases involving bedload in deep flows, the foregoing remarks may be irrelevant; nonetheless, in shallow flows, an Exner-type morphological equation should be inter-

preted carefully.

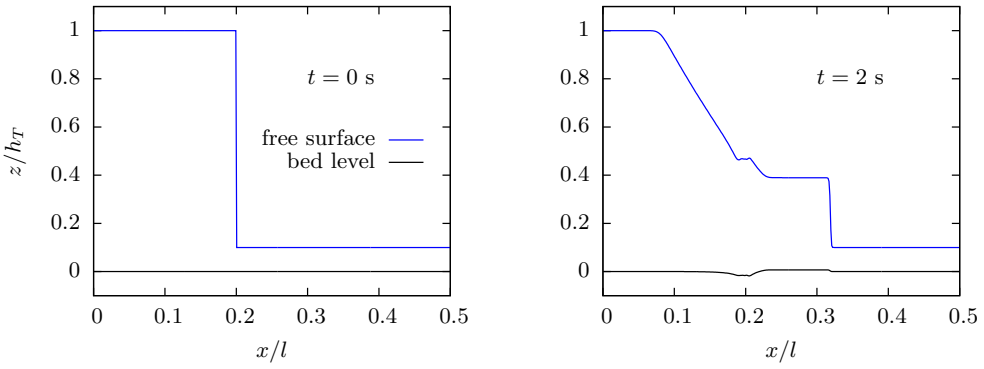

(a) Initial state **(b)** Final state

Figure 6.22: Dam-break over a flat erodible bed (solely bedload transport considered). Initial and final states depicted.

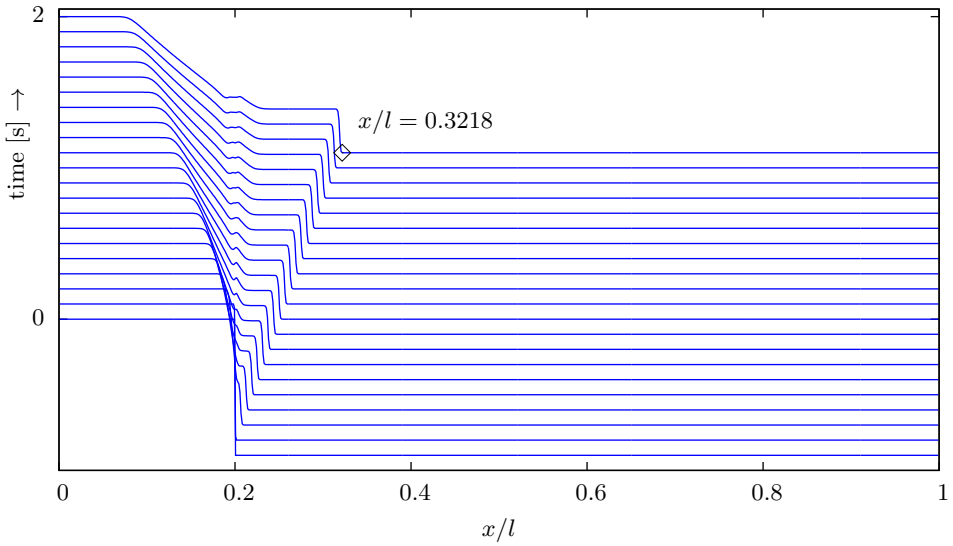

Figure 6.23: Time evolution (every 0.1 s) of the free surface during a dam-break.

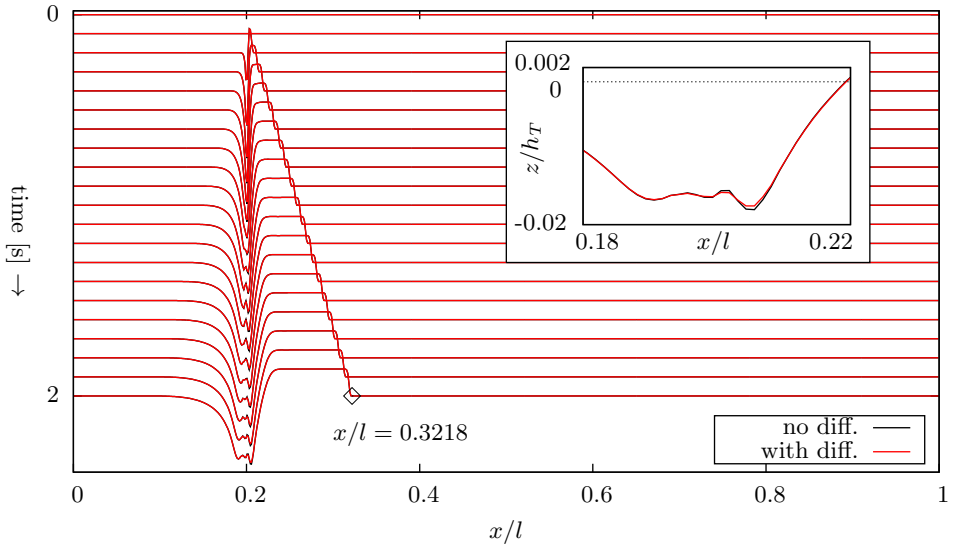

Figure 6.24: Time evolution (every 0.1 s) of the bed elevation caused by a dam-break. Comparison between the conventional approach (eqs. 4.52) with and without slope-related diffusion. Subplot depicts final bed state in the scour region.

6.5.5 A bore over an otherwise steady flow

This case study investigates the effect of bed-slope when slow and fast morphological changes occur subsequently. The numerical experiment involves two stages. In the first stage, a hump is subject to a regular flow for 10^3 s, and the bed-slope influence on bedload is considered. The final results of this stage are used as initial conditions for the regular-flow-part of the domain for the second stage of the experiment. Next, a bore is propagated over the flow for 6 s as depicted in Figure 6.25. Here, bedload is calculated using a Meyer-Peter-and-Müller-type formula, with a coefficient $A = 12$ (se eq. 4.40). This value of A is based on the recommendation made by El Kadi Abderrezzak & Paquier (2011) on the basis of their findings on sediment transport over erodible beds due to dam-breaks. A grain diameter of 2.0 mm and a Chézy coefficient of 25.0 are adopted. The Chézy coefficient is used solely for the estimation of the slope-influence, Π_{τ_0}, through (6.12), but the bed is considered frictionless (a necessary condition in the first stage of the experiment, due to the horizontal channel).

In this case, bed evolution is governed mostly by the first stage of the experiment (i.e. by the long exposure to the regular flow). The propagating bore effectively pushes the hump downstream a short distance, without significantly modifying its shape. The effect of the hump on the propagating bore seems more relevant, as observed in the reflected wave and small hydraulic jump that take place when the bore reaches the hump. Fig. 6.26 analyses the impact of neglecting the slope-influence during the bore-stage of the experiment. Such an impact is negligible, confirming findings from other investigations (e.g. Van Emelen *et al.*, 2015)

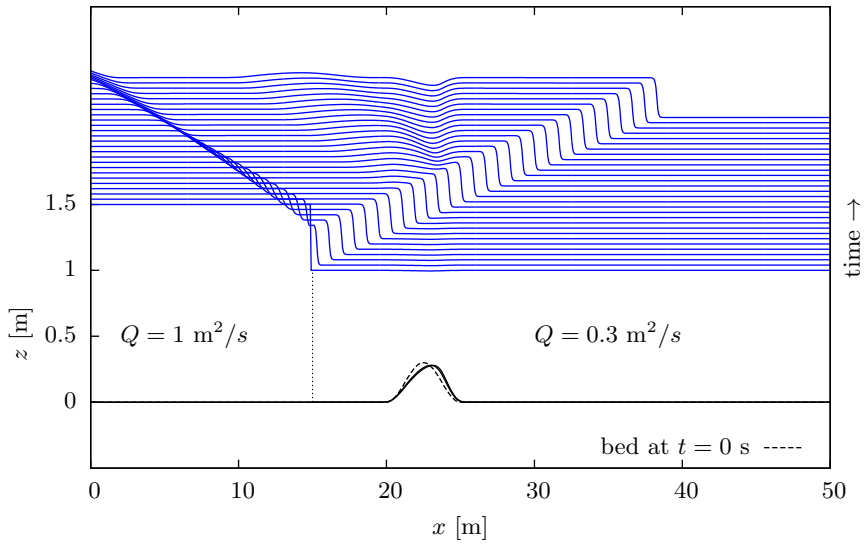

Figure 6.25: A bore (blue lines) propagating on a regular flow over an erodible channel with a hump. The stated discharges are prescribed as initial conditions for the second stage of the test (at $t = 10^3$ s). Black solid lines denote the bed level at $t =$ 1,000 and 1,006 s (they appear as overlapping in this plot).

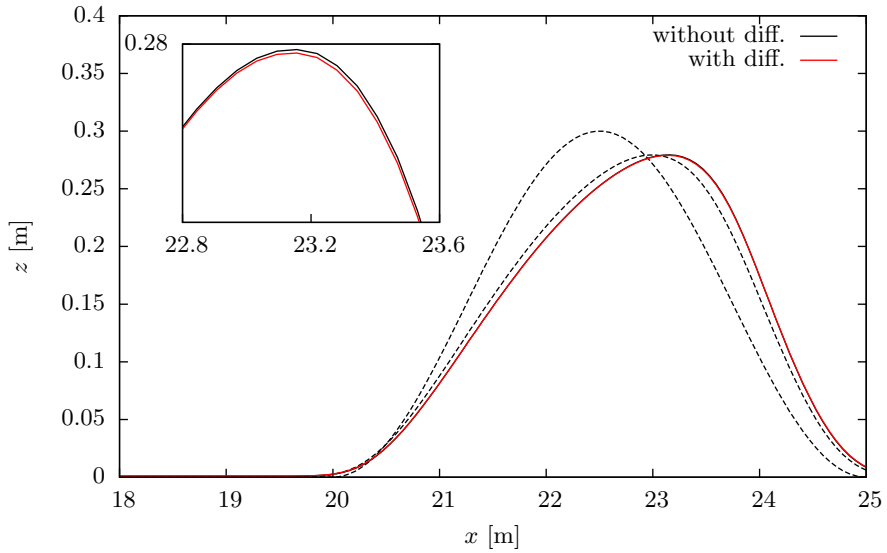

Figure 6.26: Hump at $t = 0$ s (dashed left), 1,000 s (dashed right) and 1,006 s (solid lines). Comparison between accounting for and neglecting the bed-slope-related diffusivity. Subplot illustrates the part of the hump where differences are largest.

6.6 Chapter summary

The bed-slope can impact significantly on bedload sediment transport and morphological evolution. The effect of bed-slope on bedload is maximised for cases concerning steep bed-slopes and relatively low flow velocities. The Q2L model seems to capture correctly the bed-slope influence. This is confirmed by the satisfactory validation of the model against empirical data for bedload rates in steep sloping channels. Discrepancies between the model predictions and the experimental data for steep negative slopes motivate further research into the estimation of τ_c for steep sloping channels.

The present model has been used to derive analytical expressions to quantify the bed-slope influence. Such expressions can be used to modify bedload empirical formulae originally derived for nearly-horizontal channels in order to expand their applicability to arbitrary slopes, without further increasing their level of empiricism (as with the

approach proposed by e.g. Watanabe, 1988). Conventional morphological models described by a set of equations similar to (4.52) prove to yield better results when the equations are enhanced by slope-related modifications arising from the Q2L model.

Generic expressions to account for the bed-slope influence have been derived for a given transport stage and bed shear stress; namely, Π_T and Π_{τ_0}, respectively. The former can be used directly to modify bedload formulae derived as functions of the transport stage (e.g. van Rijn, 1984a; Lee *et al.*, 2000), whereas the latter is useful in the (more-common) case of formulae expressed in terms of bed shear stress. For relatively-small bed-slopes and low transport stages, simplified expressions (6.7) and (6.12) can be invoked to estimate Π_T and Π_{τ_0}, respectively. If exact expressions for Π_T and Π_{τ_0} (eqs. 6.6 and 6.11) are to be used (e.g. for very steep slopes at low transport stages), a value of $h_0 \approx 10D$ is recommended.

For certain applications, it may be convenient to include the bed-slope influence by adding an extra term to the bedload expression for horizontal channels (see eq. 6.16). Such a term can be interpreted as a diffusive component in an Exner-type bed-update equation (eq. 4.52c), and is proportional to the local bed-slope. For relatively-mild bed-slopes ($|\tan\beta| \lesssim 0.2 \therefore |\beta| \lesssim 11.3°$), expressions for such a diffusivity parameter have been derived from the Q2L model; namely, ε_T (eq. 6.21) and ε_{τ_0} (eq. 6.26). As with Π_T and Π_{τ_0}, the choice between ε_T and ε_{τ_0} ought to be primarily based on whether the bedload formula to be modified is expressed as a function of T or τ (or a parameter related to τ, such as $\bar{u}$); although other considerations should also be taken into account (see §6.4.3). The derived expression for ε_{τ_0} is inversely proportional to $\tan\varphi$, in agreement with Bagnoldian models (see Bailard & Inman, 1981). However, unlike these models, the Q2L-model-based expression for ε_{τ_0} vanishes at large bed shear stresses (see eq. 6.26), in agreement with experimental observations. The use of

ε_{τ_0} in a conventional morphodynamic model yields stable and realistic results when simulating the evolution of an erodible hump subject to a current, as opposed to the employment of Bagnoldian-based diffusivity (which over-flattens the hump) or the exclusion of slope-related diffusion (which yields unrealistic oscillations in the hump's profile).

Case studies investigated in this chapter illustrate that the influence of bed-slope on bedload and morphology are most relevant in long-term simulations at low flow velocities and steep bed-slopes. Cases complying with such conditions can be found, for example, in coastal, estuarine, and mountain-river environments. For fast morphological changes, hydrodynamic forces overshadow the gravitational influence of the bed-slope on bedload in governing the evolution of the morphology. Inclusion of bed-slope influence on bedload does not solely obey numerical-stability reasons (i.e. to avoid unrealistic high-frequency oscillations in the bed), but it is also underpinned by phenomenological observations. In other words, realistic morphodynamic models should include the influence of the slope on bedload transport.

In the preceding chapters, the possibilities of the Q2L model to investigate various aspects of sediment transport (particularly bedload) have been explored. In the next chapter, a Lagrangian stochastic model of particle saltation is derived and employed to gain further insight into the mechanics and statistics of bedload transport.

Chapter 7

Lagrangian study of bedload

Saltation models provide considerable insight into near-bed sediment transport. This chapter outlines a simple, efficient numerical model of stochastic saltation, which is validated against previously published experimental data on saltation in a channel of nearly horizontal bed. The model is then employed to derive two criteria aimed at ensuring that statistically convergent results are achieved when similar saltation models are employed. Sensitivity of the model to the lift force formula, the friction coefficient, and the collision line level, is also investigated. Regression equations are obtained for each of the saltation characteristics. Finally, the model is used to evaluate the bedload transport rate (through two different methods), which is in satisfactory agreement with common formulae based on flume data, especially when compared against other saltation-derived expressions.

7.1 Introduction

Bedload transport consists of a combination of three different types of particle motion, namely: rolling, sliding and saltation. Whereas rolling and sliding occur near the threshold of incipient motion, saltation only occurs once the particle motion has far exceeded the threshold (van Rijn, 1984a). Saltation is then related to a higher flow shear velocity, and hence tends to be responsible for most of the total bedload transport. For this reason, saltating particle models are often used to gain insight into

bedload sediment transport. Such models, however, vary considerably from each other depending on which forces are taken to act on the grain and the approach adopted to the collision-rebound mechanism of the particle with the bed (or splash function) when continuous saltation is simulated (for single-hop models see e.g. van Rijn, 1984a; Lee & Hsu, 1994).

The most sophisticated equations of motion include effects due to turbulence, rotation of the particle (Magnus force) and changing boundary layer (Basset history term), at the cost of considerable mathematical complexity (see e.g. Niño & García, 1998b).

With regard to the splash function, stochastic methods are commonly used due to the inherent randomness of the collision-rebound phenomenon[1]. For example, Sekine & Kikkawa (1992) stated that the position of the particles' centroid forming the bed surface relative to the mean bed level followed a Gaussian distribution. Niño & García (1994) assumed the bed was composed of uniformly packed spheres. Niño & García then defined a collision surface which angle, with respect to the horizontal, was generated as a random number from a uniform distribution dependent on the incidence angle. In both the foregoing models, after defining the friction and restitution coefficients, geometrical considerations were adopted to obtain the take-off conditions (i.e. magnitude and direction of particle velocity). For this class of stochastic models, it is usual to report the average value of the characteristics measured after a certain number of hops have been simulated. However, the number of hops is often set in a rather arbitrary fashion (e.g. Niño & García, 1998b simulate 400 hops, whereas Lee *et al.*, 2000 choose only 55 saltations and Sekine & Kikkawa, 1992 work with the range between 100 and 500 realisations); and thus, there is no guarantee that

1. Deterministic methodologies have also been developed, but these usually require highly idealised assumptions concerning the composition of the bed; see e.g. Yan (2010)

statistically convergent results will be achieved.

The model presented herein belongs to the stochastic-type of continuous-saltation models. However, it differs from others (e.g. Sekine & Kikkawa, 1992; Niño & García, 1994) in that no explicit assumptions are made regarding the structure of the bed. Instead, laboratory data are used to predict directly the take-off angle (by means of randomly generated numbers), hence leaving the friction coefficient as the sole calibration parameter to be determined in order to continue the saltation process. The main advantage of this alternative approach is the considerable simplification of the mathematical model and computer code required. Hence, the present model is referred to as Simple Saltating Particle (SSP) model.

The model is validated against available empirical data. Then, it is used to develop two criteria aimed at estimating the minimum number of hops to be simulated in order to ensure statistically convergent results when similar saltating particle models are employed. The sensitivity of the model to variations in the friction coefficient (often considered constant) and the level at which the particle strikes the bed (herein referred to as the 'collision line') is also assessed. The choice of lift force formula is also examined analytically. Regression equations are used in order to derive formulae for the different saltation characteristics. These equations are utilised to estimate the bedload transport through two different methods; such predictions are then compared against formulae available in the literature. Some concluding remarks are presented at the end of the chapter.

7.2 Model description

The model solves the equations of motion for a saltating spherical particle in combination with a stochastic approach in order to simulate the collision-rebound mechanism of a saltating particle with the bed, as explained below. (See Fig. 7.1 for reference)

7.2.1 Equations of motion

The equations of motion of a saltating particle include contributions from inertia, lift, drag, and submerged weight. The Basset history term (related to the time-changing boundary layer on the particle) and the Magnus force (associated with the rotation of the particle) are not considered herein in order to retain model simplicity. Stochastic methods are used in an attempt to account for the idealisations considered (e.g. Basset history term, Magnus force, irregularity in shape and layout of particles on the bed surface, etc.).

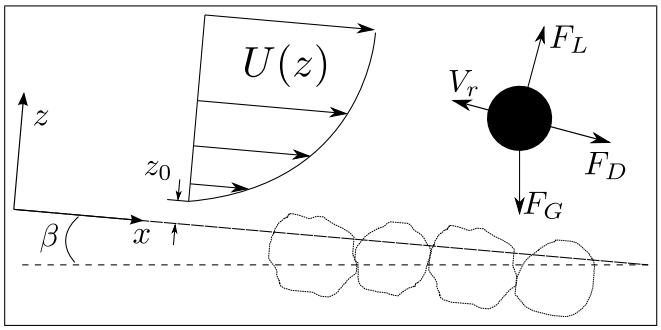

Figure 7.1: Definition sketch for the SSP model.

The governing equations are (see e.g. van Rijn, 1984a; Lee & Hsu, 1994):

$$m\ddot{x} = F_L\left(\frac{\dot{z}}{V_r}\right) + F_D\left(\frac{U-\dot{x}}{V_r}\right) + F_G \sin\beta^- \tag{7.1a}$$

$$m\ddot{z} = F_L\left(\frac{U-\dot{x}}{V_r}\right) - F_D\left(\frac{\dot{z}}{V_r}\right) - F_G \cos\beta^- \tag{7.1b}$$

where x and z are the stream-wise and bed-normal centroid displacements of the par-

ticle; $m = (\rho_s + \alpha_m \rho_w)\pi D^3/6$ is the total mass of the particle; α_m is the added mass coefficient, theoretically equal to 0.5; F_L, F_D and F_G are the lift, drag and gravitational force components, respectively; β^- represents the bed-slope angle with a positive value in the down-sloping direction (i.e. as opposed to the definition of β used in other chapters of this thesis[2]); $U = U(z)$ is the horizontal velocity component of the fluid; and V_r is the slip or relative velocity of the particle evaluated at its centroid as follows:

$$V_r^2 = (\dot{x} - U)^2 + \dot{z}^2. \tag{7.2}$$

The drag force, acting in the direction opposite to that of the relative velocity, is caused by a combination of form drag and skin friction (Lee & Hsu, 1994) and is expressed, for spherical particles, as:

$$F_D = \frac{1}{8} C_D \, \pi D^2 \, \rho_w \, V_r^2, \tag{7.3}$$

where C_D is the drag coefficient. However, the behaviour of C_D for unsteady flow has not been widely analysed (Niño & García, 1998b) and so it is usual to estimate its value from that of a single, steady, free-falling particle. The empirical formula given by Swamee & Ojha (1991) is employed herein, namely:

$$C_D = 0.5 \left\{ 16 \left[\left(\frac{24}{\mathrm{Re}} \right)^{1.6} + \left(\frac{130}{\mathrm{Re}} \right)^{0.72} \right]^{2.5} + \left[\left(\frac{40,000}{\mathrm{Re}} \right)^2 + 1 \right]^{-0.25} \right\}^{0.25}, \tag{7.4}$$

where $\mathrm{Re} = |V_r| D/\nu$ is the particle Reynolds number.

Less is known about the lift force than the drag. Until few decades ago, the very existence of the lift force (in the context of saltating particles) was questioned: Bagnold (1973) argued that the only upward impulses exerted on the particle were those due

2. This is done for consistency with similar saltation models available in the literature.

to collision with the bed. However, it is now widely accepted that there is enough evidence to state that hydrodynamic lift forces play a fundamental role in saltation (Niño & García, 1998b). Here, two formulae are used to calculate the lift force, and the results compared. The first was proposed by Saffman (1965) and used by van Rijn (1984a) in a single-hop saltating particle model, namely:

$$F_{L_1} = \alpha_L \rho_w \nu^{0.5} D^2 V_r \left(\frac{\partial U}{\partial z} \right)^{0.5}, \tag{7.5}$$

where α_L is the lift coefficient. Equation (7.5) was originally derived for small Reynolds numbers but later applied to the turbulent regime with a linearly varying α_L until it reached a maximum value (van Rijn, 1984a). Nonetheless, the lift coefficient α_L is herein used as a constant-value calibration parameter within the model (following the usual convention).

The second formula for F_L comes from Anderson & Hallet (1986) who considered wind-driven sediment transport, and is expressed for spherical particles as:

$$F_{L_2} = \frac{1}{8} C_L \rho_w \pi D^2 (V_{rT}^2 - V_{rB}^2), \tag{7.6}$$

where V_{rT} and V_{rB} are the relative velocities calculated using (7.2), evaluating U at the top and bottom of the particle, respectively. C_L in the above equation represents the lift coefficient, which is used as a calibration parameter.

The submerged weight is expressed as:

$$F_G = \frac{1}{6} \pi (\rho_s - \rho_w) g D^3. \tag{7.7}$$

The time-averaged vertical structure of the flow velocity is assumed to follow a logarithmic profile, given by:

$$U(z) = \frac{U_*}{\kappa} \ln(z/z_0). \tag{7.8}$$

The bed level at which velocity is zero, z_0, is herein computed in a different manner as in §3.2; namely: $z_0 = 0.11(\nu/U_*) + 0.033k_s$; where k_s is the equivalent roughness height of Nikuradse, taken to be proportional to the diameter of the bed material ($k_s \propto D$). This expression to estimate z_0 is employed following Lee & Hsu (1994) and Soulsby (1997), who recommend its use for hydrodynamically transitional flows ($5 \leq U_* k_s/\nu \leq 70$), which is the case for the validation of this model (see §7.3). It is important to mention that the use of the above velocity logarithmic profile assumes a low concentration of particles in the bedload area (when relating the mechanics of a single saltating particle to the study of bedload transport), which agrees with experimental findings (e.g. Fernández Luque & van Beek, 1976). For higher concentrations, the effect of particles on the fluid vertical structure and that of inter-particle collisions would not be negligible.

Equations (7.1) are transformed into a system of first-order ordinary differential equations and then integrated in time using a fourth-order Runge-Kutta method.

7.2.2 Collision-rebound mechanism (splash function)

Consider the collision-rebound event depicted in Fig. 7.2. From the equations of motion, the velocity vector at the moment of collision, $\vec{V}_{in} = (\dot{x}, \dot{z})_{in}$, is determined. For simplicity, it is assumed that $\vec{V}_{in} = \vec{V}_n$; in other words, equal to that immediately before the event. As the vertical position at collision is known (the level z_{in} defines the collision line), the time needed for the particle to reach that line can be obtained as:

$t_{in} = (z_n - z_{in})/\dot{z}_n$, and the horizontal position of collision as: $x_{in} = \dot{x}_{in} t_{in} + x_n$. Notice that $t_{in} < \Delta t$, where Δt represents the numerical time step. The point $(n+\Delta t)_{virtual}$ in Figure 7.2 represents the point predicted by the solution of the governing equations for which the condition $z < z_{in}$ is first verified, i.e. when the collision line is virtually 'crossed'.

The take-off angle is then generated as a random number, which probability distribution is based on measurements reported in the literature (see e.g. Niño & García, 1998a; Lee *et al.*, 2000). Based on previous experimental observations, herein this angle is assumed to follow a normal distribution, i.e. $\theta_{out} \sim N(\mu_s, \sigma_s^2)$, where μ_s and σ_s^2 are the angle mean value and variance, respectively. The striking horizontal velocity, $\dot{x}_{in}$, is thought to be reduced after collision by a factor f, allowing therefore the calculation of the take-off stream-wise and vertical velocities as $\dot{x}_{out} = f\,\dot{x}_{in}$ and $\dot{z}_{out} = \dot{x}_{out} \tan\theta_{out}$, respectively. Notice that the restitution coefficient, defined as $e = -\dot{z}_{out}/\dot{z}_{in}$, is herein a result of the splash function rather than a tuning parameter. An alternative approach would be to set e as the tuning variable, leading to f $(= \dot{x}_{out}/\dot{x}_{in})$ being the resultant variable instead. However, it has been found from laboratory data that, unlike the restitution coefficient, the friction coefficient exhibits fairly constant behaviour (Niño & García, 1998a) and thus it is chosen to be the main calibration parameter within the model.

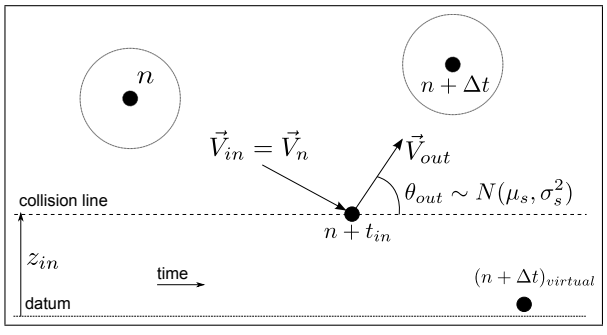

Figure 7.2: Sketch of the splash function.

It is worth mentioning that attention ought to be paid to the definitions of e and f adopted, especially when compared to other studies. For instance, Niño & García (1998a) define the coefficients as reductions in the tangential and vertical velocity components with respect to the collision surface, which does not necessarily coincide with the stream-wise plane (as in the present model). It should therefore not be expected that the values of e and f should be the same. For model validation, the friction coefficient, f, and the position of the collision line, z_{in}, may be considered constant. This simplification is revised in §7.6.

Once the take-off velocity, $\vec{V}_{out} = (\dot{x}, \dot{z})_{out}$, is obtained, the new position of the particle is found by linear interpolation as follows:

$$x_{n+\Delta t} = x_{in} + \dot{x}_{out}(\Delta t - t_{in}) \tag{7.9a}$$

$$z_{n+\Delta t} = z_{in} + \dot{z}_{out}(\Delta t - t_{in}) \tag{7.9b}$$

The post-rebound velocity is assumed to be equal to the take-off one; i.e. $\vec{V}_{n+\Delta t} = \vec{V}_{out}$. From this point on, the numerical integration of the governing equations continues as normal until the particle again encounters the collision line.

It is important to highlight that the present model does not replicate the actual behaviour of a saltating particle, such as the eventual rest to which a particle comes when trapped by the local bed topology. Hence the term *bed surface* is deliberately avoided and the term *collision line* is used instead. Following the idea behind Monte Carlo simulation, continuous saltation of the particle is modelled until statistical convergence of the sampled characteristics is achieved. The main goal of the model is to evaluate these average characteristics. The results presented here should then be interpreted as probabilistic tendencies arising from a statistical analysis of saltation (based on a

combination of laboratory data and relatively simple governing equations), rather than as findings resulting from strictly physics-based numerical simulations.

7.3 Validation

Model predictions (SSP F_{L_1} and SSP F_{L_2}) are compared against the experimental results reported by Francis (1973) (F), Lee & Hsu (1994) (LH), Niño & García (1994) (NG A 1 and NG A2, where the datasets differ from each other with respect to the diameters measured) and Niño & García (1998a) (NG). The characteristics measured include the saltation height, δ_s, length, λ_s, and stream-wise velocity of the particle, u_s, as depicted in Figure 7.3, which illustrates a typical trajectory followed by the centroid of a saltating particle. The stream-wise velocity, u_s, is here defined as the average stream-wise velocity of the particle during a hop; i.e. $u_s \equiv \lambda_s/t_s$, where t_s is the time between the rebound and eventual collision of the particle with the bed (thus $u_s \neq \dot{x}$). The conditions replicated in the simulations are those of the experiments by Niño & García (1998a). A particle diameter of 0.5 mm is used and values of the shear velocity, U_*, in the range from 0.0207 to 0.0321 m/s are modelled. During the comparison, the transport stage, defined as τ_*/τ_{*c}, is used as the independent variable (the abscissa in Figures 7.4 to 7.6). τ_* denotes the dimensionless bed shear stress evaluated as $\tau_* \equiv U_*^2/[g(s-1)D]$; τ_{*c} represents the dimensionless critical shear stress for sediment motion (i.e. $\tau_{*c} = \theta_c$), obtained from the Shields curve. Note that the values of τ_*/τ_{*c} herein computed do not match those of Niño & García (1998a). The reason is that Niño & García report variations in the measured particle size and therefore τ_* and τ_{*c}, which are functions of D, are affected.

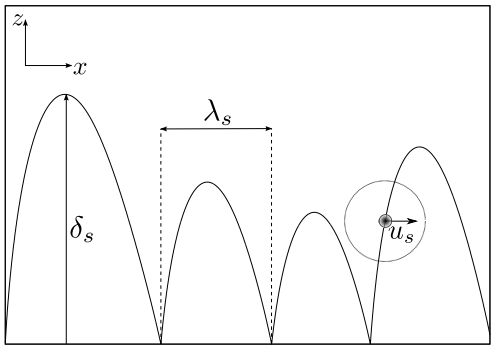

Figure 7.3: Typical saltation trajectory and characteristics measured.

As input data the following values are used: $D = 0.5$ mm, $\rho_w = 1{,}000$ kg/m^3, $\rho_s = 2{,}650$ kg/m^3, $\nu = 1.1 \times 10^{-6}$ m^2/s, $k_s = 1D$ and $\beta^- = 0.05\,^\circ$ (down-slope). Values of θ_{out} are generated as a random number following a normal distribution with parameters $\mu_s = 25^\circ$ and $\sigma_s \approx 14^\circ$ ($\sigma_s^2 = 200$ deg^2). The values of μ_s and σ_s are estimated from the work of Niño & García (1998a) and Lee *et al.* (2000). Following van Rijn (1984a), the collision line is set to be $0.6D$ above the datum, i.e. $z_{in} = 0.6D$. Two variables are used as calibration parameters: the lift coefficient, $\alpha_L|C_L$ (depending on the formula for lift force employed), and the friction coefficient, f. Three hundred continuous hops are simulated for every scenario. This number is of a similar order to those commonly reported in experiments and it is sufficient to make the influence of arbitrary initial conditions negligible, herein set to $x = 0$, $z = 0.6D$ and $\dot{x} = \dot{z} = 2.5U_*$ (van Rijn, 1984a). Section 7.5 presents further discussion on the adequate number of hops to be simulated. First, the friction coefficient is considered to be constant; later the influence of randomness is also tested (see §7.6). From the calibration process, the optimum values of the tuning parameters are found to be $\alpha_L = 10 \mid C_L = 0.75$ and $f = 0.85$. This value of f is in perfect agreement with the findings of Fernández Luque & van Beek (1976).

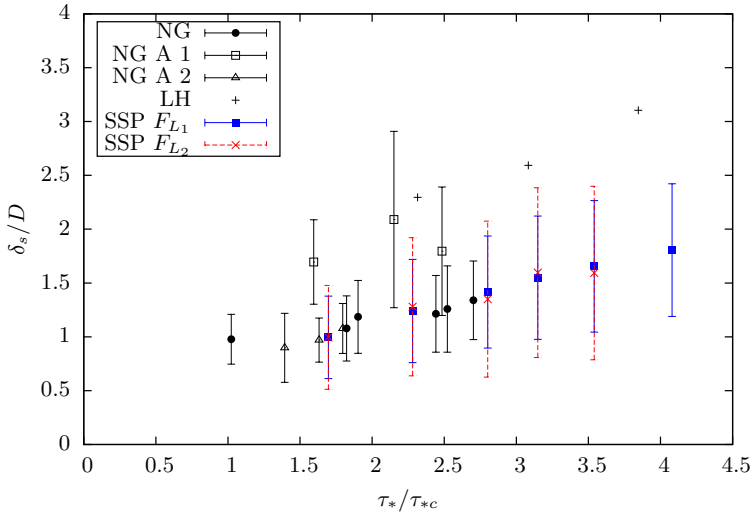

Figure 7.4: Dimensionless saltation height versus transport stage. [Symbols represent mean values and vertical lines represent the total length of two standard deviations; in legend, NG denotes Niño & García (1998a), NG A 1 and 2 denote Niño & García (1994) where the datasets differ from each other on the diameters measured, LH denotes Lee & Hsu (1994) and SSP (Simple Saltating Particle) denotes the present model]

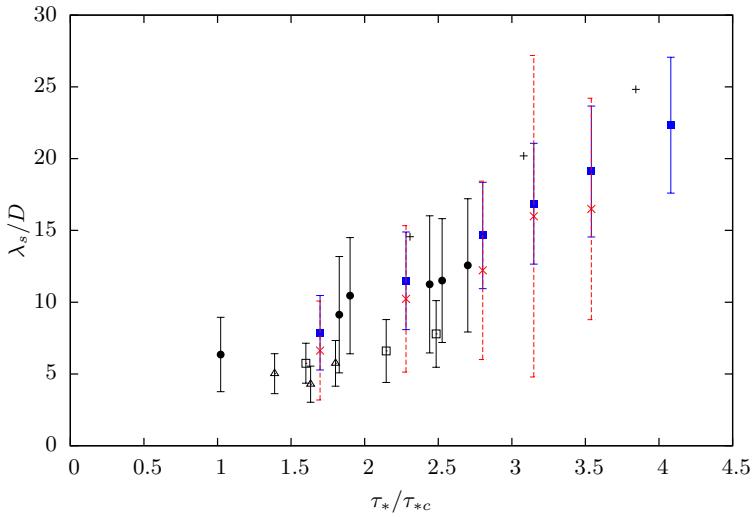

Figure 7.5: Dimensionless saltation length versus transport stage. [Symbols, vertical lines and legend as in Figure 7.4]

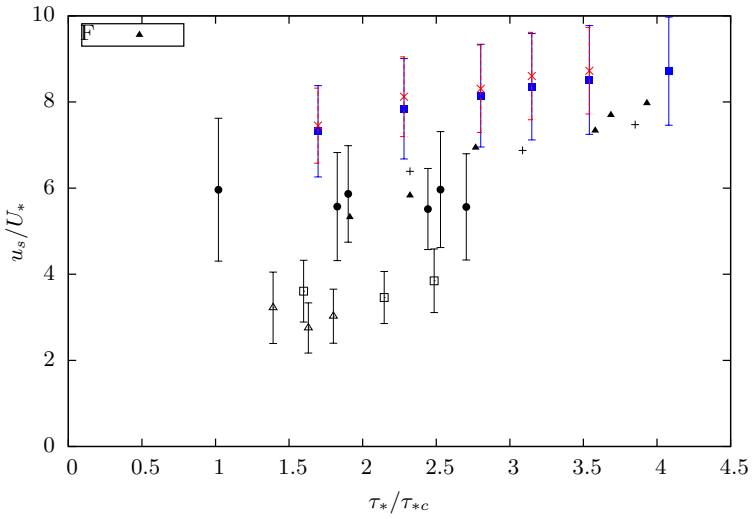

Figure 7.6: Dimensionless saltation stream-wise velocity versus transport stage. [In legend, F denotes Francis (1973); the remaining symbols are as in Figures 7.4 and 7.5]

Figures 7.4 and 7.5 show the non-dimensional saltation height and length as functions of the transport stage. Fig. 7.6 illustrates the corresponding plot of non-dimensional saltation stream-wise velocity (made dimensionless with the shear velocity). The definition of saltation height given in the open literature is often ambiguous; here the definition stated by Niño & García (1998a) is adopted, i.e. the maximum distance reached during a hop between the centroid of the particle and the top of the bed grains. The top of the bed grains –not the same as the collision line– is assumed to be $0.25D$ above the datum (van Rijn, 1984a). This assumption underpins the values depicted in Figure 7.4. The model shows generally good agreement (both in mean values and standard deviations) with the experimental data considered, particularly those of Niño & García (1998a), whose experiments are simulated in this work. Overestimations of u_s can be perceived, which may be related to the formula used to compute the drag coefficient; however, the model seems to predict well the asymptotic behaviour of this variable for increasing flow velocity, in accordance with previous work (see e.g. Fernández Luque & van Beek, 1976). Comparing the formulae for the lift force (points

sharing the exact same values of τ_*/τ_{*c} in the figures), two main conclusions arise: i) except for the case of u_s, F_{L_2} shows a larger scatter (standard deviation) than F_{L_1} for the same simulation conditions; and ii) when using F_{L_2}, the model eventually becomes unstable for increasing flow velocities, which has made it impossible to obtain results for $\tau_*/\tau_{*c} > 4$. Due to this limitation, hereafter F_{L_1} will be used within the model. In the next section, these two alternative formulations to estimate the lift force are investigated analytically.

7.4 Analysis of F_{L_1} and F_{L_2}

The main difference between the two expressions is that, whereas F_{L_1} predicts that the lift force is proportional to the slip (relative) velocity of the particle multiplied by the square root of the vertical gradient of the horizontal flow velocity component, F_{L_2} states that such a force is instead proportional to the difference between the squares of the slip velocity components at the top and bottom of the particle; in other words, $F_{L_1} \propto V_r\,(\partial U/\partial z)^{1/2}$ and $F_{L_2} \propto (V_{rT}^2 - V_{rB}^2)$. The equivalence (or non-equivalence) between these two expressions for the limiting case of a small particle is explored next.

Invoking (7.2), the difference between the squares of the slip velocity components at the top and bottom of the particle can be expressed as follows:

$$V_{rT}^2 - V_{rB}^2 = (\dot{x} - U_T)^2 + \dot{z}^2 - (\dot{x} - U_B)^2 - \dot{z}^2$$

$$= U_T^2 - U_B^2 - 2\dot{x}(U_T - U_B), \tag{7.10}$$

where U_T and U_B represent the fluid horizontal velocity evaluated at the top and bottom of the particle, respectively. Without subscripts T and B, variables U and V_r are

evaluated at the centroid of the particle.

For a sufficiently small particle, it can be assumed that:

$$\frac{U_T - U_B}{D} \approx \frac{\partial U}{\partial z}, \tag{7.11}$$

from which it follows that:

$$(U_T - U_B) = D\frac{\partial U}{\partial z},$$

and

$$U_T^2 - U_B^2 = 2DU_B\frac{\partial U}{\partial z} + \left(D\frac{\partial U}{\partial z}\right)^2,$$

hence allowing to rewrite (7.10) as:

$$V_{rT}^2 - V_{rB}^2 = 2DU_B\frac{\partial U}{\partial z} + \left(D\frac{\partial U}{\partial z}\right)^2 - 2\dot{x}D\frac{\partial U}{\partial z}$$

$$= \left[(U_B - \dot{x}) + \frac{D}{2}\frac{\partial U}{\partial z}\right] 2D\frac{\partial U}{\partial z}. \tag{7.12}$$

Recalling assumption (7.11), the above expression can be further manipulated as follows:

$$V_{rT}^2 - V_{rB}^2 = \left(U_B + \frac{U_T - U_B}{2} - \dot{x}\right) 2D\frac{\partial U}{\partial z}$$

$$= \left(\frac{U_B + U_T}{2} - \dot{x}\right) 2D\frac{\partial U}{\partial z},$$

and assuming $U = (U_B + U_T)/2$:

$$V_{rT}^2 - V_{rB}^2 = 2D(U - \dot{x})\frac{\partial U}{\partial z} = 2DV_{rx}\frac{\partial U}{\partial z}, \tag{7.13}$$

where V_{rx} is the x-component of V_r. Recalling the definition of F_{L_2} given by (7.6), it can be concluded that:

$$F_{L_2} \propto V_{rx}\frac{\partial U}{\partial z}, \tag{7.14}$$

whilst (from eq. 7.5),

$$F_{L_1} \propto V_r\left(\frac{\partial U}{\partial z}\right)^{1/2}. \tag{7.15}$$

For the velocity profile herein adopted (eq. 7.8), $\partial U/\partial z = U_*/(\kappa z)$. Thus, near the bed ($z \to 0$), F_{L_2} will increase at a significantly larger rate than F_{L_1}. This is illustrated in Fig. 7.7, which also shows that the lift force predicted by F_{L_2} increases substantially with U_* near the bed, thus explaining why the present model becomes unstable for larger values of the bed shear stress when F_{L_2} is employed.

Fig. 7.8 depicts the failure of the model when F_{L_2} and a relatively large U_* are considered. When the take-off velocity (related in turn to the take-off angle) of the particle is not sufficient for it to 'escape' the (near-bed) zone where the vertical gradient of the fluid velocity maximises the lift force, the vertical component of the lift force will eventually equal the vertical component of the gravitational force, hence causing the particle to remain (unrealistically) in suspension without further colliding with the bed surface. Although this behaviour is not observed when F_{L_1} is utilised, it should not be concluded that F_{L_1} is a 'better' formula than F_{L_2}, given that conditions necessary for F_{L_2} to render the model unstable arise from the stochastic approach herein adopted to simulate the collision-rebound mechanism. An strict process-based model may not necessarily replicate the conditions that invalidate the use of F_{L_2} (e.g. in a process-

based model, a combination of small take-off angle and velocity may conclude in the particle coming to rest). However, for a stochastic saltation model of this type, the use of a formula similar to F_{L_1} is recommended.

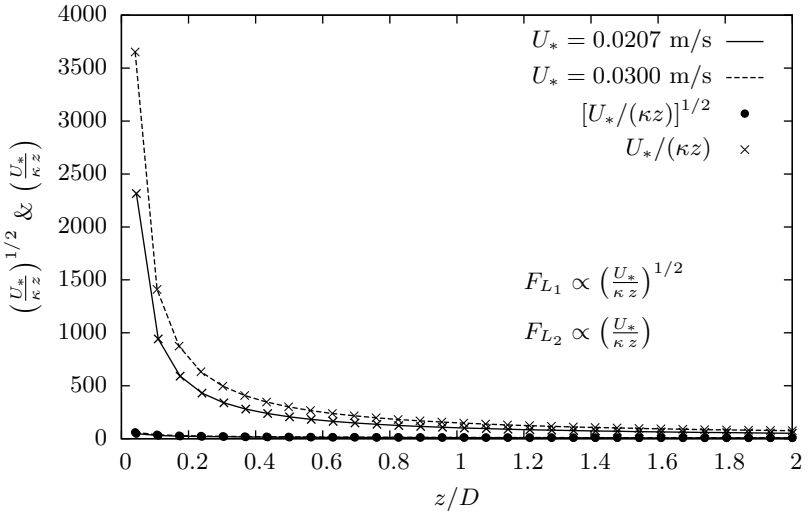

Figure 7.7: Comparison of approximate rate of change in the lift force ($V_r \sim V_{rx}$ assumed for both formulae) with vertical distance from the bed predicted by F_{L_1} and F_{L_2}, for two values of U_*.

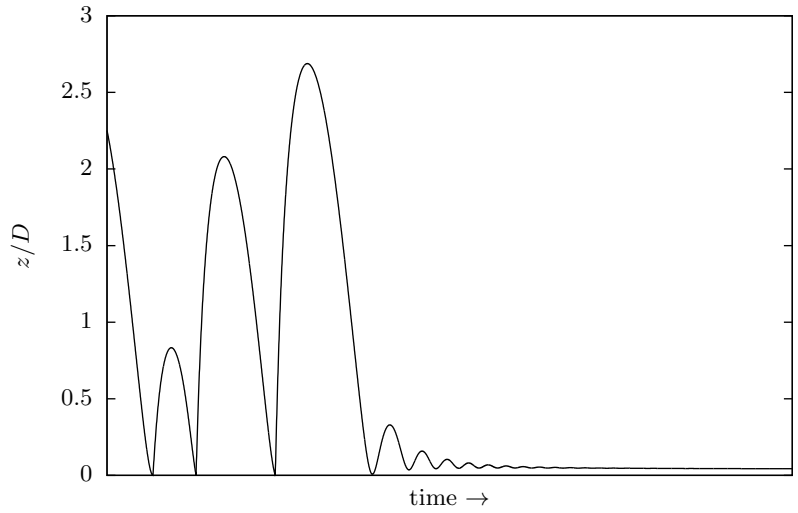

Figure 7.8: Trajectory followed by the centroid of the particle illustrating failure of the model (particle remains in suspension) when F_{L_2} is employed.

7.5 Study of statistical convergence

The basic idea behind Monte Carlo methods is the repeated sampling of random (formally pseudo-random) numbers in order to simulate complex systems. These methods vary considerably, but conventionally, m random numbers are sampled from a given probability distribution (input variables) and a deterministic computation is carried out in order to obtain the solution to the problem (output of the system). This process is repeated n times until statistically convergent results are achieved. In the present work, this is translated as follows: n numerical experiments are executed, each consisting of m hops performed by the particle. Thus, for each experiment m values of the take-off angle (the only variable so far defined as random) are generated. The deterministic algorithm applied to the input random variable is the solution to the equations of motion defining the path of the particle between the rebound and eventual collision with the bed. Notice that because of the nature of this problem, an equivalent approach to the n experiments of m hops each is to carry out a single numerical experiment simulating $m \times n$ hops (this deduction has been verified numerically). As stated previously, the main outputs of the system are the saltation characteristics, i.e. particle saltation height, length and stream-wise velocity. In order to assess the statistical convergence of the results, two simple criteria are adopted. The idea is to provide a quick assessment on the statistical convergence, and so only the first moment of the output probability distribution (mean value) is quantified (first criterion), whereas higher-order moments (e.g. variance and skewness) are solely evaluated from a qualitative perspective. The two criteria are described below.

A reference scenario is obtained by simulating a fairly large number of hops (i.e. 10^6), and different n-hops runs are compared against this case. The first convergence criterion is defined as the percentage error in the mean value of an individual n-hops

run in relation to the reference case, as follows:

$$\text{error}_n = \left| \frac{X_n - X_{\text{ref}}}{X_{\text{ref}}} \right| \times 100 \,, \tag{7.16}$$

where X_n can be the average value of any measured characteristic (i.e. λ_s, δ_s or u_s) for n number of hops simulated, and the subscript 'ref' denotes the reference scenario (i.e. the 10^6–hops simulation, in this case).

The second criterion for evaluating statistical convergence is here defined by assessing how close or far a given output sample is from a well-defined probability distribution (that is, a well characterised distribution determined by a large number –one million– of saltation). Thus the second criterion compares, in a rather qualitative fashion, the probability density obtained from the diverse n-hops cases against the one obtained from the reference scenario.

Five different numbers of hops have been simulated, varying from 10^2 to 10^6 increasing every intermediate order of magnitude. This is repeated for three values of the transport stage (TS), namely: $\tau_*/\tau_{*c} = 2.8$, 4.1 and 10 (TS 1, TS 2 and TS 3, respectively); in order to analyse the influence of increasing flow velocities. The grain diameter considered in the validation of the model is adopted, $D = 0.5$ mm. Figure 7.9 summarises the results. The saltation height has been selected as the target variable for clarity and because it is representative of the convergence behaviour followed by the other two variables. In order to avoid confusion, hereafter δ_s is defined as the maximum height reached by the centroid of the particle during a hop in relation to the collision line, as illustrated in Figure 7.3.

Points with vertical lines represent the mean values and standard deviations of δ_s

divided by the reference average value, $\delta_{s_{\text{ref}}}$, for $\tau_*/\tau_{*c} = 4.1$ (left y-axis). In order to provide further insight, Figure 7.9 also includes three curves showing the percentage error (right y-axis) corresponding to different transport stages. The lower part of Figure 7.9 shows the probability density of the averaged non-dimensional saltation height for different numbers of hops modelled for $\tau_*/\tau_{*c} = 4.1$. In all cases, the Freedman-Diaconis rule has been used in order to set the number of bins.

Several features arise from analysis of Figure 7.9. It can be noted that mean values are usually relatively close to the reference case, with errors no larger than 10%; also, that this error decreases to less than 1% if 10^3 or more hops are simulated. The reference case shows a well defined (from an informal, qualitative evaluation) gamma-type distribution that starts to be clearly recognisable after 10^4 hops. Hence, based on the first convergence criterion, it can be argued that 10^3 hops seem sufficient to assure convergence. However, in accordance with the second criterion, 10^4 hops appear to be better. This is interesting as most studies on continuous saltation report results for simulations of the order of hundreds of hops or less (e.g. Niño & García, 1998b; Lee *et al.*, 2000; Sekine & Kikkawa, 1992). Furthermore, the magnitude of the standard deviation seems to be independent of the number of hops.

Although a qualitative interpretation of higher-order moments (i.e. standard deviation, skewness and kurtosis) of the output distributions (second criterion) confirms the findings from a quantitative reading of the first moment (i.e. that the number of hops to be simulated should be $\geq 10^3$), a rigorous, quantitative evaluation of such moments should be carried out in order to confirm these results. This is, however, outside the scope of the present work, which seeks to provide a first, simple, general guideline (manifested also in the selection of a simple set of deterministic governing equations) to choose a number of hops to be modelled. A rigorous, quantitative statistical analysis

would probably be most beneficial when applied to a more sophisticated, physics-based model of particle saltation than the one herein adopted.

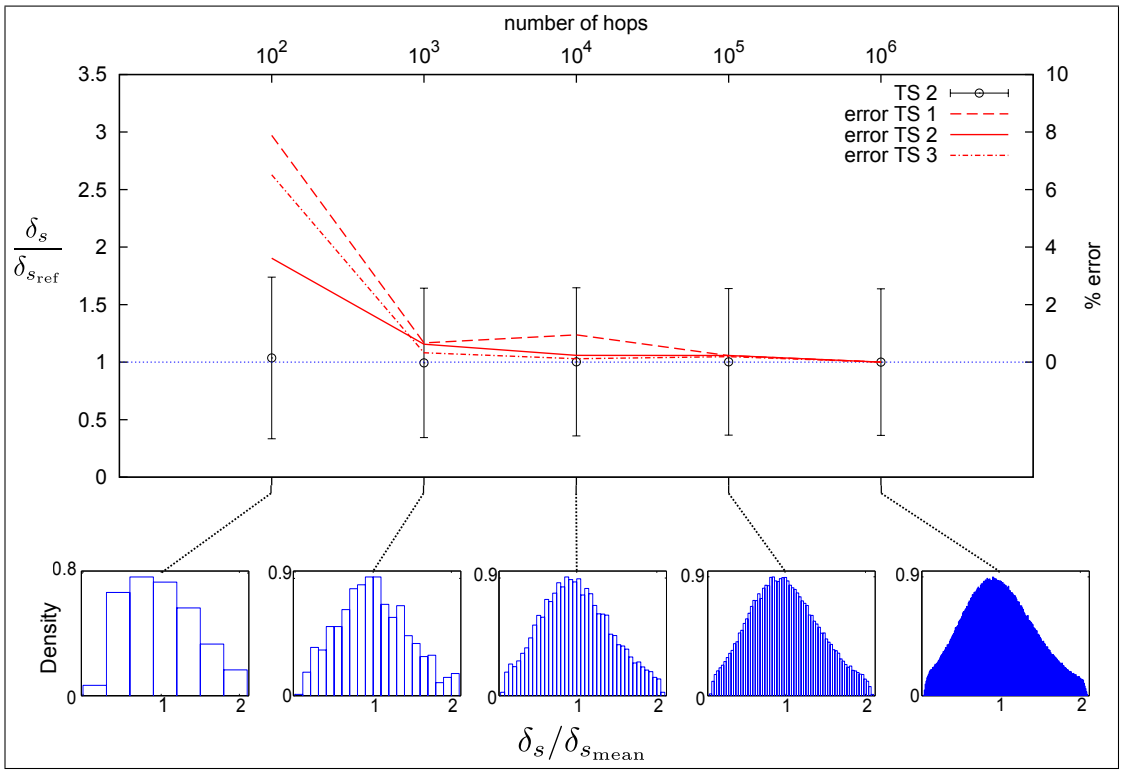

Figure 7.9: First and second convergence criteria, corresponding to upper and lower parts of the figure, respectively [In the legend, TS 1, 2 and 3 denote the three values of the transport stage simulated; i.e. $\tau_*/\tau_{*c} = 2.8$, 4.1 and 10, respectively]. The upper plot shows mean values (points) and two standard deviations (vertical lines) of δ_s for TS 2 divided by the mean value of the reference scenario, $\delta_{s_{\mathrm{ref}}}$ (left y-axis). Percentage errors (red lines) are superimposed for the three values of the TS modelled (right y-axis). The lower plots comprise probability densities of δ_s divided by the mean value given a number of hops simulated, for the case of TS 2.

Figure 7.10 illustrates how the measured δ_s tends towards the mean value (i.e. the standard deviation decreases) for increasing flow velocity conditions. Hence, it can be concluded that as the flow velocity increases, its influence on the saltation process also increases progressively by reducing the scatter in saltation characteristics caused by the (highly random) collision-rebound phenomenon. In other words, for increasing flow velocities, the fluid becomes the dominant agent in the saltation process, minimising

the influence that the random particle collision and rebound with the bed has on the deviation from the mean value of the saltation characteristics (i.e. it reduces such deviation).

The relationship between the variance found in the output variable δ_s and the variance set to generate the input variable θ_{out} has also been studied. For values of the variance of θ_{out} in the range of 200-400 deg^2 (Niño & García, 1998a), a linear response in the variance of δ_s/D occurs in the range of 0.28-0.35. Hence, a large increase in the variance of the input variable θ_{out} (i.e. 100%) corresponds to a relatively small response in the variance of the output variable δ_s D ($\approx 25\%$). Therefore, the variance of δ_s is not only independent of the number of hops simulated, but also weakly dependent on the input variance of θ_{out}.

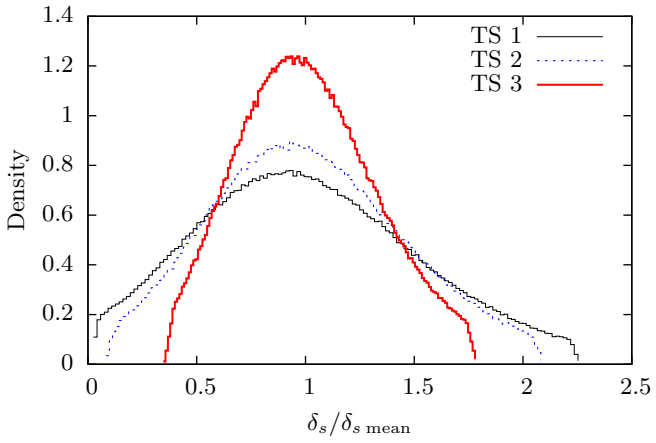

Figure 7.10: Probability densities of δ_s divided by the globally mean values for different transport stages (results shown after one million hops).

Figure 7.11 depicts the probability distributions followed by the three main saltation characteristics after one million hops; for illustration, the case of $\tau_*/\tau_{*c} = 4.1$ (TS 2) is considered. Notice that, of the three variables, δ_s exhibits the largest deviation from the mean value, whereas values of u_s tend to concentrate around the mean. Visual

inspection and quick distribution-fitting tests suggest that the probability density of the saltation characteristics is closest to the gamma-type family. This is in accordance with previous findings. Lee *et al.* (2000) concluded that δ_s and λ_s followed a Pearson Type III distribution, and that the measured(simulated) u_s followed a normal(uniform) distribution. Lee *et al.*'s results also show simulated values of u_s being concentrated around the mean. Experiments by Roseberry *et al.* (2012) and Furbish *et al.* (2012b) suggest an exponential distribution of the particle stream-wise velocity; however, it should be noted that their definition of such a velocity is instantaneous (i.e. $\dot{x}$) as opposed to the hop-averaged definition of u_s herein adopted.

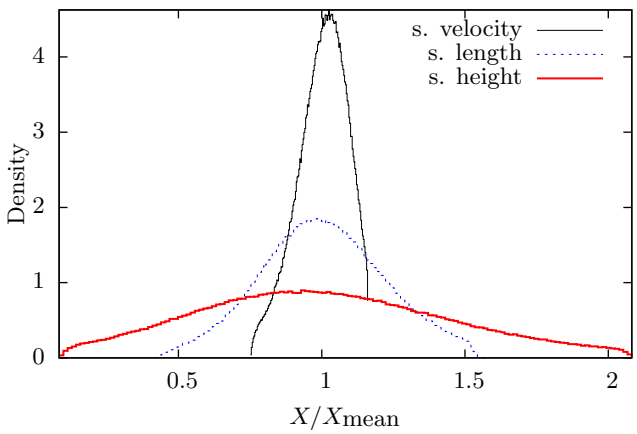

Figure 7.11: Probability densities of the saltation characteristics divided by the globally mean values, for the case of TS 2 (results shown after one million hops).

This study of statistical convergence also demonstrates an important feature of the present model: its mathematical simplifications permit a fast computer program to be used in order to simulate a large number of hops in an efficient manner. As an illustration, 10,000 hops can be simulated in about 1 minute (depending on the value of the shear velocity modelled) using a standard PC (i.e. Intel Core i3 3.10 GHz processor, 4 GB RAM). This feature is particularly important in the studies carried out in the following sections.

7.6 Sensitivity analysis

A constant value of f (which is the usual approach) implies that the stream-wise reduction of particle momentum is constant (i.e. collision-rebound events always occur in the same way). However, even though data reported in literature show an arguably constant behaviour of this coefficient, unsurprisingly, they also exhibit clear scatter (see e.g. Niño & García, 1998a). For this reason, the possibility of having a variable friction coefficient is now tested, by generating f from a uniform probability distribution, such that $f \sim U(f_{min}, f_{max})$. Hence, f_{min} and f_{max} denote the minimum and maximum values of f permitted, respectively. In a similar fashion to f, the influence of randomness on the collision line level, z_{in}, is also evaluated. This is done with the aim of taking into account the diverse irregularities inherent to the grains within the near-bed area (e.g. size, position, shape, etc.), both while saltating and resting on the bed, and which directly affect the position of the collision line.

These two factors have been selected for the sensitivity analysis given their direct impact on the collision-rebound mechanism (considered herein as the main goal of investigation within the saltation phenomenon). Sensitivity of the model to other factors so far neglected (such as Magnus force, turbulent fluctuations in the velocity profile, etc.) would provide a more profound insight into the understanding of a saltating particle; however, such analysis would probably merit another piece of work for future research.

By giving f and z_{in} (which have been treated as constants up to this point) values associated with a probability distribution, the influence of randomness is assessed from the effect it has on the mean values and standard deviations of the saltation characteristics, as well as on their statistical convergence. The Base Case is taken where

both f and z_{in} are constant, as previously validated. Three different combinations are tested, as explained below.

Case 1: constant f, random z_{in}. Whereas the friction coefficient has a calibrated constant value, i.e. $f = 0.85$, the value of z_{in} is generated from the uniform distribution, ranging from a lower limit of $0.6D$ (van Rijn, 1984a) up to a value of $0.75D$. These limits are obtained from geometrical considerations, as depicted in Figure 7.12.

Case 2: random f, constant z_{in}. For the reasons discussed above, the friction coefficient is generated as a uniformly distributed random number. Based on the available published literature, the value of this coefficient is allowed to vary within ± 0.1 from the calibrated constant value, hence $f \sim U(0.75, 0.95)$. The collision line is given as a constant value, fixed at $0.6D$ above the datum.

Case 3: random f, random z_{in}. In this case, the combined influence of randomness on the two variables is tested. The values of f and z_{in} are generated as described above.

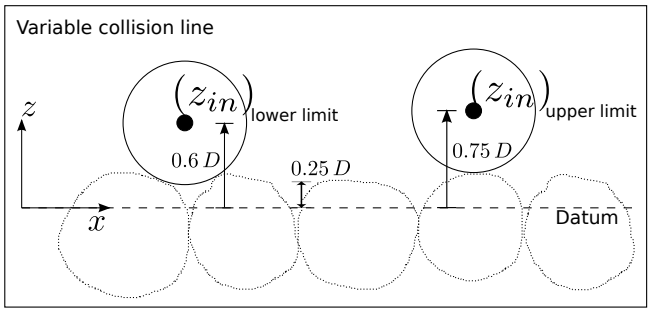

Figure 7.12: Sketch illustrating lower and upper limits of a variable collision line.

The same methodology described in §7.5 is applied herein to study statistical convergence. A reference scenario of 10^6 hops is simulated for each case and results from different n-hops runs are compared against the reference results. Mean values

and standard deviations of the three saltation characteristics, obtained after 10^6 hops, are compared for each case against the Base Case (where both f and z_{in} are constant). The transport stage modelled is $\tau_*/\tau_{*c} = 4.1$.

Figure 7.13 illustrates the percentage changes in mean and standard deviation of saltation height, length and velocity for each case, with respect to the Base Case. It can be observed that for all cases, the variation in the mean values falls within $\pm 2.5\%$ with respect to the Base Case. Regarding the standard deviations, variations of δ_s and u_s range from approximately -1 to 4%. However, a larger increase is present in the standard deviation for λ_s, up to values of about 12 and 15% for Cases 2 and 3, respectively, demonstrating the direct impact that a variation of the friction coefficient (reduction of the stream-wise velocity) has on the stream-wise distance reached by the particle during a hop (i.e. saltation length).

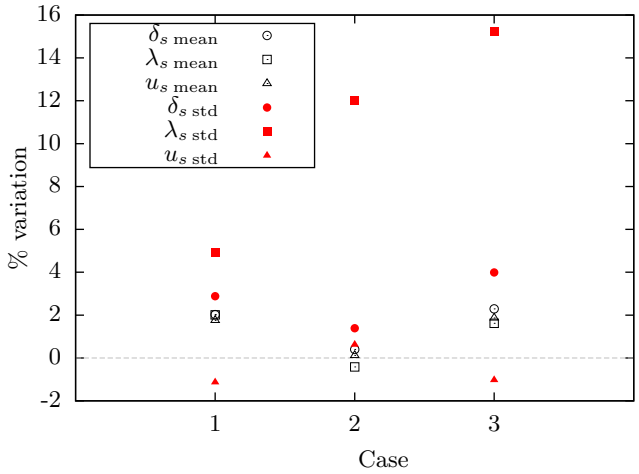

Figure 7.13: Percentage variation of the saltation characteristics for each case in relation to the Base Case (i.e. f and z_{in} constant). Unfilled symbols represent mean values; filled points denote standard deviations.

The first criterion for statistical convergence is depicted in Figure 7.14, where the percentage error of δ_s, calculated from (7.16), for each case is presented as a function of

the number of hops. The Base Case (curve 'error TS 2' in Figure 7.9) is also included. Observe that errors for 10^6 hops are not plotted because these are equal to zero by definition. The second convergence criterion is shown in Figure 7.15, which illustrates the probability density of the saltation height obtained for each case and the number of hops simulated. The saltation height and transport stage are representative of the behaviour of the other saltation characteristics and values of τ_*/τ_{*c} regarding statistical convergence.

Figures 7.14 and 7.15 confirm the conclusions found in §7.5 regarding statistical convergence, namely: at least 10^3 hops have to be simulated in order to assure a mean value of the characteristics with an error smaller than 1% (first criterion); and 10^4 hops or more should be modelled so that the probability distribution followed by the resultant saltation features resembles sufficiently the final gamma-type distribution obtained after 10^6 hops (second criterion).

Fig. 7.15 also shows an interesting feature of the final distribution resulting from Cases 2 and 3 (middle and bottom most-right panels): a small peak in the density as $\delta_s/\delta_{s_{\text{mean}}} \to 0$. Given that Cases 2 and 3 both have uniformly distributed friction coefficients, this peak seems to occur when a small value of f coincides (in a collision event) with a small value of θ_{out}, therefore resulting in a small and predominantly-streamwise-oriented take-off velocity (and hence limited height reached by the particle). This peak is related to the joint probability of occurrence of simultaneously small values of both f and θ_{out}. Furthermore, it should be noted that, as in the Base Case, the deviation from the mean value (i.e. the magnitude of the standard deviation) is independent of the number of hops for the three cases studied. Overall, it can be concluded that the influence of randomness on f and z_{in} is negligible when focusing on the mean values and convergence behaviour presented by the saltation characteristics.

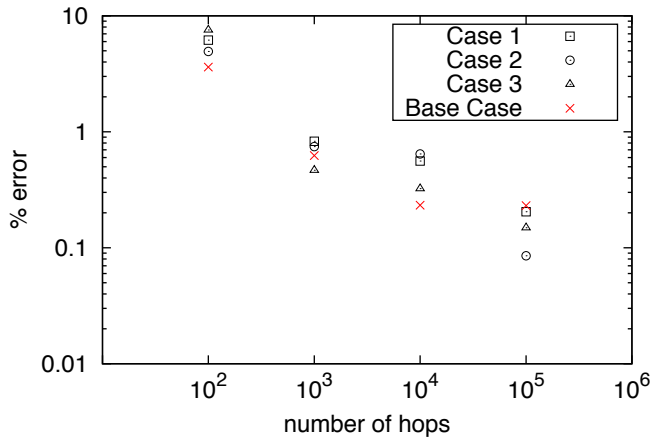

Figure 7.14: First convergence criterion for the three cases and the Base Case, for δ_s.

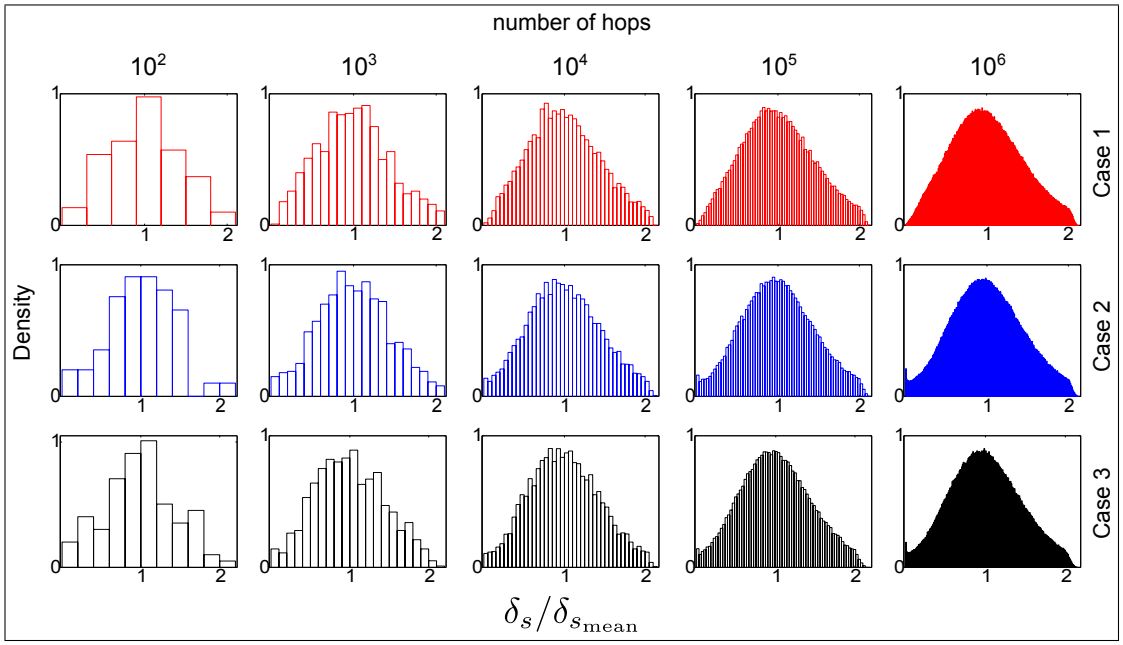

Figure 7.15: Probability densities of δ_s divided by the mean value (second convergence criterion) for Cases 1, 2 and 3 (top to bottom) and different numbers of hops simulated.

7.7 Regression equations

Ninety combinations are simulated, including 6 different particle sizes (D =0.1, 0.25, 0.5, 1.0, 2.0 and 4.0 mm) and values of τ_*/τ_{*c} in the range of 1 to 16. In accordance with the convergence criteria previously developed, 10^4 hops are simulated for each combination of D and τ_*/τ_{*c} in order to compute the mean value of the saltation characteristics. Regression equations are then obtained for the three saltation characteristics. Based on the work of other authors (see e.g. Lee *et al.*, 2000; van Rijn, 1984a), equations of the form $X_* = aD_*^b T_*^c$ are adopted; where X_*, $D_*(\equiv D[(s-1)g/\nu^2]^{1/3})$ and $T_*(\equiv \tau_*/\tau_{*c})$ denote the non-dimensional saltation characteristic, diameter and transport stage, respectively; a, b and c are coefficients. For the saltation velocity, the form $u_s/U_* = a + b\ln D_* + cT_*^{-0.5}$ is also tested.

The saltation length exhibits behaviour not predicted by other studies, to the author's knowledge. Figure 7.16 presents the variation in λ_s/D with D_* and T_*. It can be seen that, for a given T_*, the profile of λ_s/D evolves with D_* to drop rapidly to a minimum value at $D_* = 11.87$ (corresponding to $D = 0.5$ mm in this case); from that point on, it grows in an asymptotic fashion. Note that this value of the diameter corresponds to the minimum critical shear stress in the Shields curve. The other saltation characteristics do not present similar behaviour.

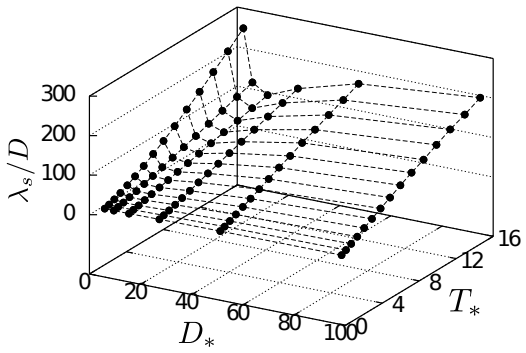

Figure 7.16: Simulated non-dimensional saltation length versus dimensionless diameter and transport stage.

When λ_s/D is instead plotted against bed shear stress (Fig. 7.17), the non-dimensional saltation length progressively increases with both D and τ_* in the range of $D \leq 2.0$ mm. At large particle diameters, the difference in λ_s/D for a given τ_* decreases. For $D = 4.0$ mm, the saltation length seems to decrease very slightly as compared to $D = 2.0$ mm, for a given bed shear stress. This can be related to the influence of the gravitational force on the saltation process. For a given bed bed shear stress, the non-dimensional saltation length increases with the particle diameter, up to a point (coarse sediments) where the self weight of the particle becomes a dominant agent in the saltation process, limiting the stream-wise distance reached by a particle during a hop in relation to its diameter (i.e. λ_s/D).

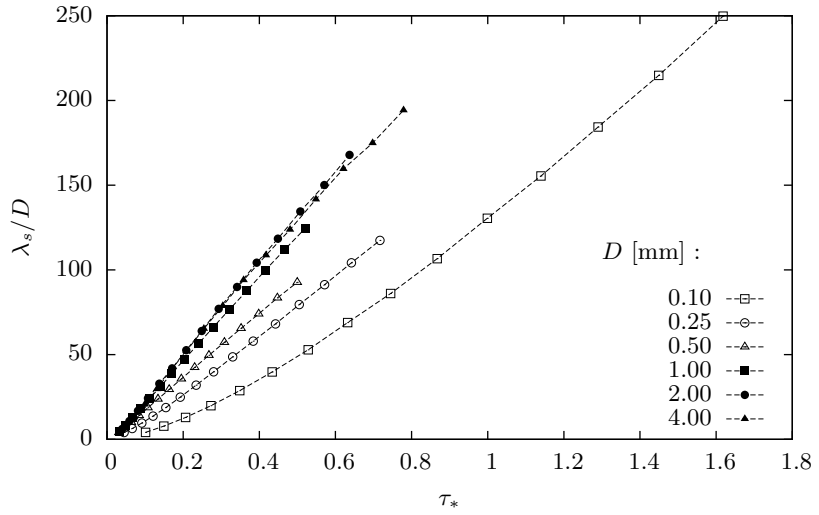

Figure 7.17: Simulated non-dimensional saltation length versus dimensionless bed shear stress for different particle sizes.

The above discussion underlines the importance of selecting an adequate independent variable (τ_* vs T_*) in studies of particle saltation. A step function is herein adopted in the regression equation for λ_s/D as $f(D_*, T_*)$. It should be noted that in practice most approaches to the bedload transport using saltating particle models disregard the saltation length; typically, bedload transport is modelled as the product $\delta_s u_s c_0$, where c_0 represents the sediment concentration within the bedload layer. However. further

discussion on this is made in §7.8.

The regression equations obtained, valid for $T_* \geq 1$, are:

$$\delta_s/D = 0.154\, D_*^{0.495}\, T_*^{0.73}\ , \tag{7.17}$$

$$\lambda_s/D = \begin{cases} 11.25\, D_*^{-0.62}\, T_*^{1.3} & \text{if } D_* < 12 \\ \\ 2.327\, D_*^{0.35}\, T_*^{1.03} & \text{if } D_* \geq 12 \end{cases}\ , \tag{7.18}$$

and

$$u_s/U_* = 4.355\, D_*^{0.14}\, T_*^{0.19} \tag{7.19a}$$

$$u_s/U_* = 8.328 + 1.328 \ln D_* - 6.232 T_*^{-0.5}\ . \tag{7.19b}$$

The corresponding values of the correlation coefficient R^2 for equations (7.17), (7.18), (7.19a) and (7.19b) are 0.98, 0.99, 0.93 and 0.94, respectively. Care should be taken when comparing against similar equations in the literature, given that different definitions of the transport stage, T_*, may be used. For example, another conventional definition of the transport stage is: $(U_*^2 - U_{*c}^2)/U_{*c}^2$ (where U_{*c} is the critical shear velocity for initiation of motion), which is equal to $T_* - 1$, with T_* as defined herein (i.e. $T_* \equiv \tau_*/\tau_{*c}$).

7.8 Bedload transport rate

The study of saltation is very useful when attempting to understand the mechanics of bedload transport. However, when saltating particle models are used to compute the bedload sediment transport rate, q_b, several considerations have to be taken into account. For instance, at low flow regimes (near the threshold of motion), rolling and sliding may be prominent modes of transport and so a saltating-particle-derived formula for q_b could underestimate the bedload transport rate under those conditions. On the other hand, at higher flow velocities, more particles are expected to entrain motion. However, if the number of grains in saltation is sufficiently large, results from an analysis like the present may lose validity due to the influence that a large number of particles in saltation may have on the fluid velocity and the effect of inter-particle collisions. Nonetheless, the present model is utilised in order to calculate bedload transport and compare it against other formulae available in the literature.

Figure 7.18 depicts a comparison between the non-dimensional bedload transport, $\Phi(\equiv q_b/[g(s-1)D^3]^{1/2})$, calculated using the present model against the saltating-particle-derived (SP) formulae of Lee *et al.* (2000) (L) and van Rijn (1984a) (vR), and the commonly used flume-data-derived expressions of Meyer-Peter & Müller (1948) (MPM), Soulsby (1997) (S) and Fernández Luque & van Beek (1976) (FLB). A grain diameter of 2 mm with $\rho_s = 2{,}650$ kg/m^3 has been used in all calculations. The relatively large discrepancies between the saltation-based expressions of Lee *et al.* (2000) and van Rijn (1984a) and the flume-data-based formulae, may be due to the observations stated above in this paragraph, the definition of bedload layer, and the consequent estimation of its sediment concentration. The present model yields a more satisfactory agreement with the formulae by Meyer-Peter & Müller (1948), Soulsby (1997) and Fernández Luque & van Beek (1976) (in comparison with the other two

saltation-based formulae), by computing bedload as $q_b = h_b c_0 u_s$; where the bedload layer concentration, evaluated as $c_0 = 0.117(T_* - 1)/D_*$ (van Rijn, 1984a), is taken as the sediment concentration of a bedload layer defined by the thickness h_b, related in turn to δ_s (calculated from eq. 7.17) through idealised geometrical considerations as $h_b = \delta_s + D$ (see Figure 7.19). For the sake of simplicity, u_s is evaluated using (7.19a) instead of (7.19b). The curve calculated with the present model has been plotted up to a value of τ_* roughly corresponding to $c_b = 0.25$, which has been experimentally found to be the average maximum concentration in a bedload layer (Spinewine, 2005).

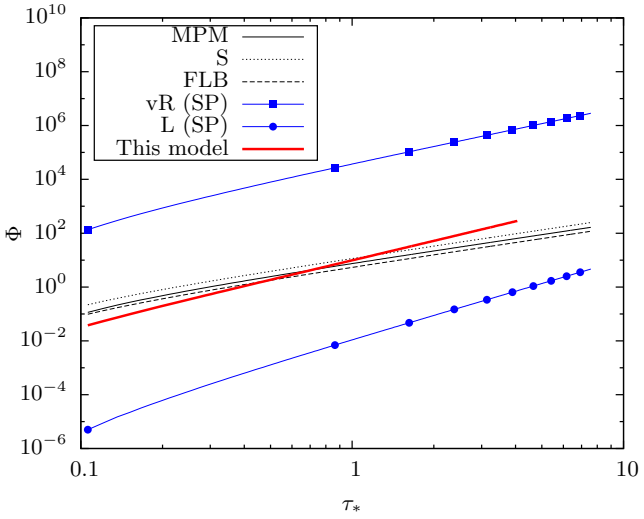

Figure 7.18: Non-dimensional bedload transport versus non-dimensional bed shear stress [Acronyms in legend defined in corresponding paragraph].

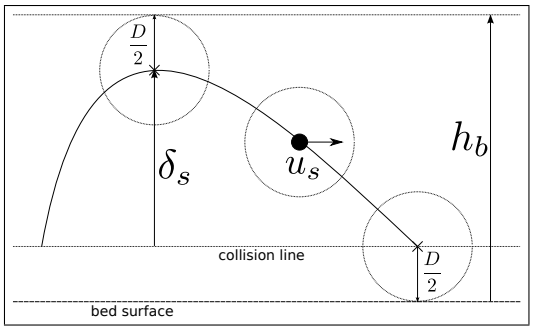

Figure 7.19: Sketch depicting relation between bedload layer thickness and particle saltation height.

An alternative method to estimate bedload transport rate is next examined. The bedload layer sediment concentration can be related to the probability of finding a particle in saltation at a given time (Wiberg & Smith, 1989). Here, it is assumed that such a probability is in turn proportional to the time a particle remains in saltation and inversely proportional to a control volume (related to the bedload layer). In other words, the longer the particle remains in saltation and the smaller (in its vertical dimension) the control volume, the more likely it will be to detect a saltating particle (from a side-view of the channel). In non-dimensional form, this can be expressed as follows:

$$c_{0*} \equiv \frac{c_0}{c_b} \propto \frac{t_{s*}}{h_{b*}}, \tag{7.20}$$

where the non-dimensional saltation time and bedload layer are given by $t_{s*} = \lambda_{s*}/u_{s*} = (\lambda_s/D)/(u_s/U_*)$ and $h_{b*} \equiv h_b/D$, respectively, thus yielding:

$$\frac{c_0}{c_b} \propto \frac{\lambda_s U_* D}{D u_s h_b}$$

$$\Rightarrow c_0 = K_c \frac{\lambda_s U_*}{u_s h_b}, \tag{7.21}$$

where K_c is a non-dimensional calibration constant. Recalling (7.18) and (7.19a), it can be noticed that the above expression predicts, on average, a roughly linear relationship between c_0 and the bed shear stress, in agreement with previous approaches (Fernández Luque & van Beek, 1976; van Rijn, 1984a; Wiberg & Smith, 1989).

The bedload transport rate, evaluated as $q_b = h_b c_0 u_s$, becomes:

$$q_b = h_b \left(K_c \frac{\lambda_s U_*}{u_s h_b} \right) u_s$$

$$= K_c \lambda_s U_* \, . \tag{7.22}$$

Fig. 7.20 compares the bedload transport estimated from (7.22) ('SSP independent') against the methodology described before (based on van Rijn's expression for bedload concentration: 'SSP-van Rijn') and the empirical formulae (saltation-based expressions by van Rijn, 1984a and Lee *et al.*, 2000 are excluded) depicted in Fig. 7.18. Four particle diameters are considered. A value of $K_c = 0.03$ is employed in all cases.

The bedload predicted by (7.22) yields significantly better agreement with empirical formulae as compared to the SSP-van Rijn approach. This good agreement holds for different particle sizes, though it is better for coarser sediments. This can be explained by analysing (7.22). Recalling that $\tau_* \propto U_*^2$ and invoking (7.18), it can be seen that for coarse sediments, (7.22) predicts approximately $\Phi \propto \tau_*^{3/2}$, in agreement with numerous empirical formulae. These results suggest that the assumption (7.20) is a sensible and practical approach to simulate bedload sediment concentration and bedload transport rate (bearing in mind the observations pointed out previously in this section) from saltation characteristics of the particle. Similar expressions to (7.22) have been proposed by other authors based on probabilistic ideas (e.g. Furbish *et al.*, 2012a; Seminara *et al.*, 2002).

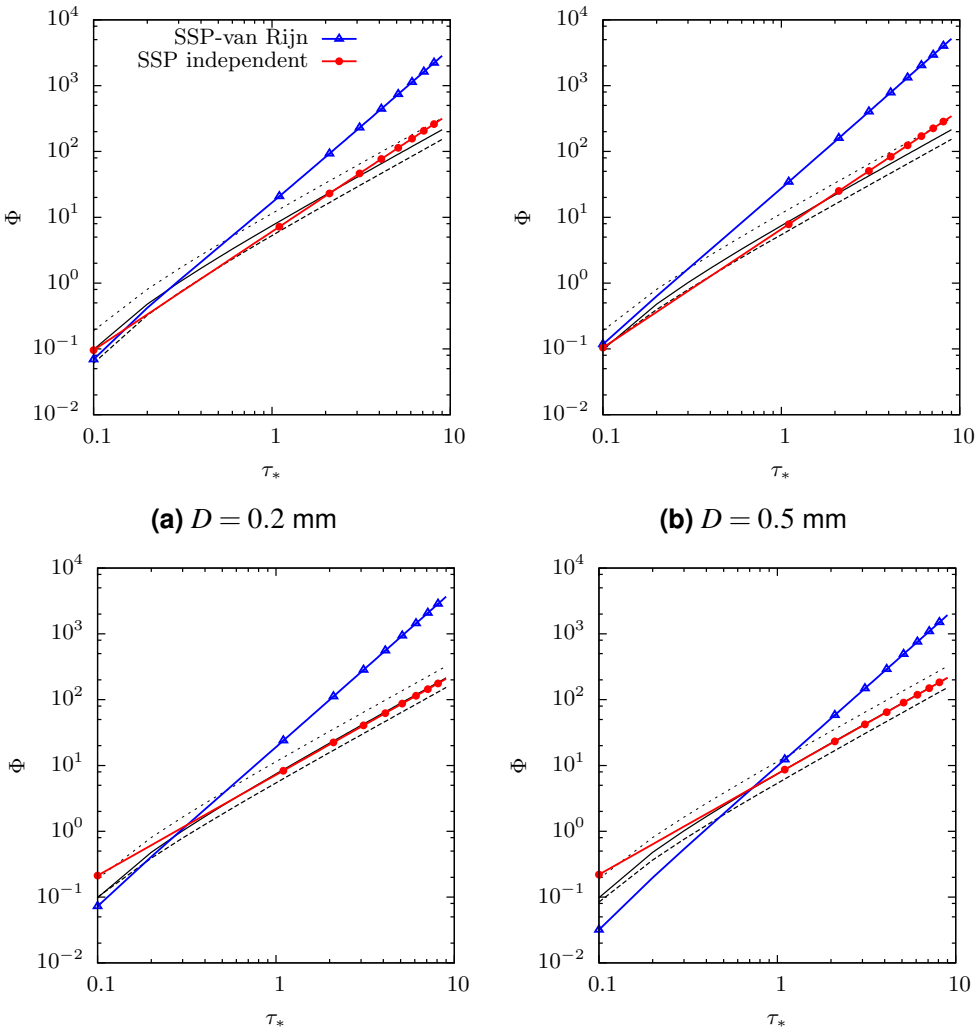

(a) $D = 0.2$ mm **(b)** $D = 0.5$ mm

(c) $D = 1.0$ mm **(d)** $D = 2.0$ mm

Figure 7.20: Non-dimensional bedload transport versus non-dimensional bed shear stress for four particle diameters. Comparison between present model standalone method (red line), the saltation-based approach based on van Rijn (1984a), and empirical bedload formulae (see legend in Fig. 7.18).

7.9 Chapter summary

A fast, efficient numerical model for stochastic saltation has been developed utilising a simple splash function and governing equations, and validated satisfactorily against experimental data on saltation height, length, and velocity, previously reported in the

literature.

Two criteria for statistical convergence were identified: one, of quantitative nature, is related to the error in the mean values of the saltation characteristics between different n-hops runs and a large-n-hops (i.e. 10^6 hops) reference scenario; the other, rather qualitative, is concerned with the deviation in the sampled characteristics from a well-defined probability distribution achieved after a large number of hops (i.e. 10^6) has been simulated. Model convergence tests show that at least 10^3 particle hops are needed to satisfy the first criterion, whereas 10^4 hops appear more convenient if the second criterion is to be satisfied. This finding is relevant, given that several previous studies report results after only a few hundred, or less, particle hops have been simulated.

The choice of empirical formula for the lift force component is important. The present work has shown that, for a stochastic saltation model of this kind, a formula dependent on the slip (relative) velocity of the particle multiplied by the vertical gradient of the horizontal flow velocity component (i.e. F_{L_1}, see eq. 7.5) gives more stable results than a formula dependent on the difference between the squares of the slip velocity components at the top and bottom of the particle (i.e F_{L_2}, see eq. 7.6).

A sensitivity analysis has shown that variations in the bed friction coefficient and the position of the collision line have almost no effect on the mean values and convergence behaviour presented by the saltation characteristics.

The saltation height and velocity both increase monotonically with increasing particle diameter. The saltation length is also dependent on the particle diameter for a given value of τ_*/τ_{*c}, but with a minimum at a critical value of the non-dimensional particle diameter ($D_* \sim 12$, corresponding to a particle diameter of about 0.5 mm for the

test cases considered herein). This confirms the importance of the selection of an appropriate variable (τ_* vs T_*) when analysing the saltation characteristics. Regression analysis has been used to determine empirical formulae for the saltation height, length and stream-wise velocity of a particle over a nearly horizontal bed.

The model has been used to compute the bedload transport rate through two methods: i) an available empirical formula for bedload concentration; and ii) a proposed alternative method for the estimation of c_0 based on saltation characteristics and a calibration parameter. Both methods provide results in good agreement with those from commonly used formulae by Meyer-Peter & Müller (1948), Soulsby (1997) and Fernández Luque & van Beek (1976) (especially when compared against the saltation-derived expressions proposed by Lee *et al.*, 2000 and van Rijn, 1984a). The second method, however, yields better agreement with results from the reference formulae than the first method. The very satisfactory and robust predictive behaviour of the second method suggests that the proposed alternative to estimate c_0 and q_b from saltation characteristics is based on sensible assumptions; i.e. that c_0 is proportional to a non-dimensional saltation time and inversely proportional to a control volume defined by a non-dimensional bedload layer.

This model could also be used to gain further insight into the saltation mechanism in steep sloping channels, thus complementing the work carried out in Chapter 6. Appendix C illustrates how the present Lagrangian model can be utilised as a complementary tool to the Q2L model here derived. In future, it would be useful to integrate a full Lagrangian model of saltation, rolling and sliding, to generate a more complete and insightful representation of bedload transport.

Chapter 8

Conclusions and future research

This thesis is primarily concerned with the study, through theoretical tools, of sediment transport (particularly bedload). Two models have been derived; namely: a Quasi-2-Layer model for sediment transport rates and morphological evolution (Chapters 2 to 6), and a stochastic Lagrangian model of particle saltation aimed at investigating the mechanics and statistics of bedload transport (Chapter 7).

This concluding chapter summarises the findings achieved throughout this thesis, identifies the main limitations and states some recommendations for future work.

8.1 Concluding remarks

8.1.1 On the Q2L model

A physics-based Quasi-2-Layer model for predicting sediment transport rates and morphological evolution has been presented. The model is a particular case of a 2-Layer SWE-based flow over an erodible bed. The main advantages of the model are:

- It reduces the high degree of empiricism (by being free from the selection of a particular empirical formula for sediment transport rates) common in conventional morphodynamic models.
- It captures accurately the physics behind sediment transport and morphological change caused by bed erosion in horizontal, sloping, flat and irregular beds.

- It naturally deals with the ambiguity inherent in the distinction between bedload and suspended load.
- It provides a closer representation of near-bed phenomena (e.g. flow velocity and sediment concentration profiles, bedload transport)

The model can simulate 3 modes of transport: no sediment transport at all, bedload only, and total load (i.e. bedload plus suspended load). Two main calibration parameters are required; namely, $c^{(b)}$ and $c^{(i)}$. The model can be tuned either from hydrodynamic data (information on the flow vertical distribution of the horizontal velocity) or by comparing it against sediment transport rates (measurements or empirical formulae). It is shown that both approaches yield mutually consistent estimations of the tuning parameters. Predicted bedload transport rates solely depend on $c^{(b)}$, whereas total load is dependent on both $c^{(b)}$ and $c^{(i)}$. As first approximation for practical applications, values of $c^{(b)}/c_f \in [4,6]$ (or $0.01 \lesssim c^{(b)} \lesssim 0.07$) and $c^{(b)} \sim c^{(i)}$ are anticipated. The thickness of the bedload layer, h_0, is set arbitrarily. However, it is demonstrated that within a pragmatic range of parameters, the Q2L model is weakly dependent on this variable. A default value of $h_0 = 10D$ is advised.

Analytical solutions to the model have been derived for the three modes of transport, for the case of a steady uniform flow over an erodible bed. These solutions provide a powerful tool to analyse the model in depth, and permit its insightful comparison against similar hydrodynamic and morphodynamic models, and general theory of sediment transport. The analytical solutions could also be used by fluvial engineers (given that river environments may often present steady or quasi-steady uniform flow) to estimate sediment transport rates based on river's physical characteristics (e.g. depth, bed material, slope).

The model is validated against empirical and semi-empirical expressions for bedload

an total load, yielding satisfactory results. For the case of bedload, the Q2L model is also thoroughly analysed analytically. The following remarks can be drawn from such an analysis:

- The bedload rate predicted by the model follows the general form $\Phi = A(\theta - \theta_c)\theta^{1/2}$, where A is a function of flow and sediment characteristics. This is in agreement with commonly employed formulae and experimental observations.
- Under sheet flow regime, the model predicts $q_b = B\bar{u}^3$. The proportionality $q_b \propto \bar{u}^3$ for sheet flow is widely accepted. An expression for B (see eq. 4.45) is derived. The thickness of a sheet layer can also be estimated from the model, consistent with estimates from previous approaches.
- Within the framework of the Q2L model, confronting views (Bagnoldian ideas vs their critics) about the behaviour of shear stress under sediment-transport conditions, seem to reconcile.

The Q2L model has been compared against a conventional morphodynamic model (consisting of a coupling between the SWE, the Exner equation, and the Grass formula for bedload; see eqs. 4.52) for the benchmark case of an erodible migrating hump subject to a subcritical current. When solved using finite differences, the aforementioned conventional model is known to predict the development of unrealistic high-frequency oscillations in the bed elevation, which eventually render the model unstable. However, using the same numerical solver, the Q2L model does not predict the appearance of such oscillations, and it reproduces correctly the expected (from a qualitative viewpoint) behaviour of the hump; i.e. the hump migrates downstream and its lee steepens with time. In this sense, the Q2L model outperforms the conventional approach, presumably because, unlike the latter, the former inherently includes the effect of local bed-slopes on bedload transport, which prevents unrealistic oscillations from developing. This hypothesis has motivated a thorough investigation into the influence of bed-slope on bedload.

Analysis of the bed-slope influence on bedload is presented in Chapter 6. The inherent ability of the Q2L model to capture the effect of bed-slope on sediment transport is confirmed through validation against empirical data from a steep sloping channel. The influence of bed-slope on bedload is found (confirmed) to be maximum for steep bed-slopes and slow flow velocities (i.e. near incipient sediment motion), and to vanish at large flow velocities.

The model is then used to derive analytical expressions whose goal is to modify bed-load empirical formulae (originally derived for nearly horizontal channels) in order to render them applicable to steep stream-wise slopes. Inclusion of such slope-related expressions in a conventional model (eqs. 4.52) is proven to improve it significantly, by yielding stable, realistic results. Other alternatives to account for the bed-slope influence tend to yield unrealistic results (e.g. Bailard & Inman, 1981), further increase the level of empiricism (e.g. Watanabe, 1988), or imply a substantial degree of complexity and/or empiricism (e.g. Parker *et al.*, 2003;Damgaard *et al.*, 1997; Smart, 1984). The Q2L model provides relatively simple, reliable means of enhancing a conventional morphodynamic model for its use in arbitrary stream-wise sloping channels.

A set of case studies has demonstrated that the bed-slope influence on bedload and morphology is most important for long-term predictions at low flow velocities and steep slopes. Such conditions can be found in practice, for example, in coastal, estuarine, and mountain-river environments. When fast morphological changes take place (e.g. due to a dam-break), the fast flow velocities involved overshadow the gravitational effect of bed-slope on sediment transport (and thus, on morphological evolution).

8.1.2 On the Lagrangian study of bedload

A mathematically-simple and computationally-efficient model for stochastic particle saltation has been proposed. The model utilises relatively simple equations governing the trajectory followed by a spherical particle during saltation, in combination with a laboratory-data-based stochastic approach to the splash function (i.e. particle collision with the bed and consequent rebound). The model is satisfactorily validated against empirical data for particle saltation.

When similar saltation models are used, the number of hops to be simulated is often selected in a rather arbitrary fashion. This thesis outlines two criteria for the number of hops to be modelled, aimed at ensuring that final results are free from statistical errors emanating from the size of the sample. According to the first criterion (a quantitative indicator), a minimum of 10^3 hops ought to be considered, whereas the second criterion (of a rather qualitative nature) suggests than at least 10^4 realisations are required to ensure statistical convergence of the measured variables (i.e. the saltation characteristics). These findings are relevant given that previous studies on particle saltation tend to report results after only a few hundred, or less, hops have been simulated.

Two different types of formulae to estimate the lift force on a saltating particle are commonly used in the literature. This study shows that, for a model similar to the one herein presented, a formula dependent on the slip (relative) velocity of the particle multiplied by the vertical gradient of the horizontal flow velocity component (i.e. F_{L_1}, see eq. 7.5) gives more stable results than a formula dependent on the difference between the squares of the slip velocity components at the top and bottom of the particle (i.e F_{L_2}, see eq. 7.6).

Sensitivity analysis demonstrates that variations in the friction coefficient f (commonly considered constant) and the position of the collision line have negligible influence on the statistical behaviour of a saltating particle.

Finally, the model is employed to estimate bedload transport rate (cautionary remarks regarding the use of saltating particle models for bedload prediction are also provided). Two methodologies are followed; namely:

- Bedload is computed as the product $h_b c_0 u_s$, where h_b is related to δ_s, and c_0 is computed from the empirical formula by van Rijn (1984a).
- Based on the assumption that the bedload sediment concentration is proportional to a non-dimensional saltation time and inversely proportional to a particle-related non-dimensional control volume, bedload is calculated as $q_b = K_c \lambda_s U_*$.

Both of the above approaches yield satisfactory agreement with popular bedload formulae, especially when compared against the performance of other saltation-based bedload expressions. The second approach, however, proves to be a more accurate and robust method to estimate bedload from saltation characteristics.

8.2 Limitations and future work

The Q2L model has proved to be a valuable tool for predicting morhodynamics and analysing particular aspects of sediment transport. This thesis is primarily concerned with bedload; however, the Q2L model has also demonstrated to be potentially useful in cases where suspended load is present. Further research is then encouraged regarding the use of the model in scenarios dealing with total load.

The validity of the conclusions achieved with respect to bedload are limited to predominantly 1D cases (e.g. rivers). The expansion of the Q2L model to 2DH would

enable the analysis of a larger spectrum of case studies. For example, the combined influence of stream-wise and transverse bed-slopes could be investigated. Phenomena present in coastal environments could also be studied; e.g. formation and behaviour of beach cusps, sand bars, and complex morphological patterns in tidal inlets. Previous numerical investigations on the aforementioned features have proven to be influenced by uncertainty arising from empirical expressions for sediment transport rates (e.g. Dodd *et al.*, 2008; Garnier *et al.*, 2006; Dissanayake *et al.*, 2009), and so the Q2L model could generate meaningful insight into these cases. When dealing with the shore environment, however, wet-dry fronts are commonly encountered. Thus, the inclusion of a wetting-and-drying algorithm would represent a very valuable addition to the model.

Numerical solvers based on finite differences (herein adopted) have some limitations, for example, when dealing with sharp gradients in the free surface and flow velocity. Therefore, developing and adopting a finite-volume shock-capturing numerical solver would allow the Q2L model to be used for cases involving fast morphological changes (e.g. dam-breaks over erodible beds, a swash event on a beach). To this end, a good starting point would be the work of e.g. Li *et al.* (2013); Hu *et al.* (2012); Lee (2011); Apostolidou (2011); Fraccarollo & Capart (2002); Chacón Rebollo *et al.* (2003); Toro (2001); Spinewine (2005).

In this thesis, uniform sediment size has been assumed. In order to expand the applicability of the Q2L model to more realistic scenarios, variable particle sizes should be considered. Given that the model is designed to represent bedload and suspended load separately, a natural candidate to account for variable sediment diameter is the two-fraction approach (Wilcock, 1998; Wilcock & Kenworthy, 2002). This model divides the bed sediment in sand and gravel. The Q2L model then would tentatively treat sand

as suspended load, and gravel as bedload.

An intensive parameter study should be undertaken in order to assess the influence that the estimation of, for example, τ or τ_c, has on the prediction of sediment transport rates and morphological evolution. In this thesis, the friction coefficient $c^{(b)}$ is considered a calibration constant. Such an assumption is sensible for most of the case studies herein investigated. Nevertheless, it would be interesting to further investigate and enhance this parameter. For example, it would be useful to express $c^{(b)}$ as a function of a Chézy or Manning coefficient, and to analyse the potential effect that bed features (e.g. ripples) and oscillatory flow may have in the value of $c^{(b)}$.

Further validation of the Q2L model against experiments and benchmark case studies is encouraged. In particular, it would be interesting to compare the predictions of A (see eq. 4.41) against a large data set of bedload measurements, encompassing diverse flow conditions and sediment characteristics.

With respect to the Lagrangian study of bedload, the proposed Simple Saltating Particle model could be used to predict the statistical behaviour of a saltating particle in steep sloping channels (to the author's knowledge, relevant experimental data are very scarce). The derivation of two simple criteria for statistical convergence has been motivated by the idea of generating a first-approximation guideline to the number of particle saltations to be simulated. However, a more thorough statistical analysis of convergence, which quantifies higher-order statistical moments, would be highly desired. Expansion of the SSP model to 3D (i.e. inclusion of the transverse deviation of the saltating particle) would generate further insight into the mechanics of saltation. An integrated model of particle saltation, rolling and sliding, would lead to a more complete representation of bedload transport. Findings arising from the Lagrangian

investigation of bedload would complement the analysis undertaken by means of the Q2L model.

Appendix A

Bedload formulae

Compilation of some works providing either a novel or modified version of a previously derived bedload formula. The list is sorted chronologically.

1. Schoklitsch (1934)
2. Meyer-Peter & Müller (1948)
3. Einstein (1950)
4. Bagnold (1963)
5. Yalin (1963)
6. Engelund & Hansen (1967)
7. Bijker (1968)
8. Ashida & Michue (1972)
9. Ackers & White (1973)
10. Fernández Luque & van Beek (1976)
11. Engelund & Fredsøe (1976)
12. Bailard & Inman (1981)
13. Grass (1981)
14. White & Day (1982)
15. Smart (1984)
16. van Rijn (1984a)
17. Wilson (1987)

18. Wiberg & Smith (1989)
19. Parker (1990)
20. Madsen (1991)
21. Nielsen (1992)
22. Dibajnia & Watanabe (1992)
23. Nnadi & Wilson (1992)
24. Ribberink & Al-Salem (1994)
25. Inui *et al.* (1995)
26. Soulsby (1997)
27. Damgaard *et al.* (1997)
28. Ribberink (1998)
29. Niño & García (1998b)
30. Wu *et al.* (2000)
31. Lee *et al.* (2000)
32. Wilcock & Kenworthy (2002)
33. Cheng (2002)
34. Abrahams (2003)
35. Barry *et al.* (2004)
36. Camenen & Larson (2005)
37. Wong & Parker (2006)
38. Abrahams & Gao (2006)
39. Rosgen *et al.* (2006)
40. Yager *et al.* (2007)
41. Chiari *et al.* (2010)
42. Kuhnle *et al.* (2013)

Appendix B

On Exner equation

Consider the Exner equation:

$$\frac{\partial z_b}{\partial t} + \xi \frac{\partial q_b}{\partial x} = 0, \tag{B.1}$$

An equation of the same type as (B.1) can be derived from the framework of the present model by considering the conservation of sediment mass in the bed (L_b) and the transport layer above it (L_0). In layers L_b and L_0, the amount of sediment mass at a given time per unit channel width in a volume longitudinally defined by Δx is $\rho_s(c_b z_b + c_0 h_0)\Delta x$, where c_b is the bed sediment concentration, c_0 denotes the sediment concentration within L_0, and ρ_s is the density of sediment. The rate of sediment mass entering the control volume is $\rho_s c_0 h_0 u_{s0}$, where u_{s0} is the sediment particles streamwise velocity in L_0 (note that no sediment enters or leaves horizontally the static layer L_b because its velocity is by definition $u_b = 0$, as shown in Fig. 2.1.a). Ignoring non-linear terms in the Taylor series expansion, the rate of sediment leaving the control volume is $\rho_s c_0 h_0 u_{s0} + \Delta x \partial(\rho_s c_0 h_0 u_{s0})/\partial x$. Hence, the temporal variation of sediment in the control volume is given by:

$$\frac{\partial[\rho_s(c_b z_b + c_0 h_0)]}{\partial t}\Delta x = \rho_s c_0 h_0 u_{s0} - \left(\rho_s c_0 h_0 u_{s0} + \frac{\partial(\rho_s c_0 h_0 u_{s0})}{\partial x}\Delta x\right)$$

$$\Rightarrow \frac{\partial(c_b z_b)}{\partial t} + h_0 \frac{\partial c_0}{\partial t} + \frac{\partial(c_0 h_0 u_{s0})}{\partial x} = 0.$$

Noting that $c_0 h_0 u_{s0}$ represents the volumetric sediment transport rate per unit width within the bedload layer, $q_b = c_0 h_0 u_{s0}$, and that c_b is the complement of the bed porosity ($c_b = 1 - e_b$), the above expression can be written as:

$$\frac{\partial z_b}{\partial t} + \xi h_0 \frac{\partial c_0}{\partial t} + \xi \frac{\partial q_b}{\partial x} = 0, \tag{B.2}$$

where $\xi = 1/c_b = 1/(1 - \varepsilon_b)$. The above equation is the same as Exner equation, except for the term $\xi h_0 \partial c_0/\partial t$, which is related to the adaptation time required for accelerating/de-accelerating sediment particles when crossing the interface (b) between layers with different velocities (i.e. L_b and L_0). The above derivation thus proves, or confirms, that i) the Exner equation does not strictly represent conservation of mass in the bed –as often referred to in the literature– but denotes conservation of sediment mass in the bed and bedload layer; and ii) the Exner equation is a particular case of (B.2) when sediment transport steady or quasi-steady conditions are considered (i.e. such that $\partial c_0/\partial t \approx 0$).

Appendix C

Sediment particle velocity vs sediment-water mixture velocity

Throughout this thesis, it has been assumed that the velocity of the water-sediment-mixture layers (u_0 and u_1) can be employed instead of that of the sediment particles transported in such layers (u_{s0} and u_{s1}), when estimating sediment transport rates. Such an assumption is often taken to be valid in the case of suspended load (i.e. $u_{s1} = u_1$), where sediment is transported at approximately the same speed of the flow. However, within the near-bed region, the streamwise velocity of the sediment particles may differ significantly from that of the driving flow. In this section, results from Chapters 4 and 7 are employed to investigate the relationship between u_{s0} and u_{s1}.

Whereas in Chapter 4, the bedload rate is estimated as $q_b = h_0 c_0 u_0$, strictly u_0 should be replaced by u_{s0}, as q_b represents the *sediment* transport rate transported as bedload. Hence, the *exact* bedload sediment transport rate is given by:

$$q_b = h_0 c_0 u_{s0}. \tag{C.1}$$

Results from Chapter 7 –which investigates bedload from a Lagrangian framework– can be used to find a relation between velocities u_{s0} and u_0. In §7.7, based on the work by van Rijn (1984a) and Engelund & Fredsøe (1976), an equation of the form $u_s/U_* = \widehat{a} + \widehat{b} \ln D_* + \widehat{c} T_*^{-1/2}$ (where $\widehat{a}$, $\widehat{b}$ and $\widehat{c}$ are calibration coefficients) was employed in

the regression analysis applied to values of the non-dimensional streamwise particle velocity, u_s/U_*, obtained from numerical experiments. From such analysis, the value of $\widehat{c}$ was found to be negative ($\widehat{c} = -6.232$), and so the expression for u_s/U_* can be alternatively written as:

$$u_s/U_* = \widehat{a} + \widehat{b}\ln D_* - \widehat{c}T_*^{-1/2}, \tag{C.2}$$

where $\widehat{c}$ is expected to be a positive number. Consider now the following relations:

$$T_* \equiv \frac{\tau_*}{\tau_{*c}} = \frac{\tau}{\tau_c}; \tag{C.3}$$

and

$$\tau = \rho_w U_*^2 = \tau_0^{(b)} = \rho_0 c^{(b)} u_0^2; \tag{C.4}$$

with the variables defined in the Nomenclature section.

For a given particle diameter, the streamwise particle velocity can be written as:

$$u_s = \widehat{d}U_* - \widehat{c}\left(\frac{U_*^2}{U_{*c}^2}\right)^{-1/2} U_*$$

$$= \widehat{d}U_* - \widehat{c}U_{*c}, \tag{C.5}$$

where $\widehat{d} = \widehat{a} + \widehat{b}\ln D_*$. Invoking (C.4), the above equation yields:

$$u_s(= u_{s0}) = \widehat{d}\left(\frac{\rho_0 c^{(b)}}{\rho_w}\right)^{1/2} u_0 - \widehat{c}\left(\frac{\tau_c}{\rho_w}\right)^{1/2}. \tag{C.6}$$

Observe that for conditions well beyond the threshold of motion ($\tau_c \approx 0$), a linear

relationship between u_{s0} and u_0 holds, namely:

$$u_s(=u_{s0}) = \widehat{d}\left(\frac{\rho_0 c^{(b)}}{\rho_w}\right)^{1/2} u_0. \tag{C.7}$$

Recall the analytical solution for bedload derived in §4.1.3, eq. (4.21), rewritten here for convenience:

$$q_b = \frac{\left(\tau_0^{(b)} - \tau_c\right)}{(\rho_s - \rho_w) g \tan\varphi} u_0$$

$$= \frac{\left(\tau_0^{(b)} - \tau_c\right)}{(\rho_s - \rho_w) g \tan\varphi} \left(\frac{\tau_0^{(b)}}{\rho_0 c^{(b)}}\right)^{1/2}. \tag{C.8}$$

Substitution of u_0 in the above equation by u_{s0} given by (C.6) (assuming $\tau_c \approx 0$), yields:

$$q_b = \frac{\left(\tau_0^{(b)} - \tau_c\right)}{(\rho_s - \rho_w) g \tan\varphi} u_{s0}$$

$$= \frac{\left(\tau_0^{(b)} - \tau_c\right)}{(\rho_s - \rho_w) g \tan\varphi} \widehat{d}\left(\frac{\rho_0 c^{(b)}}{\rho_w}\right)^{1/2} u_0$$

$$= \frac{\left(\tau_0^{(b)} - \tau_c\right)}{(\rho_s - \rho_w) g \tan\varphi} \widehat{d}\left(\frac{\rho_0 c^{(b)}}{\rho_w}\right)^{1/2} \left(\frac{\tau_0^{(b)}}{\rho_0 c^{(b)}}\right)^{1/2}$$

$$= \widehat{d}\frac{\left(\tau_0^{(b)} - \tau_c\right)}{(\rho_s - \rho_w) g \tan\varphi} \left(\frac{\tau_0^{(b)}}{\rho_w}\right)^{1/2}. \tag{C.9}$$

Eq. (C.9) shows that the predicted bedload is not dependent any more on the parameter $c^{(b)}$; however, coefficient $\widehat{d}$ has now to be set instead. In other words, by considering

u_{s0} instead of u_0 in the computation of q_b, the calibration of the model simply switches from coefficient $c^{(b)}$ to coefficient $\widehat{d}$. In fact, for conditions well beyond the threshold of motion, both coefficients relate through:

$$\widehat{d}\left(\frac{1}{\rho_w}\right)^{1/2} = \left(\frac{1}{\rho_0 c^{(b)}}\right)^{1/2}. \tag{C.10}$$

Observe also that when u_{s0} is employed in the estimation of q_b, the bedload rate is not dependent on the arbitrary selection of h_0; i.e. $q_b \neq f(h_0)$. Conversely, when u_0 is used in q_b, then $q_b = f(h_0)$ (through ρ_0). Note that, as demonstrated in §4.4, the dependence of q_b on h_0 is nevertheless weak. Thus, the results from this section may suggest that, when rigorously estimated (i.e. use of u_{s0}), the bedload predicted by the model has the advantage of being independent from the arbitrary selection of h_0. However, note that in such a case, two tuning parameters, $\widehat{a}$ and $\widehat{b}$, still have to be set ($\widehat{d} = \widehat{a} + \widehat{b}\ln D_*$) – here, they have been estimated from numerical experiments (see §7.7).

The above analysis has focused on flow conditions well beyond the threshold of motion, mainly because in the incipient motion regime, uncertainty in the quantification of bedload is inherently large (for example, because of the difficult estimation of an accurate τ_c under this condition; see §1.1.6). However, it is also interesting to consider the condition $\tau \sim \tau_c$. Under such circumstances, use of (C.6) in (4.21), leads to:

$$q_b = \frac{\left(\tau_0^{(b)} - \tau_c\right)}{(\rho_s - \rho_w) g \tan\varphi}\left[\widehat{d}\left(\frac{\tau_0^{(b)}}{\rho_w}\right)^{1/2} - \widehat{c}\left(\frac{\tau_c}{\rho_w}\right)^{1/2}\right]. \tag{C.11}$$

Note that the above equation follows the form of expressions for bedload proposed by Ashida & Michue (1972) (see Table 4.1) and Madsen (1991).

Based on numerical experiments within a Lagrangian framework, in §7.7 the following

values of the calibration parameters required in (C.11) were obtained: $\widehat{d} = 8.328 + 1.328 \ln D_*$ and $\widehat{c} = 6.232$. Fig. C.1 compares the bedload rate predicted by (C.11), using the aforementioned values of the coefficients, against the analytical solution derived in §4.1.3 (eq. C.8). Two particle diameters are considered. Fig. C.1 confirms the similarity between the two expressions found above mathematically. Slight differences in the slopes of the curves can be perceived, which result from variations of ρ_0 in (C.8) with $\tau_0^{(b)}$. For $c^{(b)} \approx 0.01$, both expressions yield very similar results. However, this is only the case for the considered values of calibration coefficients $\widehat{a}$, $\widehat{b}$ and $\widehat{c}$, which result from particular ranges of particle diameter and flow velocity investigated in §7.7.

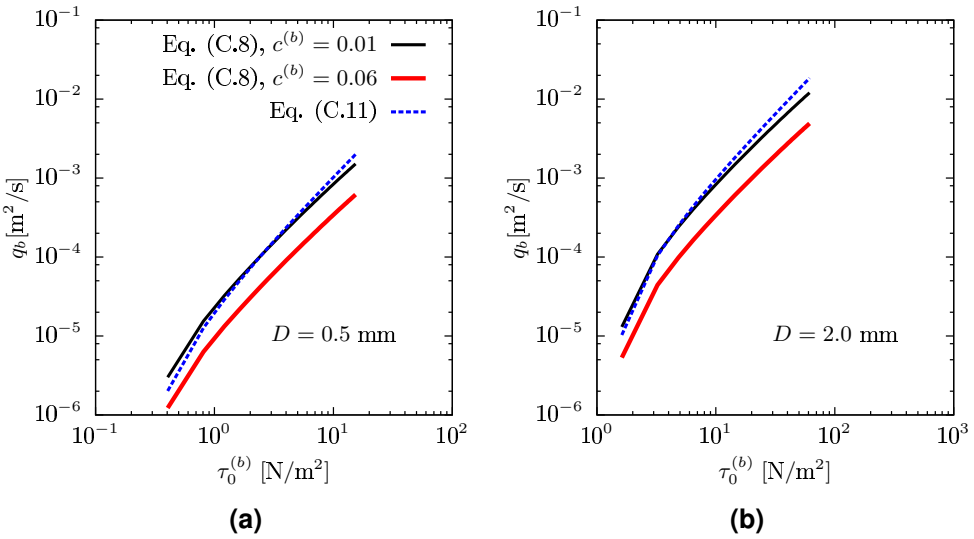

Figure C.1: Comparison between dimensional bedload predicted by $q_b = f(u_{s0})$ (eq. C.11) and $q_b = f(u_0)$ (eq. C.8) –for two values of $c^{(b)}$– for two different sediment diameters.

The present Appendix proves that the results and analysis presented throughout this thesis regarding the Q2L model, based on the assumption $u_0 \approx u_{s0}$, hold valid from a practical viewpoint. Also, from a rigorous position, bedload transport rates predicted by the Q2L model should use u_{s0} instead of u_0. To this end, the Lagrangian model presented in Chapter 7 can be used as an auxiliary tool to estimate the relation between both variables.

Bibliography

Abbott, M. (1979). *Computational Hydraulics: Elements of the Theory of Free Surface Flows.* Ashgate, Great Britain.

Abrahams, A. D. (2003). Bed-Load Transport Equation for Sheet Flow. *Journal of Hydraulic Engineering*, 129(2):159–163.

Abrahams, A. D. and Gao, P. (2006). A bed-load transport model for rough turbulent open-channel flows on plane beds. *Earth Surface Processes and Landforms*, 31(7):910–928.

Absi, R. (2011). An ordinary differential equation for velocity distribution and dip-phenomenon in open channel flows. *Journal of Hydraulic Research*, 49(1):82–89.

Ackers, P. and White, W. R. (1973). Sediment transport: new approach and analysis. *Journal of the Hydraulics Division*, 99.

Amoudry, L. O. and Souza, A. J. (2011). Deterministic coastal morphological and sediment transport modeling: A review and discussion. *Reviews of Geophysics*, 49(2010):1–21.

Ancey, C. (2010). Stochastic modeling in sediment dynamics: Exner equation for planar bed incipient bed load transport conditions. *Journal of Geophysical Research: Earth Surface (2003–2012)*, 115(F2).

Ancey, C., Böhm, T., Jodeau, M. and Frey, P. (2006). Statistical description of sediment transport experiments. *Physical Review E - Statistical, Nonlinear, and Soft Matter Physics*, 74:1–14.

Ancey, C., Iverson, R. M., Rentschler, M. and Denlinger, R. P. (2008). An exact solution for ideal dam-break floods on steep slopes. *Water Resources Research*, 44(1):1–10.

Anderson, R. S. and Hallet, B. (1986). Sediment transport by wind: Toward a general model. *Geological Society of America Bulletin*, 97(5):523–535.

Apostolidou, I.-G. (2011). *Variable Density Shallow Flow Model for Flood Simulation.* DPhil thesis, University of Oxford, Oxford, U.K.

Armanini, A. and Di Silvio, G. (1988). A one-dimensional model for the transport of a sediment mixture in non-equilibrium conditions. *Journal of Hydraulic Research*, 26:275–292.

Ashida, K. and Michue, M. (1972). Study on hydraulic resistance and bed-load transport rate in alluvial streams. *Journal of Civil Engineering, Jpn Soc Civil Engineers*, 206:59–69.

Bagnold, R. A. (1956). The Flow of Cohesionless Grains in Fluids. *Philosophical Transactions of the Royal Society A: Mathematical, Physical and Engineering Sciences*, 249(964):235–297.

Bagnold, R. A. (1963). Mechanics of marine sedimentation. In Hill, M. N., editor, *The sea*, volume 3. Interscience Publishers, Great Britain.

Bagnold, R. A. (1973). The Nature of Saltation and of 'Bed-Load' Transport in Water. *Proceedings of the Royal Society A: Mathematical, Physical and Engineering Sciences*, 332:473–504.

Bailard, J. A. and Inman, D. L. (1981). An energetics bedload model for a plane sloping beach: Local transport. *Journal of Geophysical Research*, 86(C3):2035.

Bakhtyar, R., Yeganeh-Bakhtiary, A., Barry, D. A. and Ghaheri, A. (2009). Two-phase hydrodynamic and sediment transport modeling of wave-generated sheet flow. *Advances in Water Resources*, 32(8):1267–1283.

Barry, J. J., Buffington, J. M. and King, J. G. (2004). A general power equation for predicting bed load transport rates in gravel bed rivers. *Water Resources Research*, 40(10):1–22.

Bathurst, J., Graf, W. and Cao, H. (1983). Initiation of sediment transport in steep channels with coarse bed material. In Sumer, B. and Müller, A., editors, *Mechanics of Sediment Transport*. A.A..Balkema, Rotterdam, Netherlands.

Bayazit, M. (1983). Flow structure and sediment transport mechanics in steep channels. In Sumer, B. and Müller, A., editors, *Mechanics of Sediment Transport*. A.A..Balkema, Rotterdam, Netherlands.

Bijker, E. W. (1968). Littoral drift as function of waves and current. *Coastal Eng. 1968*, pages 415–435.

Bonakdari, H., Larrarte, F., Lassabatere, L. and Joannis, C. (2008). Turbulent velocity profile in fully-developed open channel flows. *Environmental Fluid Mechanics*, 8:1–17.

Callaghan, D. P., Saint-Cast, F., Nielsen, P. and Baldock, T. E. (2006). Numerical solutions of the sediment conservation law; a review and improved formulation for coastal morphological modelling. *Coastal Engineering*, 53:557–571.

Camenen, B. and Larroudé, P. (2003). Comparison of sediment transport formulae for the coastal environment. *Coastal Engineering*, 48:111–132.

Camenen, B. and Larson, M. (2005). A general formula for non-cohesive bed load sediment transport. *Estuarine, Coastal and Shelf Science*, 63(1-2):249–260.

Cao, Z. and Carling, P. A. (2002a). Mathematical modelling of alluvial rivers: reality and myth. part 1: General review. *Proceedings of the ICE-Water and Maritime Engineering*, 154(3):207–219.

Cao, Z. and Carling, P. A. (2002b). Mathematical modelling of alluvial rivers: reality and myth. Part 2: Special issues. *Proceedings of the ICE - Water and Maritime Engineering*, 154(4):297–307.

Cao, Z., Day, R. and Egashira, S. (2002). Coupled and Decoupled Numerical Modeling of Flow and Morphological Evolution in Alluvial Rivers. *Journal of Hydraulic Engineering*, 128(3):306–321.

Cao, Z., Pender, G., Wallis, S. and Carling, P. (2004). Computational Dam-Break Hydraulics over Erodible Sediment Bed. *Journal of Hydraulic Engineering*, 130(7):689–703.

Capart, H. and Young, D. (1998). Formation of a jump by the dam-break wave over a granular bed. *Journal of Fluid Mechanics*, 372:165–187.

Castro Díaz, M. J., Fernández-Nieto, E. D. and Ferreiro, A. M. (2008). Sediment transport models in Shallow Water equations and numerical approach by high order finite volume methods. *Computers & Fluids*, 37:299–316.

Chacón Rebollo, T., Domínguez Delgado, A. and Fernández Nieto, E. D. (2003). An entropy-correction free solver for non-homogeneous shallow water equations. *ESAIM: Mathematical Modelling and Numerical Analysis*, 37(05):755–772.

Chen, X., Ma, J. and Dey, S. (2010). Sediment Transport on Arbitrary Slopes: Simplified Model. *Journal of Hydraulic Engineering*, 136(May):311–317.

Cheng, N.-S. (2002). Exponential Formula for Bedload Transport. *Journal of Hydraulic Engineering*, 128(10):942–946.

Chiari, M., Friedl, K. and Rickenmann, D. (2010). A one-dimensional bedload transport model for steep slopes. *Journal of Hydraulic Research*, 48(2):152–160.

Chiew, Y.-M. and Parker, G. (1994). Incipient sediment motion on non-horizontal slopes. *Journal of Hydraulic Research*, 32(5):649–660.

Damgaard, J. S., Whitehouse, R. J. S. and Soulsby, R. L. (1997). Bed-Load Sediment Transport on Steep Longitudinal Slopes. *Journal of Hydraulic Engineering*, 123:1130–1138.

De Vriend, H., Zyserman, J., Nicholson, J., Roelvink, J., Pechon, P. and Southgate, H. (1993). Medium-term 2DH coastal area modelling. *Coastal Engineering*, 21(1):193–224.

Denlinger, R. P. and O'Connell, D. R. (2008). Computing Nonhydrostatic Shallow-Water Flow over Steep Terrain. *Journal of Hydraulic Engineering*, 134(November):1590–1602.

Dey, S. (2003). Threshold of sediment motion on combined transverse and longitudinal sloping beds. *Journal of Hydraulic Research*, 41:405–415.

Dey, S. and Debnath, K. (2001). Sediment Pickup on Streamwise Sloping Beds. *Journal of Irrigation and Drainage Engineering*, 127(1):39–43.

Dibajnia, M. and Watanabe, A. (1992). Sheet flow under nonlinear waves and currents. *Coastal Engineering Proceedings*, 1(23).

Diplas, P., Dancey, C. L., Celik, A. O., Valyrakis, M., Greer, K. and Akar, T. (2008). The Role of Impulse on the Initiation of Particle Movement Under Turbulent Flow Conditions. *Science*, 322(5902):717–720.

Dissanayake, D. M. P. K., Roelvink, J. A. and van der Wegen, M. (2009). Modelled channel patterns in a schematized tidal inlet. *Coastal Engineering*, 56(11-12):1069–1083.

Dodd, N., Stoker, A. M., Calvete, D. and Sriariyawat, A. (2008). On beach cusp formation. *Journal of Fluid Mechanics*, 597:145–169.

Du Boys, M. P. (1879). Le rhône et les rivières à lit affouillable. In *Annales des ponts et chaussees*, 5.

Einstein, H. a. (1950). The bed-load function for sediment transport in open channel flows. *Agriculture. Soil Conservation Service. Tech. Bull*, 1026.

El Kadi Abderrezzak, K. and Paquier, A. (2011). Applicability of Sediment Transport Capacity Formulas to Dam-Break Flows over Movable Beds. *Journal of Hydraulic Engineering*, 137(2):209–221.

Engelund, F. (1981). The motion of sediment particles on an inclined bed. *Progress Rep*, 53.

Engelund, F. and Fredsøe, J. (1976). A sediment transport model for straight alluvial channels. *Nordic Hydrology*, 7(5):293–306.

Engelund, F. and Hansen, E. (1967). A monograph on sediment transport in alluvial streams. Technical report, TEKNISKFORLAG Skelbrekgade 4 Copenhagen V, Denmark.

Falconer, R. A. (1993). An introduction to nearly horizontal flows. *Coastal, estuarial and harbour engineers' reference book*, pages 27–36.

Fang, H.-W. and Wang, G.-Q. (2000). Three-Dimensional Mathematical Model of Suspended-Sediment Transport. *Journal of Hydraulic Engineering*, 126(8):578–592.

Fernández Luque, R. and van Beek, R. (1976). Erosion And Transport Of Bed-Load Sediment. *Journal of Hydraulic Research*, 14(October 2014):127–144.

Fleming, C. A. and Hunt, J. N. (1976). Application of a sediment transport model. *Coastal Engineering Proceedings*, 1(15).

Fraccarollo, L. and Capart, H. (2002). Riemann wave description of erosional dam-break flows. *Journal of Fluid Mechanics*, 461:183–228.

Francis, J. R. D. (1973). Experiments on the Motion of Solitary Grains Along the Bed of a Water-Stream. *Proceedings of the Royal Society A: Mathematical, Physical and Engineering Sciences*, 332:443–471.

Fredsøe, J. and Deigaard, R. (1992). *Mechanics of Coastal Sediment Transport*, volume 3 of *Advanced series on ocean engineering*. World Scientific, Singapore.

Furbish, D. J., Haff, P. K., Roseberry, J. C. and Schmeeckle, M. W. (2012a). A probabilistic description of the bed load sediment flux: 1. Theory. *Journal of Geophysical Research: Earth Surface*, 117(January).

Furbish, D. J., Roseberry, J. C. and Schmeeckle, M. W. (2012b). A probabilistic description of the bed load sediment flux: 3. the particle velocity distribution and the diffusive flux. *Journal of Geophysical Research: Earth Surface*, 117(January).

Garnier, R., Calvete, D., Falqués, A. and Caballeria, M. (2006). Generation and non-linear evolution of shore-oblique/transverse sand bars. *Journal of Fluid Mechanics*, 567:327.

Gaudio, R., Miglio, A. and Dey, S. (2010). Non-universality of von Kármán's κ in fluvial streams. *Journal of Hydraulic Research*, 48:658–663.

Gomez, B. and Church, M. (1989). An assessment of bed load sediment transport formulae for gravel bed rivers. *Water Resources Research*, 25(6):1161.

Graf, W. (1984). *Hydraulics of Sediment Transport*. Water Resources Publications, LLC, U.S.A.

Grass, A. (1981). *Sediment transport by waves and currents*. University College London, Dept. of Civil Engineering, London, U.K.

Greco, M., Iervolino, M., Leopardi, A. and Vacca, A. (2013). A two-phase model for fast geomorphic shallow flows. *International Journal of Sediment Research*, 27(4):409–425.

Haddadian, S., Bahmanpouri, F. and Namin, M. M. (2014). Experimental and Numerical Investigation of Bed Compaction Effect on Dam Break Flow over Movable Bed. In *11th International Congress on Advances in Civil Engineering*.

Hergarten, S. and Robl, J. (2015). Modelling rapid mass movements using the shallow water equations in Cartesian coordinates. *Natural Hazards and Earth System Science*, 15(3):671–685.

Hinton, D. D. (2012). *Complexity of Bedload Transport in Gravel Bed Streams: Data Collection, Prediction, and Analysis*. PhD thesis, Brigham Young University, Provo, Utah, U.S.A.

Hu, D., Saito, Y. and Kempe, S. (1998). Sediment and nutrient transport to the coastal zone. *Asian change in the context of global climate change: impact of natural and anthropogenic changes in Asia on global biogeochemical cycles*, 3:245–270.

Hu, P., Cao, Z. and Pender, G. (2012). Well-balanced two-dimensional coupled modelling of submarine turbidity currents. *Proceedings of the ICE-Maritime Engineering*, 165(4):169–188.

Huai, W. X., Zeng, Y. H., Xu, Z. G. and Yang, Z. H. (2009). Three-layer model for vertical velocity distribution in open channel flow with submerged rigid vegetation. *Advances in Water Resources*, 32(4):487–492.

Huang, J., Borthwick, A. G. L. and Soulsby, R. L. (2008). One-dimensional modelling of fluvial bed morphodynamics. *Journal of Hydraulic Research*, 46(5):636–647.

Hudson, J. and Sweby, P. K. (2003). Formulations for Numerically Approximating Hyperbolic Systems Governing Sediment Transport. *Journal of Scientific Computing*, 19(December):225–252.

Inui, T., Dibajnia, M., Isobe, M. and Watanabe, A. (1995). A transport rate formula for mixed-size sands and its application. In *Proc. 42nd Japanese Annual Conf. on Coastal Eng., JSCE, (in Japanese)*.

Johnson, H. K. and Zyserman, J. a. (2002). Controlling spatial oscillations in bed level update schemes. *Coastal Engineering*, 46:109–126.

Kleinhans, M. G., Buskes, C. J. J. and de Regt, H. W. (2005). Terra Incognita: Explanation and Reduction in Earth Science. *International Studies in the Philosophy of Science*, 19:289–317.

Kleinhans, M. G. and van Rijn, L. C. (2002). Stochastic Prediction of Sediment Transport in Sand-Gravel Bed Rivers. *Journal of Hydraulic Engineering*, 128(4):412–425.

Komar, P. (1998). *Beach Processes and Sedimentation*. Prentice Hall PTR.

Kovacs, A. and Parker, G. (1994). A new vectorial bedload formulation and its application to the time evolution of straight river channels. *Journal of Fluid Mechanics*, 267:153.

Kuhnle, R. A., Wren, D. G., Langendoen, E. J. and Rigby, J. R. (2013). Sand Transport over an Immobile Gravel Substrate. *Journal of Hydraulic Engineering*, 139(2):167–176.

Lavelle, J. W. and Mofjeld, H. O. (1987). Do Critical Stresses for Incipient Motion and Erosion Really Exist? *Journal of Hydraulic Engineering*, 113(3):370–385.

Lee, H. and Hsu, I. (1994). Investigation of Saltating Particle Motions. *Journal of Hydraulic Engineering*, 120(7):831–845.

Lee, H.-Y., Chen, Y.-H., You, J.-Y. and Lin, Y.-T. (2000). Investigations of Continuous Bed Load Saltating Process. *Journal of Hydraulic Engineering*, 126(9):691–700.

Lee, W.-K. (2011). *Chaotic Mixing in Wavy-type Channels and Two-layer Shallow Flows*. DPhil thesis, University of Oxford, Oxford, U.K.

Li, J., Cao, Z., Pender, G. and Liu, Q. (2013). A double layer-averaged model for dam-break flows over mobile bed. *Journal of Hydraulic Research*, 51:518–534.

Madsen, O. S. (1991). Mechanics of cohesionless sediment transport in coastal waters. In *Coastal Sediments (1991)*, pages 15–27. ASCE.

Maldonado, S. and Borthwick, A. G. L. (2015). Sensitivity Analysis and Statistical Convergence of a Saltating Particle Model. *Journal of Hydraulic Engineering*, 141(5):04014091.

Manes, C. and Brocchini, M. (2015). Local scour around structures and the phenomenology of turbulence. *Journal of Fluid Mechanics*, 779:309–324.

Marusic, I., Mathis, R. and Hutchins, N. (2010). Predictive Model for Wall-Bounded Turbulent Flow. *Science*, 329(5988):193–196.

Meyer-Peter, E. and Müller, R. (1948). Formulas for Bed-Load Transport. *International Association for Hydraulic Structures Researach - Zweite Tagung - Second meeting - Deuxième réunion*.

Moulton, M., Elgar, S. and Raubenheimer, B. (2014). A surfzone morphological diffusivity estimated from the evolution of excavated holes. *Geophysical Research Letters*, 41.

Ni, J. R., Wang, G. Q. and Borthwick, A. G. L. (2000). Kinetic Theory for Particles in Dilute and Dense Solid-Liquid Flows. *Journal of Hydraulic Engineering*, 126(12):893–903.

Niño, Y. and García, M. (1994). Gravel Saltation: 2. Modeling. *Water Resources Research*, 30(6):1915–1924.

Niño, Y. and García, M. (1998a). Experiments on Saltation of Sand in Water. *Journal of Hydraulic Engineering*, 124(10):1014–1025.

Niño, Y. and García, M. (1998b). Using Lagrangian particle saltation observations for bedload sediment transport modelling. *Hydrological Processes*, 12:1197–1218.

Nielsen, P. (1992). *Coastal bottom boundary layers and sediment transport*, volume 4. World scientific.

Nikora, V., Ballio, F., Coleman, S. and Pokrajac, D. (2013). Spatially Averaged Flows over Mobile Rough Beds: Definitions, Averaging Theorems, and Conservation Equations. *Journal of Hydraulic Engineering*, 139(8):803–811.

Nikora, V., McEwan, I., McLean, S., Coleman, S., Pokrajac, D. and Walters, R. (2007). Double-averaging concept for rough-bed open-channel and overland flows: Theoretical background. *Journal of Hydraulic Engineering*.

Nnadi, F. N. and Wilson, K. C. (1992). Motion of Contact-Load Particles at High Shear Stress. *Journal of Hydraulic Engineering*, 118(12):1670–1684.

Parker, G. (1990). Surface-based bedload transport relation for gravel rivers. *Journal of Hydraulic Research*, 28(4):417–436.

Parker, G., Paola, C. and Leclair, S. (2000). Probabilistic Exner sediment continuity equation for mixtures with no active layer. *Journal of Hydraulic Engineering*, 126(11):818–826.

Parker, G., Seminara, G. and Solari, L. (2003). Bed load at low Shields stress on arbitrarily sloping beds: Alternative entrainment formulation. *Water Resources Research*, 39(7):1–11.

Pritchard, D. (2005). On fine sediment transport by a flood surge. *Journal of Fluid Mechanics*, 543:239–248.

Pu, J. (2013). Universal Velocity Distribution for Smooth and Rough Open Channel Flows. *Journal of Applied Fluid Mechanics*, 6(3):413–423.

Pugh, F. J. and Wilson, K. C. (1999). Velocity and concentration distributions in sheet flow above plane beds. *Journal of Hydraulic Engineering*, 125(2):117–125.

Radice, A., Nikora, V., Campagnol, J. and Ballio, F. (2013). Active interactions between turbulence and bed load: Conceptual picture and experimental evidence. *Water Resources Research*, 49(1):90–99.

Razavitoosi, S. L., Ayyoubzadeh, S. A. and Valizadeh, A. (2014). Two-phase SPH modelling of waves caused by dam break over a movable bed. *International Journal of Sediment Research*, 29(3):344–356.

Reynolds, O. (1885). On the dilatancy of media composed of rigid particles in contact. with experimental illustrations. *The London, Edinburgh, and Dublin Philosophical Magazine and Journal of Science*, 20(127):469–481.

Ribberink, J. S. (1998). Bed-load transport for steady flows and unsteady oscillatory flows. *Coastal Engineering*, 34(1-2):59–82.

Ribberink, J. S. and Al-Salem, A. A. (1994). Sediment transport in oscillatory boundary layers in cases of rippled beds and sheet flow. *Journal of Geophysical Research: Oceans (1978–2012)*, 99(C6):12707–12727.

Roelvink, J. a. (2006). Coastal morphodynamic evolution techniques. *Coastal Engineering*, 53:277–287.

Rosatti, G. and Fraccarollo, L. (2006). A well-balanced approach for flows over mobile-bed with high sediment-transport. *Journal of Computational Physics*, 220:312–338.

Roseberry, J. C., Schmeeckle, M. W. and Furbish, D. J. (2012). A probabilistic description of the bed load sediment flux: 2. Particle activity and motions. *Journal of Geophysical Research: Earth Surface*, 117(January).

Rosgen, D. L., Silvey, H. L. and Frantila, D. (2006). *Watershed assessment of river stability and sediment supply (WARSSS)*. Wildland Hydrology.

Saffman, P. G. (1965). The lift on a small sphere in a slow shear flow. *Journal of Fluid Mechanics*, 22:385.

Sarma, K. V. N., Lakshminarayana, P. and Rao, N. S. L. (1983). Velocity Distribution in Smooth Rectangular Open Channels. *Journal of Hydraulic Engineering*, 109:270–289.

Schoklitsch, A. (1934). Der geschiebetrieb und die geschiebefracht. *Wasserkraft Wasserwirtschaft*, 4:1–7.

Sekine, M. and Kikkawa, H. (1992). Mechanics of Saltating Grains. II. *Journal of Hydraulic Engineering*, 118:536–558.

Sekine, M. and Parker, G. (1992). Bed-Load Transport on Transverse Slope. I. *Journal of Hydraulic Engineering*, 118(4):513–535.

Seminara, G., Solari, L. and Parker, G. (2002). Bed load at low Shields stress on arbitrarily sloping beds: Failure of the Bagnold hypothesis. *Water resources research*, 38(11):31–1.

Shang, P. and Kamae, S. (2005). Fractal nature of time series in the sediment transport phenomenon. *Chaos, Solitons & Fractals*, 26(3):997–1007.

Shang, P., Na, X. and Kamae, S. (2009). Chaotic analysis of time series in the sediment transport phenomenon. *Chaos, Solitons & Fractals*, 41(1):368–379.

Shields, A. (1936). Anwendung der Aehnlichkeitsmechanik und der Turbulenzforschung auf die Geschiebebewegung. Technical report, Preussischen Versuchsanstalt für Wasserbau.

Silva Casarín, R., Ruiz Martínez, G., Mariño-Tapia, I., Posada Vanegas, G., Mendoza Baldwin, E. and Escalante Mancera, E. (2012). Manmade vulnerability of the Cancun beach system: the case of hurricane Wilma. *CLEAN–Soil, Air, Water*, 40(9):911–919.

Sivakumar, B. (2004). Chaos theory in geophysics: past, present and future. *Chaos, Solitons & Fractals*, 19(2):441–462.

Smart, G. M. (1984). Sediment Transport Formula for Steep Channels. *Journal of Hydraulic Engineering*, 110(3):267–276.

Soulsby, R. (1997). *Dynamics of Marine Sands: A Manual for Practical Applications*. Thomas Telford, Great Britain.

Soulsby, R. L. and Damgaard, J. S. (2005). Bedload sediment transport in coastal waters. *Coastal Engineering*, 52:673–689.

Spinewine, B. (2005). *Two-layer flow behaviour and the effects of granular dilatancy in dam-break induced*. PhD thesis, Université catholique de Louvain, Louvain-la-Neuve, Belgium.

Stive, M. J. F., de Schipper, M. A., Luijendijk, A. P., Aarninkhof, S. G. J., van Gelder-Maas, C., van Thiel de Vries, J. S. M., de Vries, S., Henriquez, M., Marx, S. and Ranasinghe, R. (2013). A new alternative to saving our beaches from sea-level rise: The sand engine. *Journal of Coastal Research*, 29(5):1001–1008.

Swamee, P. K. and Ojha, C. S. P. (1991). Drag Coefficient and Fall Velocity of nonspherical particles. *Journal of Hydraulic Engineering*, 117(5):660–667.

Talmon, A., Struiksma, N. and Van Mierlo, M. (1995). Laboratory measurements of the direction of sediment transport on transverse alluvial-bed slopes. *Journal of Hydraulic Research*, 33(4):495–517.

Toro, E. F. (2001). *Shock-Capturing Methods for Free-Surface Shallow Flows*. John Wiley & Sons, LTD, Great Britain.

Tregnaghi, M., Bottacin-Busolin, A., Marion, A. and Tait, S. (2012). Stochastic determination of entrainment risk in uniformly sized sediment beds at low transport stages: 1. Theory. *Journal of Geophysical Research: Earth Surface*, 117:1–15.

Van Emelen, S., Zech, Y. and Soares-Frazão, S. (2015). Impact of sediment transport formulations on breaching modelling. *Journal of Hydraulic Research*, 53(1):60–72.

van Rijn, L. C. (1984a). Sediment transport, part I: bed load transport. *Journal of Hydraulic Engineering*, 110(10):1431–1456.

van Rijn, L. C. (1984b). Sediment transport, part II: suspended load transport. *Journal of hydraulic engineering*, 110(11):1613–1641.

Wang, H., Yang, Z., Saito, Y., Liu, J. P., Sun, X. and Wang, Y. (2007). Stepwise decreases of the Huanghe (Yellow River) sediment load (1950–2005): Impacts of climate change and human activities. *Global and Planetary Change*, 57(3):331–354.

Watanabe, A. (1988). Modeling of sediment transport and beach evolution. In Horikawa, K., editor, *Nearshore Dynamics and Coastal Processes*, chapter 4, pages 292–302. University of Tokyo Press, Tokyo, Japan.

White, W. and Day, T. (1982). Transport of graded gravel bed material. *Gravel-Bed Rivers, Fluvial Processes, Engineering and Management*, pages 181–223.

Whitehouse, R. and Hardisty, J. (1988). Experimental assessment of two theories for the effect of bedslope on the threshold of bedload transport. *Marine Geology*, 79(1-2):135–139.

Wiberg, P. and Smith, J. (1989). Model for calculating bed load transport of sediment. *Journal of Hydraulic Engineering*, 115(1):101–123.

Wilcock, P. R. (1998). Two-Fraction Model of Initial Sediment Motion in Gravel-Bed Rivers. *Science*, 280(5362):410–412.

Wilcock, P. R. and Kenworthy, S. T. (2002). A two-fraction model for the transport of sand/gravel mixtures. *Water Resources Research*, 38(10):12–1.

Wilson, K. C. (1966). Bed-load transport at high shear stress. *Journal of the Hydraulics Division*, 92(6):49–59.

Wilson, K. C. (1987). Analysis of Bed-Load Motion at High Shear Stress. *Journal of Hydraulic Engineering*, 113(1):97–103.

Wong, M. and Parker, G. (2006). Reanalysis and Correction of Bed-Load Relation of Meyer-Peter and Müller Using Their Own Database. *Journal of Hydraulic Engineering*, 132(11):1159–1168.

Wu, W., Wang, S. S. and Jia, Y. (2000). Nonuniform sediment transport in alluvial rivers. *Journal of Hydraulic Research*, 38(6):427–434.

Yager, E. M., Kirchner, J. W. and Dietrich, W. E. (2007). Calculating bed load transport in steep boulder bed channels. *Water Resources Research*, 43(7):1–24.

Yalin, M. S. (1963). An expression for bed-load transportation. *Journal of the Hydraulics Division*, 89(3):221–250.

Yalin, S. (1977). *Mechanics of Sediment Transport*. Pergamon Press, Great Britain, second edition.

Yan, K. (2010). *Coastal Flood Inundation and Morphodynamic Change*. DPhil thesis, University of Oxford, Oxford, U.K.

Yang, C. T. and Wan, S. (1991). Comparisons of Selected Bed-Material Load Formulas. *Journal of Hydraulic Engineering*, 117(8):973–989.

Yang, S.-Q., Tan, S.-K. and Lim, S.-Y. (2004). Velocity Distribution and Dip-Phenomenon in Smooth Uniform Open Channel Flows. *Journal of Hydraulic Engineering*, 130(12):1179–1186.

Yeganeh, A., Gotoh, H. and Sakai, T. (2000). Applicability of Euler-Lagrange coupling multiphase-flow model to bed-load transport under high bottom shear. *Journal of Hydraulic Research*, 38(5):389–398.

Yen, B. C. (2002). Stochastic Inference to Sediment and Fluvial Hydraulics. *Journal of Hydraulic Engineering*, 128:365–367.

Zech, Y., Soares-Frazão, S., Spinewine, B. and Le Grelle, N. (2008). Dam-break induced sediment movement: Experimental approaches and numerical modelling. *Journal of Hydraulic Research*, 46:176–190.

Ziaei, A. N., Keshavarzi, A. R. and Homayoun, E. (2005). Fractal scaling and simulation of velocity components and turbulent shear stress in open channel flow. *Chaos, Solitons & Fractals*, 24(4):1031–1045.

Zou, S. (2007). *Coastal Sediment Transport Simulation by Smoothed Particle Hydrodynamics*. PhD thesis, The Johns Hopkins University, Baltimore, Maryland, U.S.A.